Future Physics Programme of BESIII*

Abstract: There has recently been a dramatic renewal of interest in hadron spectroscopy and charm physics. This renaissance has been driven in part by the discovery of a plethora of charmonium-like *XYZ* states at BESIII and *B* factories, and the observation of an intriguing proton-antiproton threshold enhancement and the possibly related *X*(1835) meson state at BESIII, as well as the threshold measurements of charm mesons and charm baryons. We present a detailed survey of the important topics in tau-charm physics and hadron physics that can be further explored at BESIII during the remaining operation period of BEPCII. This survey will help in the optimization of the data-taking plan over the coming years, and provides physics motivation for the possible upgrade of BEPCII to higher luminosity.

DOI: 10.1088/1674-1137/44/4/040001

Received 25 December 2019, Published online 26 March 2020

* Supported in part by National Key Basic Research Program of China (2015CB856700); National Natural Science Foundation of China (NSFC) (11335008, 11425524, 11625523, 11635010, 11735014, 11822506, 11935018); the Chinese Academy of Sciences (CAS) Large-Scale Scientific Facility Program; the CAS Center for Excellence in Particle Physics (CCEPP); Joint Large-Scale Scientific Facility Funds of the NSFC and CAS (U1532257, U1532258, U1732263); CAS Key Research Program of Frontier Science (QYZDJ-SSW-SLH003, QYZDJ-SSW-SLH040); 100 Talents Program of CAS; CAS PIFI; the Thousand Talents Program of China; INPAC and Shanghai Key Laboratory for Particle Physics and Cosmology; German Research Foundation DFG under Contracts Nos. Collaborative Research Center CRC 1044, FOR 2359; Istituto Nazionale di Fisica Nucleare, Italy; Koninklijke Nederlandse Akademie van Wetenschappen (KNAW) (530-4CDP03); Ministry of Development of Turkey (DPT2006K-120470); National Science and Technology fund; The Knut and Alice Wallenberg Foundation (Sweden) (2016.0157); The Swedish Research Council; U. S. Department of Energy (DE-FG02-05ER41374, DESC-0010118, DE-SC-0012069); University of Groningen (RuG) and the Helmholtzzentrum fuer Schwerionenforschung GmbH (GSI), Darmstadt; the Russian Ministry of Science and Higher Education (14.W03.31.0026)

M. Ablikim[1,§] M. N. Achasov[10,d,§] P. Adlarson[58,§] S. Ahmed[15,§] M. Albrecht[4,§] M. Alekseev[57A,57C,§] A. Amoroso[57A,57C,§]
F. F. An[1,§] Q. An[54,42,§] Y. Bai[41,§] O. Bakina[27,§] R. Baldini Ferroli[23A,§] Y. Ban[35,§] K. Begzsuren[25,§] J. V. Bennett[5,§]
N. Berger[26,§] M. Bertani[23A,§] D. Bettoni[24A,§] F. Bianchi[57A,57C,§] J Biernat[58,§] J. Bloms[51,§] I. Boyko[27,§] R. A. Briere[5,§]
L. Calibbi[34,¶] H. Cai[59,§] X. Cai[1,42,§] A. Calcaterra[23A,§] G. F. Cao[1,46,§] N. Cao[1,46,§] S. A. Cetin[45B,§] J. Chai[57C,§]
J. F. Chang[1,42,§] W. L. Chang[1,46,§] J. Charles[I,¶] G. Chelkov[27,b,c,§] Chen[6,§] G. Chen[1,§] H. S. Chen[1,46,§] J. C. Chen[1,§]
M. L. Chen[1,42,§] S. J. Chen[33,§] Y. B. Chen[1,42,§] H. Y. Cheng[VI,¶] W. Cheng[57C,§] G. Cibinetto[24A,§] F. Cossio[57C,§]
X. F. Cui[34,§] H. L. Dai[1,42,§] J. P. Dai[37,h,§] X. C. Dai[1,46,§] A. Dbeyssi[15,§] D. Dedovich[27,§] Z. Y. Deng[1,§] A. Denig[26,§]
I. Denysenko[27,§] M. Destefanis[57A,57C,§] S. Descotes-Genon[IV,¶] F. De Mori[57A,57C,§] Y. Ding[31,§] C. Dong[34,§] J. Dong[1,42,§]
L. Y. Dong[1,46,§] M. Y. Dong[1,42,46,§] Z. L. Dou[33,§] S. X. Du[62,§] S. I. Eidelman[II,V,VIII,¶] J. Z. Fan[44,§] J. Fang[1,42,§]
S. S. Fang[1,46,§] Y. Fang[1,§] R. Farinelli[24A,24B,§] L. Fava[57B,57C,§] F. Feldbauer[4,§] G. Felici[23A,§] C. Q. Feng[54,42,§]
M. Fritsch[4,§] C. D. Fu[1,§] Y. Fu[1,§] Q. Gao[1,§] X. L. Gao[54,42,§] Y. Gao[44,§] Y. Gao[55,§] Y. G. Gao[6,§] Z. Gao[54,42,§]
B. Garillon[26,§] I. Garzia[24A,§] E. M. Gersabeck[49,§] A. Gilman[50,§] K. Goetzen[11,§] L. Gong[34,§] W. X. Gong[1,42,§]
W. Gradl[26,§;1)] M. Greco[57A,57C,§] L. M. Gu[33,§] M. H. Gu[1,42,§] Y. T. Gu[13,§] A. Q. Guo[22,§] F. K. Guo[VII,46,¶] L. B. Guo[32,§]
R. P. Guo[1,46,§] Y. P. Guo[26,§] A. Guskov[27,§] S. Han[59,§] X. Q. Hao[16,§] F. A. Harris[47,§] K. L. He[1,46,§] F. H. Heinsius[4,§]
T. Held[4,§] Y. K. Heng[1,42,46,§] Y. R. Hou[46,§] Z. L. Hou[1,§] H. M. Hu[1,46,§] J. F. Hu[37,h,§] T. Hu[1,42,46,§] Y. Hu[1,§]
G. S. Huang[54,42,§] J. S. Huang[16,§] X. T. Huang[36,§] X. Z. Huang[33,§] Z. L. Huang[31,§] N. Huesken[51,§] T. Hussain[56,§]
W. Ikegami Andersson[58,§] W. Imoehl[22,§] M. Irshad[54,42,§] Q. Ji[1,§] Q. P. Ji[16,§] X. B. Ji[1,46,§] X. L. Ji[1,42,§] H. L. Jiang[36,§]
X. S. Jiang[1,42,46,§] X. Y. Jiang[34,§] J. B. Jiao[36,§] Z. Jiao[18,§] D. P. Jin[1,42,46,§] S. Jin[33,§] Y. Jin[48,§] T. Johansson[58,§]
N. Kalantar-Nayestanaki[29,§] X. S. Kang[31,§] R. Kappert[29,§] M. Kavatsyuk[29,§] B. C. Ke[1,§] I. K. Keshk[4,§] T. Khan[54,42,§]
A. Khoukaz[51,§] P. Kiese[26,§] R. Kiuchi[1,§] R. Kliemt[11,§] L. Koch[28,§] O. B. Kolcu[45B,f,§] B. Kopf[4,§] M. Kuemmel[4,§]
M. Kuessner[4,§] A. Kupsc[58,§] M. Kurth[1,§] M. G. Kurth[1,46,§] W. Kühn[28,§] J. S. Lange[28,§] P. Larin[15,§] L. Lavezzi[57C,§]
H. Leithoff[26,§] T. Lenz[26,§] C. Li[58,§] Cheng Li[54,42,§] D. M. Li[62,§] F. Li[1,42,§] F. Y. Li[35,§] G. Li[1,§] H. B. Li[1,46,§,★]
H. J. Li[9,j,§] J. C. Li[1,§] J. W. Li[40,§] Ke Li[1,§] L. K. Li[1,§] Lei Li[3,§] P. L. Li[54,42,§] P. R. Li[30,§] Q. Y. Li[36,§] W. D. Li[1,46,§]
W. G. Li[1,§] X. H. Li[54,42,§] X. L. Li[36,§] X. N. Li[1,42,§] X. Q. Li[34,§] Z. B. Li[43,§] H. Liang[1,46,§] H. Liang[54,42,§]
Y. F. Liang[39,§] Y. T. Liang[28,§] G. R. Liao[12,§] L. Z. Liao[1,46,§] J. Libby[21,§] C. X. Lin[43,§] D. X. Lin[15,§] Y. J. Lin[13,§]
B. Liu[37,h,§] B. J. Liu[1,§] C. X. Liu[1,§] D. Liu[54,42,§] D. Y. Liu[37,h,§] F. H. Liu[38,§] Fang Liu[1,§] Feng Liu[6,§] H. B. Liu[13,§]
H. M. Liu[1,46,§] Huanhuan Liu[1,§] Huihui Liu[17,§] J. B. Liu[54,42,§] J. Y. Liu[1,46,§] K. Y. Liu[31,§] Ke Liu[6,§] Q. Liu[46,§]
S. B. Liu[54,42,§] T. Liu[1,46,§] X. Liu[30,§] X. Y. Liu[1,46,§] Y. B. Liu[34,§] Z. A. Liu[1,42,46,§] Zhiqing Liu[26,§] Y. F. Long[35,§]
X. C. Lou[1,42,46,§] H. J. Lu[18,§] J. D. Lu[1,46,§] J. G. Lu[1,42,§] Y. Lu[1,§] Y. P. Lu[1,42,§] C. L. Luo[32,§] M. X. Luo[61,§]
P. W. Luo[43,§] T. Luo[9,j,§] X. L. Luo[1,42,§] S. Lusso[57C,§] X. R. Lyu[46,§,★;2)] F. C. Ma[31,§] H. L. Ma[1,§] L. L. Ma[36,§]
M. M. Ma[1,46,§] Q. M. Ma[1,§] X. N. Ma[34,§] X. X. Ma[1,46,§] X. Y. Ma[1,42,§] Y. M. Ma[36,§] F. E. Maas[15,§] M. Maggiora[57A,57C,§]
S. Maldaner[26,§] S. Malde[52,§] Q. A. Malik[56,§] A. Mangoni[23B,§] Y. J. Mao[35,§] Z. P. Mao[1,§] S. Marcello[57A,57C,§]
Z. X. Meng[48,§] J. G. Messchendorp[29,§] G. Mezzadri[24A,§] J. Min[1,42,§] T. J. Min[33,§] R. E. Mitchell[22,§] X. H. Mo[1,42,46,§]
Y. J. Mo[6,§] C. Morales Morales[15,§] N.Yu. Muchnoi[10,d,§] H. Muramatsu[50,§] A. Mustafa[4,§] S. Nakhoul[11,g,§] Y. Nefedov[27,§]
F. Nerling[11,g,§] I. B. Nikolaev[10,d,§] Z. Ning[1,42,§] S. Nisar[8,k,§] S. L. Niu[1,42,§] S. L. Olsen[46,§] Q. Ouyang[1,42,46,§]
S. Pacetti[23B,§] Y. Pan[54,42,§] M. Papenbrock[58,§] P. Patteri[23A,§] M. Pelizaeus[4,§] H. P. Peng[54,42,§] K. Peters[11,g,§]
A. A. Petrov[X,¶] J. Pettersson[58,§] J. L. Ping[32,§] R. G. Ping[1,46,§] A. Pitka[4,§] R. Poling[50,§] V. Prasad[54,42,§] M. Qi[33,§]
T. Y. Qi[2,§] S. Qian[1,42,§] C. F. Qiao[46,§] N. Qin[59,§] X. P. Qin[13,§] X. S. Qin[4,§] Z. H. Qin[1,42,§] J. F. Qiu[1,§] S. Q. Qu[34,§]
K. H. Rashid[56,i,§] C. F. Redmer[26,§] M. Richter[4,§] M. Ripka[26,§] A. Rivetti[57C,§] V. Rodin[29,§] M. Rolo[57C,§] G. Rong[1,46,§]
J. L. Rosner[IX,¶,★] Ch. Rosner[15,§] M. Rump[51,§] A. Sarantsev[27,e,§] M. Savrié[24B,§] K. Schoenning[58,§] W. Shan[19,§]
X. Y. Shan[54,42,§] M. Shao[54,42,§] C. P. Shen[2,§] P. X. Shen[34,§] X. Y. Shen[1,46,§] H. Y. Sheng[1,§] X. Shi[1,42,§] X.D Shi[54,42,§]
J. J. Song[36,§] Q. Q. Song[54,42,§] X. Y. Song[1,§] S. Sosio[57A,57C,§] C. Sowa[4,§] S. Spataro[57A,57C,§] F. F. Sui[36,§] G. X. Sun[1,§]
J. F. Sun[16,§] L. Sun[59,§] S. S. Sun[1,46,§] X. H. Sun[1,§] Y. J. Sun[54,42,§] Y.K Sun[54,42,§] Y. Z. Sun[1,§] Z. J. Sun[1,42,§]
Z. T. Sun[1,§] Y.T Tan[54,42,§] C. J. Tang[39,§] G. Y. Tang[1,§] X. Tang[1,§] V. Thoren[58,§] B. Tsednee[25,§] I. Uman[45D,§]
B. Wang[1,§] B. L. Wang[46,§] C. W. Wang[33,§] D. Y. Wang[35,§] H. H. Wang[36,§] K. Wang[1,42,§] L. L. Wang[1,§] L. S. Wang[1,§]
M. Wang[36,§] M. Z. Wang[35,§] Wang Meng[1,46,§] P. L. Wang[1,§] R. M. Wang[60,§] W. P. Wang[54,42,§] X. Wang[35,§]

X. F. Wang[1,§] X. L. Wang[9,j,§] Y. Wang[54,42,§] Y. F. Wang[1,42,46,§] Z. Wang[1,42,§] Z. G. Wang[1,42,§] Z. Y. Wang[1,§]
Zongyuan Wang[1,46,§] T. Weber[4,§] D. H. Wei[12,§] P. Weidenkaff[26,§] H. W. Wen[32,§] S. P. Wen[1,§] U. Wiedner[4,§]
G. Wilkinson[52,§] M. Wolke[58,§] L. H. Wu[1,§] L. J. Wu[1,46,§] Z. Wu[1,42,§] L. Xia[54,42,§] Y. Xia[20,§] S. Y. Xiao[1,§]
Y. J. Xiao[1,46,§] Z. J. Xiao[32,§] Y. G. Xie[1,42,§] Y. H. Xie[6,§] T. Y. Xing[1,46,§] X. A. Xiong[1,46,§] Q. L. Xiu[1,42,§] G. F. Xu[1,§]
L. Xu[1,§] Q. J. Xu[14,§] W. Xu[1,46,§] X. P. Xu[40,§] F. Yan[55,§] L. Yan[57A,57C,§] W. B. Yan[54,42,§] W. C. Yan[2,§] Y. H. Yan[20,§]
H. J. Yang[37,h,§] H. X. Yang[1,§] L. Yang[59,§] R. X. Yang[54,42,§] S. L. Yang[1,46,§] Y. H. Yang[33,§] Y. X. Yang[12,§]
Yifan Yang[1,46,§] Z. Q. Yang[20,§] M. Ye[1,42,§] M. H. Ye[7,§] J. H. Yin[1,§] Z. Y. You[43,§] B. X. Yu[1,42,46,§] C. X. Yu[34,§]
J. S. Yu[20,§] C. Z. Yuan[1,46,§;3)] X. Q. Yuan[35,§] Y. Yuan[1,§] A. Yuncu[45B,a,§] A. A. Zafar[56,§] Y. Zeng[20,§] B. X. Zhang[1,§]
B. Y. Zhang[1,42,§] C. C. Zhang[1,§] D. H. Zhang[1,§] H. H. Zhang[43,§] H. Y. Zhang[1,42,§] J. Zhang[1,46,§] J. L. Zhang[60,§]
J. Q. Zhang[4,§] J. W. Zhang[1,42,46,§] J. Y. Zhang[1,§] J. Z. Zhang[1,46,§] K. Zhang[1,46,§] L. Zhang[44,§] S. F. Zhang[33,§]
T. J. Zhang[37,h,§] X. Y. Zhang[36,§] Y. Zhang[54,42,§] Y. H. Zhang[1,42,§] Y. T. Zhang[54,42,§] Yang Zhang[1,§] Yao Zhang[1,§]
Yi Zhang[9,j,§] Yu Zhang[46,§] Z. H. Zhang[6,§] Z. P. Zhang[54,§] Z. Q. Zhang[III,¶] Z. Y. Zhang[59,§] G. Zhao[1,§] J. W. Zhao[1,42,§]
J. Y. Zhao[1,46,§] J. Z. Zhao[1,42,§] Lei Zhao[54,42,§] Ling Zhao[1,§] M. G. Zhao[34,§] Q. Zhao[1,§] S. J. Zhao[62,§] T. C. Zhao[1,§]
Y. B. Zhao[1,42,§] Z. G. Zhao[54,42,§] A. Zhemchugov[27,b,§] B. Zheng[55,§] J. P. Zheng[1,42,§] Y. Zheng[35,§] Y. H. Zheng[46,§]
B. Zhong[32,§] L. Zhou[1,42,§] L. P. Zhou[1,46,§] Q. Zhou[1,46,§] X. Zhou[59,§] X. K. Zhou[46,§] X. R. Zhou[54,42,§] Xingyu Zhou[2,§]
Xiaoyu Zhou[20,§] Xu Zhou[20,§] A. N. Zhu[1,46,§] J. Zhu[34,§] J. Zhu[43,§] K. Zhu[1,§] K. J. Zhu[1,42,46,§] S. H. Zhu[53,§]
W. J. Zhu[34,§] X. L. Zhu[44,§] Y. C. Zhu[54,42,§] Y. S. Zhu[1,46,§] Z. A. Zhu[1,46,§] J. Zhuang[1,42,§] B. S. Zou[1,§] J. H. Zou[1,§]

[1]Institute of High Energy Physics, Beijing 100049, China
[2]Beihang University, Beijing 100191, China
[3]Beijing Institute of Petrochemical Technology, Beijing 102617, China
[4]Bochum Ruhr-University, D-44780 Bochum, Germany
[5]Carnegie Mellon University, Pittsburgh, Pennsylvania 15213, USA
[6]Central China Normal University, Wuhan 430079, China
[7]China Center of Advanced Science and Technology, Beijing 100190, China
[8]COMSATS University Islamabad, Lahore Campus, Defence Road, Off Raiwind Road, 54000 Lahore, Pakistan
[9]Fudan University, Shanghai 200443, China
[10]G.I. Budker Institute of Nuclear Physics SB RAS (BINP), Novosibirsk 630090, Russia
[11]GSI Helmholtzcentre for Heavy Ion Research GmbH, D-64291 Darmstadt, Germany
[12]Guangxi Normal University, Guilin 541004, China
[13]Guangxi University, Nanning 530004, China
[14]Hangzhou Normal University, Hangzhou 310036, China
[15]Helmholtz Institute Mainz, Johann-Joachim-Becher-Weg 45, D-55099 Mainz, Germany
[16]Henan Normal University, Xinxiang 453007, China
[17]Henan University of Science and Technology, Luoyang 471003, China
[18]Huangshan College, Huangshan 245000, China
[19]Hunan Normal University, Changsha 410081, China
[20]Hunan University, Changsha 410082, China
[21]Indian Institute of Technology Madras, Chennai 600036, India
[22]Indiana University, Bloomington, Indiana 47405, USA
[23](A)INFN Laboratori Nazionali di Frascati, I-00044, Frascati, Italy; (B)INFN and University of Perugia, I-06100, Perugia, Italy
[24](A)INFN Sezione di Ferrara, I-44122, Ferrara, Italy; (B)University of Ferrara, I-44122, Ferrara, Italy
[25]Institute of Physics and Technology, Peace Ave. 54B, Ulaanbaatar 13330, Mongolia
[26]Johannes Gutenberg University of Mainz, Johann-Joachim-Becher-Weg 45, D-55099 Mainz, Germany
[27]Joint Institute for Nuclear Research, 141980 Dubna, Moscow region, Russia
[28]Justus-Liebig-Universitaet Giessen, II. Physikalisches Institut, Heinrich-Buff-Ring 16, D-35392 Giessen, Germany
[29]KVI-CART, University of Groningen, NL-9747 AA Groningen, The Netherlands
[30]Lanzhou University, Lanzhou 730000, China
[31]Liaoning University, Shenyang 110036, China
[32]Nanjing Normal University, Nanjing 210023, China
[33]Nanjing University, Nanjing 210093, China
[34]Nankai University, Tianjin 300071, China
[35]Peking University, Beijing 100871, China
[36]Shandong University, Jinan 250100, China
[37]Shanghai Jiao Tong University, Shanghai 200240, China
[38]Shanxi University, Taiyuan 030006, China
[39]Sichuan University, Chengdu 610064, China
[40]Soochow University, Suzhou 215006, China
[41]Southeast University, Nanjing 211100, China
[42]State Key Laboratory of Particle Detection and Electronics, Beijing 100049, Hefei 230026, China
[43]Sun Yat-Sen University, Guangzhou 510275, China

[44]Tsinghua University, Beijing 100084, China
[45](A)Ankara University, 06100 Tandogan, Ankara, Turkey; (B)Istanbul Bilgi University, 34060 Eyup, Istanbul, Turkey; (C)Uludag University, 16059 Bursa, Turkey; (D)Near East University, Nicosia, North Cyprus, Mersin 10, Turkey
[46]University of Chinese Academy of Sciences, Beijing 100049, China
[47]University of Hawaii, Honolulu, Hawaii 96822, USA
[48]University of Jinan, Jinan 250022, China
[49]University of Manchester, Oxford Road, Manchester, M13 9PL, United Kingdom
[50]University of Minnesota, Minneapolis, Minnesota 55455, USA
[51]University of Muenster, Wilhelm-Klemm-Str. 9, 48149 Muenster, Germany
[52]University of Oxford, Keble Rd, Oxford, UK OX13RH
[53]University of Science and Technology Liaoning, Anshan 114051, China
[54]University of Science and Technology of China, Hefei 230026, China
[55]University of South China, Hengyang 421001, China
[56]University of the Punjab, Lahore-54590, Pakistan
[57](A)University of Turin, I-10125, Turin, Italy; (B)University of Eastern Piedmont, I-15121, Alessandria, Italy; (C)INFN, I-10125, Turin, Italy
[58]Uppsala University, Box 516, SE-75120 Uppsala, Sweden
[59]Wuhan University, Wuhan 430072, China
[60]Xinyang Normal University, Xinyang 464000, China
[61]Zhejiang University, Hangzhou 310027, China
[62]Zhengzhou University, Zhengzhou 450001, China
[I]Aix-Marseille Univ, Université de Toulon, CNRS, CPT, Marseille, France
[II]Budker Institute of Nuclear Physics, SB RAS, Novosibirsk, 630090, Russia
[III]Laboratoire de l'Accélérateur Linéaire, IN2P3-CNRS et Université Paris-Sud 11, F-91898, Orsay Cedex, France
[IV]Laboratoire de Physique Théorique, UMR 8627, CNRS, Univ. Paris-Sud, Université Paris-Saclay, 91405 Orsay Cedex, France
[V]Lebedev Physical Institute RAS, 119991 Moscow, Russia
[VI]Institute of Physics, Academia Sinica, Taiwan 115, China
[VII]Institute of Theoretical Physics, Beijing 100190, China
[VIII]Novosibirsk State University, Novosibirsk, 630090, Russia
[IX]University of Chicago, 5620 S. Ellis Avenue, Chicago, IL 60637, USA
[X]Wayne State University, Detroit, MI 48201, USA
[a]Also at Bogazici University, 34342 Istanbul, Turkey
[b]Also at the Moscow Institute of Physics and Technology, Moscow 141700, Russia
[c]Also at the Functional Electronics Laboratory, Tomsk State University, Tomsk, 634050, Russia
[d]Also at the Novosibirsk State University, Novosibirsk, 630090, Russia
[e]Also at the NRC "Kurchatov Institute", PNPI, 188300, Gatchina, Russia
[f]Also at Istanbul Arel University, 34295 Istanbul, Turkey
[g]Also at Goethe University Frankfurt, 60323 Frankfurt am Main, Germany
[h]Also at Key Laboratory for Particle Physics, Astrophysics and Cosmology, Ministry of Education; Shanghai Key Laboratory for Particle Physics and Cosmology; Institute of Nuclear and Particle Physics, Shanghai 200240, China
[i]Also at Government College Women University, Sialkot - 51310. Punjab, Pakistan.
[j]Also at Key Laboratory of Nuclear Physics and Ion-beam Application (MOE) and Institute of Modern Physics, Fudan University, Shanghai 200443, China
[k]Also at Harvard University, Department of Physics, Cambridge, MA, 02138, USA

★ Editor
§ BESIII collaborator
¶ External contributing author

1) E-mail: gradl@uni-mainz.de
2) E-mail: xiaorui@ucas.ac.cn
3) E-mail: yuancz@ihep.ac.cn

Chapter 1

Introduction

1.1 Motivation

The purpose of this White Paper is to examine the BESIII program [1], to consider further physics opportunities, and to plan for possible upgrades of the BEPCII accelerator and the BESIII detector [2], in order to fulfill the physics potentials of the BESIII experiment. The BESIII Yellow Book [1] documented the original plan for the BESIII physics program before its commissioning. The discovery of the $Z_c(3900)$ [3], followed by many experimental results for the *XYZ* hadrons by BESIII [4-6], were pleasant surprises, which were not foreseen in the Yellow Book. Another surprise came from the first systematic absolute measurements of the Λ_c^+ decay properties based on the thereshold $\Lambda_c^+\bar{\Lambda}_c^-$ pair production [7, 8]. The physics of the *XYZ* hadrons and (heavier) charmed baryons has also become the focal point of the Belle II and LHCb experiments, and is an exciting area for the BESIII experiment in the future. In addition, a full spectrum of other important experimental opportunities, as discussed in this White Paper, will be continually pursued by BESIII, such as light hadron spectroscopy and charmed meson physics.

The integration of quantum theory and Maxwell 's electrodynamics has led to a new, powerful theoretical scenario, quantum electrodynamics (QED), which was the first building block of what is called today the Standard Model (SM) of particle physics. Experimental progress led to discoveries of new particles and characterization of their properties, which helped to develop the theoretical framework towards a common understanding of the weak and electromagnetic interactions, called the electroweak theory. The modern theory of the strong interaction, called quantum chromodynamics (QCD), was modeled in a similar way and based on the exact color *SU*(3) symmetry of quarks and gluons.

Despite being very successful, several issues remain un-answered in SM. The strong interaction only allows the existence of composite objects; free quarks and gluons have never been observed. This is called confinement, but it is far from being theoretically understood due to its non-perturbative nature. A detailed study of composite objects and their properties will shed light on this part of QCD. Furthermore, it is suspected that additional features or underlying symmetries beyond SM might not have been discovered yet, which is usually summarized by the term 'new physics'.

The hadron physics experiments in the 1970 's and 1980's concentrated on studying the spectroscopy of the newly discovered hadrons containing relatively heavy charm and bottom quarks, or tried to understand specific questions in the light-hadron sector with dedicated experiments. For the heavy-quark mesons, no clearly superfluous or ambiguous hadron states have been reported. The recent discoveries of 'exotic ' charmonium-like states have made the picture more complicated [9-12]. Furthermore, the situation has always been less straightforward for light mesons and baryons containing only light quarks [13]. Here, the high density of states and their broad widths often make the identification and interpretation of observed signals rather ambiguous. So far the unambiguous identification and understanding of gluonic hadrons is clearly missing. However, the self-interaction of gluons is central to QCD and leads to a flux tube of gluons binding the quarks together inside a hadron. Due to the self-interaction, bound states of pure gluons (named glueballs), or their mixing with conventional mesonic state, should exist as well as the so-called hybrids, where quarks and gluonic excitations contribute explicitly to the quantum numbers.

The energy regime in which BESIII is operating and the detector design allow a detailed study of charmonium and the light-quark region. Charmonium physics received a major renewal of interest in the 2000 's when many new, unexpected resonances, called *X*, *Y* and *Z* states [9-12], were discovered but could not be accommodated by the quark model. Many of those were found by Belle, BaBar, CDF, D0 and later the LHC experiments, but only BESIII is dedicated to the energy region where most of these states appear. It is therefore not surprising that detailed studies with a much higher statistics can only be performed at BESIII. Nowadays, BESIII is one of the main contributors to the understanding of the *XYZ* states. At the same time, the high production cross-section of charmonia at BEPCII together with a modern, almost hermetic detector for charged and neutral particles, allows also high-precision studies of light-quark hadrons in the decay of charmonia. Since this decay into light quarks proceeds via gluons, it is likely that the desired studies of gluonic excitations may be performed at BESIII, as is shown in this White Paper.

Despite the discovery of the charm quark more than 40 years ago, many questions about charmed particles still remain unsolved [9-12]. An upgraded BEPCII and BESIII can make key contributions to the lepton flavor universality, unitarity of the Cabibbo-Kobayashi-Maskawa (CKM) matrix, validity of lattice QCD (LQCD), as well as theories of decay constants and form

factors, by studying the leptonic and semileptonic decays of charmed particles. These studies can give insight into the applicability of QCD in low-energy nonperturbative context and can greatly expand our knowledge of charmed baryon properties. Open questions include the missing Λ_c decay modes (*e.g.* those with as yet undetected neutral or excited final-state baryons) and baryon electromagnetic structure.

1.2 The BESIII detector and its upgrades

The BESIII detector and BEPCII accelerator represent major upgrades over the previous version of BES [14, 15] and BEPC [16]; the facility is used for studies of hadron physics and τ-charm physics. The BEPCII collider, installed in the same tunnel as BEPC, is a double-ring multi-bunch collider with a design luminosity of 1×10^{33} cm^{-2}s^{-1} optimized at a center-of-mass (cms) energy of 2×1.89 GeV, an increase of a factor of 100 over its predecessor. The design luminosity was reached in 2016, setting a new world record for the accelerator in this energy regime [17].

The BESIII detector is designed to fulfill the physics requirements and the technical requirements for a high luminosity multi-bunch collider. Detailed description of the BESIII detector can be found in Ref. [2]. Figure 1.1 shows a schematic view of the BESIII detector, which covers 93% of the 4π solid angle. It consists of the following components:

- Helium-gas based drift chamber (MDC) with a single wire resolution that is better than 120 μm and a dE/dx resolution better than 6%. The momentum resolution in the 1.0 T magnetic field is better than 0.5% for charged tracks with a momentum of 1 GeV/c.
- CsI(Tl) crystal calorimeter with an energy resolution that is better than 2.5% and position resolution better than 6 mm for 1 GeV electrons and gammas.
- Time-of-Flight (TOF) system with an intrinsic timing resolution of 68 ps in the barrel part and 110 ps in the end-cap part.
- Super-conducting solenoid magnet with a central field of 1.0 Tesla.
- 9-layer RPC-based muon chamber system with a spatial resolution that is better than 2 cm.

Details of each sub-detector and their performance, together with the trigger system, are discussed in Ref. [2].

The BESIII detector has been operating since 2009, and BEPCII has delivered around 30 fb^{-1} of integrated luminosity at different cms energies. The experiment has received several upgrades, and new upgrades of both the detector and accelerator are being considered.

1.2.1 Upgrade of ETOF

In order to improve the capability for particle identification of the BESIII experiment, the end-cap time-of-flight (ETOF) detector was upgraded with the multi-gap resistive plate chamber (MRPC) technology in 2015 [18]. MRPC is a new type of gaseous detector that has been successfully used as TOF detector in several experiments. The new ETOF system of BESIII consists of two end-caps; each end-cap station has 36 trapezoidal shaped MRPC modules arranged in circular double layers as shown in Figs. 1.2 and 1.3. Each MRPC is divided into 12 readout strips which are read out from both ends in order to improve the timing resolution. The readout electronics system of MRPC detectors consists of FEE boards, time-to-digital conversion modules, calibration-threshold-test-power board, fast control module and a clock module in NIM crates that communicates with and is controlled by the data acquisition system. A multi-peak

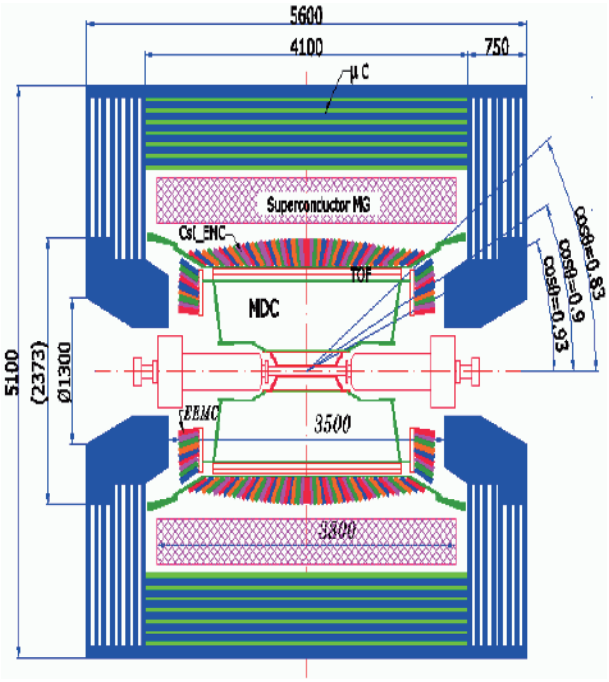

Fig. 1.1. (color online) An overview of the BESIII Detector.

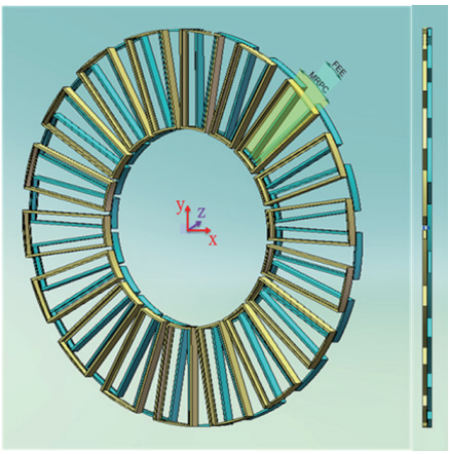

Fig. 1.2. (color online) Schematic drawing of MRPC ETOF at BESIII.

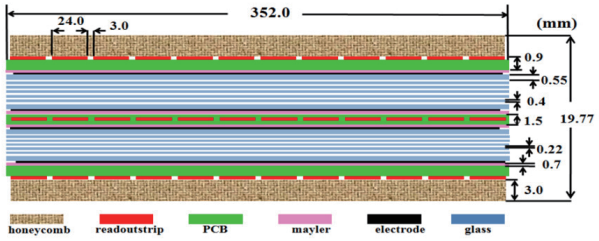

Fig. 1.3. (color online) The cross-sectional view of the MRPC module along its length.

phenomenon in the time-over-threshold distribution was observed, and the reflection of the inductive signal at the ends of the strip is the main contribution. An empirical calibration function based on the analysis of the correlation of raw measured time, time-over-threshold and extrapolated hit position of the charged particle, is implemented using the real data for Bhabha events. Performance checks show that the overall time resolution for pions with a momentum around 0.8 GeV/c is about 65 ps, which is better than the original design goal.

1.2.2 Upgrade of Inner MDC with a CGEM inner tracker

MDC is the main tracker of BESIII with the capability of accurate measurements of the position and momentum of charged particles produced in e^+e^- collisions, as well as charged particles identification by measuring dE/dx. MDC is a low-mass cylindrical wire chamber with small-cell geometry, using helium-based gas and operating in a 1 T magnetic field. It consists of an inner chamber (8 layers) and an outer chamber (35 layers), which are joined together at the endplates and share a common gas volume. After running since 2009, MDC is suffering from ageing due to beam-induced background with a hit rate up to 2 kHz/cm^2 [19], which has caused the cell gains of the inner chamber to drop dramatically (about 39% drop for the first layer cells in 2017 as shown in Fig. 1.4), and has furthermore led to a degradation of the spatial resolution and reconstruction efficiency. Because of the

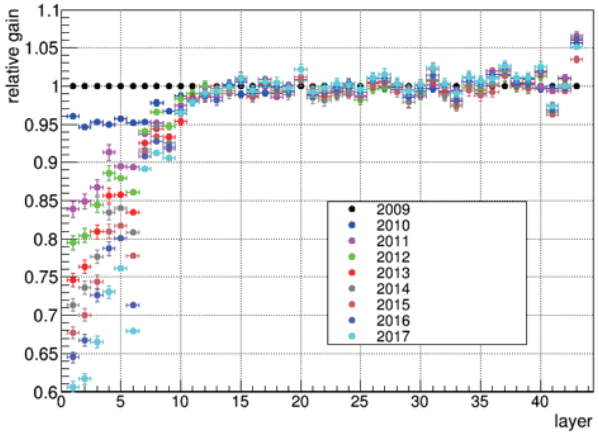

Fig. 1.4. (color online) Relative gain decrease of the cells in the MDC layers for each year of operation.

radiation damage of the inner chamber, a cylindrical gas electron multiplier (CGEM) has been selected as one of the options for the upgrade, due to its attractive features such as high counting rate capability and low sensitivity to ageing. The CGEM inner tracker (CGEM-IT) project deploys a series of innovations and special attributes in order to cope with the requirements of BESIII, as listed in Table 1.1.

Table 1.1. List of requirements for the new inner tracker.

Value	Requirements
σ_{xy}	$\leqslant$130 μm
σ_z	$\leqslant$1 mm
dp/p for 1 GeV/c	0.5%
Material budget	$\leqslant$1.5% X_0
Angular Coverage	93%×4π
Hit Rate	10^4 Hz/cm^2
Minimum Radius	65.5 mm
Maximum Radius	180.7 mm

CGEM-IT consists of three layers of triple cylindrical GEM [20], shown in Fig. 1.5. Each layer is assembled with five cylindrical structures: one cathode, three GEMs and the anode readout (see Fig. 1.5) [21]. The GEMs and electrode foils are produced in planes and then shaped as cylinders. The assembly is performed inside a vertical inserting machine. To minimize the material budget, there are no support frames inside the active area, and the GEM foils are mechanically stretched as they are glued to Permaglass rings at their ends. The Permaglass rings are used only outside the active area and operate as gas sealing structure and gap spacers. A sandwich of PMI foam, called Rohacell, and kapton is used to provide mechanical rigidity to the anode and cathode electrodes. Rohacell is a very light material that limits the material budget to 0.3% of the radiation length (X_0) per layer.

The readout anode circuit is manufactured with a 5 μm copper clad, 50 μm thick polyimide substrate. Two foils with copper segmented strips are used to provide two-dimensional readout. The strip pitch is 650 μm, with

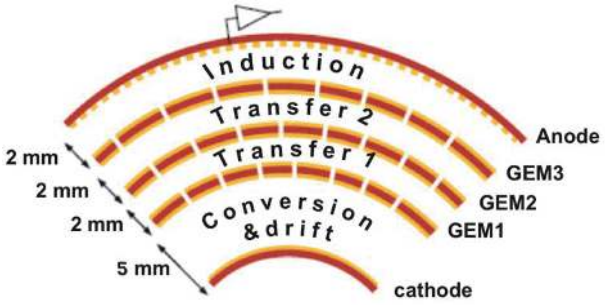

Fig. 1.5. (color online) Cross-section of the triple GEM detector used in BESIII CGEM-IT.

570 μm wide X-strips parallel to the CGEM axis providing the $r-\phi$ coordinates. The V-strips, having a stereo angle with respect to the X-strips, are 130 μm wide and together with the other view, give the z coordinate. The stereo angle depends on the layer geometry. A jagged-strip layout is used to reduce the inter-strip capacitance up to 30%. An innovative readout based on analogue information and data-pushing architecture has been developed. A dedicated ASIC has been developed to provide time and charge information from each strip.

In order to verify that CGEM-IT can reach the required performance, an extensive series of beam tests has been conducted in the last few years as part of the test beam activities of the RD51 Collaboration at CERN. The tests were performed both of the 10×10 cm^2 planar GEM chambers and of the cylindrical prototype with the dimension of the second layer of the final CGEM-IT [22]. All tests were performed in the H4 line of the SPS, in the CERN North Area. Since CGEM-IT will operate in a magnetic field, all test chambers were placed inside Goliath, a dipole magnet that can reach up to 1.5 T with both polarities. Pion and muon beams with a momentum of 150 GeV/c were used. Two scintillators were placed upstream and downstream of the magnet and operated as a trigger. A typical setup using the cylindrical prototype is shown in Fig. 1.6.

The performance of the planar GEM chambers in a magnetic field was studied with the charge centroid method. The presence of an external magnetic field induces a deformation of the avalanche shape at the anode due to the Lorentz force: the performance of the charge centroid method degrades almost linearly with the magnetic field strength, as shown in Fig. 1.7. It is still possible to improve the performance by a proper optimization of the drift field, as shown in Fig. 1.8. With the proper choice of the gas mixture (Ar/iC$_4$H$_{10}$(90/10)) and drift field (2.5 kV/cm), it is possible to achieve a resolution of 190 μm in a 1 T magnetic field.

μ-TPC is another available method for track reconstruction. It is an innovative approach that exploits the

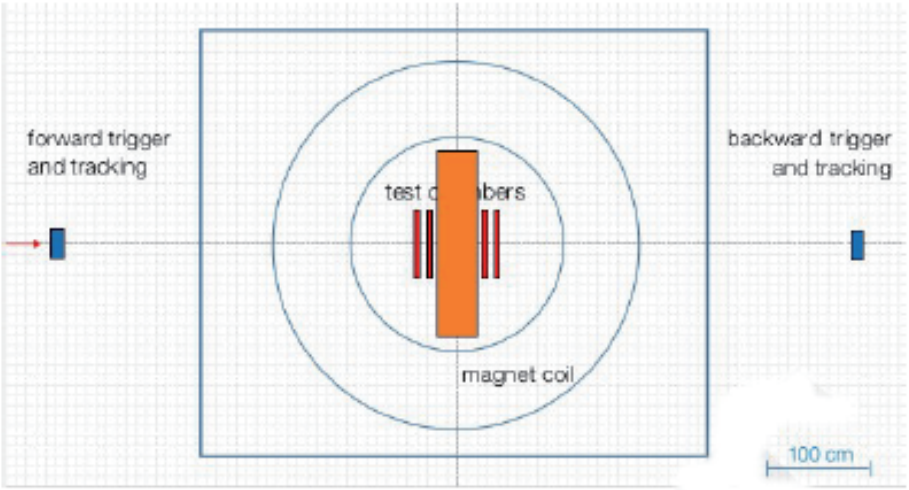

Fig. 1.6. (color online) Sketch of the setup of the CGEM test beam.

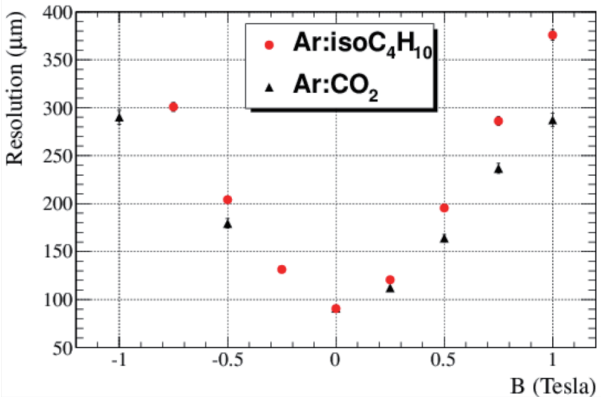

Fig. 1.7. (color online) Resolution as a function of the magnetic field strength for Ar/iC$_4$H$_{10}$(90/10) and Ar/CO$_2$ (70/30).

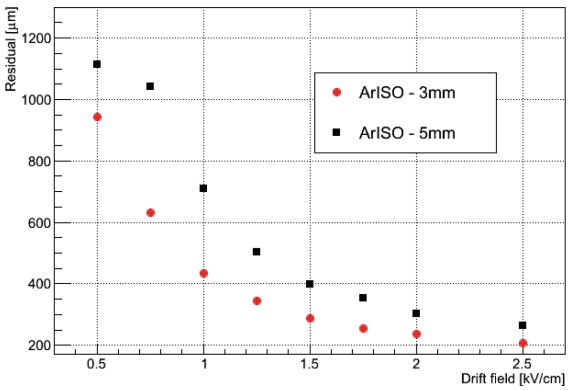

Fig. 1.8. (color online) Resolution as a function of drift field in the 1 T magnetic field for two drift gaps: 3 mm drift gap and 5 mm drift gap.

drift gap of a few millimeters as a Time Projection Chamber. Indeed, the time of arrival of the induced charge on the strip can be used to reconstruct the first ionization position in the drift gap, and thus improve the spatial resolution. The μ-TPC method can improve and overcome the limits of the charge centroid method, resulting in a spatial resolution lower than 200 μm for a large angle interval, as shown in Fig. 1.9. Further studies are ongoing. By merging the two methods it will be possible for the spatial resolution of CGEM-IT to satisfy the requirements of BESIII.

After the completion of CGEM-IT, a long term cosmic-ray test will be performed to evaluate the performance of the whole CGEM-IT before the replacement of the inner chamber of MDC.

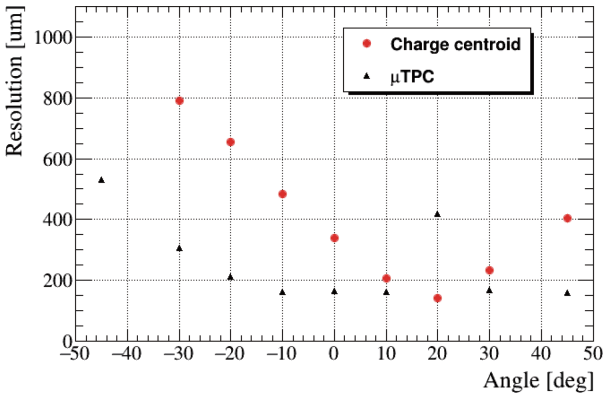

Fig. 1.9. (color online) Spatial resolution of the charge centroid and μ-TPC methods as a function of the incident angle of the track in the 1 T magnetic field.

1.2.3 Upgrade of Inner Chamber with an improved inner MDC

In addition to the construction of CGEM-IT, an improved inner MDC has been built that can replace the aged inner part of the MDC if needed [23].

The new inner MDC is designed with multi-stepped end-plates. Each step contains one sense-wire layer and one field-wire layer, which can shorten the wire length which exceeds the effective detection sold angle, and minimize the ineffective area in the very forward and backward region, thus reducing the background event rate of all cells, as shown in Fig. 1.10. The maximum reduction of the rate of background events is more than 30% for the first layer cells. With this design, the new inner MDC is expected to have a longer lifetime and improved performance due to the lower occupancy.

The new inner MDC consists of two multi-stepped endplates and an inner carbon fiber cylinder. The length of the new inner chamber is 1092 mm, and the radial extent is from 59 mm to 183.5 mm, including 8 stereo sense wire layers, comprising 484 cells in total. Similar to the old chamber, the drift cells of the new chamber have a

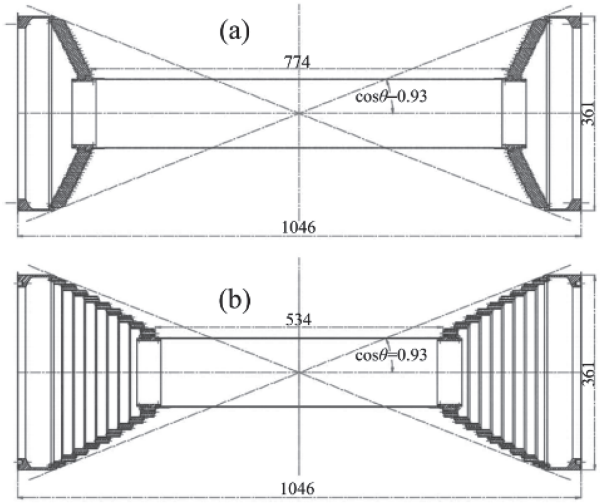

Fig. 1.10. Overview of the mechanical structure of the inner MDC. (a) The old inner chamber. (b) The new inner chamber.

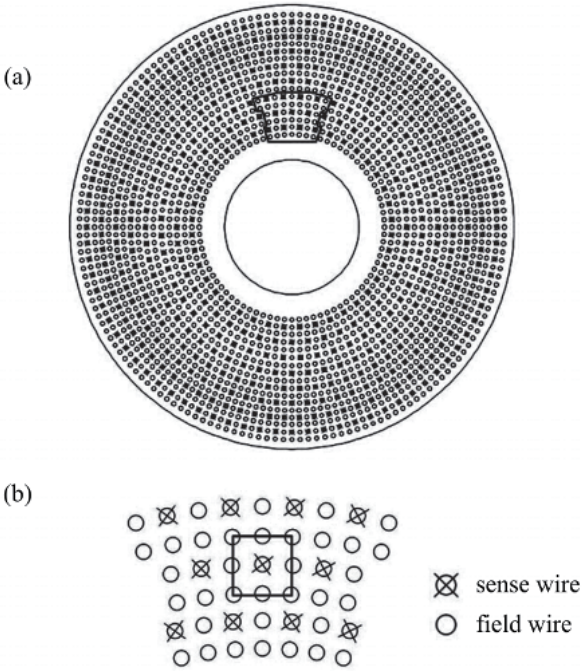

Fig. 1.11. End view of the new inner chamber and the layout of the cells. (a) End view of the new inner chamber. (b) The drift cells of the chamber.

nearly square shape, as shown in Fig. 1.11. The size of each cell is about 12 mm×12 mm with a sense wire located in the center, surrounded by eight field wires. The sense wires are 25 μm gold-plated tungsten wires, while the field wires are 110 μm gold-plated aluminum wires.

For the construction of the new inner chamber, two aluminum endplates were manufactured with an eight-step structure for each one. A total of 2096 wire holes with a diameter of 3.2 mm were drilled in each endplate

with the mean tolerance of 14 μm. A carbon fiber inner cylinder with a thickness of 1.0 mm, was covered with two layers of 100 μm thick aluminum foils on its inner and outer surfaces for electromagnetic shielding. The endplates and the cylinder were assembled with a precision better than 30 μm. Wire stringing was performed after the mechanical structure was assembled. Good quality of wire stringing was achieved by monitoring the wire tension and leakage current during the stringing. The non-uniformity of wire tension was less than 10%, and the leakage current was lower than 2 nA for each wire.

After the completion of the construction of the new chamber, a cosmic-ray test without magnetic field was carried out to evaluate its performance, shown in Fig. 1.12. The results of the cosmic-ray test showed that the new inner chamber achieves a spatial resolution of 127 μm and a dE/dx resolution of 6.4%, shown in Fig. 1.13 and Fig. 1.14, which satisfy the design specifications. These measurements verified the successful construction of the new chamber. The new inner chamber is now ready to be used if needed.

A decision on whether to install CGEM or the new inner MDC will be made according to the results of their beam and cosmic-ray tests.

Fig. 1.12. (color online) The cosmic-ray test of the new inner MDC.

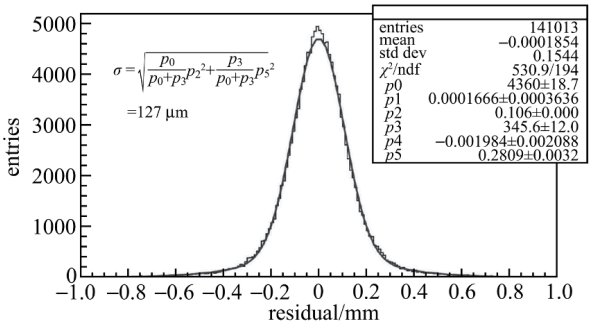

Fig. 1.13. Residual distribution of the new inner MDC showing the results of a fit with a double Gaussian function.

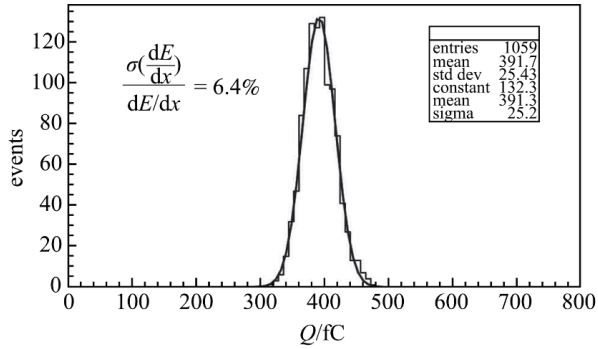

Fig. 1.14. The dE/dx resolution of the new inner MDC showing the results of a fit with a single Gaussian function.

1.3 BEPCII upgrades

BEPCII delivered its first physics data in 2009 at the $\psi(3686)$ resonance. Since then, BESIII has collected about 30 fb^{-1} of integrated luminosity at different energies, from 2.0 to 4.6 GeV. By using these data samples, the BESIII collaboration has published more than 270 papers, which have made significant contributions to hadron spectroscopy, tests of various aspects of QCD, charmed hadron decays, precision tests of SM, probes of new physics beyond SM, as well as τ mass measurement. Nowadays, the BESIII experiment plays a leading role in the study of the τ-charm energy region.

During the past 10 years of successful running, a better understanding of the machine was achieved. With the increasing physics interest, two upgrade plans of BEPCII were proposed and approved. The first one is to increase the maximum beam energy to 2.45 GeV, to expand the energy territory. The second is the top-up injection to increase the data taking efficiency. The activities related to these two upgrades began in 2017.

Before 2019, the beam energy of BEPCII ranged from 1.0 to 2.3 GeV. In order to extend the physics potential of BESIII, an upgrade project to increase the beam energy to 2.45 GeV was initiated. In order to achieve this goal, some hardware modifications were necessary, including the power supplies of the dipole magnets, power supplies of the special magnets in the interaction region, and the septum magnet and its water cooling system. These hardware modifications were completed during the summer shutdown in 2019, while the commissioning will be finished by the end of 2019. However, it is expected that when the machine is running in the high energy region above 1.89 GeV, the beam current will decrease due to the limitations related to the radio frequency (RF) power and difficulties in controlling the bunch length and emittance. Hence, the peak luminosity decreases when the beam energy is increased, as shown in Fig. 1.15. In the future, it would be interesting to investigate the possibilities of a slight increase of the beam energy to 2.5 GeV and

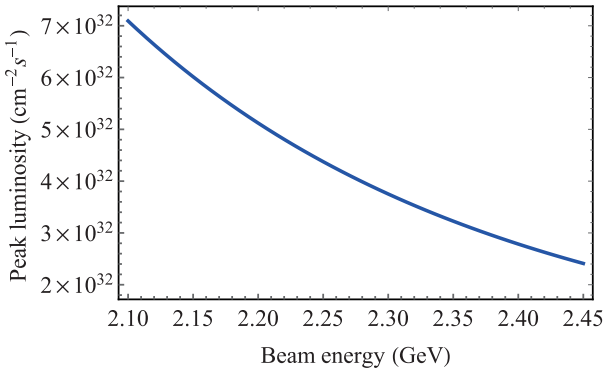

Fig. 1.15. (color online) The estimated peak luminosity of BEPCII in the energy region above 2.1 GeV.

a slight decrease to 0.9 GeV, that are interesting for the studies of Ξ_c and nucleon production, respectively.

The top-up injection is a highly efficient operation scheme for the accelerator [24], which provides a nearly constant beam current. As there is no stop for beam refilling, the integrated luminosity can be increased by 20% to 30% for long data taking runs. The BEPCII upgrade of the top-up injection for the collision mode has started in September 2017. In order to obtain a stable online luminosity, the beam current fluctuation is controlled within 1.5% with one e^+ injection and two e^- injections every 90 seconds, so that the variation of the instantaneous luminosity is less than 3% of its nominal value. The injection rates of the e^+ and e^- bunches must be higher than 60 mA/min and 180 mA/min, respectively. The commissioning of the top-up injection began after the summer shutdown in 2019 and will be finished by the end of the year.

There are also discussions on further machine luminosity upgrades. The recently proposed crab-waist collision scheme [25] is believed to be essential for the luminosity challenge of the next-generation high luminosity e^+e^- colliders. The possibility of a crab-waist scheme at BEPCII has been considered since 2007. However, it was found impossible if only minor changes on the current design are allowed. A recent upgrade proposal of BEPCII based on the crab-waist scheme was discussed in detail in Ref. [26], which presents an upgrade project with a peak luminosity of 6.0×10^{33} cm^{-2}s^{-1}. This is 10 times higher than the achieved luminosity of BEPCII at the beam energy of 2.2 GeV. The crab-waist scheme with a large Piwinski angle is suggested to be adopted with modifications of the BEPCII parameters. The β functions at the interaction point are to be modified from 1.0 m/1.5 cm to 0.14 m/0.8 cm in the horizontal and vertical planes, respectively. The emittance is to be reduced from 140 nm to 50 nm with damping wigglers. Regarding this proposal, a detailed design of the crab-waist scheme has been studied, and many physical and technical issues were investigated, such as the injection, dynamic aperture, emittance coupling, high power RF, super-conducting quadrupoles/wigglers, strong crab sextupoles, etc. It was found that the crab-waist scheme is a complicated and time-consuming project which is not practical with the present BESIII detector.

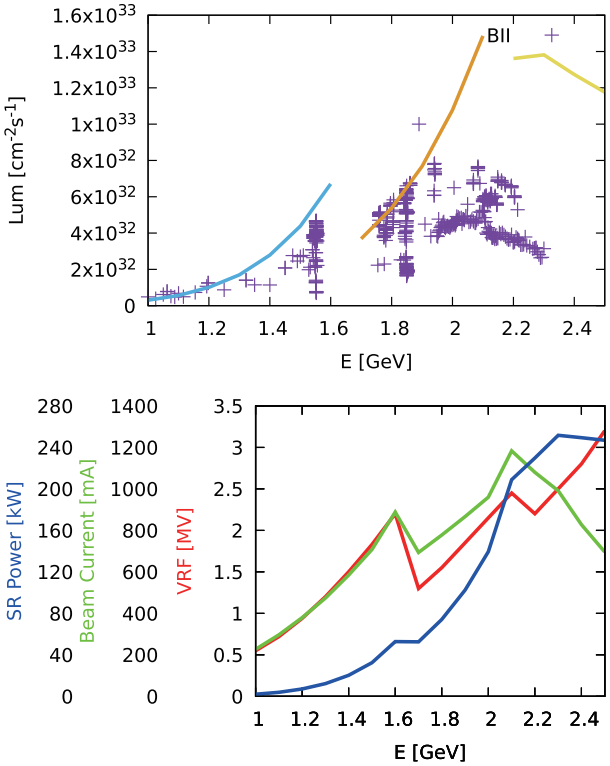

Fig. 1.16. (color online) Scenario of the BEPCII upgrade based on the increase of the beam current. The lines show the expected performance after the upgrade. The points in the upper plot show the achieved values of the current BEPCII.

Another, more economic, way to increase the luminosity is to augment the beam current, which could potentially provide a factor of 2 improvement of the peak luminosity. For this purpose, bunch lengthening needs to be suppressed, which requires higher RF voltage. The scenario of expected luminosity, beam current and SR power is shown in Fig. 1.16. The RF, cryogenic and feedback systems need to be upgraded to sustain higher beam currents. Nearly all photon absorbers along the ring and some vacuum chambers also need to be replaced in order to protect the machine from SR heating. The required budget is estimated at about 100-200 million CNY, and it will take about 3 years to prepare the equipment for the upgrade and 1 year for its installation and commissioning. The upgrade scheme with higher beam current is at present more realistic than the crab-waist scheme.

References

1 D. M. Asner *et al*., Int. J. Mod. Phys. A, **24**: S1 (2009)
2 M. Ablikim *et al*. (BESIII Collaboration), Nucl. Instrum. Methods Phys. Res., Sect. A, **614**: 345 (2010)
3 M. Ablikim *et al*. (BESIII Collaboration), Phys. Rev. Lett., **110**: 252001 (2013)
4 M. Ablikim *et al*. (BESIII Collaboration), Phys. Rev. Lett., **111**: 242001 (2013)
5 M. Ablikim *et al*. (BESIII Collaboration), Phys. Rev. Lett., **112**: 132001 (2014)
6 M. Ablikim *et al*. (BESIII Collaboration), Phys. Rev. Lett., **112**: 022001 (2014)
7 M. Ablikim *et al*. (BESIII Collaboration), Phys. Rev. Lett., **116**: 052001 (2016)
8 M. Ablikim *et al*. (BESIII Collaboration), Phys. Rev. Lett., **115**: 221805 (2015)
9 N. Brambilla, S. Eidelman, C. Hanhart, A. Nefediev, C. P. Shen, C. E. Thomas, A. Vairo and C. Z. Yuan, arXiv:1907.07583 [hep-ex]
10 F. K. Guo, C. Hanhart, U. G. Meißner, Q. Wang, Q. Zhao and B. S. Zou, Rev. Mod. Phys., **90**(1): 015004 (2018)
11 H. X. Chen, W. Chen, X. Liu, and S. L. Zhu, Phys. Rept., **639**: 1 (2016)
12 N. Brambilla *et al.*, Eur. Phys. J. C, **71**: 1534 (2011)
13 E. Klempt and A. Zaitsev, Phys. Rept., **454**: 1 (2007)
14 J. Z. Bai *et al*. (BES Collaboration), Nucl. Instrum. Methods Phys. Res., Sect. A, **344**: 319 (1994)
15 J. Z. Bai *et al*. (BES Collaboration), Nucl. Instrum. Methods Phys. Res., Sect. A, **458**: 627 (2001)
16 M. H. Ye and Z. P. Zheng, Int. J. Mod. Phys. A, **2**: 1707 (1987); S. X. Fang and S. Y. Chen, Part. Accel., **26**: 51 (1990)
17 https://phys.org/news/2016-04-bepcii-luminosity-world-11033cm2s.html
18 P. Cao *et al.*, Nucl. Instrum. Methods Phys. Res., Sect. A (in press), doi:10.1016/j.nima.2019.163053
19 M. Y. Dong *et al*., Chin. Phys. C, **40**: 016001 (2016)
20 F. Sauli, Nucl. Instrum. Methods Phys. Res., Sect. A, **386**: 531 (1997)
21 A. Amoroso *et al*., Nucl. Instrum. Methods Phys. Res., Sect. A, **824**: 515 (2016)
22 G. Mezzadri *et al*., PoS MPGD, **2017**: 048 (2019)
23 Y. J. Xie *et al*., Chin. Phys. C, **40**: 096003 (2016)
24 M. Aiba *et al*., Nucl. Instrum. Methods Phys. Res., Sect. A, **880**: 98 (2018)
25 P. Raimondi, talk presented at the 2nd Workshop on Super B factory, LNF-INFN, Frascati, 2006
26 A. Bogomyagkov, talk presented at the 14th International Workshop on Tau Lepton Physics, IHEP, Beijing, 2016

Chapter 2

Light Hadron Physics

2.1 Introduction

The generally accepted theory of the strong interaction, quantum chromodynamics (QCD), remains a challenging part of the Standard Model (SM) in the low- and medium-energy regime. In the high-energy regime, asymptotic freedom of the partons constituting hadrons allows systematic calculations in QCD using perturbation theory. In the low-energy regime where the energies are (much) smaller than a typical strong interaction scale, there is a well-established theoretical method, the chiral perturbation theory (ChPT). In the intermediate-energy regime, the non-Abelian character of QCD requires a non-perturbative approach, which must rely either on the lattice QCD (LQCD) or on the QCD-inspired models. Therefore, the study of light hadrons is central to the understanding of confinement physics.

Significant progress in the light-quark sector appeared in the last few years due to unprecedented high-statistics data sets from experiments at both electron and hadron machines. Due to the non-Abelian structure of the QCD bound states beyond the constituent quark degrees of freedom, multiquark states or states with gluonic degrees of freedom (hybrids, glueballs) are expected. Their unambiguous identification and systematic study would provide a validation of and valuable input to the quantitative understanding of QCD. Over the last decade, there have been several relevant reviews [1-6] of this subject, which cover in great detail both the meson spectroscopy and baryon spectroscopy.

Data with unprecedented statistical accuracy and clearly defined initial and final state properties resulted in significant advances in recent years, and offer great opportunities to investigate hadron spectroscopy at BESIII. The road map for the light hadron physics program at BESIII has already been defined, following the trajectory of endeavors over the last decades [7, 8]. In this document we reiterate the physics case on the basis of achieved results.

2.2 Meson spectroscopy and the search for QCD exotics

Confinement is a unique property of QCD. The quark model describes mesons as bound states of quarks and antiquarks. The LQCD and QCD-motivated models for hadrons, however, predict a richer spectrum of mesons that takes into account not only the quark degrees of freedom but also the gluonic degrees of freedom. The primary goal of the BESIII experiment is to search for and study those QCD exotics or states with a composition that is different from normal mesons and baryons. Understanding these states will provide critical information for the quantitative understanding of confinement.

2.2.1 Glueballs

The spectrum of glueballs is predicted by the quenched LQCD [9-11] with the lightest one having scalar quantum numbers 0^{++} and a mass between 1.5 GeV/c^2 and 1.7 GeV/c^2. The next-higher glueball states have non-exotic quantum numbers, 2^{++} (mass 2.3–2.4 GeV/c^2) and 0^{-+} (mass 2.3–2.6 GeV/c^2), and hence are mixed into the conventional meson spectrum and difficult to identify experimentally. This requires systematic studies to identify a glueball by searching for outnumbering of the conventional quark model states, and by comparing the properties of the candidates to the expected properties of glueballs and conventional mesons.

In a simple constituent gluon picture, these three states correspond to two-gluon systems in a relative S wave, with different combinations of helicities. Table 2.1 summarizes the quenched and unquenched lattice results for the masses of the lightest glueballs. The masses of scalar and tensor glueballs from the quenched LQCD are consistent with those obtained by the $N_f = 2$ [12] and $N_f = 2+1$ [13] unquenched LQCD.

Glueballs are expected to appear in so-called gluon-rich environments. The radiative decays of J/ψ meson provide such a gluon-rich environment and are therefore regarded as one of the most promising hunting grounds for glueballs. Recent LQCD calculations predict that the

Table 2.1. Glueball masses (in units of MeV/c^2) from the quenched [10, 11] and unquenched [12, 13] lattice QCD studies.

	m_π	$m_{0^{++}}$	$m_{2^{++}}$	$m_{0^{-+}}$
quenched Ref. [10]	–	1710(50)(80)	2390(30)(120)	2560(35)(120)
quenched Ref. [11]	–	1730(50)(80)	2400(25)(120)	2590(40)(130)
unquenched $N_f = 2$ [12]	938	1417(30)	2363(39)	2573(55)
	650	1498(58)	2384(67)	2585(65)
unquenched $N_f = 2+1$ [13]	360	1795(60)	2620(50)	–

partial width of J/ψ radiatively decaying into a pure gauge scalar glueball is 0.35(8) keV, which corresponds to a branching ratio of $3.8(9)\times10^{-3}$ [14]; the partial decay width of a tensor glueball is estimated to be 1.01(22)(10) keV, which corresponds to a large branching ratio $1.1(2)(1)\times10^{-2}$ [15]; the partial decay width of a pseudoscalar glueball is estimated to be 0.0215(74) keV, which corresponds to a branching ratio $2.31(80)\times10^{-4}$ [16]. With the unique advantage of a high-statistics J/ψ sample, a systematic research program of glueballs has been performed at BESIII. The pseudoscalar sector draws special attention due to the small number of expected resonances in the quark model. However, the experimental input is very limited and the hope is that BESIII will lead to significant improvements. In the scalar sector and tensor sector, a large number of resonances has been observed. However, the nature of these states is still controversial. The program at BESIII can provide crucial information to map out the scalar and tensor excitations.

Scalar mesons

A related review of the topic can be found in the section "Note on Scalar Mesons below 2 GeV" in PDG [17]. The most striking observation is that the $f_0(1370)$, $f_0(1500)$ and $f_0(1710)$ appear to be supernumerary. Many papers interpret the existence of these three scalars as a manifestation of the underlying light-quarkonium nonet and the lowest-mass scalar glueball.

Challenges in the interpretation of the scalar sector involve both experimental and theoretical efforts. The following key questions account for the major differences in the models of scalar mesons and need to be addressed in the future:

- Is the $f_0(1370)$ a true $q\bar{q}$ resonance or is it generated by the $\rho\rho$ molecular dynamics?
- Even though the supernumerary state is suggestive, the decay rates and production mechanisms are also needed to unravel the quark content of $f_0(1500)$ and $f_0(1710)$. In the partial wave analysis (PWA) of $J/\psi\to\gamma\eta\eta$ [18] and $J/\psi\to\gamma K_S K_S$ [19] at BESIII, the branching fractions of the $f_0(1710)$ are one order of magnitude larger than those of the $f_0(1500)$. With the new measurements from BESIII, the known branching fraction of $J/\psi\to\gamma f_0(1710)$ [5] is up to 1.7×10^{-3}, which is already comparable with the LQCD calculations of a scalar glueball ($3.8(9)\times10^{-3}$ [14]). The production property suggests that $f_0(1710)$ has a larger gluonic component than $f_0(1500)$. More precise measurements of the partial decay widths in the future will improve the understanding of the internal structure of these states. A significant property of glueball decays is their expected flavor symmetric coupling to final-state hadrons, even though some modifications from the phase space, glueball wave function and decay mechanism are expected.
- How many distinct resonances exist around 1.7 GeV/c^2? The $f_0(1710)$ and $f_0(1790)$ were observed at BES, and the $X(1810)$ was observed in $J/\psi\to\gamma\omega\phi$ [20].
- What is the nature of the $f_0(2100)$? Besides the $f_0(1710)$, large production of scalars around 2.1 GeV/c^2 was also observed in $J/\psi\to\gamma\eta\eta$ [18], $J/\psi\to\gamma\pi^0\pi^0$ [21] and $J/\psi\to\gamma K_S K_S$ [19]. The pattern of production in the gluon-rich radiative J/ψ decays agrees well with that of the ground state glueball, and its first excitation is as predicted by LQCD. It is notable that the $f_0(2100)$ is also largely produced in $p\bar{p}$ annihilation. An additional way to unveil its nature is to measure the ratio of its decay modes into $\eta\eta'$ and $\eta'\eta'$. Furthermore, the number of existing scalars in the $f_0(2100)$ region needs clarification.

Tensor mesons

In the quark model, there are two quark configurations, the $^3P_2(L=1,S=1,J=2)$ and $^3F_2(L=3,S=1,J=2)$ nonets. Hence, the tensor sector is extremely busy and a large number of tensor states appear in PDG [5]. The three tensors $f_2(2010)$, $f_2(2300)$ and $f_2(2340)$ observed in $\pi^- p\to\phi\phi n$ [22] are also observed in $J/\psi\to\gamma\phi\phi$

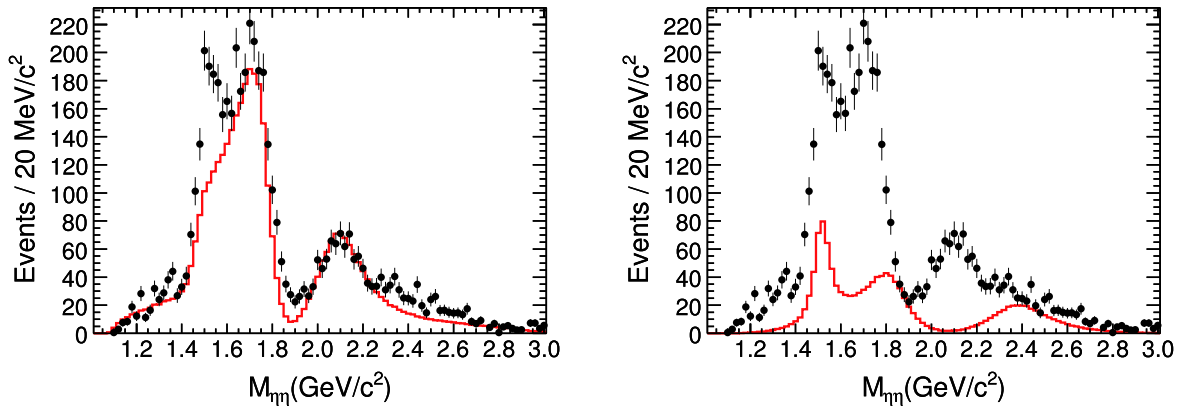

Fig. 2.1. (color online) Invariant mass distribution of $\eta\eta$ from $J/\psi\to\gamma\eta\eta$, and the projection of the PWA fit from BESIII: (a) the 0^+ component, (b) the 2^+ component [18]. Dots with error bars are the experimental data. Solid histograms are the projections of the PWA fit.

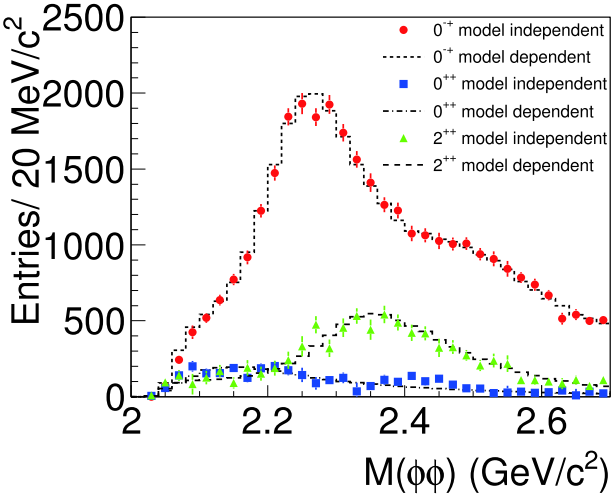

Fig. 2.2. (color online) Intensities of individual J^{PC} components from the model-independent fit of the mass distribution of $\phi\phi$ from $J/\psi \to \gamma\phi\phi$, compared with the projection of the model-dependent PWA fit from BESIII [23].

[23]. Figure 2.1 and 2.2 show the resulting PWA fit of the $\eta\eta$ and $\phi\phi$ invariant mass spectra. The large production rate of the $f_2(2340)$ in $J/\psi \to \gamma\phi\phi$ and $J/\psi \to \gamma\eta\eta$ [18] indicates that $f_2(2340)$ is a good candidate for a tensor glueball. Significant tensor contribution around 2.4 GeV/c^2 is also present in $J/\psi \to \gamma\pi^0\pi^0$ [21] and $J/\psi \to \gamma K_S K_S$ [19]. However, the measured production rate of $f_2(2370)$ appears to be substantially lower than the LQCD calculated value [15]. It is desirable to search for more decay modes to establish and characterize the lowest tensor glueball.

Pseudoscalar mesons

The $I = 0$ $J^{PC} = 0^{-+}$ ground states are η and the η'. Only radial excitations are expected in the quark model for the 0^{-+} states. The small number of expected pseudoscalars in the quark model provides a clean and promising environment for the search of glueballs.

A striking observation is that there are two pseudoscalar states near 1.4 GeV/c^2, the $\eta(1405)$ and the $\eta(1475)$, listed in PDG [5]. The $\eta(1405)$ as a supernumerary state was proposed as the ground state pseudoscalar glueball candidate. However, the extra state appears to be relatively far from the expected mass of the pseudoscalar glueball of 2 GeV/c^2. This is known as the long standing "E-ι puzzle" [24]. BESIII reported the first observation of the isospin-violating decay $\eta(1405) \to \pi^0 f_0(980)$ in $J/\psi \to \gamma 3\pi$ [25], together with an anomalous line shape of the $f_0(980)$, as shown in Fig. 2.3. The f_0 mass, deduced from the Breit-Wigner fit of the mass spectra, is slightly shifted compared to its nominal value, with a width of < 11.8 MeV (90% C.L.), much smaller than its nominal value. The observed isospin violation is (17.9 ± 4.2)%, too large to be explained by the $f_0(980)$-$a_0(980)$ mixing, also observed by BESIII [26, 27]. Based on this observation, Wu et al. [28] suggested that a triangular singularity mixing $\eta\pi\pi$ and $K^*\bar{K}$ could be large enough to account for the data. The splitting of $\eta(1405)$ and $\eta(1475)$ could also be due to this triangle anomaly.

It is also crucial to examine carefully the existence of the $\eta(1295)$ in order to nail down the first excitation of η. Alternatively, the $\eta(1295)$ could be explained as a misidentified $f_1(1285)$.

The $X(1835)$ observed in $J/\psi \to \gamma\eta'\pi^+\pi^-$, which will be discussed in Sec. 2.2.3, was determined to have the quantum numbers 0^{-+}. In the same reaction, two additional structures, the $X(2120)$ and the $X(2370)$, were observed. However, the spin-parity of these two new structures have not yet been determined. $X(2370)$ is also observed in $J/\psi \to \gamma\eta' K\bar{K}$. It is crucial to explore other decay modes of $X(2370)$ and establish its spin-parity.

Aside from the $\eta(2225)$, very little is known in the pseudoscalar sector above 2 GeV/c^2 where the lightest pseudoscalar glueball is expected based on the LQCD calculations. PWA of the decay $J/\psi \to \gamma\phi\phi$ [23] was performed in order to study the intermediate states. The most remarkable feature of the PWA results is that the 0^{-+} states are dominant. The existence of the $\eta(2225)$ was

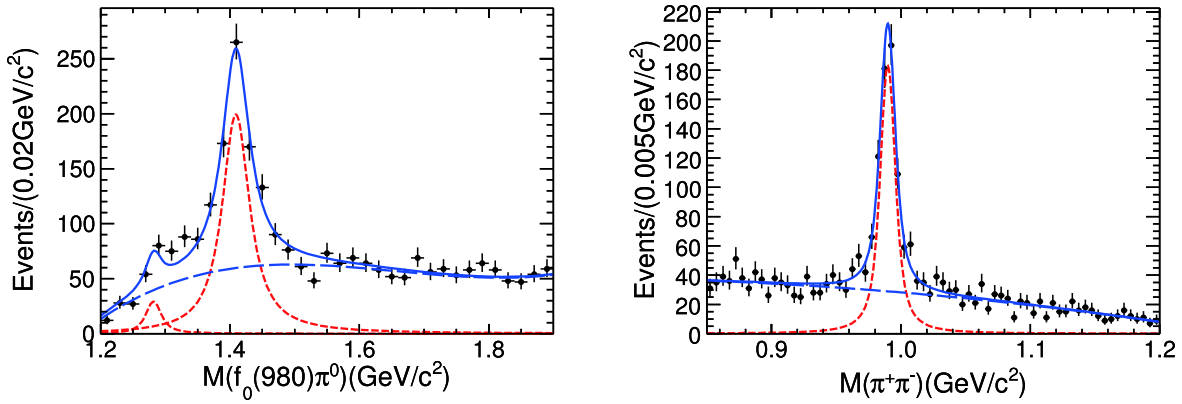

Fig. 2.3. (color online) (a) Invariant mass of $f_0(980)\pi^0$; (b) Invariant mass of $\pi^+\pi^-$ with the $\pi^+\pi^-\pi^0$ ($3\pi^0$) mass in the $\eta(1405)$ mass region, measured at BESIII [25].

confirmed and two additional pseudoscalar states, $\eta(2100)$ and $X(2500)$, were found.

Besides the radiative J/ψ decays, flavor filtering reactions could also play an important role in unraveling the quark content of the pseudoscalars (*e.g.* $J/\psi \to \gamma X$, $X \to \gamma V$ and $J/\psi \to VX$, where V stands for ρ, ω, ϕ, and X stands for the pseudoscalars). $\eta(1475) \to \gamma\phi$ and $X(1835) \to \gamma\phi$ were observed in the decay $J/\psi \to \gamma\gamma\phi$ at BESIII [29], which indicates that both $\eta(1475)$ and $X(1835)$ contain a sizeable $s\bar{s}$ component.

2.2.2 Hybrids

Since the expected quantum numbers of low-lying glueballs are not exotic, they should manifest themselves as additional states that cannot be accommodated within the $q\bar{q}$ nonets. Their unambiguous identification is complicated by the fact that they can mix when overlapping with $q\bar{q}$ states of the same quantum numbers. An easy way to avoid mixing with regular mesons are additional degrees of freedom leading to exotic quantum numbers. Such degrees of freedom could arise from explicit gluonic contributions. These particles carry a special name and are called hybrids. In many models, some of the hybrid mesons can have a unique signature, the already mentioned exotic (not allowed in a simple $q\bar{q}$ system) J^{PC} quantum numbers. This signature simplifies the spectroscopy of such exotic hybrid mesons because they do not mix with conventional $q\bar{q}$ states. LQCD calculations support the existence of exotic quantum number states within the meson spectrum, independent of specific models. As shown in Fig. 2.4 [30], LQCD calculations consistently show that the $J^{PC} = 1^{-+}$ nonet is the lightest hybrid.

Currently, there are three experimental candidates for a light 1^{-+} hybrid: the $\pi_1(1400)$ and the $\pi_1(1600)$, observed in diffractive reactions and $\bar{p}N$ annihilation, and the $\pi_1(2015)$, seen only in diffraction. The $\pi_1(1400)$ has only been observed in its decay into the $\pi\eta$ final state, and is generally considered too light to be a hybrid meson. Reviews [2, 4] provide a summary of the experimental studies.

An amplitude analysis of $\chi_{c1} \to \eta\pi^+\pi^-$ or $\chi_{c1} \to \eta'\pi^+\pi^-$ was performed at CLEO-c [31] and BESIII [32]. For these final states, the only allowed S-wave decay of χ_{c1} goes through the spin-exotic 1^{-+} wave, which then decays to $\eta(')\pi$. It turns out that a significant contribution of an exotic 1^{-+} wave is needed to describe the data in the $\eta'\pi^+\pi^-$ channel, but not in the $\eta\pi^+\pi^-$ channel.

While there is evidence for an isovector member of the $J^{PC} = 1^{-+}$ nonet, we also expect two isoscalar states (η_1 and η_1'), which are crucial to establish the nonet nature of π_1 states. However, there is still no experimental evidence for these two isoscalar states. The gluon-rich radiative J/ψ decays may provide an ideal laboratory for the search for such isoscalar 1^{-+} states. Model predictions of their decay modes are $f_1\eta$, $a_1\pi$ and $\eta\eta'$, etc. [33-36].

2.2.3 Multiquarks

An early quark model prediction was the existence of multiquark states, in particular the bound meson-antimeson molecular states. In the light-quark sector, the $f_0(980)$ and $a_0(980)$ are considered to be strong candidates for $K\bar{K}$ molecules. However, it is in general challenging to definitively identify a light multiquark state in an environment of many broad and often overlapping conventional states.

Two generic types of multiquark states have been of-

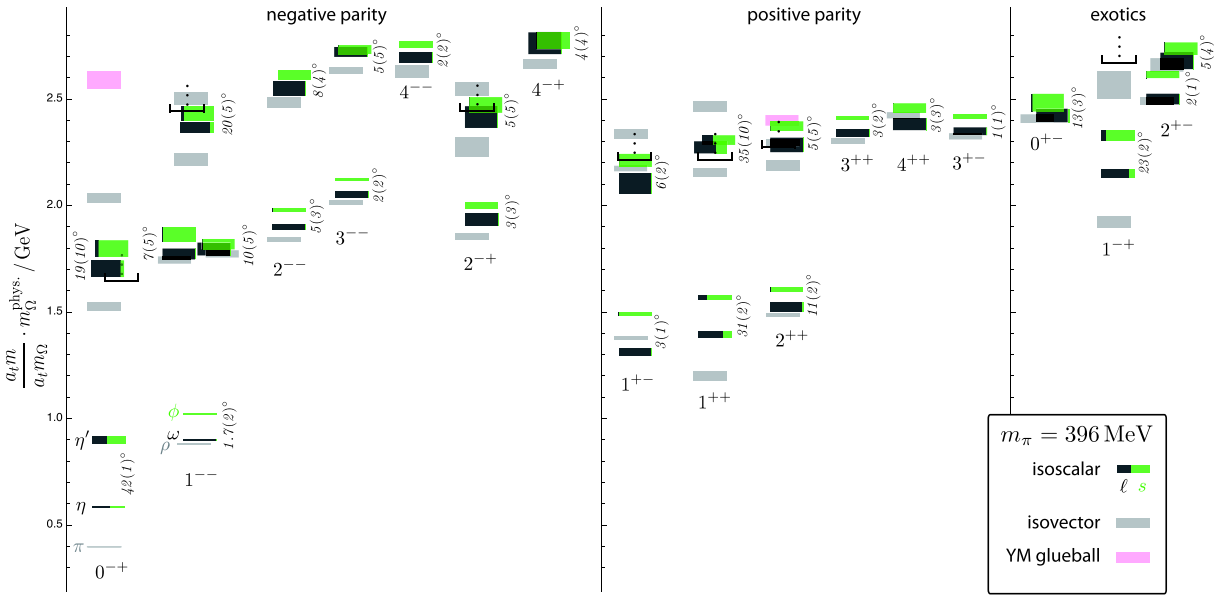

Fig. 2.4. (color online) Light-quark non-strange meson spectrum resulting from LQCD [30], sorted by the quantum numbers J^{PC}. Note that these results were obtained with an unphysical pion mass, $m_\pi = 396$ MeV/c^2.

ten discussed. Molecular state is a loosely bound state of a pair of mesons near threshold. Tetraquarks are tightly bound diquark-antidiquark states. A prediction of the tetraquark models is that they come in flavor multiplets. In addition, an enhancement may also arise from the threshold effects due to re-scattering of the two outgoing mesons close to the threshold. This could result in mass shifts due to the thresholds. Couple-channel effects result in mixing of two-meson states with $q\bar{q}$ resonances.

In general, a multiquark state is expected to be broad since it can easily decay into mesons and/or baryons when its mass is above the mass threshold for producing these hadrons. Multiquark states may only be experimentally observed when their masses are near these mass thresholds, either below or just above them. Otherwise, the multiquark states might be too wide to be experimentally distinguished from non-resonant background.

After the discoveries of $a_0(980)$ and $f_0(980)$ several decades ago, explanations of the nature of these two light scalar mesons are still controversial. These two states, with similar masses but different decay modes and isospins, are difficult to accommodate in the traditional quark-antiquark model, and many alternative formulations have been proposed to explain their internal structure, including tetra-quarks [37-41], $K\bar{K}$ molecule [42], or quark-antiquark gluon hybrid [43]. Further insights into $a_0(980)$ and $f_0(980)$ are expected from their mixing [44]. The mixing mechanism in the system of $a_0(980)-f_0(980)$ is considered to be a sensitive probe to clarify the nature of these two mesons. In particular, the leading contribution to the isospin-violating mixing transition amplitudes for $f_0(980)\to a_0^0(980)$ and $a_0^0(980)\to f_0(980)$, was shown to be dominated by the difference of the unitarity cut, which arises from the mass difference between the charged and neutral $K\bar{K}$ pairs. As a consequence, a narrow peak of about 8 MeV/c^2 is predicted between the charged and neutral $K\bar{K}$ thresholds. The corresponding signal is predicted in the isospin-violating processes of $J/\psi\to\phi a_0^0(980)$ [45, 46] and $\chi_{c1}\to\pi^0 f_0(980)$ [47]. The signals of $f_0(980)\to a_0^0(980)$ and $a_0^0(980)\to f_0(980)$ mixing were first observed in $J/\psi\to\phi f_0(980)\to\phi a_0^0(980)\to\phi\eta\pi^0$ and $\chi_{c1}\to\pi^0 a_0^0(980)\to\pi^0 f_0(980)\to\pi^0\pi^+\pi^-$ at BESIII [26, 27]. The statistical significance of the signal versus the values of $g_{a_0K^+K^-}$ and $g_{f_0K^+K^-}$ is shown in Fig. 2.5. The regions with higher statistical significance indicate larger probability for the emergence of the two coupling constants. The direct measurement of $a_0(980)$–$f_0(980)$ mixing is a sensitive probe for the internal structure of these ground state scalars and sheds important light on their nature. The new results from BESIII provide critical constraints for the development of theoretical models for $a_0(980)$ and $f_0(980)$.

The state $X(1835)$ was first observed by the BES experiment as a peak in $J/\psi\to\gamma\eta'\pi^+\pi^-$ decays [48]. This

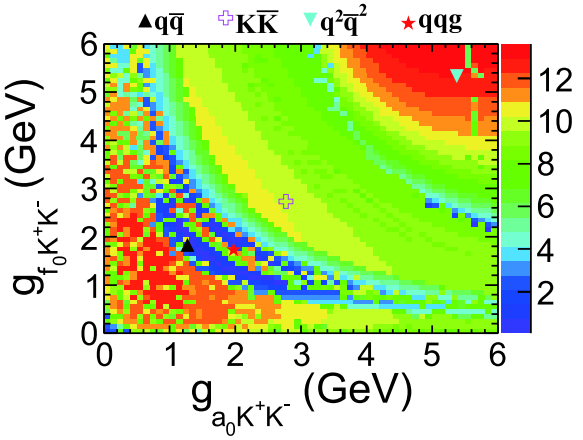

Fig. 2.5. (color online) The statistical significance of the signal scanned in the two-dimensional space of $g_{a_0K^+K^-}$ and $g_{f_0K^+K^-}$. The regions with higher statistical significance indicate larger probability for the emergence of the two coupling constants. The markers indicate predictions from various illustrative theoretical models.

observation was later confirmed by BESIII [49]. The $X(1835)$ was also observed in the $\eta K_S^0 K_S^0$ channel, where its spin-parity was determined to be $J^P=0^-$ by PWA [50]. An anomalously strong enhancement at the proton-antiproton ($p\bar{p}$) mass threshold, dubbed $X(p\bar{p})$, was first observed by BES in $J/\psi\to\gamma p\bar{p}$ decays [51]; this observation was confirmed by BESIII [52] and CLEO [53]. This enhancement was subsequently determined to have the spin-parity $J^P=0^-$ by BESIII [54]. Using a high-statistics sample of J/ψ events, BESIII studied the $J/\psi\to\gamma\eta'\pi^+\pi^-$ process and observed a significant change in the slope of the $\eta'\pi^+\pi^-$ invariant mass distribution at the proton-antiproton ($p\bar{p}$) mass threshold [55]. Two models are used to characterize the $\eta'\pi^+\pi^-$ line shape around 1.85 GeV/c^2: the first, which explicitly incorporates the opening of a decay threshold in the mass spectrum (Flatté formula) (Fig. 2.6 (a)), and the other, which is the coherent sum of two resonant amplitudes (Fig. 2.6 (b)). Both fits show almost equally good agreement with the data, and suggest the existence of either a broad state with strong couplings to the final state $p\bar{p}$, or a narrow state just below the $p\bar{p}$ mass threshold. The goodness-of-fit are equivalent for both fits. The first supports the existence of a $p\bar{p}$ molecule-like state, and the other a bound state with a significance greater than 7σ. Further study of the fine line shape of $X(1835)$ in other decay modes will provide conclusive information about the nature of the state.

An analysis of $J/\psi\to pK^-\bar{\Lambda}$ was performed at BES [56]. Enhancements both at the $p\bar{\Lambda}$ and the $K^-\bar{\Lambda}$ mass thresholds are observed. Further investigations in other decay modes and production mechanisms are needed to clarify the nature of these structures.

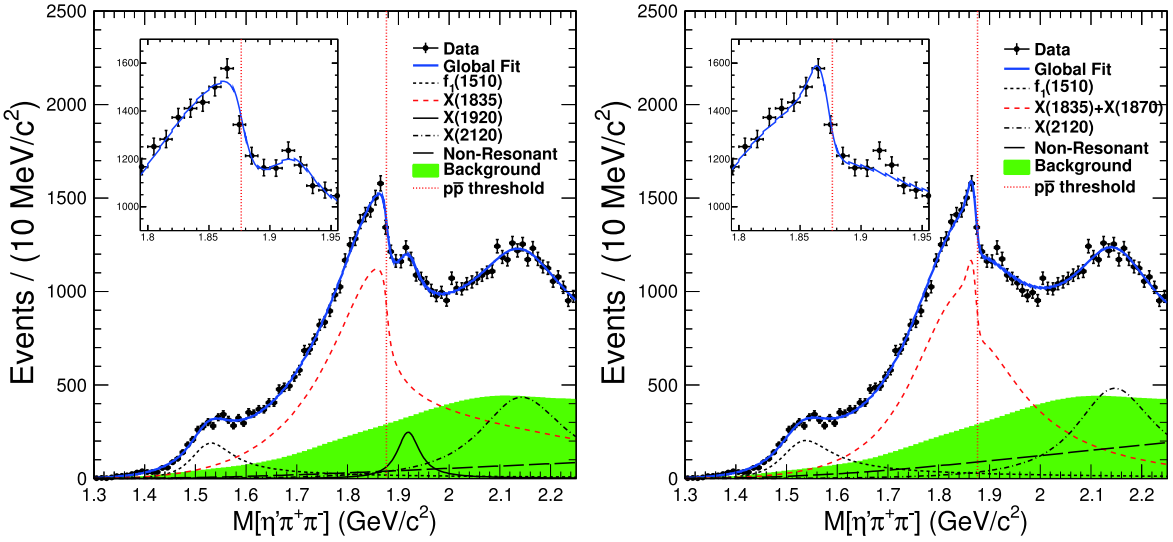

Fig. 2.6. (color online) An anomalous line shape of the $\eta'\pi^+\pi^-$ mass spectrum near the $p\bar{p}$ mass threshold in $J/\psi \to \gamma\eta'\pi^+\pi^-$. (a) shows the fit results with a Flatté formula, and (b) shows the fit results with the coherent sum of two Breit-Wigner amplitudes.

2.3 Baryon spectroscopy

Baryons are the basic building blocks of our world. Since baryons are the simplest systems in which all three QCD colors neutralize into colorless objects, understanding the baryon structure is absolutely necessary before we can claim to really understand QCD. Given many recent experimental results, our present understanding of baryon spectroscopy is clearly incomplete. Many fundamental issues in baryon spectroscopy are still not well understood [57, 58]. Most important among them is the problem of missing resonances. In quark models based on approximate flavor $SU(3)$ symmetry, it is expected that resonances form multiplets. Many excited states were predicted which have not been observed (for a review, see Ref. [59]). More recently, LQCD calculations [60] have also predicted a similar pattern as the quark models. The possibility of new, as yet unappreciated, effective symmetries could be addressed with the accumulation of more data. The new symmetries may not have obvious relation with QCD, just like nuclear shell model and collective motion model.

In addition to baryons made of u and d quarks, the search for hyperon resonances remains an important challenge. Some of the lowest excitation resonances have not yet been experimentally established, which are necessary to establish the spectral pattern of hyperon resonances.

Charmonium decays provide an excellent place to study excited nucleons and hyperons – N^*, Λ^*, Σ^* and Ξ^* resonances [61]. The corresponding Feynman graph for the production of these excited nucleons and hyperons is shown in Fig. 2.7 where ψ represents charmonium.

Complementary to other facilities, the baryon program at BESIII has several advantages [62]. For instance,

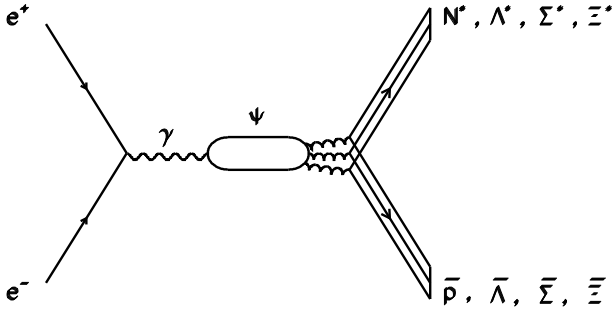

Fig. 2.7. $\bar{p}N^*$, $\bar{\Lambda}\Lambda^*$, $\bar{\Sigma}\Sigma^*$ and $\bar{\Xi}\Xi^*$ production in e^+e^- collisions through ψ meson.

πN and $\pi\pi N$ systems from the $\psi \to \bar{N}N\pi$ and $\bar{N}N\pi\pi$ processes have an isospin of 1/2 due to isospin conservation. ψ mesons decay to baryon-antibaryon pairs through three or more gluons providing a favorable place for producing hybrid ($qqqg$) baryons, and for searching for some "missing" N^* resonances which have weak coupling to both πN and γN, but stronger coupling to g^3N. The phase space for the $\psi(3686)$ decays is larger than for J/ψ decays, thus having more potential for investigating higher excitations of baryons and hyperons. In PWA of $\psi(3686) \to p\bar{p}\pi^0$ [63], two new N^* resonances, $N(2300)$ and $N(2570)$, have been observed with the J^P assignments of $1/2^+$ and $5/2^-$, respectively.

Besides the high-statistics data samples of charmonium events, the large number of Λ_c hadronic decays collected at BESIII provide a novel laboratory for studying light baryon excitations.

2.4 BESIII amplitude analysis

The basic task of an experimental study of hadron spectroscopy is to systematically map out all the reson-

ances and determine their properties like the mass, width, spin-parity, as well as partial decay widths, with high sensitivity and accuracy. Extracting the properties of resonances from the experimental data is, however, far from straightforward. Resonances tend to be broad and plentiful, leading to intricate interference patterns, or they are buried in a background of identical or other waves. The key to success lies in high statistical precision complemented with sophisticated analysis methods. PWA or amplitude analysis techniques are the state-of-the-art methods to disentangle contributions from individual, even small resonances, and to determine their quantum numbers. Multiparticle decays are usually modeled using the phenomenological approach of the isobar model, which describes a multiparticle final state by the sequential two-body decay into intermediate resonances (isobars) that eventually decay into the final state observed in the experiment. Event-based fits allow to take into account the full correlation between the final-state particles.

Facing the extremely high statistics at BESIII, the PWA fits will be computationally very expensive. The pioneer approach of harnessing GPU parallel acceleration in PWA was performed in the framework of BESIII [64]. The GPUPWA framework [65] provides facilities for amplitude calculation, minimization and plotting, and is widely used for analyses at BESIII. A high performance computing cluster has been established in the computing center at IHEP, which is equipped with hundreds of GPUs. In addition, for baryon spectroscopy analyses, the amplitudes can be extremely complicated. FDC-PWA, a package for automatic Feynman diagram calculation [66], has been extensively used to generate a complete set of Fortran source codes for PWA amplitudes.

One notoriously difficult problem is the parametrization of the dynamical properties of resonances, especially for those resonances related to thresholds. Coupled-channel analyses are mandatory to extract the partial widths and other pole properties. The correct analytical properties of the amplitude are essential for an extrapolation from the experimental data into the complex plane in order to determine the pole positions. The proper implementation of the dynamical function in PWA requires cooperation between theorists and experimentalists. In PWA of $J/\psi \to \gamma\pi^0\pi^0$ [21], $J/\psi \to \gamma K_S K_S$ [19] and $J/\psi \to \gamma\phi\phi$ [23], the results of mass-independent amplitude analysis were provided, which extract a piecewise function that describes the dynamics of the two-body meson system while making minimal assumptions about the properties and number of poles in the amplitude. Such a model-independent description allows to develop phenomenological models in a cooperation between experiment and theory, which can then be used to fit experimental data in the future. Global studies of different reactions and kinematics across experiments are also needed to clarify the underlying production mechanisms.

2.5 Other physics opportunities

2.5.1 Light meson decays

Light meson decays are an important tool for studies of the strong interaction in the non-perturbative region and for determining some SM parameters. As the neutral members of the ground state pseudoscalar nonet, both η and η' play an important role in understanding the low energy quantum chromodynamics (QCD). Decays of η/η' probe a wide variety of physics issues, *e.g.* the $\pi^0-\eta$ mixing, light-quark masses and pion-pion scattering. In particular, the η' meson, which is much heavier than the Goldstone bosons of broken chiral symmetry, plays a special role as the predominant singlet state arising from the strong axial $U(1)$ anomaly. In addition, the decays of both η and η' mesons are used to search for processes beyond SM, and to test fundamental discrete symmetries.

The main decays of η/η' mesons are hadronic and radiative. Alternatively, one can divide the decays in two classes. The first class consists of hadronic decays into three pseudoscalar mesons, such as $\eta' \to \eta\pi\pi$. These processes are already included in the lowest order, $O(p^2)$, of the chiral perturbation theory (ChPT) [67]. The second class includes anomalous processes involving an odd number of pseudoscalar mesons, such as $\eta' \to \rho^0\gamma$ and $\eta' \to \pi^+\pi^-\pi^+\pi^-$. They are driven by the "Wess-Zumino-Witten" (WZW) term [68, 69] which enters at the order of $O(p^4)$ [70]. The dynamics of η' decays remains a subject of extensive studies aiming at precision tests of ChPT in the $SU_L(3)\times SU_R(3)$ sector (*i.e.* involving an s quark). Model-dependent approaches for describing low-energy meson interactions, such as the vector meson dominance (VMD) [71, 72], and the large number of colors, N_C, extensions of ChPT [73], together with dispersive methods, could be extensively tested in η' decays.

Due to the high production rate of light mesons in charmonium (*e.g.* J/ψ) decays, the BESIII experiment also offers a unique possibility to investigate the light meson decays. The decays $J/\psi \to \gamma\eta(\eta')$ and $J/\psi \to \phi\eta(\eta')$ provide clean and efficient source of η/η' mesons for decay studies. During several runs from 2009 to 2019, a total data sample of 10^{10} J/psi events was collected with the BESIII detector [74, 75]. In recent years, considerable progress in η/η' decays was achieved at the BESIII experiment. In addition to the improved accuracy of the branching fractions of η', observations of new η' decay modes, including $\eta' \to \rho^{\mp}\pi^{\pm}$ [76] and $\eta' \to \gamma e^+e^-$ [77], $\eta' \to \pi^+\pi^-\pi^+\pi^-$, and $\eta' \to \pi^+\pi^-\pi^0\pi^0$ [78], have been reported for the first time. The precision of the $\eta' \to \pi^+\pi^-\gamma$ $M(\pi^+\pi^-)$ distribution from BESIII [79], with clear $\rho^0-\omega$ interference, is comparable to the $e^+e^- \to \pi^+\pi^-$ data and allows comparison of these two reactions with both model-dependent and model-independent methods [80, 81]. A further investigation of extra contributions, i.e. the box

anomaly or $\rho(1405)$, is necessary besides the contributions from $\rho^0(770)$ and ω. In particular, a competitive extraction of the $\omega \to \pi^+\pi^-$ branching fraction is possible [82].

Despite the impressive progress, many η/η' decays are still to be observed and explored. With the sample of 10^{10} J/ψ events collected with the BESIII detector, the available η and η' events from radiative decays $J/\psi \to \gamma\eta$, $\gamma\eta'$ and hadronic decays $J/\psi \to \phi(\omega)\eta$, $\phi(\omega)\eta'$ are summarized in Table 2.2, making possible further detailed studies of η/η' . A list of specific decay channels where new data are expected to have an important impact is shown in Table 2.3.

In addition, the high production rate of ω in J/ψ hadronic decays, *e.g.* $\mathcal{B}(J/\psi \to \omega\eta) = (1.74 \pm 0.20) \times 10^{-3}$ [5], allows to select a clean sample of 1.7×10^7 events, which offers a unique opportunity to test the theoretical calculations [84-86] by investigating the Dalitz plot of $\omega \to \pi^+\pi^-\pi^0$.

Table 2.2. Available η/η' decays calculated with the expected 1×10^{10} J/ψ events at BESIII.

Decay Mode	$\mathcal{B}(\times 10^{-4})$ [5]	η/η' events
$J/\psi \to \gamma\eta'$	51.5 ± 1.6	5.2×10^7
$J/\psi \to \gamma\eta$	11.04 ± 0.34	1.1×10^7
$J/\psi \to \phi\eta'$	7.5 ± 0.8	7.5×10^6
$J/\psi \to \phi\eta$	4.5 ± 0.5	4.5×10^6
$J/\psi \to \omega\eta$	17.4 ± 2.0	1.7×10^7
$J/\psi \to \omega\eta'$	1.82 ± 0.21	1.8×10^6

Table 2.3. A few topics for the η and η' programs.

η decay mode	physics highlight	η' mode	physics highlight
$\eta \to \pi^0 2\gamma$	ChPT	$\eta' \to \pi\pi$	CPV
$\eta \to \gamma B$	leptophobic dark boson	$\eta' \to 2\gamma$	chiral anomaly
$\eta \to 3\pi^0$	$m_u - m_d$	$\eta' \to \gamma\pi\pi$	box anomaly, form factor
$\eta \to \pi^+\pi^-\pi^0$	$m_u - m_d$, CV	$\eta' \to \pi^+\pi^-\pi^0$	$m_u - m_d$, CV
$\eta \to 3\gamma$	CPV	$\eta' \to \pi^0\pi^0\eta$	cusp effect [83]

2.5.2 Two photon physics

Production of resonances by two-photon fusion, as well as decay of resonances into two photons, provide important information about the hadron structure. The anomalous magnetic moment of the muon $\alpha_\mu \equiv (g-2)_\mu/2$ is a precision observable in SM. The accuracy of the SM prediction for $(g-2)_\mu$ is currently limited by the knowledge of the hadronic light-by-light contribution. Apart from contributing to the $(g-2)_\mu$ studies, the two-photon width can be used to identify non-$q\bar{q}$ states, because $\gamma\gamma$ decay of non-$q\bar{q}$ mesons like the glueballs, hybrids, multiquark objects, or mesonic molecules, is expected to be suppressed in various models. BESIII offers good opportunities for precision measurements of the production of low-mass hadronic systems in two-photon collisions with the two-photon invariant mass region accessible up to 3 GeV/c^2.

2.6 Prospects

Although years of continuous experimental efforts have been made to search for QCD exotic hadrons beyond the quark model, no compelling evidence has been unambiguously established yet. The experimental search for QCD exotics (glueballs, hybrids, multiquarks) continues to be an exciting problem, which is limited by the current data. Recent progress in LQCD reaffirms the existence of glueballs and hybrids. Other LQCD calculations indicate that radiative J/ψ decays are a promising hunting ground for glueballs. BESIII will continue playing a leading role in this search.

High precision data and systematic studies with various production mechanisms and decay modes are needed to determine resonance properties. The primary requirement for the data taking within the light hadron program at BESIII is to have a sufficient number of high-statistics J/ψ events for the systematic study of glueballs. The pseudoscalar glueball is clearly the main focus of research with its production rate in radiative J/ψ decays predicted to be $O(10^{-4})$ by LQCD. A major difficulty for identification of glueballs is the lack of first-principles theoretical predictions of glueball couplings and decay rates. Due to the "flavor-blindness" of gluons, there will be no dominant decay mode of a glueball. The decay rate of a glueball into a certain final state may be estimated to be at the level of $O(10^{-3}) \sim O(10^{-2})$ in analogy to the η_c or $\chi_{c0,2}$ decays. However, mixing with ordinary mesons complicates the situation in the light-quark mass range. From simulation studies, the detection efficiency of a typical decay mode of a pseudoscalar glueball is estimated to be a few percent. Recently, a new decay mode of $X(2370)$ was observed in the spectrum of $\eta' K\bar{K}$ of $J/\psi \to \gamma\eta' K\bar{K}$. We performed a feasibility study to determine the spin-parity of $X(2370)$. The neutral channel $J/\psi \to \gamma\eta' K^0_S K^0_S$ provides a clean environment for amplitude analysis as it does not suffer from significant backgrounds such as $J/\psi \to \pi^0\eta' K^0_S K^0_S$, which are present in the charged channel $J/\psi \to \pi^0\eta' K^+ K^-$. MC samples with statistics equivalent to the current data and 10 billion J/ψ were generated with a certain set of amplitude parameters. Amplitude analysis was performed of the MC samples with various hypothesis. Table 2.4 shows that the spin-parity of $X(2370)$ can be unambiguously determined with higher statistics of data. BESIII accumulated 10 billion J/ψ events, which are mandatory for mapping out the spectrum of light hadrons in J/ψ decays. In addition, $\psi(3686)$ decays have a larger phase space for studying mesons and

Table 2.4. A feasibility study for determining the spin-parity of $X(2370)$ with the amplitude analysis of $J/\psi \to \gamma\eta' K_S^0 K_S^0$. The significance is obtained by comparing the likelihoods of amplitude analyses with different spin-parity hypothesis of $X(2370)$.

	current statistics (1.3 billions of J/ψ)	expected statistics (10 billions of J/ψ)
significance for 0^{-+} assignment of $X(2370)$	3.2σ	13.2σ

baryons with higher mass, even though the production rates of light hadrons are typically suppressed with respect to J/ψ. The η_c and χ_c events from $\psi(3686)$ decays can also provide an opportunity for investigating QCD exotics. Currently, BESIII collected 450 million $\psi(3686)$ events. The light hadron physics program can benefit from the high statistics $\psi(3686)$ data set of the charmonium program in the future.

In the exploratory physics program for a future high luminosity τ-charm experiment, electromagnetic couplings to glueball candidates and their form factors can be extracted with higher accuracy, which are critical for the understanding of the nature of glueballs. High-statistics charmonium decays also provide an opportunity for investigating low-lying exotic hybrid nonets. In the future, the available high-statistics light-meson events from decays can be used not only for precision measurements of QCD at low energy, but also for probing physics beyond SM.

In the next few years, many experiments (COMPASS, BESIII) will continue to be active, while a number of new experiments (GlueX, Belle II, PANDA) appear on the horizon. Definitive conclusions about the nature of confinement will need complementary studies with these experiments. Key features of these experiments are high statistics and high sensitivity to explore hadron spectroscopy. COMPASS [87] has comprehensively studied a_J and π_J-like mesons up to the mass of 2 GeV/c^2 in diffractive scattering of hadron beams. GlueX [88] is designed to search for and measure the spectrum of light-mass hybrid mesons. It began its physics run in 2017 and will start a high luminosity run with an updated detector in 2019. An important advantage of this experiment is the use of polarized photons, which simplifies the initial states and the production process. PANDA [89] is designed for high-precision studies of the hadron spectrum at center-of-mass energies between 2.3 and 5.5 GeV. It is scheduled to start data taking in a full setup in 2026. In $\bar{p}p$ annihilations, spin-exotic states (*e.g.* oddballs) can be produced. Belle II [90] will start collecting data in 2019, and will accumulate 50 ab^{-1} of data at the $\Upsilon(4S)$ peak by 2027. Although it is not its primary goal as the next generation flavor factory, Belle II can also explore the light-quark sector using the two-photon process, because a glueball should have suppressed couplings to $\gamma\gamma$. Hadronic decays of heavy hadrons may also serve as a well-defined source for light mesons. BESIII remains unique for studying and searching for QCD exotics and new excited baryons, as its high-statistics data sets of charmonia provide a gluon rich environment with clearly defined initial and final state properties.

References

1 N. Brambilla *et al*., Eur. Phys. J. C, **74**: 2981 (2014)
2 C. A. Meyer and Y. Van Haarlem, Phys. Rev. C, **82**: 025208 (2010)
3 V. Crede and C. A. Meyer, Prog. Part. Nucl. Phys., **63**: 74 (2009)
4 E. Klempt and A. Zaitsev, Phys. Rept., **454**: 1 (2007)
5 C. Amsler and N. A. Tornqvist, Phys. Rept., **389**: 61 (2004)
6 S. Godfrey and J. Napolitano, Rev. Mod. Phys., **71**: 1411 (1999)
7 L. Kopke and N. Wermes, Phys. Rept., **174**: 67 (1989)
8 K. T. Chao and Y. F. Wang, Int. J. Mod. Phys. A, **24**: suppl. 1 (2009)
9 G. S. Bali *et al*. (UKQCD Collaboration), Phys. Lett. B, **309**: 378 (1993)
10 C. J. Morningstar and M. J. Peardon, Phys. Rev. D, **60**: 034509 (1999)
11 Y. Chen *et al*., Phys. Rev. D, **73**: 014516 (2006)
12 W. Sun *et al*., Chin. Phys. C, **42**: 093103 (2018)
13 E. Gregory *et al*., JHEP, **1210**: 170 (2012)
14 L. C. Gui *et al*. (CLQCD Collaboration), Phys. Rev. Lett., **110**: 021601 (2013)
15 Y. B. Yang *et al*. (CLQCD Collaboration), Phys. Rev. Lett., **111**: 091601 (2013)
16 L. C. Gui, J. M. Dong, Y. Chen et al, arXiv:1906.03666 [hep-lat]
17 M. Tanabashi *et al*. (Particle Data Group), Phys. Rev. D, **98**: 030001 (2018)
18 M. Ablikim *et al*. (BESIII Collaboration), Phys. Rev. D, **87**: 092009 (2013); Erratum: [Phys. Rev. D, **87**: 119901 (2013)]
19 M. Ablikim *et al*. (BESIII Collaboration), Phys. Rev. D, **98**: 072003 (2018)
20 M. Ablikim *et al*. (BESIII Collaboration), Phys. Rev. D, **87**: 032008 (2013)
21 M. Ablikim *et al*. (BESIII Collaboration), Phys. Rev. D, **92**: 052003 (2015); Erratum: [Phys. Rev. D, **93**: 039906 (2016)]
22 A. Etkin *et al*., Phys. Rev. Lett., **41**: 784 (1978); Phys. Lett. B, **165**: 217 (1985); Phys. Lett. B, **201**: 568 (1988)
23 M. Ablikim *et al*. (BESIII Collaboration), Phys. Rev. D, **93**: 112011 (2016)
24 A. Masoni, C. Cicalo, and G. L. Usai
25 M. Ablikim *et al*. (BESIII Collaboration), Phys. Rev. Lett., **108**: 182001 (2012)
26 M. Ablikim *et al*. (BESIII Collaboration), Phys. Rev. D, **83**: 032003 (2011)
27 M. Ablikim *et al*. (BESIII Collaboration), Phys. Rev. Lett., **121**: 022001 (2018)
28 J. J. Wu, X. H. Liu, Q. Zhao *et al*., Phys. Rev. Lett., **108**: 081803 (2012)
29 M. Ablikim *et al*. (BESIII Collaboration), Phys. Rev. D, **97**: 051101 (2018)
30 J. J. Dudek *et al*., Phys. Rev. D, **83**: 111502 (2011)
31 G. S. Adams *et al*. (CLEO Collaboration), Phys. Rev. D, **84**: 112009 (2011)
32 M. Ablikim *et al*. (BESIII Collaboration), Phys. Rev. D, **95**: 032002 (2017)

33 N. Isgur, R. Kokoski, and J. Paton, Phys. Rev. Lett., **54**: 869 (1985)
34 P. R. Page, E. S. Swanson, and A. P. Szczepaniak, Phys. Rev. D, **59**: 034016 (1999)
35 P. Z. Huang, H. X. Chen, and S. L. Zhu, Phys. Rev. D, **83**: 014021 (2011)
36 H. X. Chen, Z. X. Cai, P. Z. Huang *et al*., Phys. Rev. D, **83**: 014006 (2011)
37 R. L. Jaffe, Phys. Rev. D, **15**: 267 (1977)
38 M. G. Alford and R. L. Jaffe, Nucl. Phys. B, **578**: 367 (2000)
39 L. Maiani, F. Piccinini, A. D. Polosa *et al*., Phys. Rev. Lett., **93**: 212002 (2004)
40 L. Maiani, A. D. Polosa, and V. Riquer, Phys. Lett. B, **651**: 129 (2007)
41 G. 't Hooft, G. Isidori, L. Maiani *et al*., hys. Lett. B, **662**: 424 (2008)
42 J. D. Weinstein and N. Isgur, Phys. Rev. D, **41**: 2236 (1990)
43 S. Ishida et al, in *Proceedings of the 6th International Conference on Hadron Spectroscopy*, Manchester, United Kingdom, 1995 (World Scientific, Singapore, 1995), p.454
44 N. N. Achasov, S. A. Devyanin, and G. N. Shestakov, Phys. Lett. B, **88**: 367 (1979)
45 J. J. Wu, Q. Zhao, and B. S. Zou, Phys. Rev. D, **75**: 114012 (2007)
46 C. Hanhart, B. Kubis, and J. R. Pelaez, Phys. Rev. D, **76**: 074028 (2007)
47 J. J. Wu and B. S. Zou, Phys. Rev. D, **78**: 074017 (2008)
48 M. Ablikim *et al*. (BES Collaboration), Phys. Rev. Lett., **95**: 262001 (2005)
49 M. Ablikim *et al*. (BESIII Collaboration), Phys. Rev. Lett., **106**: 072002 (2011)
50 M. Ablikim *et al*. (BESIII Collaboration), Phys. Rev. Lett., **115**: 091803 (2015)
51 J. Z. Bai *et al*. (BES Collaboration), Phys. Rev. Lett., **91**: 022001 (2003)
52 M. Ablikim *et al*. (BESIII Collaboration), Chin. Phys. C, **34**: 421 (2010)
53 J. P. Alexander *et al*. (CLEO Collaboration), Phys. Rev. D, **82**: 092002 (2010)
54 M. Ablikim *et al*. (BESIII Collaboration), Phys. Rev. Lett., **108**: 112003 (2012)
55 M. Ablikim *et al*. (BESIII Collaboration), Phys. Rev. Lett., **117**: 042002 (2016)
56 M. Ablikim *et al*.. (BES Collaboration), Phys. Rev. Lett., **93**: 112002 (2004)
57 S. Capstick *et al.*, arXiv:hep-ph/0012238
58 E. Klempt and J. M. Richard, Rev. Mod. Phys., **82**: 1095 (2010)
59 S. Capstick and W. Roberts, Prog. Part. Nucl. Phys., **45**: S241 (2000)
60 R. G. Edwards, J. J. Dudek, D. G. Richards and S. J. Wallace, Phys. Rev. D, **84**: 074508 (2011)
61 B. -S. Zou, Nucl. Phys. A, **684**: 330 (2001)
62 B. S. Zou *et al*. (BES Collaboration), PiN Newslett., **16**: 174 (2002)
63 M. Ablikim *et al*. (BESIII Collaboration), Phys. Rev. Lett., **110**: 022001 (2013)
64 M. Battaglieri *et al*., Acta Phys. Polon. B, **46**: 257 (2015)
65 N. Berger, L. Beijiang, and W. Jike, J. Phys. Conf. Ser., **219**: 042031 (2010)
66 J. X. Wang, Nucl. Instrum. Methods Phys. Res., Sect. A, **534**: 241 (2004)
67 J. Gasser and H. Leutwyler, Annals Phys., **158**: 142 (1984)
68 J. Wess and B. Zumino, Phys. Lett. B, **37**: 95 (1971)
69 E. Witten, Nucl. Phys. B, **223**: 422 (1983)
70 J. Bijnens, A. Bramon, and F. Cornet, Z. Phys. C, **46**: 599 (1990)
71 J. J. Sakurai, Annals Phys., **11**: 1 (1960)
72 L. G. Landsberg, Phys. Rept., **128**: 301 (1985)
73 R. Kaiser and H. Leutwyler, Eur. Phys. J. C, **17**: 623 (2000)
74 M. Ablikim *et al*. (BESIII Collaboration), Chin. Phys. C, **36**: 915 (2012)
75 M. Ablikim *et al*. (BESIII Collaboration), Chin. Phys. C, **41**: 013001 (2017)
76 M. Ablikim *et al*. (BESIII Collaboration), Phys. Rev. Lett., **118**: 012001 (2017)
77 M. Ablikim *et al*. (BESIII Collaboration), Phys. Rev. D, **92**: 012001 (2015)
78 M. Ablikim *et al*. (BESIII Collaboration), Phys. Rev. Lett., **112**: 251801 (2014); Addendum: [Phys. Rev. Lett., **113**: 039903 (2014)]
79 M. Ablikim *et al*. (BESIII Collaboration), Phys. Rev. Lett., **120**: 242003 (2018)
80 B. Kubis and J. Plenter, Eur. Phys. J. C, **75**: 283 (2015)
81 F. Stollenwerk, C. Hanhart, A. Kupsc *et al*., Phys. Lett. B, **707**: 184 (2012)
82 C. Hanhart , S. Holz, B. Kubis *et al.*, Eur. Phys. J. C, **77**: 98 (2017); Erratum: Eur. Phys. J. C, **78**: 450 (2018)
83 B. Kubis and S. P. Schneider, Eur. Phys. J. C, **62**: 511 (2009)
84 F. Niecknig, B. Kubis, and S. P. Schneider, Eur. Phys. J. C, **72**: 2014 (2012)
85 I. V. Danilkin *et al*., Phys. Rev. D, **91**: 094029 (2015)
86 C. Terschlusen, B. Strandberg, S. Leupold *et al*., Eur. Phys. J. A, **49**: 116 (2013)
87 F. Gautheron *et al.* (COMPASS Collaboration), SPSC-P-340, CERN-SPSC-2010-014
88 P. Eugenio, PoS ConfinementX,349 (2012)
89 M. F. M. Lutz *et al.* (PANDA Collaboration), arXiv:0903.3905 [hep-ex]
90 T. Abe *et al.* (Belle II Collaboration), arXiv:1011.0352 [physics.ins-det]; E. Kou et al, arXiv:1808.10567 [hep-ex]

Chapter 3

Charmonium physics

3.1 Introduction

Heavy quarkonia are frequently referred to as the "positronium of QCD" [1] due to consistent, one-to-one correspondence of the level schemes that reflect the Coulomb-like interactions at small distances. Within the BESIII energy range, charmonium states both below and above the open-charm threshold are accessible (Figs. 3.1 and 3.2). The spectrum of charmonium states with masses below the open-charm threshold has been well-established for several decades. These states can therefore be used to precisely test predictions based on various theoretical techniques, ranging from models (like the quark model) to approximations of QCD (like non-relativistic QCD, described below) to numerical calculations of the full QCD Lagrangian (i.e., LQCD). The fact that the energy scale ranges from the charmonium mass to $\Lambda_{\rm QCD}$ makes the charmonium processes a rich laboratory to probe both perturbative and non-perturbative QCD.

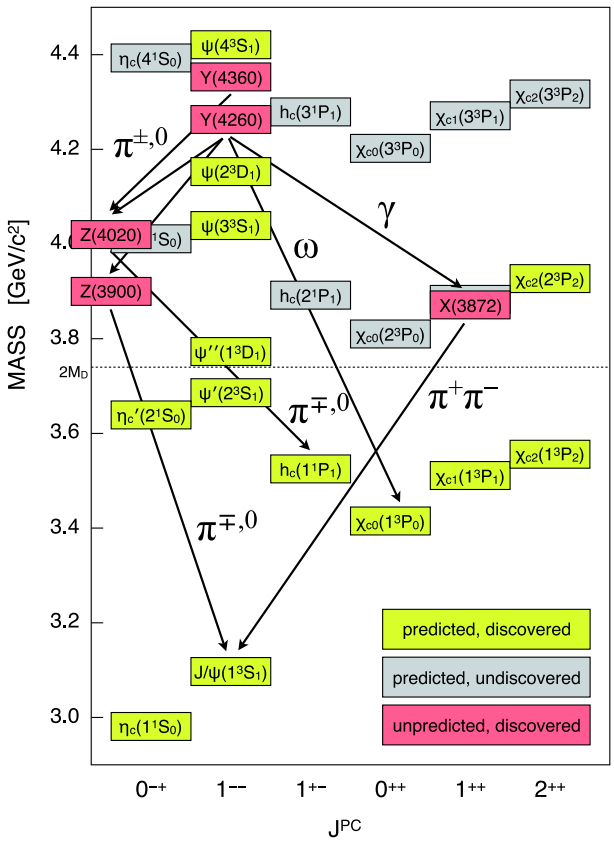

Fig. 3.1. (color online) The charmonium spectrum. Yellow boxes denote states predicted by the quark model [2] that have already been discovered; gray boxes are for predicted states that have not yet been discovered; and the red boxes are for states that were unexpectedly discovered – likely pointing towards the existence of exotic hadrons. All of these states have been studied at BESIII. A few of the key transitions studied at BESIII are indicated by black arrows.

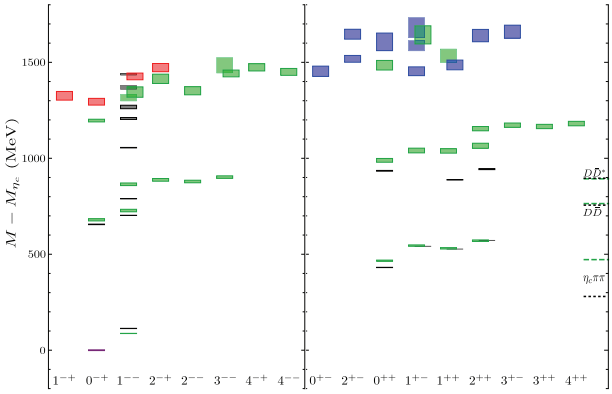

Fig. 3.2. (color online) The charmonium and hybrid spectrum. Green boxes represent masses of charmonium states calculated by the lattice QCD with $M_\pi \sim 240$ MeV [3]; red and blue boxes represent the lightest and first-excited hybrid states; black boxes are the world averaged experimental results in 2015 [4]; dashed lines show the location of some lower thresholds for strong decay from computations (coarse green) and experiments (fine grey). The states are labeled with their quantum numbers J^{PC} and their masses are shown with the η_c mass subtracted. The vertical size of the boxes denotes the standard uncertainty.

The relative simplicity of the lowest-lying (least massive) charmonium states allows precision tests of QCD and QCD-inspired models in a region where both non-perturbative and perturbative aspects of QCD play a role. The higher-mass states, on the other hand, pose serious challenges even to our qualitative understanding of mesons. Several of these states provide potential evidence of a wealth of exotic configurations of quarks and gluons, including: tetraquark states (two quarks and two antiquarks), hadronic molecules (two hadrons), hybrid mesons (a quark and antiquark with an excited gluonic field), etc.

The charmonium group studies both of these regions of the charmonium spectrum, providing a unique and important perspective on the dynamics of strong force physics. These studies include: searching for new charmonium states, determining the internal structure of previously established charmonium states, measuring masses

and widths, precisely measuring transitions (both radiative and hadronic) between charmonium states, and finding new decay channels. The capabilities of the BESIII experiment are uniquely suited to the study of both light and heavy charmonium states. The lighter charmonium states are primarily studied using large and clean samples of $\psi(3686)$ decays (i.e., $\psi(2S)$ or ψ'); the heavy charmonium states are produced using higher-energy collisions, while the exotic charmonium states are either produced directly or by decays of other states.

As noted above, the spectrum of states above open-charm threshold (Figs. 3.1 and 3.2) is clearly quite convoluted. The past decade has seen the discovery of a large number of new states that are yet to be satisfactorily understood. The "Y" states usually have $J^{PC} = 1^{--}$; the "Z" states are electrically charged; and the "X" states are the remainder. Note that the naming scheme is revised in the latest edition of the review of particle physics by PDG [5], but we use the older scheme in this White Paper for consistency. These states have been named "X", "Y", and "Z" since their internal structure is still unclear. One thing is clear: these new states cannot all be conventional bound states of a charm quark and antiquark. They are a likely evidence of more exotic configurations of quarks and gluons (such as tetraquarks, meson molecules, or hybrid mesons, etc.). Their existence therefore provides a crucial opportunity to study the dynamics of quarks and gluons in a new environment. At BESIII, the accessible e^+e^- cms energies allow to directly produce a large number of these states, which in turn allows to measure their masses, widths, and decay modes. The effort to understand these new states (which we refer to as "XYZ physics") is described further in Sec. 3.3.

Future studies of the charmonium system, both above and below the open-charm threshold, will require additional data sets. These requirements will be detailed throughout this chapter and summarized in Sec. 3.4. For further studies of charmonium below the open-charm threshold, around 3 billion $\psi(3686)$ decays are required, representing about an order-of-magnitude increase in statistics over the current sample of about 450 million $\psi(3686)$ decays. Above the open-charm threshold, we require three types of additional data samples: (1) a large number of additional data samples, each with an integrated luminosity of approximately 500 pb^{-1} and spread over a variety of cms energies, in order to study the spectrum of the Y states and the evolution of the Z states; (2) a small number of larger data samples, each of approximately 5 fb^{-1}, to perform detailed studies of the Z states; and (3) samples of higher-energy data to explore the poorly established mass region above 4.6 GeV/c^2, where mysterious peaks in the $\Lambda_c^+\bar{\Lambda}_c^-$ [6] and $\pi^+\pi^-\psi(2S)$ cross-sections [7] have been observed.

3.2 Charmonium states below the open-charm threshold

The goal of BESIII studies of charmonium states below the open-charm threshold is to investigate the spectroscopy, transitions, and decays of charmonium states mainly by analyzing (but not limited to) the $\psi(3686)$ data. The $\psi(3686)$ data is especially well suited for the study of charmonium states due to many transitions between the $\psi(3686)$ and lower-lying states. Thus, starting with a sample of $\psi(3686)$ data, one gains access to most of the charmonium states below the open-charm threshold. Figure 3.3 shows the low-lying charmonium ($c\bar{c}$) spectrum

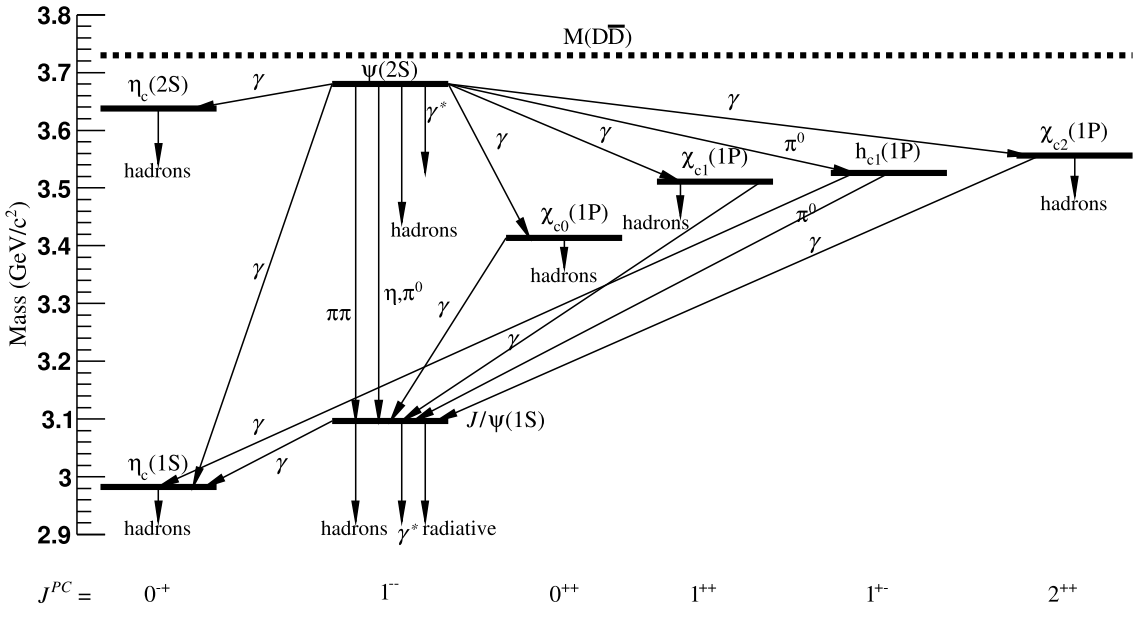

Fig. 3.3. The low-lying charmonium ($c\bar{c}$) spectrum and some observed transitions.

and some of the commonly observed transitions.

3.2.1 The theoretical framework

The charmonium meson system is an ideal, and to some extent unique, laboratory to investigate the boundary between perturbative and non-perturbative QCD in a controlled environment. Since reliable calculations of non-perturbative QCD are still difficult, several phenomenological models and effective theories have been proposed. These models and calculational techniques can be tested and further developed using the phenomenology of charmonium states. For example, the non-relativistic QCD (NRQCD) [8-10], expressed as the Pauli two-component field theory, can be constructed in correspondence with the hierarchy of energy scales in charmonium. NRQCD can be regarded as an effective theory that expands the full QCD in powers of v, where v is the relative velocity between c and $\bar{c}$ quarks.

According to the potential model calculations and lattice simulations, $v^2 \sim 0.3$ in the charmonium system [11]. For small v, a multitude of energy scales are observed as hard m_c, soft $m_c v$, and ultra-soft $m_c v^2$. The effects at energy scale m_c can be integrated out explicitly. The resultant theory, NRQCD, reduced in the number of dynamical degrees of freedom, is simpler than the full QCD, and turns out to be very useful in calculating the charmonium-relevant processes, such as the inclusive production and annihilation decays, and spectroscopy. Starting from NRQCD one can obtain the effective theory potential NRQCD (pNRQCD) [12-14] by integrating out the scale $m_c v$. Here, the role of the potentials and the quantum mechanical nature of the problem can be reduced to the zeroth order Schrödinger equation for the two heavy quarks. These effective field theories, as well as the potential models and LQCD, make it possible to calculate a wide range of charmonium observables in a controlled and systematic way, allowing an investigation of one of the most elusive sectors of SM: the low-energy QCD.

The charmonium observables can be taken from spectroscopy (e.g. masses and widths), transitions (e.g. transition rates), leptonic and electromagnetic decays, radiative decays, hadronic decays, rare and forbidden decays, and some miscellaneous topics such as the Bell inequalities in high energy physics and special topics in $B\bar{B}$ final states, where B refers to baryon. BESIII is well suited to address the remaining experimental questions that are related to the low-mass charmonium spectrum, i.e. below the open-charm threshold, such as a precise determination of the mass and width of η_c, h_c, and $\eta_c(2S)$. The QCD multipole expansion (QCDME) [15, 16] is a feasible approach for the charmonium hadronic transitions. Its results can be examined via observations at BESIII such as the $\pi\pi$ transitions of S-wave (P-wave or D-wave) charmonium states, the η transition $\psi(3686) \to \eta J/\psi$, and the iso-spin violating π^0 transition $\psi(3686) \to \pi^0 h_c$. Many radiative transition channels, including $E1$ (electric dipole) and $M1$ (magnetic dipole) transitions, can be investigated with the BESIII $\psi(3686)$ data sample using the cascade transition chain. Other EM related processes, such as the charmonium leptonic and EM decays, can also be studied at BESIII. In addition, studies of the hadronic decays will shed light on the $\rho-\pi$ puzzle [17] and reveal the inertial structure and decay dynamics of charmonium states. The baryonic decays are a special topic since the structure of baryons is comparatively more complicated than of mesons. BESIII can investigate the baryonic decays via the two-body, three-body, multi-body, and semi-inclusive modes. With a large $\psi(3686)$ data sample, BESIII can also search for rare and forbidden charmonium decays to explore some interesting topics such as CP violation or lepton flavor violation.

With the theory tools and the impressive number of collected charmonium states, BESIII will make a difference in the field allowing to carry out important investigations of SM and beyond.

3.2.2 Results with the current $\psi(3686)$ data set

BESIII has so far collected a total of 448 million $\psi(3686)$ decays (including 107 million in 2009 and 341 million in 2012). These data samples have led to the publication of more than 30 papers. Some of the most important results are as follows:

1. Measurement of h_c in $\psi(3686)$ decays [18]. Clear signals are observed for $\psi(3686) \to \pi^0 h_c$ with and without the subsequent radiative decay $h_c \to \gamma\eta_c$. In addition, first measurement of the absolute branching ratios $\mathcal{B}(\psi(3686) \to \pi^0 h_c) = (8.4 \pm 1.3 \pm 1.0) \times 10^{-4}$ and $\mathcal{B}(h_c \to \gamma\eta_c) = (54.3 \pm 6.7 \pm 5.2)\%$ are presented. Figure 3.4 shows the recoil mass of π^0 with and without the subsequent radiative decay $h_c \to \gamma\eta_c$.

2. Observation of the χ_{c1} decay into vector meson pairs [19]. The first measurement of the decay of χ_{c1} into vector meson pairs (VV) $\phi\phi$, $\omega\omega$, and $\omega\phi$ are presented. The branching fractions are measured as $(4.4 \pm 0.3 \pm 0.5) \times 10^{-4}$, $(6.0 \pm 0.3 \pm 0.7) \times 10^{-4}$, and $(2.2 \pm 0.6 \pm 0.2) \times 10^{-5}$, for $\chi_{c1} \to \phi\phi$, $\omega\omega$, and $\omega\phi$, respectively, which indicates that the hadron helicity selection rule is significantly violated in χ_{cJ} decays. Figure 3.5 shows the invariant mass spectra of VV in different final states.

3. Measurement of the mass and width of η_c using $\psi(3686) \to \gamma\eta_c$ [20]. A novel model that incorporates full interference between the signal reaction $\psi(3686) \to \gamma\eta_c$ and the nonresonant radiative background is used to successfully describe the line shape of η_c. The η_c mass is measured as $(2984.3 \pm 0.6 \pm 0.6)$ MeV/c^2, and the total width as $(32.0 \pm 1.2 \pm 1.0)$ MeV. Figure 3.6 shows the invariant mass distributions for the decays $K_S K^+\pi^- + c.c.$, $K^+K^-\pi^0$, $\eta\pi^+\pi^-$, $K_S K^+\pi^+\pi^-\pi^- + c.c.$, $K^+K^-\pi^+\pi^-\pi^0$, and $3(\pi^+\pi^-)$ with the fit results (for the constructed solution) superimposed.

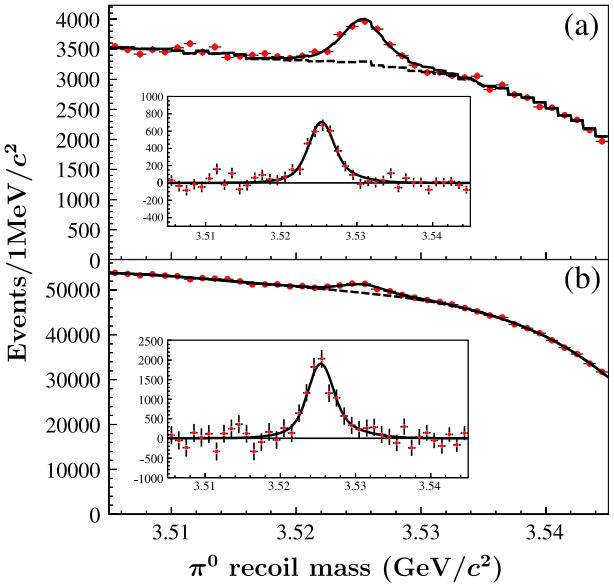

Fig. 3.4. (color online) Measurement of h_c in $\psi(3686)$ decays. (a) The π^0 recoil-mass spectrum and the fit in the $E1$-tagged analysis of $\psi(3686)\to\pi^0 h_c$, $h_c\to\gamma\eta_c$. (b) The π^0 recoil-mass spectrum and the fit in the inclusive analysis of $\psi(3686)\to\pi^0 h_c$. The fits are shown as solid lines, the background as dashed lines. The insets show the background-subtracted spectra.

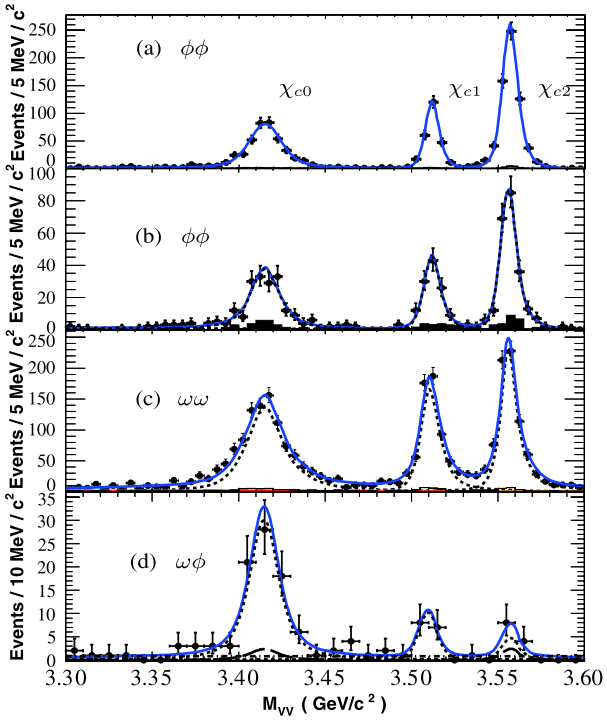

Fig. 3.5. (color online) Observation of the χ_{c1} decay into vector meson pairs. The invariant mass spectra of VV are shown for (a) $\phi\phi$ mode in the $\gamma 2(K^+K^-)$ final state, (b) $\phi\phi$ mode in the $\gamma\pi^+\pi^-\pi^0K^+K^-$ final state, (c) $\omega\omega$ mode in the $\gamma 2(\pi^+\pi^-\pi^0)$ final state, and (d) $\omega\phi$ mode in the $\gamma\pi^+\pi^-\pi^0K^+K^-$ final state.

4. First observation of the $M1$ transition between the radially excited charmonium S-wave spin-triplet and the radially excited S-wave spin-singlet states: $\psi(3686)\to\gamma\eta_c(2S)$ [21]. The analyses of the processes $\psi(3686)\to\gamma\eta_c(2S)$ with $\eta_c(2S)\to K^0_S K^\pm\pi^\mp$ and $K^+K^-\pi^0$, give an $\eta_c(2S)$ signal with a statistical significance greater than 10 standard deviations under a wide range of assumptions for the signal and background properties. The product branching fraction $\mathcal{B}(\psi(3686)\to\gamma\eta_c(2S))\times\mathcal{B}\left(\eta_c(2S)\to K\bar{K}\pi\right)$ is measured as $(1.30\pm0.20\pm0.30)\times10^{-5}$. Figure 3.7 shows the invariant mass spectrum for $K^0_S K^\pm\pi^\mp$, and the simultaneous likelihood fit to the three resonances and combined background sources.

5. Observation of the h_c radiative decay $h_c\to\gamma\eta'$ [22]. Events from the reaction channels $h_c\to\gamma\eta'$ and $\gamma\eta$ are observed with a statistical significance of 8.4σ and 4.0σ, respectively, for the first time. The branching fractions for $h_c\to\gamma\eta'$ and $h_c\to\gamma\eta$ are measured as $\mathcal{B}(h_c\to\gamma\eta')=(1.52\pm0.27\pm0.29)\times10^{-3}$ and $\mathcal{B}(h_c\to\gamma\eta)=(4.7\pm1.5\pm1.4)\times10^{-4}$. Figure 3.8 shows the results of the simultaneous fit of the invariant mass distributions of $M(\gamma\eta')$ and $M(\gamma\eta)$.

The above list represents only a part of the important results from the BESIII $\psi(3686)$ data set; more results can be found on the BESIII publication page [23].

3.2.3 Prospects of the charmonium program

We continue to explore important physics topics via charmonium decays. A few of these include: searches for new decay modes of the h_c, measurements of $M1$ transition processes and properties of the associated charmonium states (an $M1$ transition working group has been formed), and systematic analyses of baryon final states. For many channels with larger statistics, amplitude analyses are being applied to extract more physics information. With more $\psi(3686)$ data, we can search for additional decay modes of the η_c, $\eta_c(2S)$ and h_c, give more precise measurements of the masses and widths of the η_c, $\eta_c(2S)$ and h_c (and better understand the line shapes associated with their production), perform partial-wave analysis (PWA) on more channels, etc. Among these topics, some important measurements may require more $\psi(3686)$ data in order to achieve the desired precision.

For $h_c\to hadrons$, at present only three channels are observed and the sum of their branching fractions is only about 1.5% [24]. Many more hadronic decay modes are expected and will be searched for at BESIII. For a 5σ significant observation of the h_c decay channel with the branching fraction of 5×10^{-4}, a sample of 2×10^9 $\psi(3686)$ events is needed with the assumption that this channel is produced via the $\psi(3686)\to\pi^0 h_c$ transition, with 10% efficiency for the detection of the final states, and a similar background level to the $\pi^+\pi^-\pi^0$ channel. With such a data sample, h_c hadronic transitions, such as

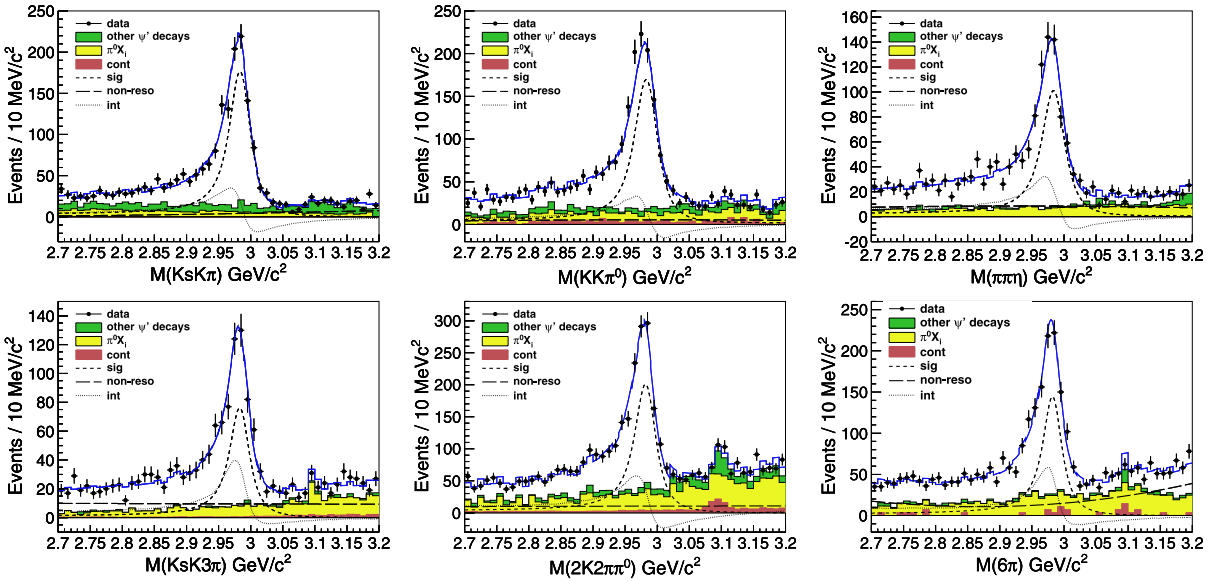

Fig. 3.6. (color online) Measurement of the mass and width of η_c using $\psi(3686)\to\gamma\eta_c$. The invariant mass distributions for the decays $K_S K^+\pi^-$, $K^+K^-\pi^0$, $\eta\pi^+\pi^-$, $K_S K^+\pi^+\pi^-\pi^-$, $K^+K^-\pi^+\pi^-\pi^0$, and $3(\pi^+\pi^-)$ are shown with the fit results (for the constructive interference solution) superimposed. Charge conjugate modes are included.

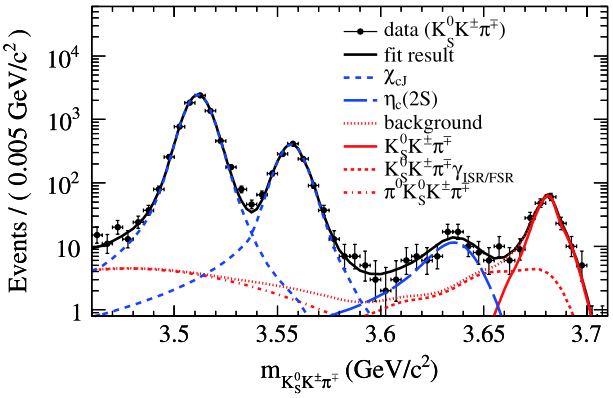

Fig. 3.7. (color online) First observation of the $M1$ transition $\psi(3686)\to\gamma\eta_c(2S)$. The invariant mass spectrum for $K^0_S K^\pm\pi^\mp$ and the simultaneous likelihood fit to the three resonances and combined background sources are shown.

the spin-flip transition $h_c\to\pi^+\pi^- J/\psi$ and its radiative decays, can also be searched for.

Compared with $E1$ transitions, the rates for $M1$ transitions between charmonium states are much lower. With the previously collected $\psi(3686)$ data sample, the first observation of the $M1$ transition $\psi(3686)\to\gamma\eta_c(2S)$ was reported by BESIII [21]. However, in order to understand $\eta_c(2S)$ better and to measure its mass, width, and decays more precisely, more $\psi(3686)$ data is necessary. For example, for the observation of the $\eta_c(2S)$ decay into a channel with the production branching fraction $\mathcal{B}(\psi(3686)\to\gamma\eta_c(2S))\times\mathcal{B}(\eta_c(2S)\to K_S K3\pi)$ of about 5×10^{-6}, a sample of 10^9 $\psi(3686)$ events is needed with the assumption that the detection efficiency is about 5%, where the low efficiency and high background levels are due to the softness of the transition photon. With such a large sample, we could also study the η_c charmonium state via the $M1$ transition to improve the precision of $\mathcal{B}(\psi(3686)\to\gamma\eta_c)$ and its comparison with theoretical predictions. A measurement of $\mathcal{B}(\psi(3686)\to\gamma\eta_c(2S))$ could be used to extract the absolute branching fractions for some specific $\eta_c(2S)$ decays. There are other radiative transitions, such as $\eta_c(2S)\to\gamma J/\psi$, $\eta_c(2S)\to\gamma h_c$, $\chi_{c2}\to\gamma h_c$, and $h_c\to\gamma\chi_{c0,1}$, that are challenges for BESIII even with a sample of 10^9 $\psi(3686)$ events because of low decay rates, or difficulties in detecting soft photons. These rates can be calculated in the potential model [1] and experimental searches are therefore important [25].

In addition to the radiative transitions, hadronic transitions are also very important and can be calculated better than the hadronic decays of charmonia. It is interesting to observe or find evidence of hadronic transitions such as the spin-flip $\chi_{c1}\to\pi\pi\eta_c$ and $h_c\to\pi\pi J/\psi$, for which only upper limits are known at present. We have estimated the needed statistics to see evidence of the transition $\chi_{c1}\to\pi^+\pi^-\eta_c$ and found that at least 10^9 $\psi(3686)$ events are needed according to the previous BESIII results [26]. Note that in Ref. [26] only two η_c hadronic decay channels were used. If more decay modes are included, a smaller data set could satisfy the requirements. To uncover evidence of $h_c\to\pi\pi J/\psi$, a sample of ot least 2×10^9 $\psi(3686)$ decays is needed with the assumption that there is no background. There are other hadronic transitions, such as $\psi(3686)\to\eta J/\psi$ and $\psi(3686)\to\pi^0 J/\psi$, that have been observed with the present BESIII $\psi(3686)$ data sample and will be im-

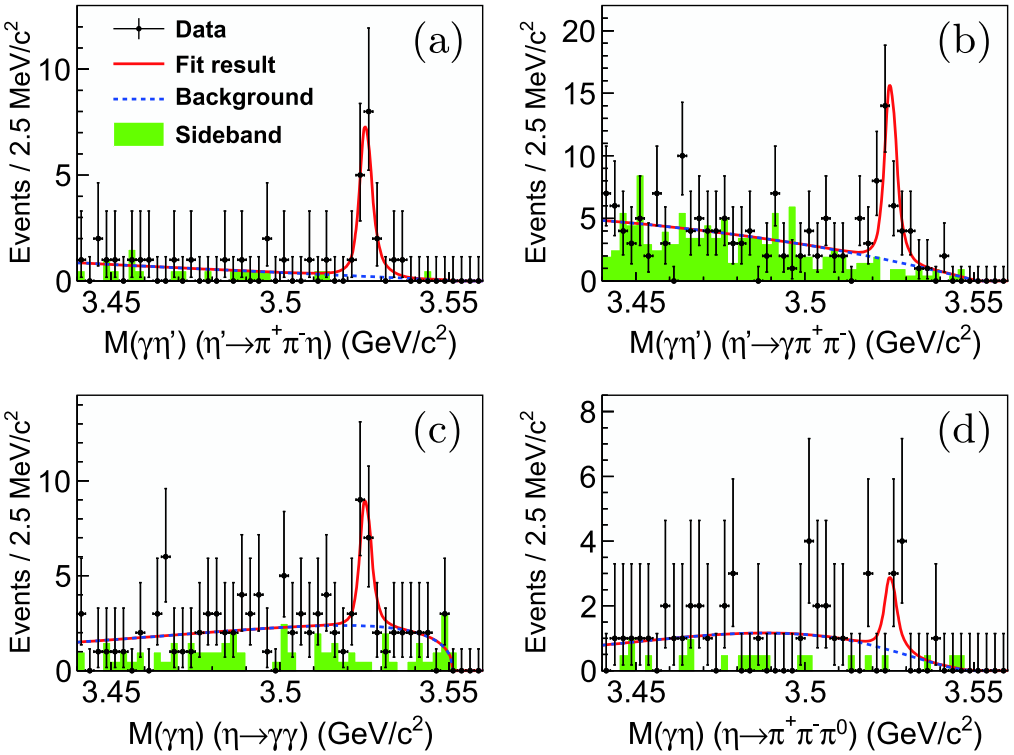

Fig. 3.8. (color online) Observation of the h_c radiative decay $h_c \to \gamma\eta'$. The results of the simultaneous fit of the two invariant mass distributions of $M(\gamma\eta')$ (top) and $M(\gamma\eta)$ (bottom) are shown; (a) $M(\gamma\eta')$ distribution for $h_c \to \gamma\eta'(\eta' \to \pi^+\pi^-\eta)$, (b) $M(\gamma\eta')$ distribution for $h_c \to \gamma\eta'(\eta' \to \gamma\pi^+\pi^-)$, (c) $M(\gamma\eta)$ distribution for $h_c \to \gamma\eta(\eta \to \gamma\gamma)$, and (d) $M(\gamma\eta)$ distribution for $h_c \to \gamma\eta(\eta \to \pi^+\pi^-\pi^0)$.

proved with a larger one.

Besides the transitions between charmonium states, there are also decays of charmonia that should be measured. Both radiative decays and hadronic decays of charmonium states should be studied for a better understanding of charmonium decay dynamics. From Ref. [27], the typical branching fraction of $\chi_{cJ} \to \gamma V$, where V represents a vector resonance, is about 10^{-6}. This means a sample of 10^9 $\psi(3686)$ events would be needed to observe the signal if we assume that the intermediate product branching fractions are 80% and the selection efficiency is 30%. Since the branching fractions for $\eta_c \to \gamma V$ are expected to be similar to $\eta_c \to \gamma\gamma$, they should be at the 10^{-4} level. The improved measurement of $\eta_c \to \gamma\gamma$ will shed light on the effects of higher order QCD corrections, as well as provide validation of the decoupling of the hard and soft contributions in the NRQCD framework due to its simplicity [28, 29]. With the present $\psi(3686)$ data sample at BESIII, the processes $\psi(3686) \to \gamma\pi^0$ and $\gamma\eta$ have been observed for the first time [30]. There are also many studies of J/ψ and $\psi(3686)$ decays into $\gamma p\bar{p}$, γK^+K^-, $\gamma\pi^+\pi^-$, etc. With a larger $\psi(3686)$ data sample, all these measurements will be improved.

Additional and better measurements of $\psi(3686)$ hadronic decays are crucial to help solve the long standing ρ-π puzzle [17]. The ratio of the branching fractions of J/ψ and $\psi(3686)$ is expected to hold to a reasonably good degree to 12% based on pQCD, for both inclusive and exclusive decays. However, this relation was observed to be severely violated for the $\rho\pi$ and several other decay channels. From the BESIII results already obtained, it has become clear that kinematic effects, which have been previously ignored, might contribute significantly, and that the amplitude analysis method might also be necessary to clarify the different dynamic processes between the J/ψ and $\psi(3686)$. For charmonium states beyond the open-charm threshold, the studies of their decay to open-charm states will not only provide information about the decay mechanism, but also serve for spectroscopy studies. Furthermore, it is interesting to study the non-$D\bar{D}$ decays of $\psi(3770)$, such as $\psi(3770) \to p\bar{p}$, $p\bar{p}\pi^0$, $\gamma\eta_c$, $\gamma\chi_{cJ}$, $\gamma\eta_c(2S)$, and $\pi^+\pi^- J/\psi$. These can be studied using the data collected on and around the $\psi(3770)$ peak.

The two-body baryonic decays of the χ_{cJ} can provide information about the color-singlet and color-octet contributions. In addition, systematic studies of two-body baryonic decays of the J/ψ and $\psi(3686)$ will shed light on the relative angle and magnitude of the electro-magnetic and strong interaction amplitudes [31]. The $\eta_c(2S)$ and h_c decays into $p\bar{p}$ have been searched for based on the 1×10^8 $\psi(3686)$ decay sample at BESII and no obvious signal has been observed [32]. To find evidence of both, a data sample of 2×10^9 $\psi(3686)$ decays will be required

under the assumption that the efficiency is about 40% and that there is no background. Also, a similar data set is needed to study the Bell inequality [33], $SU(3)$ flavor symmetry [34], and CP violation [35, 36]. Measurement of the three-body baryonic decays of higher excited charmonia will provide more information about the excited baryonic states, where amplitude analysis will be required.

Some rare decays can be searched for with larger $\psi(3686)$ data samples such as the C-violating process $J/\psi \to \gamma\gamma$ via $\psi(3686) \to \pi\pi J/\psi$. This is discussed in Chapter 6 on new physics.

For the excited conventional charmonium states beyond the open-charm threshold there are still many unsolved puzzles. There are only four 1^{--} states between 4.0 and 4.6 GeV predicted by the potential models, but the number of observed vector resonances is larger. The masses and partial widths of these states decaying into e^+e^- (Γ_{ee}) can be calculated with the potential models assuming they are conventional charmonia. However, strong coupling to open-charm meson pairs and relativistic corrections significantly change both the spectrum and Γ_{ee}. Better measurements would be very helpful to clarify the situation. BESIII has observed the $\psi(1^3D_2)$ state $X(3823)$ via its decay into $\gamma\chi_{c1}$ [37], but many predicted states, such as $1F$, $3S$, $2D$, $1G$, $3P$, $2F$, $4S$, $3D$ and $2G$ have not been observed yet. The properties of the excited conventional charmonia will be studied with the data sets collected for the XYZ states.

BESIII has already collected scan samples around the J/ψ, $\psi(3686)$, and $\psi(3770)$ peaks, as well as those above 4.0 GeV. These samples are dedicated to some specific problems that can be studied better at BESIII than elsewhere, such as the determination of resonance parameters, line shapes, interference between strong and EM amplitudes in resonance decay, etc.

Some tentative measurements and the needed $\psi(3686)$ samples are listed in Table 3.1. From this table, a sample of 3×10^9 $\psi(3686)$ events may guarantee the expected precision and lead to exciting discoveries. However, at present we consider that XYZ physics is a higher priority, and prefer to take the $\psi(3686)$ data only after finishing the proposed XYZ program.

3.3 *XYZ* Physics

The discovery of the XYZ states has opened a new era in the study of the charmonium spectrum [38-43]. Before the discovery of the $X(3872)$ in 2003 [44], every meson in the mass region between 2.9 and 4.5 GeV/c^2 could be successfully described as a $c\bar{c}$ bound state. Simple potential models, using the QCD-inspired potentials binding quarks and antiquarks, could reproduce the spectrum of charmonium states all the way from the $\eta_c(1S)$ (the ground state) up to the $\psi(4415)$ (usually considered as the third radial excitation of J/ψ) [2]. This simple model of charmonium spectrum has since broken down in a dramatic fashion. Following the discovery of the XYZ states (Fig. 3.1), we now observe exotic hadronic configurations containing charm and anticharm quarks. These new configurations, such as tetraquarks, hadronic molecules, and hybrid mesons, allow us to probe the mysterious nonperturbative QCD which underlies how quarks and gluons combine into larger hadronic composites.

The $X(3872)$, the first of the XYZ states discovered, was discovered in 2003 by the Belle Collaboration in the process $B \to KX(3872)$ with $X(3872) \to \pi^+\pi^- J/\psi$ [44]. Its unexpected appearance, combined with its narrow width and the fact that its mass is very close to the $D^0\bar{D}^{*0}$ mass threshold, immediately signaled that the $X(3872)$ is an unusual meson. Since its discovery, many of its properties have been determined [5]. For example, its total width is less than 1.2 MeV, its mass is within 0.18 MeV/c^2 of the $D^0\bar{D}^{*0}$ threshold, it has $J^{PC} = 1^{++}$, and in addition to $\pi^+\pi^- J/\psi$, it decays to $D^0\bar{D}^{*0}$ with a large branching fraction, $\gamma J/\psi$, $\gamma\psi(3686)$ and $\omega J/\psi$. It is currently believed to be a mixture of the $\chi_{c1}(2P)$ and a tetraquark or meson molecule [38-43]. However, many important open questions remain and further investigation is needed.

In 2013, BESIII discovered a way to experimentally access the $X(3872)$ via the process $e^+e^- \to \gamma X(3872)$ using cms energies in the vicinity of 4.26 GeV [45], which in itself provides an important hint of the relation between the $Y(4260)$ and $X(3872)$ [46]. This discovery has initiated a

Table 3.1. Some tentative measurements and required $\psi(3686)$ sample to achieve the desired precision. The observations and evidence correspond to the 5σ and 3σ significance of the signal.

measurement	expected sensitivity on branching fraction	needed $\psi(3686)$ sample in 10^9
$h_c \to hadrons$	observation of 5×10^{-4}	2
$\eta_c(2S) \to X$	observation of 1×10^{-6}	5
$\chi_{c1} \to \pi^+\pi^-\eta_c$	evidence of 3×10^{-3}	>1
$h_c \to \pi^+\pi^- J/\psi$	evidence of 2×10^{-3}	>2
$\chi_{cJ} \to \gamma V$	observation of 1×10^{-6}	1
$h_c \to p\bar{p}$	evidence of 2×10^{-4}	>2

new and vigorous program at BESIII of searching for new decay modes of the $X(3872)$, which in turn offer new insight into its nature.

The discovery of the $X(3872)$ quickly led to the discovery of many more states with exotic configurations of quarks and gluons. For example, the search for the decay $X(3872)\to\omega J/\psi$ led to the discovery of the $X(3915)$ in the process $B\to KX(3915)$ with $X(3915)\to\omega J/\psi$ [47]. This state was originally a candidate for the quark model $\chi_{c0}(2P)$ state, but its mass and decay patterns were inconsistent with that interpretation. Moreover, since that time a better candidate for the $\chi_{c0}(2P)$ state, the $X(3860)$, was discovered [48] (see also in Ref. [49]). This leaves the nature of the $X(3915)$ an unsettled question. Searching for the $X(3915)$ in the process $e^+e^-\to\gamma X(3915)$ is currently an important topic at BESIII. In addition, it is also important to search for resonant signals for the broad the $X(3860)$ and the conjectured narrow 2^{++} X_2 with a mass around 4 GeV/c^2 [50], the predicted spin partner of the $X(3872)$, in the process $e^+e^-\to\gamma D\bar{D}$.

Following the discovery of the $X(3872)$, $Y(4260)$ was discovered by BaBar using the Initial State Radiation (ISR) process $e^+e^-(\gamma_{\rm ISR})\to Y(4260)$ with $Y(4260)\to\pi^+\pi^- J/\psi$ [51]. Because of its production mechanism, we can immediately infer that it has $J^{PC}=1^{--}$. However, its mass is inconsistent with any of the known or expected charmonium vector excitations. For example, its mass lies between the masses of the $\psi(4160)$ and $\psi(4415)$. It is therefore supernumerary. LQCD calculations [52], as well as other models [53], suggest that the $Y(4260)$ could be a hybrid meson. Another intriguing model that considers the $Y(4260)$ as strongly coupled to the $D_1(2420)\bar{D}$ predicts a nontrivial behavior of its line shape [54, 55]. At BESIII, the $Y(4260)$ can be produced directly by simply tuning the cms energy of e^+e^- collisions to the mass of the $Y(4260)$. In the same way, BESIII can also directly produce the $Y(4360)$ (seen in $e^+e^-\to\pi^+\pi^-\psi(3686)$), and can search for new Y states. The BESIII discovery of a multitude of new Y states (or the discovery of a complicated coupled-channel system) is further described in the next section (Sec. 3.3.1).

The final, and perhaps the most interesting, class of exotic structures are the isovector Z_c states. Since they are known to contain an isosinglet $c\bar{c}$ pair, they must also contain light quarks to account for the non-zero isospin. One of the first of these states to be observed, the $Z_c(3900)$, was discovered by BESIII in the process $e^+e^-\to\pi^\mp Z_c(3900)^\pm$ with $Z_c(3900)^\pm\to\pi^\pm J/\psi$ [56]. Its two distinctive features are that it carries an electric charge and it has a mass near the $D\bar{D}^*$ threshold. This suggests that it is a candidate for a meson molecule or tetraquark with rescattering effects due to the presence of the $D\bar{D}^*$ threshold, and that more complicated kinematical singularities are also expected to be important. The line shape of the $Z_c(3900)$ and how that shape evolves with cms energy will be one of the keys to its interpretation. As described in more detail later, disentangling the nature of the $Z_c(3900)$ is one of the primary goals of the BESIII XYZ program.

Since the discovery of the $Z_c(3900)$, other Z_c states have also been discovered. For example, BESIII discovered the $Z_c(4020)$ in the process $e^+e^-\to\pi^\mp Z_c(4020)^\pm$ with $Z_c(4020)^\pm\to\pi^\pm h_c(1P)$ [57]. Its mass is close to the $D^*\bar{D}^*$ threshold, suggesting it is closely related to the $Z_c(3900)$.

So far, the $Z_c(3900)$ and $Z_c(4020)$ have only been produced in e^+e^- collisions with cms energies around 4.2–4.4 GeV with possible connection to the reported Y states. Other potential production mechanisms, such as $B\to KZ_c$ decays, appear to be insensitive to the $Z_c(3900)$ and $Z_c(4020)$ states. A different class of Z_c states has been discovered in B decays, among which the most prominent one is the $Z_c(4430)$ seen in $B\to KZ_c(4430)$ with $Z_c(4430)^\pm\to\pi^\pm\psi(3686)$ [58]. The reason why one class of Z_c states is produced in e^+e^- collisions and a different class in B decays remains a fascinating open question.

3.3.1 Overview of BESIII accomplishments

The goal of the XYZ physics program at BESIII is to understand the novel phenomena apparent in the spectrum of charmonium states with masses above the open-charm threshold, as outlined in the previous section. The presence of the XYZ states provides an ideal opportunity for BESIII to study exotic and unexplored features of the strong force. BESIII is currently in a unique position to both directly access a large number of these states and to search for new states in their decays. Note that a given Y state, because it has $J^{PC}=1^{--}$, can be produced directly at BESIII by the appropriate choice of the cms energy of e^+e^- collisions.

BESIII has already made significant progress in the studies of XYZ states. The existing data sets are shown in Fig. 3.9. We originally had "large" data sets (with integrated luminosity at or above 500 pb^{-1}) at only a few e^+e^- cms energies: 4.01, 4.18 (primarily used for D_s physics), 4.23, 4.26, 4.36, 4.42 and 4.6 GeV. In 2017, we collected large samples at seven additional energies between 4.19 and 4.27 GeV, and in 2019, eight additional energies between 4.28 and 4.44 GeV.

Using the limited amount of data collected prior to 2017, we have already made a number of important discoveries and measurements. Here we highlight eight of the most important measurements:

1. We discovered the $Z_c(3900)$ in the process $e^+e^-\to\pi^\mp Z_c^\pm$ with $Z_c^\pm\to\pi^\pm J/\psi$ [56], shown in Fig. 3.10(a). Since the $Z_c(3900)$ has a mass in the charmonium mass region and decays to J/ψ, we know that it includes $c\bar{c}$ quarks.

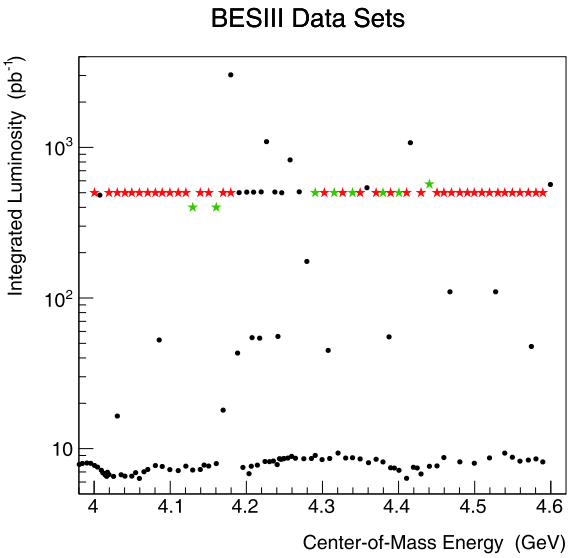

Fig. 3.9. (color online) BESIII data sets that are relevant for *XYZ* physics. The data sets collected prior to 2019 are shown in black, those collected in 2019 are in green, and those considered for potential future measurements are shown in red.

However, since it has an electric charge, it must include additional quarks. The $Z_c(3900)$ is therefore a good candidate for a tetraquark or meson molecule.

With 680 citations (as of Oct. 9, 2019), this publication is the most-cited of all BES papers (including BES and BESIII). Additional work is ongoing to better determine the internal structure of the $Z_c(3900)$.

2. We discovered the $Z_c(4020)$ in the process $e^+e^- \to \pi^\mp Z_c^\pm$ with $Z_c^\pm \to \pi^\pm h_c$ [57], shown in Fig. 3.10(b). Like the $Z_c(3900)$, the $Z_c(4020)$ contains $c\bar{c}$ quarks and is electrically charged. While the $Z_c(3900)$ is near the $D\bar{D}^*$ threshold, the $Z_c(4020)$ is near the $D^*\bar{D}^*$ threshold. With 337 citations (as of Oct. 9, 2019), this publication is the second-most cited BESIII paper.

3. We observed the $Z_c(3900)$ decay into the open-charm channel $(D\bar{D}^* + c.c.)^\pm$ [59], shown in Fig. 3.10(c). With 258 citations (as of Oct. 9, 2019), this publication is the fourth-most-cited BESIII paper.

4. Similarly, we observed the $Z_c(4020)$ decay into the open-charm channel $(D^*\bar{D}^*)^\pm$ [60], shown in Fig. 3.10(d). Observation of the $Z_c(3900)$ and $Z_c(4020)$ decays into the open-charm channels (and the lack of evidence of $Z_c(4020)$ decays into $(D\bar{D}^* + c.c.)^\pm$), combined with the fact that their masses are close to threshold, suggests that the nature of the $Z_c(3900)$ and $Z_c(4020)$ is somehow intimately tied to these channels. With 291 citations (as of Oct. 9, 2019), this publication is the third-most-cited BESIII paper.

5. We precisely measured the cross-section of $e^+e^- \to \pi^+\pi^- J/\psi$ [61]. Since this reaction led to the discovery of the $Y(4260)$, the aim of our measurement was to precisely determine the parameters of the $Y(4260)$. Instead, what we observed was a cross-section that was inconsistent with that arising from a single ordinary resonance, as shown in Fig. 3.10(e). The cross-section was successfully fitted using two resonances: one with a narrow total width and mass around 4.22 GeV/c^2 , and the other with a wider total width and mass around 4.32 GeV/c^2. Thus, the $Y(4260)$, one of the first *XYZ* states to be discovered, is either composed of two resonances or has a highly nontrivial line shape due to other dynamics, such as strong coupling to the $D_1(2420)\bar{D}$. In addition, we observed the decay $Y(4260) \to \pi^0\pi^0 J/\psi$ and the neutral $Z_c(3900)$ in $e^+e^- \to \pi^0 Z_c^0 \to \pi^0\pi^0 J/\psi$ [62]. This further cements the case that the $Z_c(3900)$ is an isospin-1 state with $c\bar{c}$ core.

6. We discovered two peaks in the cross-section of $e^+e^- \to \pi^+\pi^- h_c$ [63], shown in Fig. 3.10(f). Along with the above described measurement of $e^+e^- \to \pi^+\pi^- J/\psi$, this indicates that the family of Y states is more complicated than was originally thought. In particular, these two final states have different total spins of the charm and anticharm quark pair. The masses and widths of the peaks in $\pi^+\pi^- h_c$ and $\pi^+\pi^- J/\psi$ are inconsistent.

7. We discovered a peak in $e^+e^- \to \omega\chi_{c0}$ [64], shown in Fig. 3.10(g), that is inconsistent with the reported parameters of the $Y(4260)$. This suggests that either there is another Y state in this mass region, or that the mass of the $Y(4260)$ should be shifted downwards.

8. We discovered the process $e^+e^- \to \gamma X(3872)$ [45], shown in Fig. 3.10(h), which hints at the existence of radiative decay $Y(4260) \to \gamma X(3872)$. This is a unique transition in the sense that it is a transition between two states whose nature is unclear. This suggests that there is an intimate connection between the $Y(4260)$ and the $X(3872)$.

There is currently a great interest of the community in *XYZ* physics, as is clear from the high profile of BESIII papers mentioned above. Since the nature of most of these phenomena is yet to be understood, the theory community has been especially active in developing new techniques to aid the interpretation of *XYZ* states [38-43]. This has led to many innovations. What is currently needed, however, is more high precision data. Therefore, new data that BESIII will provide is much anticipated and will be put to immediate use.

3.3.2 Broad problems in *XYZ* physics

The *XYZ* results from BESIII have helped uncover several broad problems in the field, and these are the subject of intense studies at BESIII. Below, they are labeled the "Y problem", the "Z problem", and the "X problem". With more data, BESIII is in the unique position to definitively address all three. This section includes a description of the problems and indicates a variety of ways they can be addressed at BESIII.

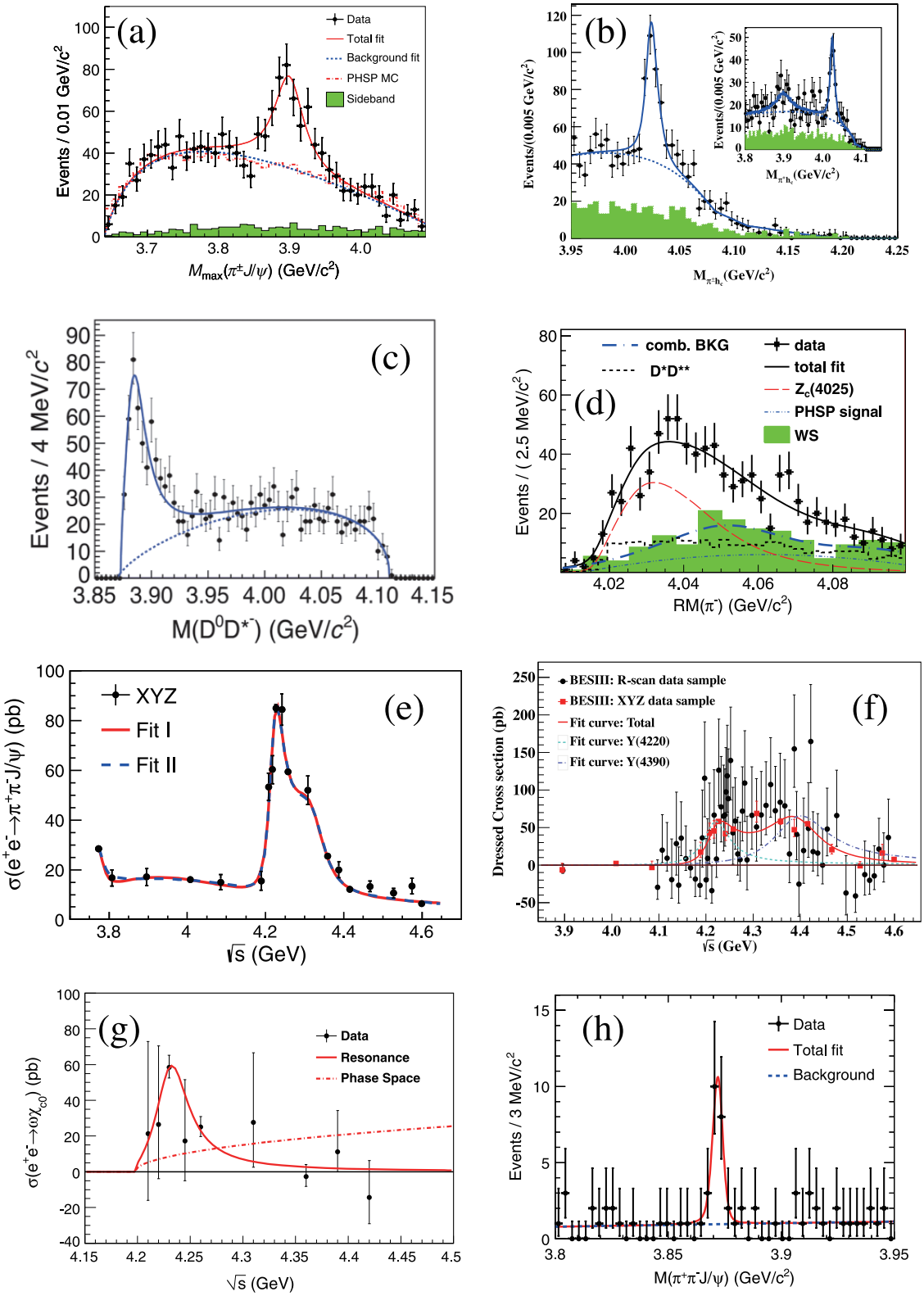

Fig. 3.10. (color online) A selection of *XYZ* results from BESIII: (a) discovery of the $Z_c(3900)$ [56]; (b) discovery of the $Z_c(4020)$ [57]; (c) discovery of the open-charm decays of the $Z_c(3900)$ [59]; (d) discovery of the open-charm decays of the $Z_c(4020)$ [60]; (e) observation of $Y(4260) \to \pi^+\pi^- J/\psi$ [61]; (f) discovery of two peaks in $e^+e^- \to \pi^+\pi^- h_c$ [63]; (g) discovery of a peak in $e^+e^- \to \omega\chi_{c0}$ [64]; (h) discovery of $e^+e^- \to \gamma X(3872)$ [45].

(1) The Y problem

Exclusive e^+e^- cross-sections have shown surprisingly complex behavior as a function of cms energy. The $Y(4260)$ is more complex than a single ordinary resonance, as shown by the complicated line shape of the $e^+e^- \to \pi^+\pi^- J/\psi$ cross-section in Fig. 3.10(e); the $Y(4360)$ and $Y(4660)$ are seen in $e^+e^- \to \pi^+\pi^-\psi(3686)$; two other peaks are seen in $e^+e^- \to \pi^+\pi^- h_c$ in Fig. 3.10(f); the $Y(4220)$ is seen in $e^+e^- \to \omega\chi_{c0}$ in Fig. 3.10(g), etc. A summary of the masses and widths of resonances extracted from recent BESIII results is shown in Fig. 3.11. There is currently very little consistency between different reactions. Furthermore, none of these complicated features are apparently present in the inclusive e^+e^- cross-section, which only shows evidence of the $\psi(3770)$, $\psi(4040)$, $\psi(4160)$, and $\psi(4415)$ [65]. This is the "Y" problem. Are the many peaks seen in the e^+e^- cross-sections really new states? Or are they the results of more subtle effects? With new data, will new patterns emerge? What are their exact line shapes? Will they match theoretical predictions, such as a very asymmetric line shape of the Y(4260) obtained in the molecular frame [55]? With limited number of data points (cms energies), there is little hope of resolving the issue. We require (1) more data for a variety of cms energies, and (2) a global and simultaneous analysis of many final states. The latter effort will likely require close collaboration with the theory community, in particular in view of amplitude analysis.

(2) The Z problem

BESIII discovered the $Z_c(3900)$ in the $e^+e^- \to \pi^+\pi^- J/\psi$ events at a single cms energy of 4.26 GeV, as shown in Fig. 3.10(a). Higher-energy data, however, revealed more complex structures. There is a similar situation in $e^+e^- \to \pi^+\pi^-\psi(3686)$, where the lower-energy data appear relatively simple, but the Dalitz plots at higher energies are more complex [66]. This is the "Z" problem. How do the Z_c structures produced in e^+e^- annihilation change as a function of the e^+e^- cms energy? Will their properties remain constant, as would be expected for a true resonance, or will their properties change, which would indicate a discovery of other effects (which are also important to study)? Again, BESIII is in a unique position to address this problem. Again, we require large data sets at a variety of energies, and we require closer cooperation with the theory community.

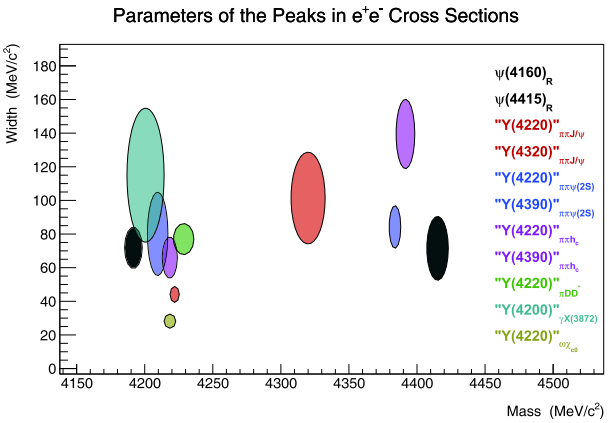

Fig. 3.11. (color online) A collection of resonance parameters as determined from fits to e^+e^- cross sections. Each ellipse encloses 1σ around the measurements of resonance parameters, where the size of the ellipses are determined by adding together the statistical and systematic uncertainties in quadrature. The parameters are from inclusive hadronic cross sections [65]; $\pi^+\pi^- J/\psi$ [61]; $\pi^+\pi^-\psi(3686)$ [66]; $\pi^+\pi^- h_c$ [63]; $\pi D\bar{D}^* + c.c.$ [67]; $\gamma X(3872)$ [68]; and $\omega\chi_{c0}$ [69].

Using the existing data samples, BESIII has successfully determined the quantum numbers of the $Z_c(3900)$ as $J^P = 1^+$ [70]. However, the data samples have so far been insufficient to measure the phase of the $Z_c(3900)$ with respect to the other amplitudes present in $e^+e^- \to \pi^+\pi^- J/\psi$. Such an effort to measure the Argand diagram for the $Z_c(3900)$ is currently being explored. Determining the line shape of $Z_c(3900)$ and studying its phase motion would allow to distinguish between different models of the nature of the $Z_c(3900)$ [71]. There are at least two challenges. First, a larger data sample at a single cms energy is required. Second, and perhaps more importantly, we must understand all the other resonances that are present in the $\pi^+\pi^- J/\psi$ Dalitz plots. The measurement of the phase of the $Z_c(3900)$ (and even the magnitude of its amplitude) is only as good as our understanding of the parametrization of the rest of the Dalitz plot. This is a challenging issue.

Another route for understanding the nature of the $Z_c(3900)$ would be to look for patterns of other Z_c states. BESIII has already discovered the $Z_c(4020)$, which seems to indicate that the $D\bar{D}^*$ and $D^*\bar{D}^*$ thresholds play an important role in the properties of Z_c. Another important subject may be the putative strange hidden-charm states, like Z_{cs}, where the up or down quark in Z_c is replaced with a strange quark. If a Z_{cs} state exists, perhaps decaying to KJ/ψ, this would provide another crucial handle for the nature of Z_c states. To search for heavier Z_{cs} states, larger samples of higher-energy data will be required.

(3) The X problem

The interpretation of the $X(3872)$ is intimately related to the problem of determining the parameters of the conventional $2P$ $c\bar{c}$ states – the spin-triplet $\chi_{cJ}(2P)$ and the spin-singlet $h_c(2P)$. This is because the $X(3872)$ with $J^{PC} = 1^{++}$ certainly contains some admixture of the $\chi_{c1}(2P)$ state. Sorting out the spectrum of states in this region, and determining which are exotic and which are conventional and how they mix, is the "X" problem.

One important piece of information in the program of sorting out the $2P$ states is the mass of the $h_c(2P)$. Once

this state is found, it will indicate where the $\chi_{cJ}(2P)$ states are located. Then the states deviating from this pattern can be identified as exotic. Since there is clear evidence of $e^+e^- \to \pi^+\pi^-\psi(1S,2S)$ and $\pi^+\pi^-h_c(1P)$ at BESIII, one also expects to produce the $\pi^+\pi^-h_c(2P)$. Search is underway, but larger data sets at higher cms energies are needed.

At least in principle, BESIII also has access to a variety of other X states via radiative transitions $e^+e^- \to \gamma X$, in a similar way that the $X(3872)$ is produced. This is being used, for example, to search for the $X(3915)$ in the process $e^+e^- \to \gamma\omega J/\psi$, and to search for the $X(4140)$ in $e^+e^- \to \gamma\phi J/\psi$.

3.3.3 Possibilities for *XYZ* data taking

The X, Y and Z problems are all Tier A physics priorities for the charmonium group. All could benefit from additional data sets. Three qualitatively different types of data taking plans are discussed below, each targeting different topics.

(1) High-statistics scan from 4.0 to 4.6 GeV

To study the Y problem, we need a detailed scan of the cross-sections between 4.0 and 4.6 GeV. The range is chosen in order to study a wide range of channels, important to achieve a more global picture of this region. We propose 500 pb^{-1} per energy point, and points spaced in intervals of 10 MeV. The intervals were chosen to cover the possibility of narrow features – the narrowest of the *XYZ* states discovered by BESIII is currently the $Z_c(4020)$ with a width of 7 MeV, and the $\pi\pi J/\psi$ cross-section shows rapid changes between 4.20 and 4.23 GeV. Other cross-sections are likely to include other rapidly changing features. A series of simulations are shown in Fig. 3.12. The background rates and efficiencies are based on the existing data. The cross-section shapes are only guesses; they need to be measured. Statistical fluctuations are not included. The error bars, however, are reliable estimates. The top part of Table 3.2 shows the precision with which cross-sections could be measured for a few select channels at 4.30 GeV.

This high-statistics scan would also allow to study the way the Z_c states evolve with cms energy. Changes in the shape of the peaks and/or their production cross-sections would provide clues about the nature of Z_c. By combining data sets at different cms energies, we could also better explore the X problem.

(2) A series of higher-statistics points

For the Z problem, especially for the detailed studies of the Argand diagrams, we require very high statistics samples at a few points. We currently have 1 e^+e^- of data at the e^+e^- cms energy of 4.42 GeV. For the $\pi\pi J/\psi$ channel, this is not sufficient to definitely resolve the substructure. We require of the order of 5 fb^{-1} per point to have adequate statistics for an unambiguous analysis of the Dalitz plot. Three or four of these high-statistics points would likely reveal the nature of the energy dependence of the Dalitz plot. A working group is studying the substructure in the various channels using the 4.42 GeV data. As the working group progresses, the requirements for the future data taking will become clearer. The lower part of Table 3.2 lists the expected number of events for a few channels given future 5 fb^{-1} data samples.

(3) Possibilities for data above 4.6 GeV

If BESIII could provide data above 4.6 GeV, a number of new exciting possibilities would become accessible. Here we list five cases. (1) We know that there is an unexplained peak at 4.66 GeV in the $e^+e^- \to \pi^+\pi^-\psi(3686)$ cross-section. BESIII would be able to produce and study it directly. (2) We could also study the peak at 4.63 GeV in the $\Lambda_c^+\bar{\Lambda}_c^-$ cross-section. (3) We could search for new peaks; it seems likely that not only these two exist. These three goals would extend our study of the Y problem. (4) Production of a Z_{cs} tetraquark candidate in the process $e^+e^- \to KZ_{cs}$ with $Z_{cs} \to KJ/\psi$ would require cms energies above 4.6 GeV if Z_{cs} is near the $D_s\bar{D}^*$ or $D_s^*\bar{D}$ threshold. (5) Data significantly above 4.6 GeV provide access to additional charmed baryon thresholds. BESIII would thus be able to study charmed baryons in a uniquely clean environment. (6) Data above 4.6 GeV would provide a unique opportunity to search for the excited 1^{+-} h_c state, expected to be around 3.9 GeV as shown in $e^+e^- \to \eta D\bar{D}^*$. The identification of this state would likely help clarify many of the J^{++} states between 3.8 and 4.0 GeV.

Table 3.2. Requirements for *XYZ* data taking for a few select channels.

channel	data plan	luminosity	cross-section precision	# of events
$\pi^+\pi^-J/\psi$	(1)	500 pb^{-1} at 4.30 GeV	3%	1270
$\pi^+\pi^-h_c(1P)$	(1)	500 pb^{-1} at 4.30 GeV	9%	220
$\eta J/\psi$	(1)	500 pb^{-1} at 4.30 GeV	30%	28
$\pi^+\pi^-\psi(3686)$	(1)	500 pb^{-1} at 4.30 GeV	3%	230
$\pi^+\pi^-J/\psi$	(2)	5 fb^{-1} at 4.23 GeV	<1%	18k
$\pi^+\pi^-J/\psi$	(2)	5 fb^{-1} at 4.42 GeV	3%	3k
$\pi^+\pi^-\psi(3686)$	(2)	5 fb^{-1} at 4.42 GeV	2%	4k

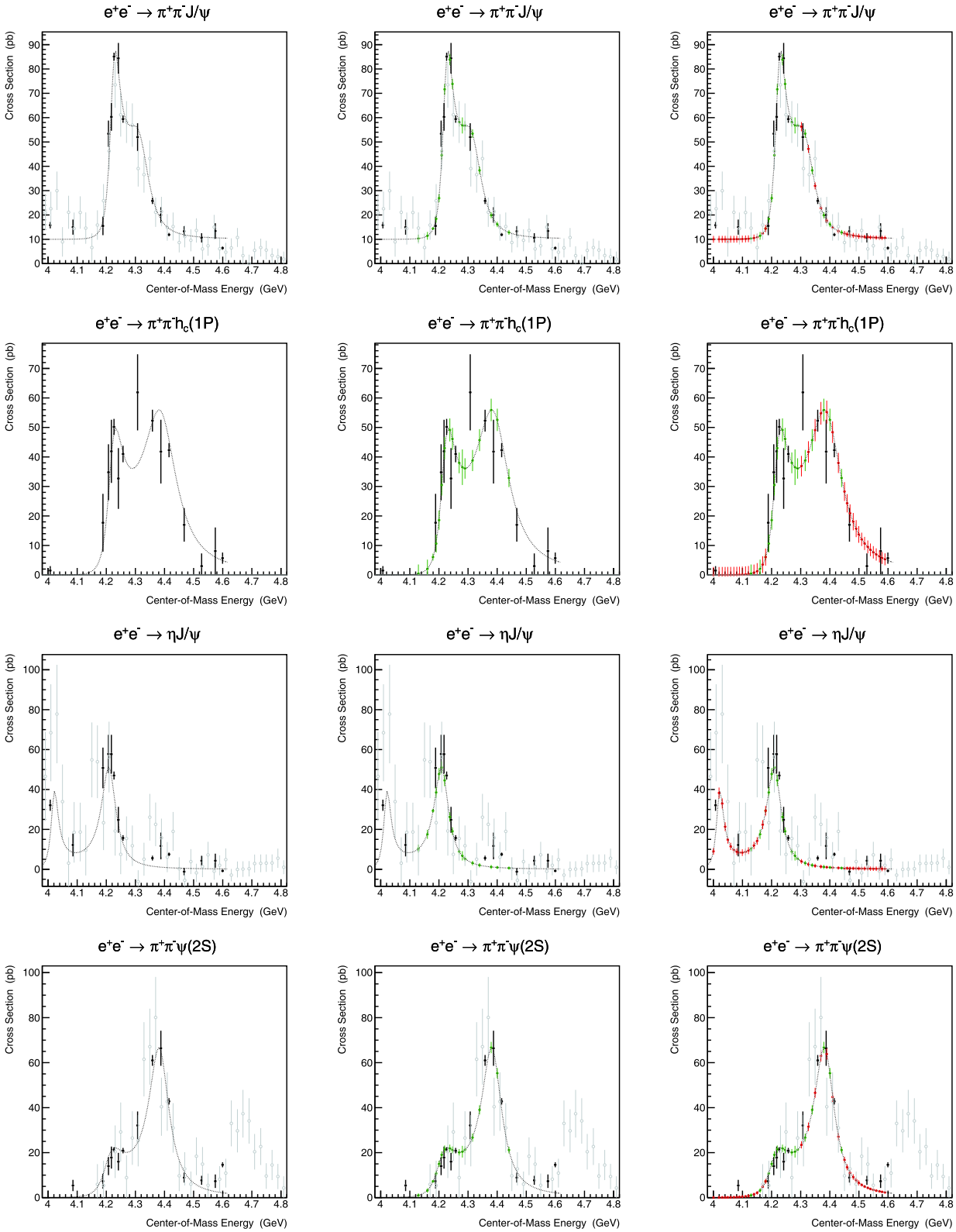

Fig. 3.12. (color online) Simulations of the different exclusive e^+e^- cross-sections. The black points are already measured (before 2019); the green points are projections for 2019; the red points are projections for the proposal from 4.0 to 4.6 GeV, and the gray points are from Belle. The top row shows $e^+e^- \to \pi^+\pi^- J/\psi$; the second row shows $e^+e^- \to \pi^+\pi^- h_c$; the third row shows $e^+e^- \to \eta J/\psi$; the bottom row shows $e^+e^- \to \pi^+\pi^-\psi(3686)$.

3.3.4 Comparisons with other experiments

Belle II [72] started collecting data in 2019, and will accumulate 50 ab^{-1} data at the $\Upsilon(4S)$ peak by 2027. These data samples can be used to study the *XYZ* and charmonium states in many different ways [73], among which ISR can produce events in the same energy range covered by BESIII. Figure 3.13 shows the effective luminosity at the BEPCII energy in the Belle II data samples. We can see that 50 ab^{-1} of Belle II data correspond to 2000–2800 pb^{-1} for each 10 MeV interval between 4–5 GeV. Similar statistics will be accumulated for the modes like $e^+e^- \to \pi^+\pi^- J/\psi$ at Belle II and BESIII, taking into account the fact that Belle II has lower efficiency.

Table 3.3 lists the expected ratio of number of events at BESIII and Belle II given the BESIII data set with 500 pb^{-1} per point and the Belle II sample of 50 ab^{-1}. Belle II has the advantage that data at different energies will be accumulated at the same time, making the analysis simpler than the BESIII scans over many data points. On the other hand, Belle II needs to integrate over large energy bins, while the BESIII data are collected at individual energy points with an energy spread of around 2 MeV.

The LHCb experiment has also made a large contribution to our understanding of the *XYZ* mesons. The strength of LHCb for studies of *B* decays to final states where all particles are charged cannot be matched by the e^+e^- facilities. For example, LHCb has made a precision measurement of the $X(3872)$ in the process $B \to KX$ with $X \to \pi^+\pi^- J/\psi$ and $J/\psi \to \mu^+\mu^-$ [74]. The discovery of the process $B \to KY(4260)$ with $Y(4260) \to \pi Z_c(3900)$ at D0 [75, 76] may give LHCb an opportunity to study the $Y(4260)$ and $Z_c(3900)$ in detail. However, since most of the *XYZ* particles decay to final states with neutral particles, the LHCb experiment is mostly complementary to the BESIII experiment. In contrast to BESIII, LHCb does not feature a high quality electromagnetic calorimeter. Thus, the identification of soft neutral pions and photons is difficult.

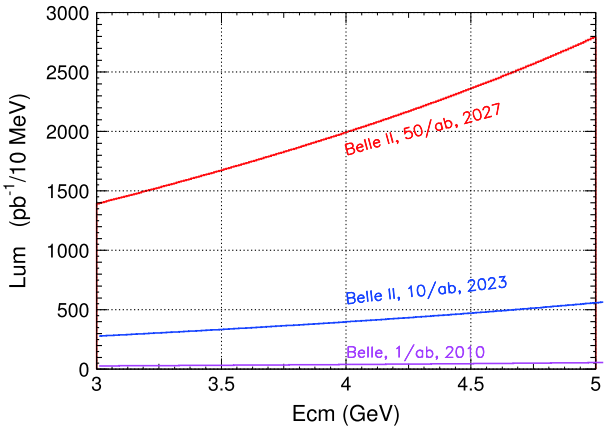

Fig. 3.13. (color online) Effective luminosity at the low energy in the Belle and BelleII $\Upsilon(4S)$ data samples.

Finally, it should be noted that all three experiments have rather different systematics, which emphasizes their complementarity.

3.4 Summary of data requirements

Our data taking requirements are summarized in Table 3.4. Sensitivities to various channels in *XYZ* physics are given in Table 3.2; sensitivities to charmonium studies are listed in Table 3.1.

Table 3.3. A comparison of BESIII and Belle II for various channels at a few e^+e^- cms energies assuming 50 ab^{-1} of Belle II data in 10 MeV energy bins. *L* and *N* denote the expected luminosity and the number of observed events.

ISR mode	$L_{\rm BESIII}/L_{\rm Belle\ II}$	$\varepsilon_{\rm BESIII}/\varepsilon_{\rm Belle\ II}$	$N_{\rm BESIII}/N_{\rm Belle\ II}$
$\pi^+\pi^- J/\psi$ at 4.26 GeV	0.5 fb^{-1}/2.2 fb^{-1}	46%/10%	1.07
$\pi^+\pi^-\psi(3686)$ at 4.36 GeV	0.5 fb^{-1}/2.3 fb^{-1}	41%/5%	1.82
$\pi^+\pi^-\psi(3686)$ at 4.66 GeV	0.5 fb^{-1}/2.5 fb^{-1}	35%/6%	1.19
$\pi^+\pi^- h_c$ at 4.26 GeV	0.5 fb^{-1}/2.2 fb^{-1}	2.7%/-%	>5
$K^+K^- J/\psi$ at 4.6 GeV	0.5 fb^{-1}/2.4 fb^{-1}	29%/7.5%	0.81
$K^+K^- J/\psi$ at 4.9 GeV	0.5 fb^{-1}/2.7 fb^{-1}	≈29%/10%	0.54
$\Lambda_c^+\bar{\Lambda}_c^-$ at 4.6 GeV	0.5 fb^{-1}/ 2.4 fb^{-1}	51%/7.5%	1.42
$\Lambda_c^+\bar{\Lambda}_c^-$ at 4.9 GeV	0.5 fb^{-1}/2.7 fb^{-1}	≈37%/7.5%	0.91

Table 3.4. Data taking requirements for *XYZ* physics and charmonium physics.

plan	data sets
XYZ plan (1)	500 pb^{-1} at a large number of points between 4.0 and 4.6 GeV
XYZ plan (2)	5 fb^{-1} at 4.23, 4.42 GeV for large Z_c samples
XYZ plan (3)	5 fb^{-1} above 4.6 GeV
charmonium plan	3×10^9 $\psi(3686)$ decays

References

1 T. Appelquist and H.D. Politzer, Phys. Rev. Lett., **34**: 43 (1975)
2 T. Barnes, S. Godfrey, and E. S. Swanson, Phys. Rev. D, **72**: 054026 (2005)
3 G. K. C. Cheung *et al.* (Hadron Spectrum Collaboration), JHEP, **1612**: 089 (2016)
4 K. A. Olive *et al*. (Particle Data Group), Chin. Phys. C, **38**: 090001 (2014) and 2015 update
5 M. Tanabashi *et al*. (Particle Data Group), Phys. Rev. D, **98**: 030001 (2018)
6 G. Pakhlova *et al*. (Belle Collaboration), Phys. Rev. Lett., **101**: 172001 (2008)
7 X. L. Wang *et al*. (Belle Collaboration), Phys. Rev. Lett., **99**: 142002 (2007)
8 W. E. Caswell and G. P. Lepage, Phys. Lett. B, **167**: 437 (1986)
9 G. P. Lepage, L. Magnea, C. Nakhleh *et al*., Phys. Rev. D, **46**: 4052 (1992)
10 G. T. Bodwin, E. Braaten, and G. P. Lepage, Phys. Rev. D, **51**: 1125 (1995); Erratum: [Phys. Rev. D, **55**: 5853 (1997)]
11 Alexey A. Petrov, Andrew E. Blechman, "Effective Field Theories", World Scientific Publishing Company Pte Limited, 2015, ISBN 9789814434935
12 A. Pineda and J. Soto, Nucl. Phys. Proc. Suppl., **64**: 428 (1998)
13 N. Brambilla, A. Pineda, J. Soto *et al*., Nucl. Phys. B, **566**: 275 (2000)
14 N. Brambilla, A. Pineda, J. Soto *et al*., Rev. Mod. Phys., **77**: 1423 (2005)
15 Y. P. Kuang, Front. Phys. China, **1**: 19 (2006)
16 N. Brambilla *et al*. (Quarkonium Working Group), arXiv:hep-ph/0412158
17 M. E. B. Franklin *et al*., Phys. Rev. Lett., **51**: 963 (1983)
18 M. Ablikim *et al*. (BESIII Collaboration), Phys. Rev. Lett., **104**: 132002 (2010)
19 M. Ablikim *et al*. (BESIII Collaboration), Phys. Rev. Lett., **107**: 092001 (2011)
20 M. Ablikim *et al*. (BESIII Collaboration), Phys. Rev. Lett., **108**: 222002 (2012)
21 M. Ablikim *et al*. (BESIII Collaboration), Phys. Rev. Lett., **109**: 042003 (2012)
22 M. Ablikim *et al*. (BESIII Collaboration), Phys. Rev. Lett., **116**: 251802 (2016)
23 http://english.ihep.cas.cn/chnl/245/index.html
24 M. Ablikim *et al*. (BESIII Collaboration), Phys. Rev. D, **99**: 072008 (2019)
25 D. M. Asner *et al*., Int. J. Mod. Phys. A, **S1**: 24 (2009)
26 M. Ablikim *et al*. (BESIII Collaboration), Phys. Rev. D, **87**: 012002 (2013)
27 Y. J. Gao, Y. J. Zhang, and K. T. Chao, Chin. Phys. Lett., **23**: 2376 (2006)
28 F. Feng, Y. Jia, and W. L. Sang, Phys. Rev. Lett., **115**: 222001 (2015)
29 F. Feng, Y. Jia, and W. L. Sang, Phys. Rev. Lett., **119**: 252001 (2017)
30 M. Ablikim *et al*. (BESIII Collaboration), Phys. Rev. Lett., **105**: 261801 (2010)
31 K. Zhu, X. H. Mo, and C. Z. Yuan, Int. J. Mod. Phys. A, **30**: 1550148 (2015)
32 M. Ablikim *et al*. (BESIII Collaboration), Phys. Rev. D, **88**: 112001 (2013)
33 N. A. Tornqvist, Phys. Lett. A, **117**: 1 (1986)
34 L. Kopke, talk presented at XXIIrd Intern Conf. on High Energy Physics, Berkeley, USA, 1986
35 X. G. He, J. P. Ma, and B. McKellar, Phys. Rev. D, **47**: 1744(R) (1993)
36 X. G. He, J. P. Ma, and B. McKellar, Phys. Rev. D, **49**: 4548 (1994)
37 M. Ablikim *et al*. (BESIII Collaboration), Phys. Rev. Lett., **115**: 011803 (2015)
38 R. F. Lebed, R. E. Mitchell, and E. S. Swanson, Prog. Part. Nucl. Phys., **93**: 143 (2017)
39 H. X. Chen, W. Chen, and X. Liu, Phys. Rept., **639**: 1 (2016)
40 A. Esposito, A. Pilloni, and A. D. Polosa, Phys. Rept., **668**: 1 (2016)
41 F.-K. Guo, C. Hanhart, and U.-G. Meißner, Rev. Mod. Phys., **90**: 015004 (2018)
42 A. Ali, J. S. Lange, and S. Stone, Prog. Part. Nucl. Phys., **97**: 123 (2017)
43 S. L. Olsen, T. Skwarnicki, and D. Zieminska, Rev. Mod. Phys., **90**: 015003 (2018)
44 S. K. Choi *et al*. (Belle Collaboration), Phys. Rev. Lett., **91**: 262001 (2003)
45 M. Ablikim *et al*. (BESIII Collaboration), Phys. Rev. Lett., **112**: 092001 (2014)
46 F.-K. Guo, C. Hanhart, U.-G. Meißner *et al*., Phys. Lett. B, **725**: 127 (2013)
47 K. Abe *et al*. (Belle Collaboration), Phys. Rev. Lett., **94**: 182002 (2005)
48 K. Chilikin *et al*. (Belle Collaboration), Phys. Rev. D, **95**: 112003 (2017)
49 F.-K. Guo and U.-G. Meißner, Phys. Rev. D, **86**: 091501 (2012)
50 F.-K. Guo, U.-G. Meißner, and Z. Yang, Phys. Lett. B, **740**: 42 (2015)
51 B. Aubert *et al*. (BaBar Collaboration), Phys. Rev. Lett., **95**: 142001 (2005)
52 L. Liu *et al*. (Hadron Spectrum Collaboration), JHEP, **1207**: 126 (2012)
53 F. E. Close and P. R. Page, Phys. Lett. B, **628**: 215 (2005)
54 Q. Wang, C. Hanhart, and Q. Zhao, Phys. Rev. Lett., **111**: 132003 (2013)
55 M. Cleven, Q. Wang, and F. K. Guo *et al*., Phys. Rev. D, **90**: 074039 (2014)
56 M. Ablikim *et al*. (BESIII Collaboration), Phys. Rev. Lett., **110**: 252001 (2013)
57 M. Ablikim *et al*. (BESIII Collaboration), Phys. Rev. Lett., **111**: 242001 (2013)
58 S. K. Choi *et al*. (Belle Collaboration), Phys. Rev. Lett., **100**: 142001 (2008)

59 M. Ablikim *et al*. (BESIII Collaboration), Phys. Rev. Lett., **112**: 022001 (2014)
60 M. Ablikim *et al*. (BESIII Collaboration), Phys. Rev. Lett., **112**: 132001 (2014)
61 M. Ablikim *et al*. (BESIII Collaboration), Phys. Rev. Lett., **118**: 092001 (2017)
62 M. Ablikim *et al*. (BESIII Collaboration), Phys. Rev. Lett., **115**: 112003 (2015)
63 M. Ablikim *et al*. (BESIII Collaboration), Phys. Rev. Lett., **118**: 092002 (2017)
64 M. Ablikim *et al*. (BESIII Collaboration), Phys. Rev. Lett., **114**: 092003 (2015)
65 M. Ablikim *et al.* (BES Collaboration), eConf C 070805, 02 (2007) [Phys. Lett. B, **660**: 315 (2008)]
66 M. Ablikim *et al*. (BESIII Collaboration), Phys. Rev. D, **96**: 032004 (2017)
67 M. Ablikim *et al*. (BESIII Collaboration), Phys. Rev. Lett., **122**: 102002 (2019)
68 M. Ablikim *et al*. (BESIII Collaboration), Phys. Rev. Lett., **122**: 232002 (2019)
69 M. Ablikim *et al*. (BESIII Collaboration), Phys. Rev. D, **99**: 091103 (2019)
70 M. Ablikim *et al*. (BESIII Collaboration), Phys. Rev. Lett., **119**: 072001 (2017)
71 E. S. Swanson, Int. J. Mod. Phys. E, **25**: 1642010 (2016)
72 T. Abe *et al*. (Belle II Collaboration), arXiv:1011.0352 [physics.ins-det]; E. Kou et al, (Belle-II Collaboration), PTEP, **2019**: 123C01 (2019)
73 A. J. Bevan *et al*. (BaBar and Belle Collaborations), Eur. Phys. J. C, **74**: 3026 (2014)
74 R. Aaij *et al*. (LHCb Collaboration), Phys. Rev. D, **92**: 011102 (2015)
75 V. M. Abazov *et al*. (D0 Collaboration), Phys. Rev. D, **98**: 052010 (2018)
76 V. M. Abazov *et al*. (D0 Collaboration), Phys. Rev. D, **100**: 012005 (2019)

Chapter 4

R values, QCD and τ physics

4.1 Introduction

The *R*-QCD-τ working group studies various aspects of QCD, the accepted theory of strong interactions in the Standard Model of particle physics. The cms energy of BEPCII is ideally suited to study the transition region between non-perturbative and perturbative aspects of QCD [1]. It offers a unique laboratory for testing not only the validity of QCD in the few-GeV energy range, but also the validity of effective theories and hadronic models at higher energies.

BESIII has already demonstrated that the high statistics and accuracy of the data, illustrated in Fig. 4.1, allow to measure form factors of mesons and baryons with unprecedented accuracy, with a paramount impact on hadron structure investigation. These form factors are not only accessible in the time-like domain via electron-positron annihilations, but can also be determined in the space-like domain in two-photon scattering.

As is well known, the measurement of electron-positron annihilation into hadrons is of the utmost importance for precision tests of SM. While the measurement of exclusive hadronic channels is needed for the hadronic vacuum polarization contribution to the anomalous magnetic moment of the muon, $(g-2)_\mu$, the inclusive measurement of the hadronic cross-section above 2 GeV can be used to improve the knowledge of the fine structure constant at the *Z*-pole. The latter is currently limiting the precision tests in the electroweak sector of SM. Thus, its improvement is of central importance for the physics programs at the future high-energy electron-positron colliders, such as the Higgs factories [2, 3]. The exclusive channels can be measured by BESIII via the initial state radiation (ISR) technique, while the accuracy of the inclusive *R*-measurement will be further improved with respect to measurements by BES and KEDR. Regarding $(g-2)_\mu$, BESIII can also measure the transition form factors of pseudoscalar mesons, motivated by the hadronic light-by-light scattering contribution to $(g-2)_\mu$.

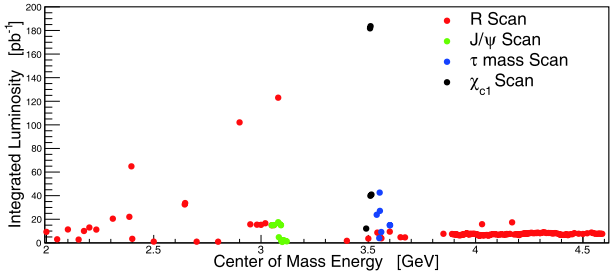

Fig. 4.1. (color online) Overview of the data sets and integrated luminosities analyzed by the *R*-QCD-τ working group. *R* scan data (red) were collected from 2012-2015, the J/ψ line shape scan (green) was performed in 2012, a search for the production of χ_{c1} (black) was carried out in 2017, and the latest τ mass scan data (blue) were acquired in 2018.

The analysis of the high-statistics energy scan between 2.0 and 4.6 GeV allows a first precision measurement of the neutron and hyperon form factors. In the case of hyperons, their self-analyzing decay does not only provide access to the absolute values of the electric and magnetic form factors, but allows also to extract the relative phase between them. A complementary view on hadron structure is possible via the measurement of the Collins asymmetries. The recent result obtained by BESIII extends the previously available knowledge, which was restricted to measurements at *B* factories, towards lower energies. The picture of the non-perturbative features of QCD can be further extended by the investigation of fragmentation functions.

Naturally, the research program of the τ-QCD working group comprises measurements of such fundamental parameters of SM as the mass of the τ lepton. It can be determined via an energy scan in the threshold region. The first result by BESIII is already the most precise measurement in the world. Further improvement is expected with new data. Moreover, the mass of the charm quark is accessible by determining the cross-section of $e^+e^- \to c\bar{c}$, which relates the physics of hadronic cross-section measurements to yet another precision observable of SM.

Finally, the precise measurements of the *R* value and the τ mass allow detailed investigation of the production of charmonium resonances. The line shape of vector charmonium resonances might reveal, using the relative phase of strong and electromagnetic decay amplitudes, a more detailed picture of their internal structure. Even the production of non-vector resonances, like χ_{c1} in e^+e^- annihilation, might be observed via interference patterns with the continuous background. Another exciting spin-off of the BESIII *R* program is the investigation of the light hadron spectrum, enabling studies of potentially exotic resonances, such as $\phi(2170)$.

4.2 BESIII measurements related to precision variables $(g-2)_\mu$ and $\alpha_{\rm em}(s)$

4.2.1 The anomalous magnetic moment of the muon $(g-2)_\mu$

At present, the SM prediction and the experimental

value of the anomalous magnetic moment of the muon, $a_\mu = (g-2)_\mu/2$ [4], are determined with a relative uncertainty of about one half part per million:

$$a_\mu^{\rm SM} = (11\,659\,182.04 \pm 3.56)\times 10^{-10} \quad \text{[Keshavarzi et al.] [5]}, \tag{4.1}$$

$$a_\mu^{\rm exp} = (11\,659\,208.9\ \pm 6.3)\times 10^{-10} \quad \text{[BNL}-\text{E821] [6]}. \tag{4.2}$$

A second evaluation of $a_\mu^{\rm SM}$ by Davier et al. resulted in $a_\mu^{\rm SM} = (11\,659\,182.3 \pm 4.3)\times 10^{-10}$ [7]. Depending on the value used for $a_\mu^{\rm SM}$, a difference of $3.5-3.7$ standard deviations between the SM prediction and the direct measurement of a_μ is observed, as illustrated in Fig. 4.2.

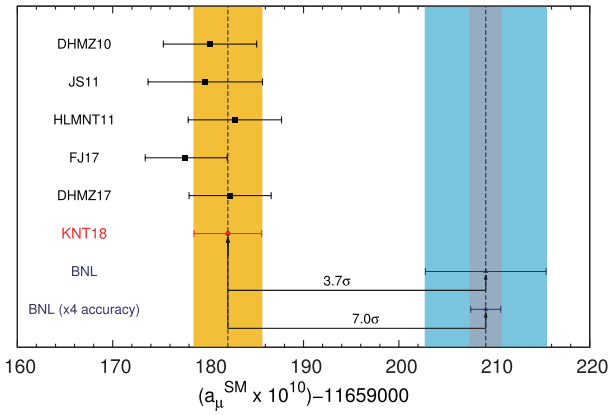

Fig. 4.2. (color online) Compilation of recent results for $a_\mu^{\rm SM}$ (figure taken from Ref. [5]). The "DHMZ17" and "KNT18" points correspond to Refs. [7] and [5], respectively. Also shown is the accuracy of the upcoming FNAL measurement of $a_\mu^{\rm exp}$ with the assumption that the central mean value of $a_\mu^{\rm exp}$ remains unchanged.

Currently, the SM prediction of a_μ is slightly more precise than the experimental value, but the situation will change soon [8]. New direct measurements have started at FNAL [9] and a complementary project is under construction at J-PARC [10]. Both aim to reduce the experimental uncertainty by a factor of four. The light grey band in Fig. 4.2 represents the hypothetical situation that the new FNAL measurement yields the same mean value for $a_\mu^{\rm exp}$ with fourfold improved accuracy.

The main uncertainties in $a_\mu^{\rm SM}$ originate from hadronic effects, in particular the contributions of the hadronic vacuum polarization (HVP), $a_\mu^{\rm HVP}$, and the hadronic light-by-light scattering (HLbL), $a_\mu^{\rm HLbL}$, as shown in Fig. 4.3. It is of vital importance to investigate whether physics models beyond SM [11], or poorly understood hadronic effects, are responsible for the observed difference. This is one of the main goals of the R-QCD research program.

The current estimate of $a_\mu^{\rm HVP}$, which enters the SM prediction, is based on the dispersion theory, in which the

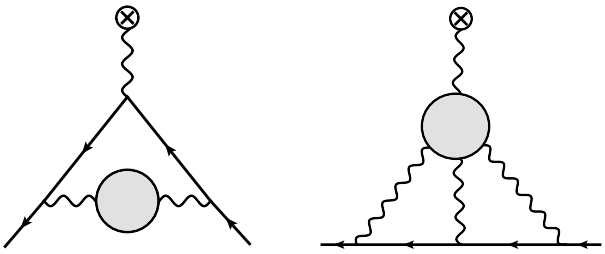

Fig. 4.3. (color online) The HVP (left panel) and HLbL (right panel) contributions to the anomalous magnetic moment of the muon.

experimental measurements of the annihilation cross-section $e^+e^- \to$ hadrons are used as input for the evaluation of the dispersion integral:

$$a_\mu^{\rm HVP} = \left(\frac{\alpha m_\mu}{3\pi}\right)^2 \int_{4m_\pi^2}^{\infty} {\rm d}s \frac{R_{\rm had}(s)K(s)}{s^2}, \tag{4.3}$$

where $K(s)$ is a kernel varying from 0.63 at $s = 4m_\pi^2$ to 1.0 at $s = \infty$, and $m_\mu(m_\pi)$ is the nominal mass of the pion (muon).

In Ref. [5], the leading order hadronic contribution was calculated as $a_\mu^{\rm HVP} = (684.68 \pm 2.42)\times 10^{-10}$. At BESIII, we are aiming at a further reduction of the uncertainty of $a_\mu^{\rm HVP}$ by measuring the exclusive channels of $R_{\rm had}$ in the most relevant energy range. Figure 4.4 shows the contributions of various exclusive hadronic channels to the absolute value (left) and the uncertainty (right) of $a_\mu^{\rm HVP}$. As can be seen, the channels with $\pi^+\pi^-$, $\pi^+\pi^-\pi^0$, $\pi^+\pi^-\pi^0\pi^0$, and $K\bar{K}$ are the most relevant, and the current efforts at BESIII are precisely focused on these channels. A major program of hadronic cross-section measurements, which is presented in detail in Sec. 4.2.3, has been launched.

Beyond HVP, the next important contribution to the uncertainty of $(g-2)_\mu$ is the HLbL contribution, shown in the right panel of Fig. 4.3. The leading contribution in the HLbL diagram is the coupling of photons to pseudoscalar mesons π^0, η, η', as well as the channels $\pi\pi$ and $\pi\eta$, as shown in Fig. 4.9. So far, hadronic models have been used for the calculation of the HLbL diagram. Although most groups report similar absolute values of the HLbL contribution, the assumed uncertainties largely differ. The calculation with the lowest uncertainties is from Prades, de Rafael, and Vainshtein [12], who find $a_\mu^{\rm HLbL} = (10.5 \pm 2.6)\times 10^{-10}$.

Very recently, new theoretical approaches to calculate the HLbL contribution were proposed by the groups from Bern and Mainz [13-19] by exploiting the dispersion relations. Measurements of the form factor of the two-photon coupling $\gamma\gamma \to P$, where P is a one-hadron or two-hadron system, are of special interest. The Belle and BaBar collaborations have determined these couplings, referred to as meson TFF, for the lightest pseudoscalar

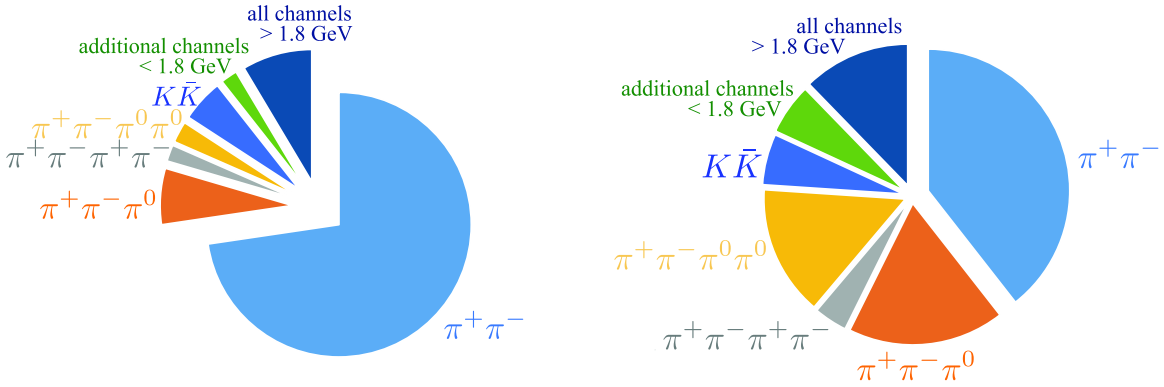

Fig. 4.4. (color online) Contributions of the different channels and energy ranges to the absolute value (left) and the uncertainty (right) of $a_\mu^{\rm HVP}$, demonstrating the importance of the processes $e^+e^- \to \pi^+\pi^-$, $e^+e^- \to \pi^+\pi^-\pi^0$, $e^+e^- \to \pi^+\pi^-2\pi^0$, and $e^+e^- \to K\bar{K}$ (numbers taken from Ref. [5]).

mesons. However, the results at the B-factories were only obtained for very large momentum transfers above 2 GeV, while measurements at low momentum transfers are required for the HLbL contribution. This is illustrated in Fig. 4.5, which shows the weight of the light pseudoscalar TFFs in the HLbL calculations [20] as a function of the two virtualities Q_1 and Q_2 of the photons. It can clearly be seen that the region of small momentum transfer is the most relevant. This is exactly where BESIII can provide precision results.

In summary, an improvement of the SM prediction of $(g-2)_\mu$ is urgently needed in view of the two upcoming direct measurements of a_μ at Fermilab and J-PARC with a fourfold improved precision. In the White Paper of 2013 [21], it was argued that new experiments, like the ones carried out at BESIII, should lead to a reduction of the SM uncertainty of a_μ down to 3.5×10^{-10}. Recent evaluations in Refs. [5, 7, 22] showed that such accuracy has almost been achieved. BESIII contributed to this achievement. The future program at BESIII, together with new analyses by BaBar, Belle II and elsewhere, will lead to an additional significant reduction. The midterm goal is to reduce the HVP and HLbL uncertainties to the level similar to the future experimental uncertainty, i.e. 1.6×10^{-10}. It should also be mentioned that since 2017 the theoretical and experimental work in view of $a_\mu^{\rm SM}$ is coordinated by the $g-2$ *Theory Initiative* [23], which is a consortium of theoretical and experimental physicists working towards an improved SM prediction. Members of the BESIII collaboration are part of this consortium.

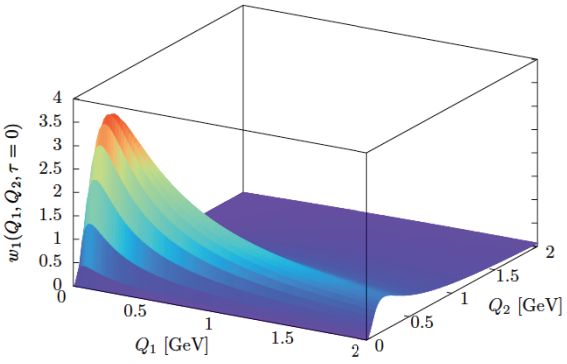

Fig. 4.5. (color online) Weight of the transition form factors of the lightest pseudoscalar mesons in the calculations of $a_\mu^{\rm HLbL}$ as a function of the virtualities of the two photons. Figure taken from Ref. [20].

4.2.2 The running of the electromagnetic fine structure constant, $\alpha_{\rm em}(s)$

Due to vacuum polarization effects, the electromagnetic fine structure constant $\alpha_{\rm em}$ is a "running" quantity. Its value increases with increasing momentum transfer s of the scattering process. The effective running of the fine structure constant as a function of s is usually parametrized in SM in the following way:

$$\alpha_{\rm em}(s) = \frac{\alpha(0)}{(1-\Delta\alpha_{\rm em}(s))}, \tag{4.4}$$

$$\Delta\alpha_{\rm em}(s) = \Delta\alpha_{\rm em}^{\rm lept}(s) + \Delta\alpha_{\rm em}^{\rm had(5)}(s) + \Delta\alpha_{\rm em}^{\rm top}(s). \tag{4.5}$$

In the above formula, $\Delta\alpha_{\rm em}^{\rm lept}$ denotes the vacuum polarization effects due to lepton loops, $\Delta\alpha_{\rm em}^{\rm had(5)}$ accounts for the effects due to loop contributions of the five lightest quarks, and the loop contributions due to the top quark are given by $\Delta\alpha_{\rm em}^{\rm top}$. The leptonic contribution can be computed in QED with very high precision, while the top-quark loop contribution is very small. Therefore, the total uncertainty of $\Delta\alpha_{\rm em}$ is entirely limited by $\Delta\alpha_{\rm em}^{\rm had(5)}$. As in the case of $(g-2)_\mu$, a dispersion relation can be used to relate experimental hadronic cross-section data with $\Delta\alpha_{\rm em}^{\rm had(5)}$.

Of special interest is the knowledge of $\Delta\alpha_{\rm em}$ for $s = M_Z^2$, since most of the electroweak precision tests have been performed at the Z^0 peak at LEP. The total correction to the fine structure constant amounts to [5]

$$\Delta\alpha_{\rm em}(M_Z^2) = (276.11 \pm 1.11) \times 10^{-4}, \quad (4.6)$$

and the value of $\alpha_{\rm em}$ at the Z pole mass is therefore

$$\alpha_{\rm em}^{-1}(M_Z^2) = 128.947 \pm 0.012. \quad (4.7)$$

A similar result, $\alpha_{\rm em}^{-1}(M_Z^2) = 128.946 \pm 0.015$, was found in Ref. [7]. The current uncertainty of $\Delta\alpha_{\rm em}$ is a severe limitation for the electroweak precision fits in SM (see the review of the electroweak model and constraints on new physics in Ref. [24]). Typically, these fits are performed using three independent input variables, such as $\alpha_{\rm em}(M_Z^2)$, the Fermi constant G_μ, and M_Z. Of these three quantities, $\alpha_{\rm em}(M_Z^2)$ is known with least precision. Its relative uncertainty is 1×10^{-4}, while G_μ and M_Z are known with uncertainties of 5×10^{-7} and 2×10^{-5}, respectively. In the past, insufficient knowledge of $\Delta\alpha_{\rm em}$ led to imprecise predictions of the Higgs mass. Now that the Higgs mass is known with high accuracy, any new precision measurement of an electroweak observable (for instance, of the electroweak mixing angle $\sin^2(\Theta_W)$) is a significant test of the electroweak SM. The smaller the uncertainty of $\Delta\alpha_{\rm em}(M_Z^2)$, the more powerful is the test. As discussed in Sec. 4.2.4, the goal of the new BESIII measurement is to reduce the uncertainty of the R measurement to 3%, which allows to improve the accuracy of the prediction of $\Delta\alpha_{\rm em}^{\rm had(5)}$.

4.2.3 Measurement of the exclusive hadronic channels via ISR

A major campaign of ISR [25-27] measurements was launched at BESIII, mainly in order to improve the HVP contribution to $(g-2)_\mu$ and to $\Delta\alpha_{\rm em}^{\rm had(5)}$. The ISR technique allows precision measurements of the hadronic cross-section at high-luminosity electron-positron colliders by using events in which either the incoming electron or positron has emitted a highly energetic photon. In this way, the available cms energy of the hadronic system varies depending on the energy of the ISR photon, which is the reason why the technique is also called Radiative Return.

From the measurement of the hadronic cross-section $\sigma(e^+e^- \to {\rm hadrons} + \gamma_{\rm ISR})$, the non-radiative cross-section $\sigma(e^+e^- \to {\rm hadrons})$ can be extracted using the radiator function from QED theory. This radiator function is known with a precision of 0.5% in the Monte Carlo (MC) generator PHOKHARA [28-30], which also simulates the most relevant exclusive final states in view of the HVP contribution to $(g-2)_\mu$.

At BESIII, the data set taken at the cms energy of 3.773 GeV is currently used for most of the ISR analyses. The total integrated luminosity at this energy is 2.9 fb^{-1}. Using this data set, the statistics of ISR hadronic events is larger than the ISR statistics of BaBar for hadronic masses above approximately 1.5 GeV. With upcoming new data, and including the already available data sets, the available ISR statistics will be similar to the BaBar statistics also for masses below 1.5 GeV.

Both the tagged and untagged ISR approaches are currently carried out at BESIII. The tagged approach requires explicit detection of the ISR photon in the calorimeter, and allows studies of the full hadronic mass range starting from the di-pion mass threshold. An untagged measurement corresponds to the usage of ISR events, in which the ISR photon is emitted at very small polar angles, essentially collinear with the electron beam. Although tagging of these photons is not feasible, the momentum information can be extracted from the missing momentum of the fully reconstructed hadronic system. For kinematic reasons, the untagged approach is limited to the energy of hadron production above approximately 1 GeV. Above 1.5 GeV, it provides significantly improved statistics compared to the tagged measurement, and furthermore, guarantees low background conditions.

The main results of the ISR program at BESIII can be summarized as follows:

- **Time-like pion form factor: $e^+e^- \to \pi^+\pi^-$**

A new measurement of the hadronic cross-section of the channel $e^+e^- \to \pi^+\pi^-$ was performed in the energy range between 600 and 900 MeV, which corresponds to the peak region of the $\rho(770)$ resonance [31]. In this energy range, the two-pion channel indeed contributes more than 50% to $a_\mu^{\rm HVP}$, and the uncertainty of this exclusive channel is therefore decisive for the SM error of $(g-2)_\mu$. Thus, this is the flagship analysis of the BESIII ISR program. A total systematic uncertainty of 0.9% for the cross-section measurement has already been achieved. The two limiting contributions to the total systematic uncertainty are from the luminosity measurement and the theoretical radiator function, with 0.5% each. As is discussed below, with improved calculations of the radiator function, by including larger data sets, and by an overall improved understanding of the detector performance, the errors of these contributions can be reduced from 0.5% to 0.2% each, yielding a reduced total systematic uncertainty. The mass range studied in this analysis is accessible via the tagged ISR approach only. The same holds for the mass range from the di-pion mass threshold to 600 MeV, which will be studied in the future, along with the mass range above 900 MeV, where the investigations can be performed in the untagged ISR approach as well.

In this analysis, the experimental detection efficiencies, the luminosity, as well as the knowledge of background channels, need to be determined at the per mil level. A separation of pion tracks from muon tracks turns out to be the major challenge of the analysis. As a consequence, a multivariate analysis technique is applied [32] by training an artificial neural network (ANN) for particle identification. If muon events are selected rather than pion events, the efficiency of the technique can be

tested by comparing the absolute yield of $e^+e^- \to \mu^+\mu^-\gamma$ events with the PHOKHARA [33] MC prediction. An agreement between the data and MC simulations at the level of $(0.5 \pm 0.3)\%$ was observed, demonstrating the excellent performance of ANN.

From the cross-section measurement, the time-like pion form factor $|F_\pi|$ is extracted, as shown in Fig. 4.6. An agreement between the BESIII data and the three KLOE analyses [34-36] is found up to the peak of the ρ resonance. In this mass range, the BESIII data are systematically lower than the BaBar results [37]. Above the ρ peak, the situation is reversed. In this case, the BESIII spectrum is in good agreement with BaBar, while the KLOE results are systematically lower. In Fig. 4.7, we show the impact of the new BESIII measurement on $a_\mu^{\rm HVP}$. It agrees with all three KLOE analyses in the mass range $600-900$ MeV, while deviations from the BaBar results are observed.

The good understanding of the radiative muon sample, which was achieved in this analysis, also led to two additional publications, which made use of the high statistics and quality of the muon data. In the first paper [38], the electronic width of the J/ψ resonance was determined with world-leading accuracy. In the second paper [39], a competitive dark photon limit was obtained by looking for an enhancement of events in the di-muon invariant mass between 1.5 and 3.4 GeV/c^2.

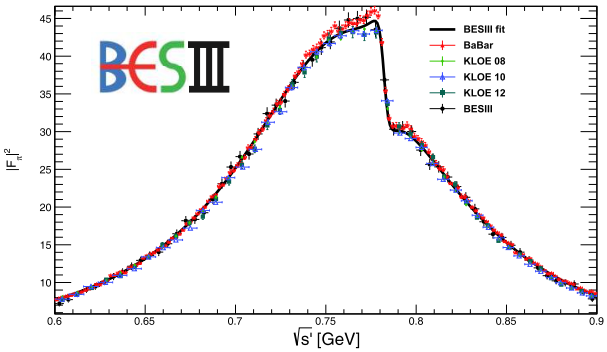

Fig. 4.6. (color online) Pion form factor measurements by BESIII [31], KLOE [34-36], and BaBar [37]. The black line is the fit of the BESIII spectrum using the Gounaris-Sakurai parametrization.

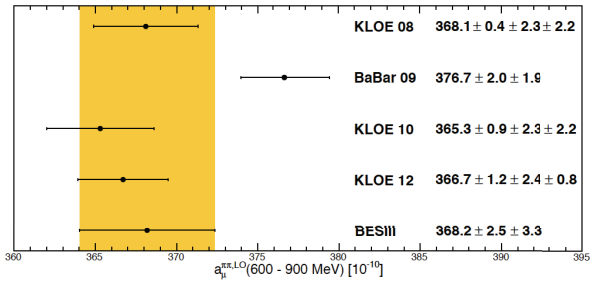

Fig. 4.7. (color online) Two-pion contribution to the hadronic vacuum polarization contribution to a_μ in the energy range between 600 and 900 MeV.

● **Cross-section of $e^+e^- \to \pi^+\pi^-\pi^0$**

The hadronic channel $e^+e^- \to \pi^+\pi^-\pi^0$, which is dominated at low energies by the $\omega(782)$ and $\phi(1020)$ resonances, was measured by the Novosibirsk experiments CMD-2 [40] and SND [41] below 1.4 GeV. These results show obvious scatter, although within the claimed accuracy, and would benefit from improved measurements. Above the $\phi(1020)$ resonance, BaBar also performed a measurement of this channel [42], and observed structures which are interpreted as two excited ω states. This BaBar result is in conflict with the old DM2 measurement [43].

In contrast to the two-pion analysis discussed above, both the tagged (in the full mass range) and the untagged ISR methods (above 1 GeV) were analyzed by BESIII. Preliminary results of the ISR measurements are already available. For the final spectrum, the tagged and untagged spectra were averaged, and a systematic uncertainty of better than 3% was achieved in a wide mass range from the threshold up to the J/ψ resonance. Assuming vector meson dominance in the fit of the mass spectrum, the mass and width of the resonances $\omega(1420)$ and $\omega(1650)$ were obtained with unprecedented accuracy. Furthermore, the branching fraction of the J/ψ decays to three pions was measured precisely.

● **Cross-section of $e^+e^- \to \pi^+\pi^-\pi^0\pi^0$**

In the channel $e^+e^- \to \pi^+\pi^-\pi^0\pi^0$, some deviations between the two Novosibirsk experiments CMD-2 [44] and SND [45] were observed below 1.4 GeV. Even larger deviations are seen in a comparison of the τ spectral functions, which can be related to the cross-section via an isospin relation. It has been speculated that large isospin violating effects might be the reason for this observation. Above approximately 1 GeV, the BaBar collaboration published an analysis in which the world data set, in terms of statistical and systematic precision, is largely exceeded [46]. It is therefore the goal of the BESIII analysis to provide an independent high-accuracy data set, besides BaBar. Furthermore, this channel is extremely interesting from the point of view of spectroscopy. It has a rich internal structure, where $\omega\pi^0$, $a_1\pi$, $\rho^+\rho^-$, and many other intermediate states play a significant role (including $f_0(500)$ and $f_0(980)$).

Preliminary results for this channel by BESIII use the tagged and untagged ISR approach. The mass range from the threshold up to 3.4 GeV was covered and the cross-section was determined with a systematic uncertainty of approximately 3%. Besides the cross-section of $e^+e^- \to \pi^+\pi^-\pi^0\pi^0$, the cross-section of the intermediate state $e^+e^- \to \omega(782)\pi^0$ was measured, and the branching fraction of the decay $J/\psi \to \pi^+\pi^-\pi^0\pi^0$ was extracted.

The existing results for $e^+e^- \to \pi^+\pi^-\pi^0$ and $e^+e^- \to$

$\pi^+\pi^-\pi^0\pi^0$ were obtained using 2.9 fb^{-1} of data at $\sqrt{s}$ = 3.773 GeV. As discussed for the $e^+e^- \to \pi^+\pi^-$ analysis, the systematic uncertainties, which are already at the world-class level, can be further reduced by combining the already existing and upcoming data sets.

4.2.4 Inclusive R scan data

Up to the energy of 2.0 GeV, the R value is determined by the sum of measured exclusive hadronic cross-sections, either via the energy scan or the ISR technique. In the case of unmeasured exclusive channels, isospin invariance is assumed in this energy range. At larger values of $\sqrt{s}$, more exclusive channels open up, so that inclusive R measurements are necessary. The energy region between 2.0 and 4.6 GeV is rich with resonances, and contains a transition between the smooth continuum region and the resonances. Figure 4.8 shows a comparison of the BES [47-51] and KEDR data [52, 53], as well as the perturbative QCD (pQCD) prediction between 2.0 and 3.7 GeV. An agreement, within uncertainties, can be observed. It should be noted that the most recent KEDR analysis in the energy interval between 3.08 and 3.72 GeV [54], is not yet included.

Regarding the hadronic vacuum polarization contribution to $(g-2)_\mu$, theorists deal in different ways with the R values in the energy region above 1.8 GeV. In Ref. [5], the dispersive evaluation is used with inclusive R values measured above 1.937 GeV. In the energy interval from 1.8 to 3.7 GeV, the contribution to the uncertainty of the muon anomaly a_μ is found to be 0.56×10^{-10}, which is roughly a factor of 3 smaller than the expected accuracy $\delta a_\mu(\text{exp}) = 16\times10^{-11}$ of the new direct measurements of a_μ. In Ref. [7], the four-loop pQCD is used in the energy region between 1.8 and 3.7 GeV, resulting in the uncertainty of 0.65×10^{-10}. The open charm region between 3.7 and 5 GeV is governed by broad resonances. Its contribution to a_μ is computed using the experimental data. However, the contribution is found to be very small (0.11×10^{-10} in Ref. [5] and 0.03×10^{-10} in Ref. [7]). At even higher energies, either the experimental data (for instance, in the bottomonium region) or pQCD are used for the evaluation of the hadronic vacuum polarization. The uncertainties of these contributions are below the level of 0.10×10^{-10}.

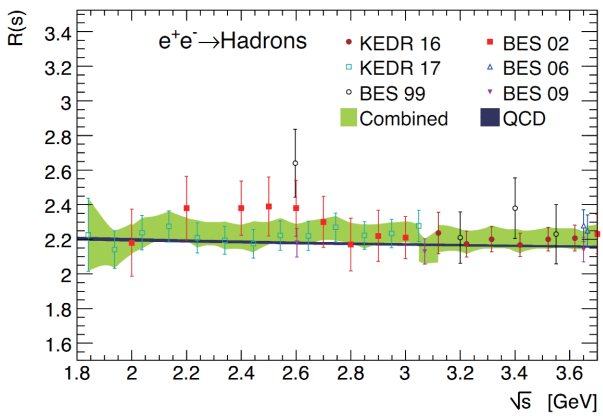

Fig. 4.8. (color online) The hadronic $R(s)$ ratio in the continuum region below the $D\bar{D}$ threshold. Shown are the results from BES and KEDR as well as their average (shaded band). The solid line shows the pQCD predictions. Plot taken from Ref. [7].

The transition region between the sum of exclusive channels and the inclusive R data is of interest and deserves re-examination. Table 4.1 summaries the values of $a_\mu^{\text{HVP,LO}}$ in the region [1.841, 2.0] GeV using different inputs [5]. The results from the inclusive data and pQCD calculations agree within uncertainties, but disagree with the exclusive sum. Hence, precise measurements of R data with the exclusive sum and inclusive methods are important for choosing the transition point between the sum of exclusive channels and the inclusive R data, and for testing the pQCD predictions of the R values in the transition region. A new scan measurement between 1.8 and 2.0 GeV would be useful to answer these questions.

Table 4.1. The values of $a_\mu^{\text{HVP,LO}}$ for $\sqrt{s}$ in the region [1.841, 2.0] GeV using different inputs. The numbers are taken from Ref. [5].

input	$a_\mu^{\text{HVP,LO}}(\times10^{10})$
exclusive sum	6.06±0.17
inclusive data	6.67±0.26
pQCD	6.38±0.11
exclusive(< 1.937 GeV) + inclusive(>1.937 GeV)	6.23±0.13

Compared to $(g-2)_\mu$, the impact of the inclusive R data on the running of the electromagnetic fine structure constant is much more pronounced as higher energy scales are very relevant in the dispersion integral for $\Delta\alpha_{\text{em}}$. In fact, in the case of $\Delta\alpha_{\text{em}}$, the total uncertainty of 1.11×10^{-4} cited in Ref. [5], stems almost entirely from the energy range between 1.19 and 11.20 GeV, which amounts to $(82.82\pm1.05)\times10^{-4}$. While Ref. [5] follows a more data-driven approach to calculate $\Delta\alpha_{\text{em}}$, the evaluation by Davier et al. in Ref. [7] relies on the pQCD calculations of the R value in the energy range between 1.8 and 3.7 GeV. Above 3.7 GeV and up to 5.0 GeV, the experimental information on R is used. In this energy range, the experimental uncertainty of 0.67×10^{-4}, out of the total uncertainty of $\Delta\alpha_{\text{em}}$ of 0.9×10^{-4}, is found. This strongly motivates the need for new data for the inclusive R ratio in the energy range covered by BESIII. The role of BESIII is twofold. On the one hand, the new data can prove the validity of pQCD for the description of R, as required by a theory-based evaluation of $\Delta\alpha_{\text{em}}$. On the other hand, the data can be directly used as input in the dispersion integral in a data-driven approach.

In order to improve the knowledge of R, the BESIII collaboration has recently carried out a series of energy scans in the range between 2.0 and 4.6 GeV, in 130 energy points and with the total integrated luminosity of about 1300 pb^{-1}. The total hadronic event yield exceeds 10^5 events at each energy, such that the accuracy of the data is entirely dominated by systematic uncertainties. The goal of the BESIII experiment is to arrive at a total accuracy of the hadronic R ratio of 3% or better. A similar systematic accuracy has already been achieved at KEDR [52] . The analysis of the data is currently ongoing, and preliminary results show that the dominant uncertainty is due to the hadronic event generator, which is also a major challenge for describing 10^5 hadronic events at each energy. MC simulation codes based on theoretical descriptions of string fragmentation functions exist, for example the LUARLW generator [55]. The KEDR collaboration used the LUARLW generator, which was also employed by the BES collaboration. With 10^5 hadronic events at each energy, the LUARLW generator was optimized and tuned. Also, a precise description of all hadronic events in one event generated was proposed. Making use of the existing measurements of many exclusive hadronic final states, the event generator CONEXC [56], which can deal with the imprecise exclusive parts of the LUARLW generator, has been considered as an alternative. Hence, a data-driven approach to the description of the total hadronic events has been identified.

The energy range between 3.85 and 4.6 GeV is rich with charmonium and charmonium-like states. Because the scan data have been collected with a small energy step, we could extract resonance parameters using the precisely measured R values. The BES collaboration did a similar analysis [47-51], but their results have a large uncertainty and are model dependent. With more studies of the charmonium and charmonium-like states, the R results could be further improved.

4.2.5 Measurements of the meson transition form factors

The main motivation for the proposed program of precision measurements of meson TFFs at BESIII is to constrain the HLbL contribution to the level set by the forthcoming $(g-2)_\mu$ experiments at FNAL and J-PARC of $\delta a_\mu = 1.6\times10^{-10}$, in order to allow a meaningful interpretation of these new measurements. Depending on the analysis of the hadronic contributions [7, 57], the present SM uncertainty is $\delta a_\mu(\text{SM}) = \pm(49-58)\times10^{-11}$, which significantly exceeds the future experimental accuracy. This motivates an intense activity to reliably estimate the contributions of hadrons to a_μ.

The leading diagram in the HLbL contribution is the pseudoscalar meson exchange, as shown in Fig. 4.9. Unlike the HVP contribution, the description of the non-perturbative light-by-light matrix element in most of the existing estimates of the HLbL contribution is based on hadronic models rather than on the experimental data. These approximations are based on a requirement of consistency with the asymptotic constraints of QCD, and predict that the hadronic corrections are dominated by the long-distance physics, namely by the exchange of the lightest pseudoscalar states. Unfortunately, a reliable estimate based on such models is possible only within certain kinematic regimes. This results in a large, mostly uncontrolled uncertainty of a_μ.

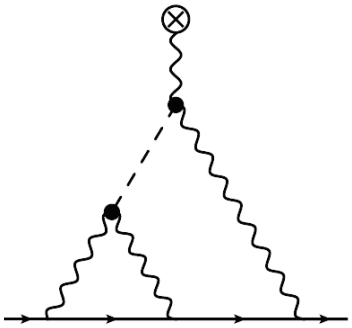

Fig. 4.9. The leading term in the hadronic light-by-light scattering (HLbL) contribution to the anomalous magnetic moment of the muon is given by the exchange of light pseudoscalar mesons, as depicted by the dashed line.

In order to reduce the model dependence, data-driven approaches for the HLbL contribution to a_μ have been proposed. Sum rules and a dispersive formalism can also provide powerful constraints on the hadronic light-by-light scattering and its contribution to a_μ. Measurements of meson TFFs are used as input in such data-driven approaches. As is discussed below, essentially all relevant channels in the space-like and time-like regions can be studied at BESIII.

TFFs describe the effect of the strong interaction on the $\gamma^*\gamma^*M$ vertex, where $M=\pi^0,\eta,\eta',\eta_c\ldots$. They are represented by functions $F_{M\gamma^*\gamma^*}(q_1^2,q_2^2)$ of the photon virtualities q_1^2 and q_2^2. For the case of pseudoscalar mesons, there is one such function [58, 59]. For scalar, axial-vector, or tensor mesons, the $\gamma^*\gamma^*M$ vertex contains in general several such TFFs.

The space-like region of TFFs is accessed at e^+e^- colliders by means of the two-photon fusion reaction $e^+e^-\to e^+e^-M$ (left panel in Fig. 4.10), where the measurement of both virtualities is still an experimental challenge. The common practice is to extract TFFs by a method where one of the outgoing leptons is tagged and the other is assumed to escape detection along the beam axis (single-tag method). The tagged lepton emits a highly off-shell photon with a transferred momentum $q_1^2\equiv-Q^2$ and is detected, while the other, untagged, is scattered at a small angle with $q_2^2\simeq0$. TFF extracted from the single-tag experiment is then $F_{M\gamma^*\gamma^*}(Q^2,0)\equiv F_{M\gamma^*\gamma}(Q^2)$. The time-

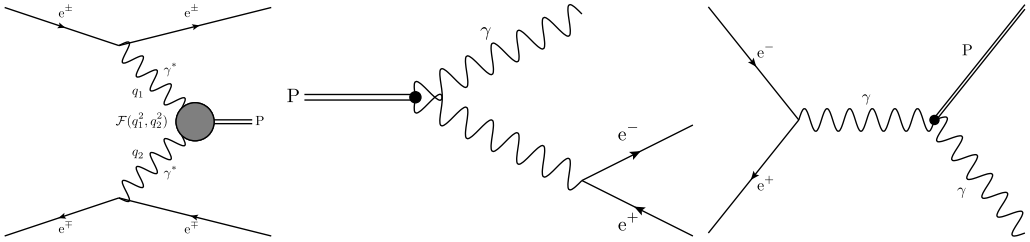

Fig. 4.10. The meson TFF in the space-like region (left panel) is accessed via the $\gamma^*\gamma^*$ annihilation process, and in the time-like region via the γe^+e^- Dalitz decay (middle panel), and via e^+e^- annihilation into $P\gamma$ (right panel), where P stands for a pseudoscalar meson.

like region of TFFs can be accessed at meson facilities via the single Dalitz decay processes $M \to l^+l^-\gamma$, which contain a single virtual photon with a transferred momentum in the range $4m_l^2 < q_1^2 < m_M^2$ (with m_l the lepton mass and m_M the meson mass), whereas $q_2^2 = 0$ (middle panel in Fig. 4.10). To complete the time-like region, e^+e^- colliders provide access to the values $q^2 > m_M^2$ via the $e^+e^- \to M\gamma$ annihilation processes (right panel in Fig. 4.10).

Besides their relation to the anomalous magnetic moment of the muon, the pseudoscalar meson TFFs provide a unique window on several symmetry-breaking mechanisms in QCD. In the limit of massless light quarks (u,d,s), i.e. the chiral limit, the QCD Lagrangian exhibits an $SU(3)_{\rm L} \times SU(3)_{\rm R}$ chiral symmetry which is spontaneously broken to $SU(3)_V$, giving rise to 8 pseudoscalar Goldstone bosons (π, K, η). The QCD Lagrangian has in addition two other global symmetries: the $U(1)_V$ symmetry leading to the conservation of baryon number, and the $U(1)_A$ symmetry which is anomalous. Since the flavor-singlet axial-vector current is not conserved in the presence of the $U(1)_A$ anomaly, the η' mass does not vanish in the chiral limit. In the massless u,d,s quark world (with the other three quarks infinitely heavy), the massive η' would be a pure flavor-singlet state $\eta^0 \equiv (u\bar{u} + d\bar{d} + s\bar{s})/\sqrt{3}$. In the real world, however, the $SU(3)_V$ flavor symmetry is explicitly broken by the quark masses, which causes a mixing among π^0, η, and η' [60, 61]. In the isospin limit ($m_u = m_d$), π^0 can be identified as a pure isotriplet state $(u\bar{u} - d\bar{d})/\sqrt{2}$. In the absence of the $U(1)_A$ anomaly (large-N_c limit of QCD), the two isosinglet pseudoscalar mass eigenstates would consist of $(u\bar{u} + d\bar{d})/\sqrt{2}$ and $s\bar{s}$ (so-called *ideally mixed* states). The $U(1)_A$ anomaly mixes these quark flavor states towards the physical η and η' mesons, which are closer to the flavor octet $\eta^8 \equiv (u\bar{u} + d\bar{d} - 2s\bar{s})/\sqrt{6}$ and flavor singlet η^0 states, respectively. The mixing in the $\eta - \eta'$ system probes the strange quark content of the light pseudoscalars, as well as the non-perturbative gluon dynamics of QCD, responsible for the $U(1)_A$ anomaly. The mixing can also be related to physical observables [60-64], in particular via the $M \to \gamma\gamma$ decay widths and the $\gamma^*\gamma^*M$ TFFs.

With the existing data, BESIII has achieved world-leading results in the field of meson TFFs, as is elaborated in the following. The overall goal of the BESIII program is to provide precision measurements of TFFs of pseudoscalar mesons, of $\pi\pi$, $\pi\eta$ and $\eta\eta$ systems, as well as of axial and tensor mesons at small momentum transfers. A future data set of 20 fb^{-1} at $\sqrt{s} = 3.773$ GeV, will make possible a first measurement of the double-virtual TFF of the lightest pseudoscalar mesons with high accuracy.

• Single-tag pseudoscalar TFFs, space-like

The first BESIII publication of the space-like TFF of the π^0 meson is based on the 2.9 fb^{-1} data sample obtained at the cms energy of 3.773 GeV. Preliminary results of the analysis are presented in Fig. 4.11. As described above for single-tag events, one of the beam particles (electron or positron) is tagged in the detector. By detecting two photons from the π^0 decay, the missing momentum can be derived for the missing positron (electron), which is further required to be scattered at very small angles. By fitting the $\gamma\gamma$ invariant mass distribution in bins of Q^2, one obtains the differential cross-section $\mathrm{d}\sigma/\mathrm{d}Q^2$ for the signal process,which is proportional to $|F(Q^2)|^2$.

Figure 4.11 shows the product $Q^2|F(Q^2)|$ as measured by BESIII together with the data from CELLO [65] and CLEO [66]. Note that the recent BaBar [67] and Belle [68] data only access the Q^2 range above 4 GeV^2, and hence, are not displayed. The BESIII analysis covers the entire Q^2 range between 0.3 and 3.1 GeV^2, which significantly improves the accuracy of the existing data sets. The accessible range of momentum transfer is limited by the detector acceptance of photons from decays of π^0 for lowest values of Q^2, and by the statistics for the largest values of Q^2. The existing data taken in the scope of the R measurement, discussed in Sec. 4.2.4, will be used to extend the covered region of momentum transfer down to approximately 0.1 GeV^2. A future data set of 20 fb^{-1} at 3.773 GeV will help to extend the covered range of momentum transfer up to approximately 10 GeV^2, which will allow to test the discrepancy of the results of B-factories, i.e. the so-called BaBar-Belle puzzle.

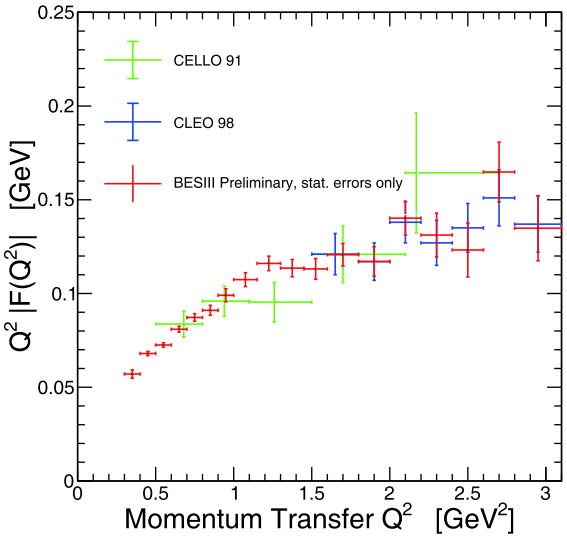

Fig. 4.11. (color online) Preliminary BESIII measurement of the space-like π^0 TFF compared with the data from CELLO [65] and CLEO [66].

The current preliminary results are in very good agreement with the recent theoretical calculations which use dispersion relations [69, 70] or LQCD [71]. The data have also been considered in a recent review of the HLbL contribution to a_μ [72], where it was demonstrated that they contribute to a significant reduction of the uncertainties.

First feasibility studies of the η and η' TFF measurements have been performed at BESIII. So far, only individual decay modes have been considered for reconstruction of mesons from the data used for pion TFF measurements. The covered range of momentum transfer is similar to the π^0 TFF range, with an accuracy similar to what was reported in previous measurements [65, 66]. The final result will make use of all major decay modes of both mesons, and will combine the existing and future data sets to obtain results of highest accuracy and impact.

● **Single-tag $\pi\pi$, $\pi\eta$, $\eta\eta$ TFFs, space-like**

Besides the lowest-lying pseudoscalar mesons, $\gamma\gamma^*$ processes also allow to access the structure of scalar, axial-vector and tensor mesons via the production of multi-meson final states. A first measurement by BESIII focused on the $\gamma^*\gamma \to \pi^+\pi^-$ channel, with one virtual photon. Data at cms energies between 3.773 and 4.6 GeV were combined to perform studies with an integrated luminosity of 7.5 fb^{-1}. Figure 4.12 shows the full simulation with 1 fb^{-1} at $\sqrt{s} = 4.23$ GeV of the single-tagged analysis of $\gamma\gamma^* \to \pi^+\pi^-$ after event selection in three relevant kinematic variables. The dominant background in the reaction $e^+e^- \to e^+e^-\mu^+\mu^-$ is rejected by employing the machine learning techniques, successfully used in the pion form factor measurements discussed in Sec. 4.2.3. The irreducible background contribution due to the time-like amplitude of $e^+e^- \to e^+e^-\pi^+\pi^-$ is subtracted using the MC derived distributions. The investigation at BESIII triggered an improvement of the EKHARA 3.0 event generator [73], which allows to properly take into account the interference between the signal and background processes. Thus, a first high-statistics result for the masses starting from the two-pion mass threshold, small momentum transfers and with a full coverage of the helicity angle of the pion system, was obtained by BESIII. While the results in the threshold region are awaited by the $(g-2)_\mu$ theory community [74, 75], such data will also provide new empirical information about pion polarization.

The analysis of the two-pion system is currently extended to the neutral pion system, where a complementary result to the recent Belle measurement at large momentum transfers [76] is expected. Future data will allow to extend the investigations also to $\pi\eta$ and $\eta\eta$ systems with high statistics. Furthermore, even higher multiplicity final states $\gamma\gamma^* \to 3\pi, \gamma\gamma^* \to 4\pi$ or $\gamma\gamma^* \to \eta\pi\pi$ can be performed to provide with high accuracy the relevant information about the axial and tensor mesons, for example $f_1(1285)$ and $a_2(1320)$, needed as input for the calculations of the HLbL contribution to $(g-2)_\mu$.

● **Double-tag π^0 TFF, space-like**

In the case that both scattered leptons are identified in the detector, the doubly-virtual TFF can be accessed. First event sample of this kind was identified in the 2.9 fb^{-1} data set at the cms energy of 3.773 GeV. With improved statistics, the measurement of the doubly-virtual TFF can be used to compute the pion-pole contribution to HLbL in a completely model-independent way. Based on a MC simulation restricted by the geometric acceptance of the BESIII detector only, the result is expected to cover the momentum transfers in the range $0.3 \leqslant (Q_1^2, Q_2^2) \leqslant 2.2$ GeV^2. This information is crucial for constraining the precision of the data-driven calculations of the HLbL contribution to $(g-2)_\mu$ [20]. In addition to the doubly-virtual TFF of π^0, the same information for η and η' mesons will be measured. The BESIII result will be complementary to the recent measurement of the doubly-virtual η' TFF by the BaBar collaboration [59], which has been obtained for large momentum transfers only.

● **Pseudoscalar TFFs at high Q^2-, time-like**

The time-like π^0 TFF has not been extracted up to now from the annihilation reaction $e^+e^- \to \pi^0\gamma$ for high momentum transfers. At BESIII, it is possible to access the time-like π^0 TFF in the Q^2 range of approximately 20 GeV^2, which allows a comparison with the space-like data from BaBar [67] and Belle [68]. In the case of η and η', in addition to the comparison to space-like measurements, the data can be compared to a time-like BaBar measurement at $Q^2 = 112$ GeV^2 [58]. Comparisons of this kind allow to test the predictions of pQCD, in which it is assumed that the space-like and time-like TFFs are

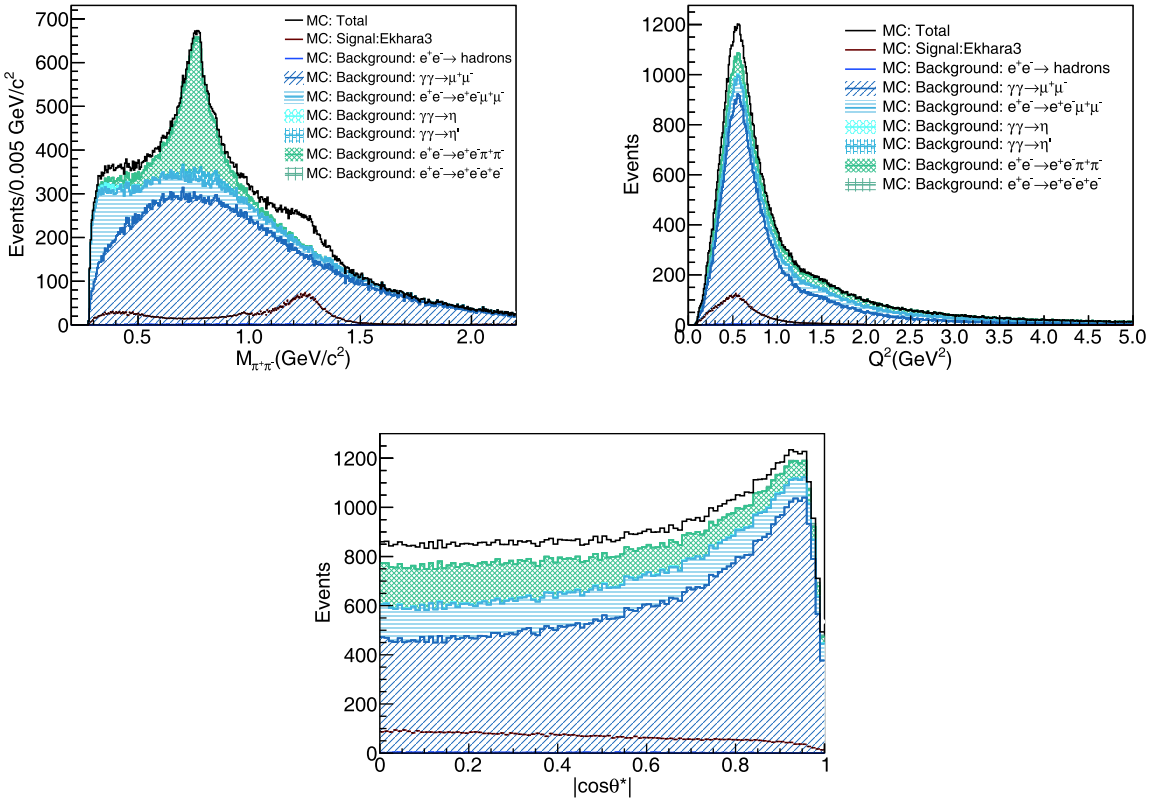

Fig. 4.12. (color online) Full simulation of the single-tagged analysis of $\gamma\gamma^* \to \pi^+\pi^-$ at $\sqrt{s} = 4.23$ GeV. Three relevant distributions of the two-pion system are shown: invariant mass of the pions (top left), momentum transfer Q^2 of the tagged lepton (top right), and helicity angle of the pions $\cos\theta^*$ (bottom).

identical and feature a Q^{-2} dependence [58].

We stress once again that the BESIII program for meson TFF measurements is of the highest relevance for constraining the HLbL contribution to $(g-2)_\mu$. In a recent review [72], the π^0 pole exchange contribution is evaluated in a simplistic model, which fulfills the basic theory constraints, and takes into account the preliminary data from BESIII. The data allow to reduce the uncertainty of this most relevant contribution to $\pm 0.2 \times 10^{-10}$, while the previous model dependent estimates have uncertainties in the range $\pm(0.9-1.2)\times 10^{-10}$ (see Table 4.2 in Ref. [72]). More elaborate and model independent evaluations of the π^0 contribution, as the dispersive calculations [69, 70], or the lattice calculations [71], which do not take into account the BESIII data, already achieve uncertainties at the level of $\pm(0.3-0.4)\times 10^{-10}$. These results can be cross checked by confronting with the present and future BESIII data. As mentioned, the goal is to achieve a total uncertainty of all hadronic contributions to a_μ at the level of 1.6×10^{-10}.

4.3 Baryon form factors

Baryons provide a unique window to the strong interaction, since they constitute the simplest system for which the non-Abelian nature of QCD is manifest [77]. The best known baryon species is the nucleon. However, despite the fact that it is known for more than a century and its importance as the main contributor to the mass of the visible Universe, its fundamental properties like the mass, spin [78, 79] and structure [80] are difficult to derive from first principles. This difficulty is a consequence of the non-perturbative interactions between the quarks inside the nucleon. At this scale, the break-down of pQCD calls for quantitative predictions from e.g. the Chiral Perturbation Theory [81, 82], Lattice QCD [83] or phenomenological models, e.g. the Skyrme models [84, 85].

The inner structure of baryons can be described and studied experimentally on a common footing via the electromagnetic form factors (EMFFs), probed by processes involving hadrons interacting with virtual photons. EMFFs are fundamental observables of non-perturbative QCD and quantify the deviation from the point-like case. If one-photon exchange is assumed, the momentum transfer squared q^2 of the virtual photon is given by $q^2 = (p_\mathrm{i} - p_\mathrm{f})^2 < 0$. Elastic, or space-like, form factors ($q^2 < 0$) have been studied since the 1960's in electron-nucleon scattering [86]. Spin $\frac{1}{2}$ baryons have two form factors, often referred to as the electric G_E and the magnetic G_M form factors. In the so-called Breit frame, these

are Fourier transforms of the charge and magnetization density, respectively. The measured charge density of the neutron is particularly intriguing. Although it is negative near the center whilst positive further out, which can be explained in the simple quark model by d quark clustering in the center surrounded by the u quark, the drop to negative values at larger distances from the center requires more elaborate models involving e.g. pion clouds [80]. One way to gain further insight into this puzzle is to replace one or several light quarks in the nucleon by heavier ones, *i.e.* to form hyperons, and study how the structure changes [87]. However, since hyperons are unstable, they are unfeasible as beams or targets, and therefore do not easily lend themselves to electron scattering experiments. Instead, their structure can be studied in the time-like region ($q^2 > 0$) via the electron-positron annihilations with subsequent production of baryon-antibaryon pairs.

The somewhat abstract time-like form factors can be related to the more intuitive space-like form factors by the dispersion relations [88]. In particular, space-like and time-like form factors should converge to the same value as $|q^2|$ reaches a certain scale [89]. For nucleons, the onset of this scale can be tested by measuring the space-like and time-like form factors with great precision and comparing them. For hyperons, this is unfeasible due to the poor experimental access to the space-like region. However, one can use the fact that time-like form factors can be complex, with a relative phase that polarizes the final state [89]. For a ground state hyperon Y, this phase is accessible, thanks to the weak, self-analyzing decays. The daughter baryon B will be emitted according to the spin of the mother hyperon Y, giving a decay angular distribution that depends on the polarization of Y:

$$W(\cos\theta_B) = \frac{1}{4\pi}(1 + \alpha_Y P_Y \cos\theta_B). \tag{4.8}$$

Since space-like form factors are real, the same must hold for time-like form factors for large $|q^2|$. Hence, the onset of the scale at which space-like and time-like form factors converge to the same value, can be obtained by finding the scale at which the phase goes to zero.

Also, the relative phase must be zero at the threshold. This is because the phase is a result of interfering amplitudes, e.g. s-waves and d-waves. At the threshold, only s-waves can contribute which means that the phase is zero. Furthermore, the absence of other waves also implies that the ratio between electric and magnetic form factors $|G_{\rm E}/G_{\rm M}|$ is equal to 1 at the threshold.

4.3.1 Formalism

For spin $\frac{1}{2}$ baryons produced via one-photon exchange in $e^+e^- \to \gamma^* \to B\bar{B}$, the Born cross-section can be parametrized in terms of $G_{\rm E}$ and $G_{\rm M}$:

$$\sigma_{B\bar{B}}(s) = \frac{4C\pi\alpha^2\beta}{3s}\left[|G_{\rm M}(s)|^2 + \frac{1}{2\tau}|G_{\rm E}(s)|^2\right]. \tag{4.9}$$

Here, $\alpha = 1/137.036$ is the fine-structure constant, $\beta = \sqrt{1 - 4m_B^2c^4/s}$ the velocity of the produced baryon, c the speed of light, s the square of the cms energy, m_B the mass of the baryon and $\tau = s/(4m_B^2)$. The Coulomb factor C is a correction to the one-photon exchange and describes the electromagnetic interaction between the outgoing B and $\bar{B}$. For neutral baryons, C is 1, which in combination with the vanishing phase space β factor, means that the cross-section should be zero at the threshold. For charged baryons, C is typically assumed to have the value of the point-like charged fermions $C = \varepsilon R_S$ [90], where $\varepsilon = \pi\alpha_{\rm em}/\beta$ is an enhancement factor. In this case, the two β factors cancel, and as a result the cross-section becomes non-zero at the threshold. The so-called Sommerfeld resummation factor

$$R_S = \sqrt{1-\beta^2}/(1 - {\rm e}^{-\pi\alpha_{\rm em}\sqrt{1-\beta^2}/\beta}) \tag{4.10}$$

causes the cross-section to rise rapidly with the fermion velocity [91].

In many experiments, the data samples are too small to separate between $G_{\rm E}$ and $G_{\rm M}$ since that requires analysis of angular distributions. In order to compare the production cross-sections of different baryon-antibaryon pairs in equivalent kinematic conditions, the effective form factor is defined:

$$|G(s)| \equiv \sqrt{\frac{\sigma_{B\bar{B}}(s)}{\left(1+\frac{1}{2\tau}\right)\left(\frac{4\pi\alpha^2\beta}{3s}\right)}} \equiv \sqrt{\frac{2\tau|G_{\rm M}(s)|^2 + |G_{\rm E}(s)|^2}{2\tau+1}}. \tag{4.11}$$

In order to extract the relative phase, a full spin decomposition of the reaction is needed. The formalism is outlined in Refs. [92, 93]. In particular, the Λ transverse polarization P_Y is given by:

$$P_Y = \frac{\sqrt{1-\eta^2}\sin\theta\cos\theta}{1+\eta\cos^2\theta}\sin(\Delta\Phi), \tag{4.12}$$

where η is the angular distribution parameter, related to the form factor ratio $\mathcal{R}$ by $\eta = (\tau - \mathcal{R}^2)/(\tau + \mathcal{R}^2)$. The polarization P_Y can be extracted from Eq. (4.8).

The formalism presented so far is based on the assumption that one-photon exchange dominates the production mechanism. It has been discussed whether two-photon exchange contributes to the production mechanism, leading to interference effects that result in an additional term $\kappa\cos\theta\sin^2\theta$ in the angular distribution [94]. As a consequence, the scattering angle distribution of the produced baryon will be slightly asymmetric. This is quantified by the asymmetry

$$\mathcal{A} = \frac{N(\cos\theta > 0) - N(\cos\theta < 0)}{N(\cos\theta > 0) + N(\cos\theta < 0)}. \tag{4.13}$$

It is related to the κ parameter in the following way:

$$\mathcal{A} = \frac{3}{4}\frac{\kappa}{3+\eta}, \tag{4.14}$$

where η is the same as in Eq. (4.12) [95]. The asymmetry $\mathcal{A}$ is straight-forward to measure and offers a convenient way to study the two-photon exchange in the time-like region.

4.3.2 State of the art

Proton EMFFs have been studied extensively in the space-like region [86]. In particular, the development of the polarization transfer technique in the late 1990's [96, 97], led to a remarkable leap in the field, enabling a model independent separation of electric and magnetic form factors. The best precision of the ratio $|G_E/G_M|$ obtained with the new technique is $\sigma_p|G_E/G_M| = 1.7\%$, achieved at JLab [98]. The previously employed Rosenbluth separation technique [99] relies on one-photon exchange, and the comparison of the data obtained with the two methods shows a large and energy dependent difference. The principal explanation is the effect of the two-photon exchange [100, 101].

The time-like region became accessible with the advent of high-precision, high-intensity electron-positron colliders at intermediate energies. The world data for $e^+e^- \to p\bar{p}$ are shown in Fig. 4.13. The advantage of electron-positron annihilations is their charge symmetry, which makes the measurements less sensitive to higher order processes such as the two-photon exchange. However, the precision achieved until recently has not been compatible with the space-like region [102]. The most precise measurements from BaBar (in $e^+e^- \to p\bar{p}$ [103]) and PS170 (in $\bar{p}p \to e^+e^-$ [104]) achieved $\sigma_p|G_E/G_M| \approx 10\%$, and differ by more than 3σ (bottom left panel of Fig. 4.13). Recent data from BESIII obtained with a beam energy scan [105], and the radiative return or ISR method [106], agree with the BaBar measurements. New data from BESIII, collected in a high-precision energy scan in 2015, will offer improved precision over a large q^2 range.

The cross-section and effective form factor show interesting features, as can be seen in the top and bottom left panels of Fig. 4.13. The BaBar collaboration reported an oscillating behavior [103, 115] that was recently confirmed by BESIII [106]. This becomes particularly striking when studied as a function of the relative momentum between the outgoing proton and antiproton. More high-precision data are needed to establish this elusive feature at the level of several standard deviations.

The large amount of high-quality data for proton EMFFs has inspired the theory community to develop various approaches to nucleon structure, based on the Chiral Perturbation Theory [116], Lattice QCD [117, 118], Vector Meson Dominance [119], relativistic Constituent Quark Models [120] and pQCD [121].

In the era of great progress in proton time-like EMFFs, the corresponding data for its isospin partner, the neutron, remain a challenge. This is primarily due to the difficulty in identifying and reconstructing the neutron and antineutron from the $e^+e^- \to n\bar{n}$ process. The cross-section has been measured by the SND experiment [122] up to 2 GeV, and by the FENICE experiment [109] between 2 and 3 GeV. FENICE collected only a small amount of data and identified $\bar{n}$ by the time-of-flight method and the annihilation pattern in the detector. The ratio $R_{np} = \sigma(e^+e^- \to n\bar{n}) / \sigma(e^+e^- \to p\bar{p})$ is expected to be close to 1 if the process is dominated by the isoscalar or isovector amplitude. In a picture where the production cross-section is proportional to the square of the leading quark charge (u quark in the case of the proton, and d quark in the case of the neutron), the ratio should instead be close to 0.25. More elaborate predictions are presented in Refs. [123, 124]. More precise data could shed further light on this issue.

Hyperon EMFFs have been a fairly unexplored territory until recently. The cross-section of the $e^+e^- \to Y\bar{Y}$ process (Y referring to various ground-state hyperons) has been studied by DM2 [125], BaBar [126], BESIII [127] and CLEO [128]. The latter measurement compared the production of several different ground-state hyperons, including Ω^-, and interpreted the results in terms of di-quark correlations. The idea that certain configurations of flavor, spin and isospin of the two quarks inside the hadron have an important impact on its structure, has been discussed since a long time [129]. In particular, the effects on Λ and Σ structures are outlined in Ref. [130]. However, it is difficult to draw definite conclusions from CLEO, since all data points coincided with charmonium resonances $\psi(3686)$, $\psi(3770)$ and $\psi(4170)$. Hence, interference effects may be important, which makes an unambiguous interpretation difficult.

Due to limited sample sizes, the electric and magnetic form factors could not be separated with any conclusive precision in neither of the aforementioned experiments. However, in a more recent measurement from BESIII, dedicated data at $q = 2.396$ GeV/c enabled a complete spin decomposition of the $e^+e^- \to \Lambda\bar{\Lambda}$ reaction, including measurement of the polarization and spin correlations. As a result, it was possible not only to separate the Λ electric and magnetic form factors, but also to determine for the first time the relative phase between $|G_E|$ and $|G_M|$. It was found to be significantly different from zero [131]. The prospect of measuring the relative phase $\Delta\Phi$ of the Λ hyperon by BESIII triggered the first theory predictions based on various $\Lambda\bar{\Lambda}$ potential models [132]. It was found that the phase is more sensitive to the potential than the $|G_E/G_M|$ ratio, which in turn is more sensitive than the cross-section. The theory predictions, as well

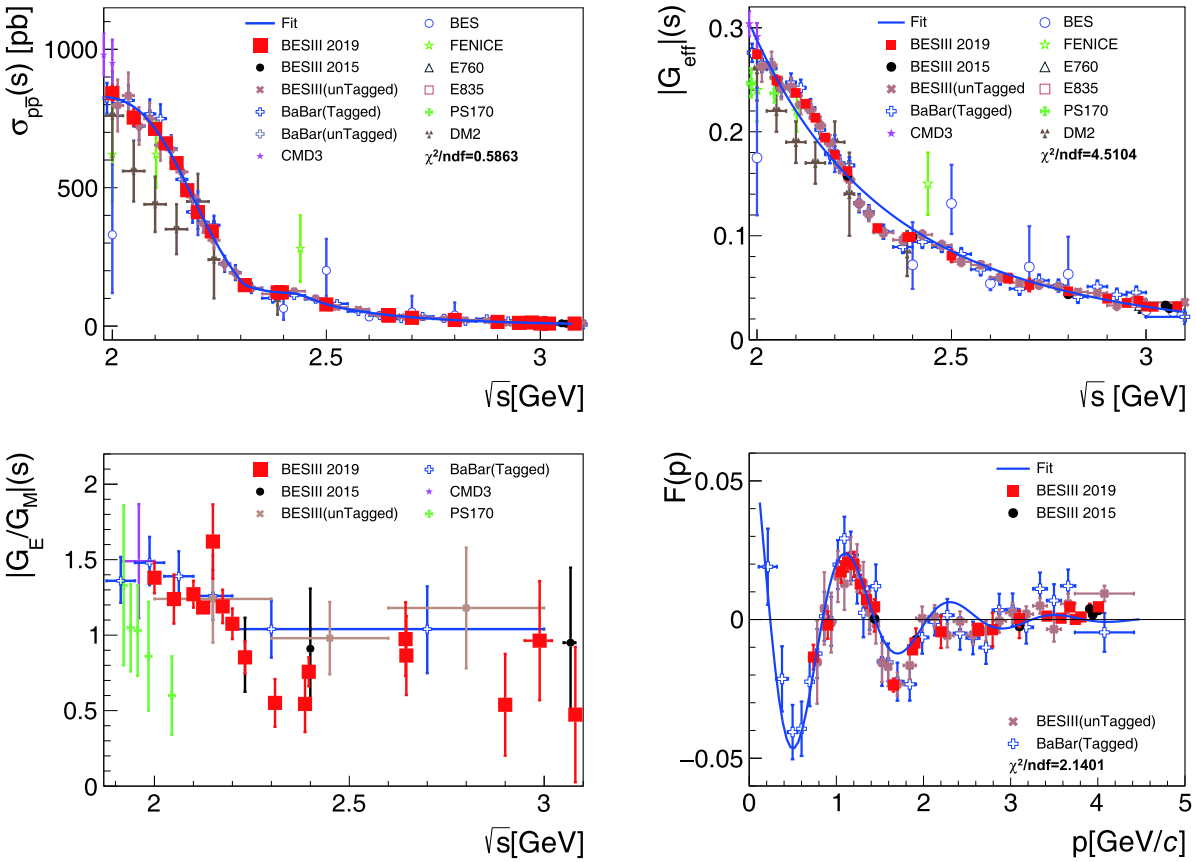

Fig. 4.13. (color online) Top left: world data for the $e^+e^- \to p\bar{p}$ cross-section. Top right: the effective proton time-like form factor. Bottom left: world data for $R = |G_E/G_M|$. Bottom right: the effective form factor after subtracting the fitted line in the top right panel. The data are from BESIII [105, 106], BaBar [103], CMD3 [107], BES [108], FENICE [109], E760 [110], E835 [111, 112] PS170 [104] and DM2 [113, 114].

as the measured values, are shown in Fig. 4.14. Note that the theory predictions were made assuming the old PDG value (from before 2019) of the Λ decay asymmetry parameter, $\alpha_\Lambda = 0.642$. The data are therefore rescaled to the old value. In Ref. [131], the phase is obtained with the 2019 update of α_Λ from PDG, $\alpha_\Lambda = 0.750$.

EMFFs of Λ_c^+ have been obtained from the measurements by Belle [133] and BESIII [134]. Furthermore, BESIII also measured the ratio $\mathcal{R}$ between the Λ_c^+ electric and magnetic form factors. In this measurement, as well as in the measurements of proton and Λ hyperon EMFFs near the threshold, interesting features can be observed: the cross-section undergoes a sharp rise close to the threshold, followed by a plateau in the case of positively charged proton [103, 107, 135] and Λ_c^+ [134], as shown in Fig. 4.15. Various FSI models have been employed to explain this behavior [116]. In the case of Λ_c^+, where there is a discrepancy between the data from Belle and BESIII, the cross-section has been studied with a model which takes into account the $Y(4630)$ resonance [139]. The threshold of the neutral Λ is particularly interesting. The cross-section of $e^+e^- \to \Lambda\bar{\Lambda}$ decreases after the sharp rise [127], which is similar to the behavior of $e^+e^- \to n\bar{n}$ [122]. It is difficult to explain with Eq. (4.9), since Λ is neutral, which means that $C = 1$, and hence the β factor should lead to a vanishing cross-section at the threshold. The non-zero cross-section near the threshold, as well as the wide plateau, have led to various interpretations, e.g. the final-state interactions [140], bound states or meson-like resonances [141, 142], and a gluon exchange contribution in the resummation factor [143, 144].

4.3.3 Prospects with BESIII

BESIII is uniquely suited for nucleon and strange hyperon form factor studies. It is currently the only running or planned e^+e^- experiment that is optimized for the energy region where nucleon-antinucleon and strange hyperons are produced in abundance. The capability of detecting and identifying charged and neutral particles, including the antineutron, is another advantage. Furthermore, the coming upgrade of the BEPCII collider up to the cms energy of 4.9 GeV will enable structure studies of single-charm hyperons. The following topics can be

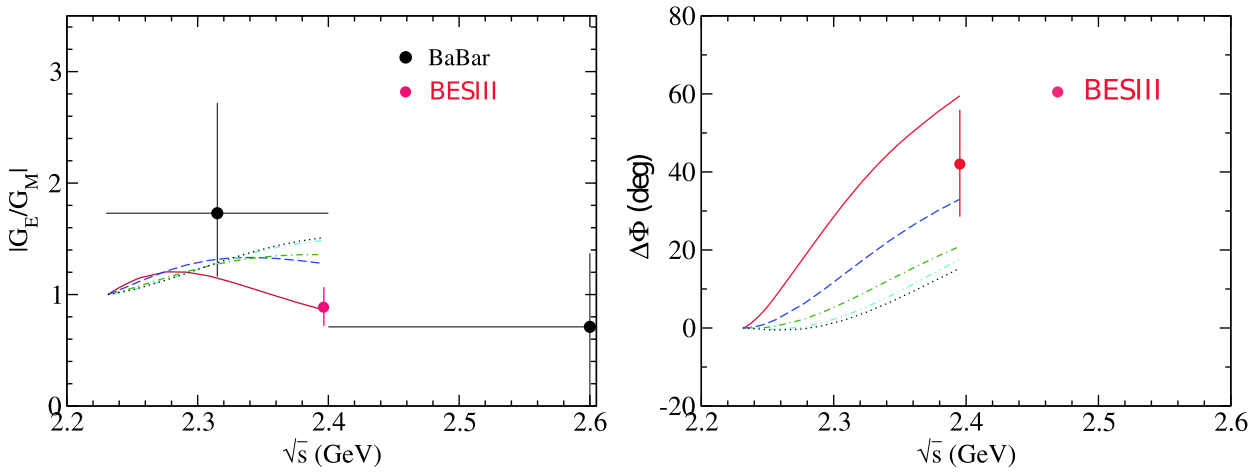

Fig. 4.14. (color online) BESIII results for $|G_E/G_M|$ and $\Delta\Phi$ compared with the theoretical predictions. The values obtained using the PDG value for α_Λ are shown since they were used for the theoretical predictions. The five lines are the different $\Lambda\bar{\Lambda}$ potentials used in [132]. Black dots are the results of BaBar [126]; red dots are the measurements by BESIII.

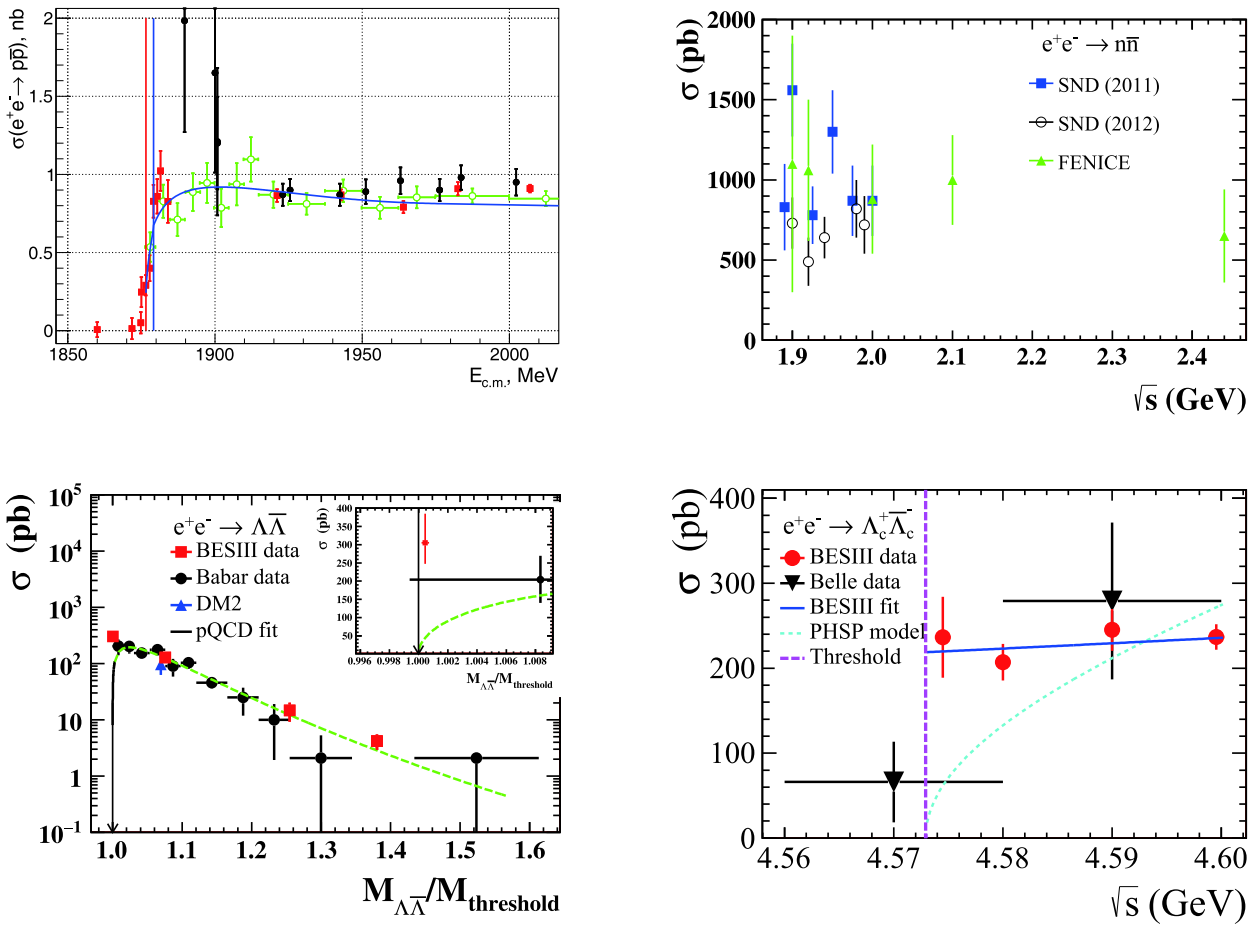

Fig. 4.15. (color online) Top left: the $e^+e^- \to p\bar{p}$ Born cross-sections measured by CMD-3 (black dots for Ref. [107], red squares for Ref. [135]) and BaBar [103] (green open circles). The solid curve shows the predictions from Ref. [136-138]. The vertical lines show the $p\bar{p}$ and $n\bar{n}$ thresholds. Top right: world data for $e^+e^- \to n\bar{n}$ (blue and white points for SND [122], and green points for FENICE [109]). Bottom left: the $e^+e^- \to \Lambda\bar{\Lambda}$ cross-section near the threshold, from BaBar [126] and BESIII [127]. Note that the scale on the y-axis is logarithmic. Bottom right: the $e^+e^- \to \Lambda_c^+\bar{\Lambda}_c^-$ cross-section from Belle [133] and BESIII [134].

addressed by BESIII in the near future:

● EMFF phase measurements of octet hyperons

Comparative studies of baryons with different isospin reveal the inner structure in terms of possible di-quark correlations [145]. For example, while the quark content of Λ and Σ^0 is the same, the isospin of the *ud* pair is different. As a consequence, the spin structure should be different. In the case of Σ^+, the isospin of the *uu* pair should be the same as of the *ud* pair in Λ. As a consequence, the cross-sections of $e^+e^- \to \Lambda\bar{\Lambda}$ and $e^+e^- \to \Sigma^+\bar{\Sigma}^-$ should be similar, as observed by CLEO. However, measurements should be performed at energies that do not coincide with charmonium resonances in order to avoid interference effects. Furthermore, spin observables should be more sensitive to the underlying quark structure. Hence, it would be important to study the EMFF phase for different octet hyperons. For the Σ triplet, simulation studies showed that $q = 2.5$ GeV/c is optimal in terms of the cross-section and reconstruction efficiency, and that 100 pb^{-1} would yield a sufficient number of events to extract the phase of Σ^+ and Σ^0. For the cascade doublet (Ξ^- and Ξ^0), the corresponding optimal point is $q = 2.8$ GeV/c.

● Energy dependence of the EMFF phase of the Λ hyperon

Preliminary calculations of the energy dependence of the Λ EMFF phase have been performed [146] in an attempt to predict the space-like EMFFs. However, the calculations call for measurements at additional energies in order to constrain the predictions. At present, the only conclusive measurement was obtained at $q = 2.396$ GeV/c. The analysis of these data, as well as simulations at other energies, show that data samples of $\approx$100 pb^{-1} are required to achieve the necessary sample size. At low energies, collecting such data samples is time consuming and the energy points should therefore be chosen very carefully. The data samples at 2.5 GeV and 2.8 GeV, proposed in the previous bullet point, coincide well with the relevant criteria, since the cross-section for these energies [126] should be sufficiently large.

● Neutron EMFFs

The analysis of the energy scan data from BESIII collected in 2015, shows that the methods for identifying neutron-antineutron final states have relatively low efficiency. In order to determine EMFFs with good precision, yet larger data samples are required. This is in line with the proposal in the previous point. In combination with the data collected in 2015 that are currently being analyzed, this will give a comprehensive picture of the neutron structure in the time-like region and enable comparative studies of proton and neutron EMFFs.

● Energy dependence of Λ_c^+ EMFFs

With the upgraded BEPCII ring, it will be possible to perform a precision scan from the $\Lambda_c^+\bar{\Lambda}_c^-$ threshold up to $q = 4.9$ GeV/c. The observed discrepancy between Belle and BESIII can be investigated and the possible importance of the $Y(4630)$ resonance can be reviewed. Furthermore, it will be possible to study the EMFF ratio and phase, as outlined in the Charm chapter.

● Threshold behavior of octet baryons

In addition to the samples collected during 2015 at the baryon-antibaryon thresholds which are currently being analyzed, additional samples are needed just below and slightly above each threshold. In this way, possible systematic effects can be detected and taken into account, and the observed behavior can be cross-checked. By comparing baryons of different charge, deeper insight can be gained, and a relation to possible resonances or interactions at the quark level can be established. In particular, a scan around the $\Sigma^+\bar{\Sigma}^-$ threshold with about 20 pb^{-1} per energy point would be very important.

● Contribution of the two-photon exchange

A contribution of the two-photon exchange would show as an asymmetry in the scattering angle distribution. This asymmetry has been measured in Ref. [131] and was found to be consistent with zero, although with a large uncertainty. Other baryon channels, for example $p\bar{p}$, where sample sizes are larger for a given integrated luminosity, can reach a precision where possible effects of the two-photon exchange can be revealed. This is particularly true if more data can be collected at a few off-resonance energies.

● Baryon form factor by the ISR method

The large amount of data that is to be collected at energies above 3.7 GeV enables studies of baryon EMFFs using the ISR method. This possibility is particularly important close to the threshold. Special event selection techniques are required for the analysis of the energy scan data due to the low momenta of the outgoing particles. Due to the boost of the ISR photon, the respective baryons have larger momenta in the laboratory frame and can be detected easier. In addition, it is currently technically challenging to collect energy scan data in the threshold region due to the design of the accelerator. However, away from the threshold, the statistical precision is generally better when using the energy scan method, as can be seen from a comparison of the proton EMFF studies using the ISR method [106] and the energy scan method [147]. Measurements of the form factor ratio and relative phase benefit from the data collected at well-defined energies with the scan method. The uncertainty in energy that is inevitable with the ISR method, propagates to the uncertainty in the ratio and phase.

4.4 Fragmentation function

The fragmentation function $D_q^h(z)$ describes the probability of a hadron h to be found in the debris of a quark (or antiquark), carrying the fraction z of the quark energy. $D_q^h(z)$ is an inherently non-perturbative object governing

hadronization. It cannot be deduced from first principles, but can be extracted from the experimental data [148, 149]. Fragmentation functions are assumed to be universal, i.e. they are not process dependent.

A large amount of data on inclusive hadron production from e^+e^- collisions has been collected in a wide energy range $10 \leqslant \sqrt{s} \leqslant 200$ GeV and $0.005 \leqslant z \leqslant 0.8$ [150]. These data sets, semi-inclusive deep-inelastic scattering (DIS) data and data sets from hadronic collisions were used to extract the fragmentation function by DSS [151], HKNS [152] and AKK08 [153]. However, the number of experimental data points is small, and the uncertainty of experimental data is large in the GeV energy region. Figure 4.16 compares the Kaon fragmentation function obtained by different fragmentation function packages; the favored $D_{\bar{s}}^{K+}(z,Q^2)$ changes very rapidly between $z = 0.2$ and $z = 0.3$ [154].

A precise determination of fragmentation functions could help to understand the internal structure of the nucleon, and resolve, for example, the strange quark polarization puzzle, i.e. the polarization of the strange quark which is positive in the measured region of Bjorken $x$obtained by semi-inclusive DIS analyses, but where inclusive DIS gives significant negative values of this quantity. It is pointed out in Ref. [155] that the polarization of the strange quark extracted from semi-inclusive DIS analyses is very sensitive to the input fragmentation functions. The semi-inclusive DIS process will be used to study the proton spin at the upgraded JLab-12 [156] and the future Electron-Ion Collider [157]. Thus, a better knowledge of fragmentation functions is needed.

DIS experiments have performed detailed studies of the transverse momentum dependence (TMD) by semi-inclusive processes. They describe the cross-sections in terms of the TMD parton density functions (PDF) and fragmentation functions. The TMD fragmentation function $D_q^h(z, P_{h\perp}^2, Q^2)$ describes a fragmentation process of an unpolarized parton q into an unpolarized hadron h, which carries the longitudinal momentum fraction z and transverse momentum $P_{h\perp}$ in the process. In order to understand TMD PDFs, knowledge of the TMD fragmentation functions is needed. Unfortunately, the determination of unpolarized TMD fragmentation functions is still missing [158]. With the data from the B factories and BESIII, the required TMD fragmentation functions could be extracted.

The Collins fragmentation function describes the spin-dependent effects in fragmentation processes [159]. It connects the transverse quark spin with a measurable azimuthal asymmetry (the so-called Collins effect) in the distribution of hadronic fragments along the initial quark momentum. This azimuthal asymmetry has been reported in semi-inclusive DIS and e^+e^- annihilation [158], where the Collins effect is studied in the e^+e^- annihilation by detecting simultaneously two hadrons, coming from the fragmentation of a quark and antiquark, in the process $e^+e^- \to h_1h_2 + X$. In this case, the observable is

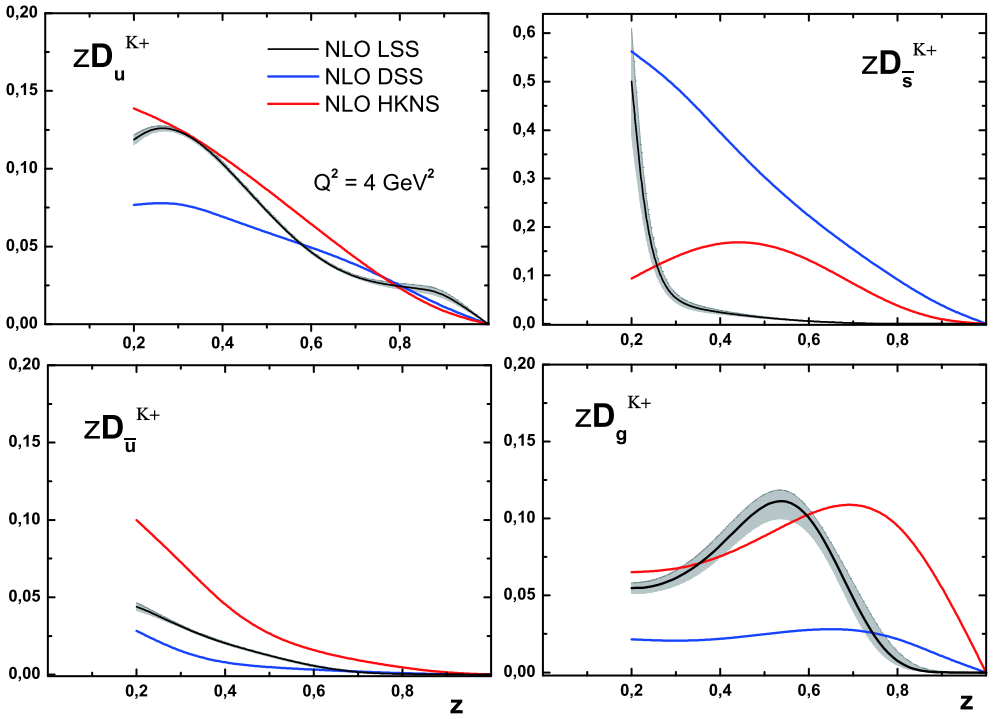

Fig. 4.16. (color online) Comparison between NLO LSS, DSS and HKNS Kaon fragmentation functions for $Q^2 = 4$ GeV^2, taken from Ref. [154].

associated with two Collins fragmentation functions.

The e^+e^- Collins asymmetries obtained by Belle and BaBar correspond to higher $Q^2(\approx 100\ \mathrm{GeV}^2)$ than the typical energy scale of existing DIS data (mostly $2-20\ \mathrm{GeV}^2$), which is similar to the scale at BESIII. Therefore, the very low cms energies at BESIII allow to investigate the energy scaling. The results are crucial for exploring the Q^2 evolution of the Collins fragmentation function and of the uncertainty of the extracted transversity, thus improving our understanding of both the Collins fragmentation function and transversity [160].

The Collins asymmetries for pion pairs have been obtained by BESIII using the data collected at $\sqrt{s}=3.65$ GeV with an integrated luminosity of 62 pb^{-1} [161]. Figure 4.17 compares the Collins effect measured by BESIII, BaBar and Belle. The measured asymmetries are almost consistent with zero for low (z_1,z_2), and rise with increasing z. The BESIII asymmetry in the last interval is about two-three times larger than measured at the B factories. Additional results are needed to confirm this observation with about 250 pb^{-1} data at 3.65 GeV. The Collins effect for strange quarks could be studied in $e^+e^-\to\pi K+X$ and $e^+e^-\to KK+X$. It is also interesting to study the Collins effect in $e^+e^-\to\pi^0\pi^0+X$, $e^+e^-\to\eta\eta+X$ and $e^+e^-\to\pi^0\eta+X$ for neutral hadrons. These results are useful for extracting TMD PDFs.

4.5 τ physics at BESIII

Since the discovery of the τ lepton in 1975 at the SPEAR e^+e^- storage ring [162], the τ lepton has been measured extensively. The properties of the τ lepton, including its mass, lifetime and decays, have been tested thoroughly [1]. As a member of the third fermion generation, it decays to the first and second generation fermions. The pure leptonic or semileptonic character of τ decays provides a clean laboratory to test the structure of the weak currents and the universality of their coupling to gauge bosons. Moreover, as τ is the only lepton massive enough to decay into hadrons, the semileptonic decays are an ideal tool for studying strong interactions.

BEPCII is a τ-charm factory with the cms energy ranging from 2.0 to 4.9 GeV, and the design peak luminosity of $10^{33}\ \mathrm{cm}^{-2}\ \mathrm{s}^{-1}$ at the cms energy of 3.773 GeV. The great advantage of BEPCII lies in running near the threshold of τ pair production, which provides an excellent opportunity for τ lepton physics. Compared with oth-

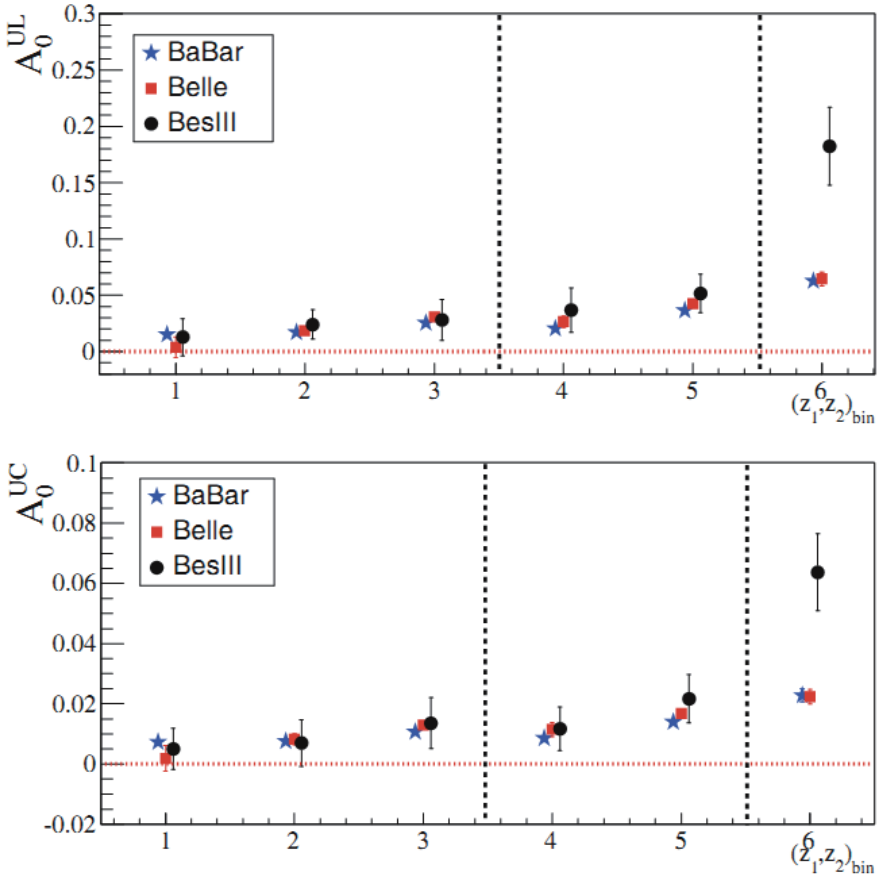

Fig. 4.17. (color online) Comparison of the measurements of the Collins effect by BESIII, BaBar and Belle. The definition of the axis can be found in Ref. [161].

er machines, the threshold region makes possible a much better control of the background and of the systematic uncertainties of measurements.

There are three energy regions which are important for experimental studies. The first is below the τ pair production threshold, around 3.50 GeV, where the light quark background can be measured and the results can be extrapolated to other energy regions. The second is at the production threshold, 3.55 GeV, where the τ lepton pair is produced at rest. It is a unique energy to study τ decays. The third region is above the τ pair production threshold, which can be further classified into two subregions: (a) below the production of open charm, around 3.69 GeV, where the background is the same as in the region below the threshold; and (b) at 4.25 GeV, where the cross-section of the τ pair production is maximum, while the charm background is an addition to the light quark background.

Figure 4.18 shows the production cross-section and the R ratio for τ pairs in the energy region of BEPCII. The luminosity at the τ lepton threshold is about 0.3×10^{33} cm^{-2}s^{-1}. Therefore several hundred thousand τ lepton pairs can be produced in a year of running (about six months). In the past years, BESIII had taken about one month of data near the τ lepton pair production threshold, i.e. about 150 pb^{-1} have been collected. Compared with the experiments at higher energies, such as the B factories and the LHC, BESIII is at a disadvantage in terms of statistics. An immense amount of data have been obtained by high energy experiments, and many measurements were performed very precisely. The energy of BEPCII is low, the produced τ leptons are almost stationary, and the equipment does not allow to measure the life time of the τ lepton accurately.

The advantage of BEPCII are the experimental conditions: the machine runs near the threshold of τ pair production, the background is simple and the systematic uncertainties can be controlled easily. The beam energy spread of BEPCII is small, about 1-2 MeV. Moreover, the beam energy measurement system (BEMS) was built such that the energy and energy spread can be controlled accurately. Therefore, BESIII has a unique advantage for performing τ mass measurements.

4.5.1 Measurement of the τ mass

τ is one of the three charged elementary leptons in Nature, and its mass is an important parameter of the Standard Model. The improvement of accuracy of τ mass (m_τ) is needed in its own right. Listed below are the measured masses of the three leptons according to PDG2012 [163]:

$$\begin{aligned} m_e &= 0.510998910\pm0.000000013\text{MeV}(\delta m_e/m_e\approx 2.554\times10^{-8}),\\ m_\mu &= 105.658367\pm0.000004\text{MeV}(\delta m_\mu/m_\mu\approx 3.786\times10^{-8}),\\ m_\tau &= 1776.82\pm0.16\text{MeV}(\delta m_\tau/m_\tau\approx 9.568\times10^{-5}). \end{aligned} \tag{4.15}$$

It can be seen that the accuracy of m_τ is almost four orders of magnitude worse than that of the other two leptons. The accuracy of the electron and muon masses is already at the level of 10^{-8}.

A well-known motivation for obtaining an accurate

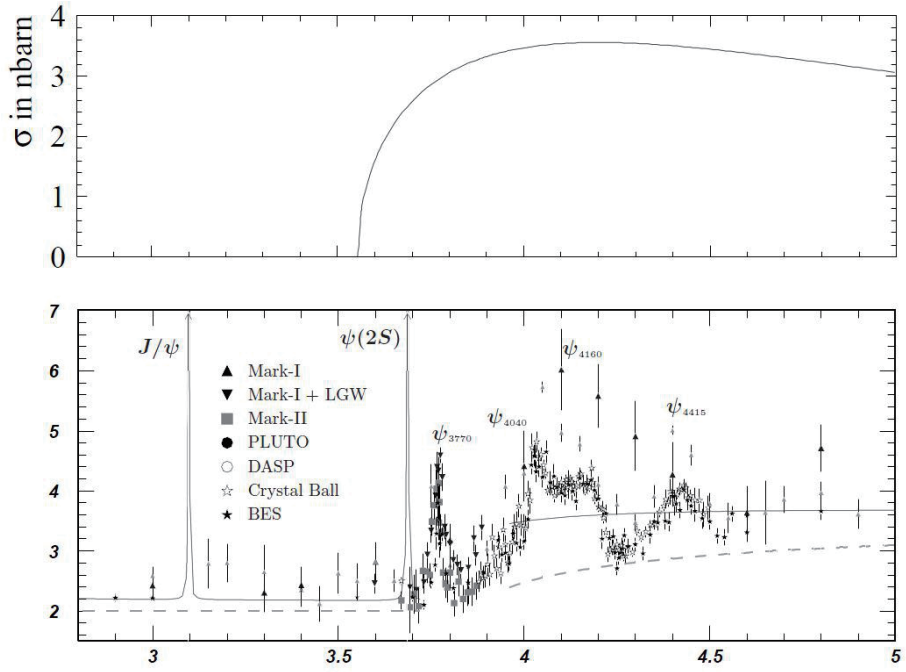

Fig. 4.18. Top: The production cross-section for τ pairs. Bottom: The R ratio, showing the expected background from quark production (from PDG). The cross-section and R values are shown as function of the cms energy in GeV on identical scales.

value of m_τ is the test of lepton universality. Lepton universality, a basic ingredient of the Standard Model, requires that the charged-current gauge coupling strengths g_e, g_μ, g_τ are identical: $g_e = g_\mu = g_\tau$. Comparing the electronic branching fractions of τ and μ, the lepton universality can be tested as:

$$\left(\frac{g_\tau}{g_\mu}\right)^2 = \frac{\tau_\mu}{\tau_\tau}\left(\frac{m_\mu}{m_\tau}\right)^5 \frac{B(\tau \to e\nu\bar{\nu})}{B(\mu \to e\nu\bar{\nu})}(1+F_W)(1+F_\gamma), \quad (4.16)$$

where F_W and F_γ are the weak and electromagnetic radiative corrections [164]. Note that $(g_\tau/g_\mu)^2$ depends on m_τ to the fifth power.

Furthermore, the precision of m_τ also restricts the final sensitivity of m_{ν_τ}. The most sensitive bound on the mass of ν_τ is derived from the analysis of the invariant mass spectrum of semi-hadronic τ decays. At present, the best limit of $m_{\nu_\tau} < 18.2$ MeV/c^2 (95% confidence level) is based on the kinematics of 2939 (52) events of $\tau^- \to 2\pi^-\pi^+\nu_\tau$ ($\tau^- \to 3\pi^-2\pi^+(\pi^-)\nu_\tau$) [165]. This method depends on the determination of the kinematic end point of the mass spectrum, thus, high precision of m_τ is needed.

Another test also depends only on the accuracy of m_τ. An interesting formula relating the three lepton masses was discovered in 1981 [166]:

$$m_e + m_\mu + m_\tau = \frac{2}{3}(\sqrt{m_e} + \sqrt{m_\mu} + \sqrt{m_\tau})^2 . \quad (4.17)$$

According to the error propagation formula (f_m indicates the difference between the right and left sides of Eq. (4.17))

$$\delta f_m = \sqrt{\sum_{k=e,\mu,\tau}\left[m_k - \frac{2}{3}\left(\sum_{i=e,\mu,\tau}\sqrt{m_k m_i}\right)\right]^2 \cdot \left(\frac{\delta m_k}{m_k}\right)^2} \approx \frac{1}{3}\delta m_\tau , \quad (4.18)$$

the test of Eq. (4.17) depends almost merely on the accuracy of m_τ.

The measurement of the τ mass has a history of more than forty years. In the first experimental paper on the τ lepton [162], m_τ is estimated to have a value in the range from 1.6 to 2.0 GeV/c^2. Since then, many measurements of m_τ have been performed [167-182], whose results are displayed in Fig. 4.19.

The results of m_τ measurements in the 21st century are summarized in Table 4.2, where two results were ob-

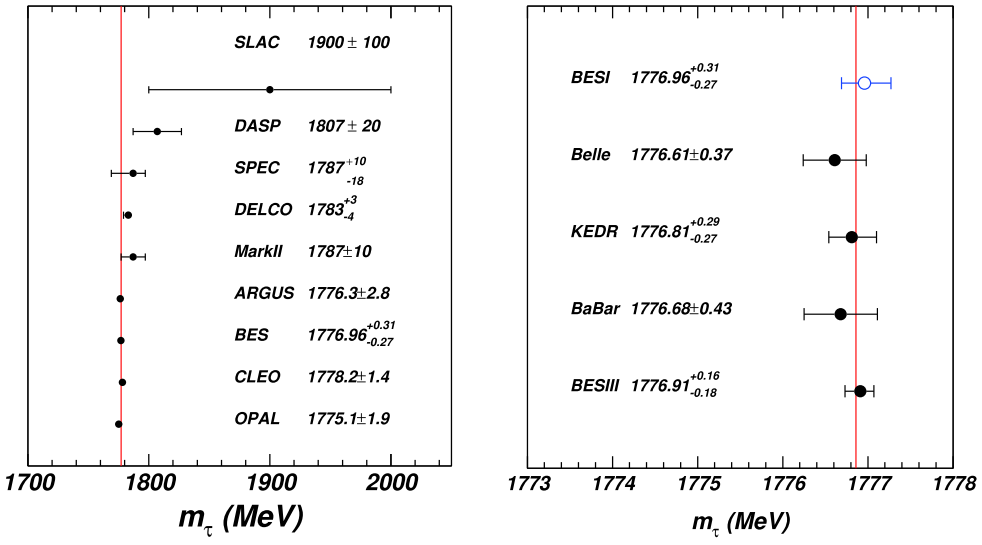

(a) m_τ measured in the 20 century (b) m_τ measured in the 21 century

Fig. 4.19. (color online) m_τ measured in the 20th and 21st century. In (a), the red line indicates the average value of m_τ in PDG2000 [183], $m_\tau = 1777.03^{+0.30}_{-0.26}$ MeV/c^2. For comparison, the measured value by BES in 1996 is plotted in (b) as a blank blue circle. The average value of m_τ in PDG2015 [184], $m_\tau = 1776.86 \pm 0.12$ MeV/c^2, is indicated by the red line in (b). It should be noted that since PDG1996 [185, 186], the results of experiments performed before 1990 were removed, except for the result of DELCO.

Table 4.2. Measurement results of m_τ in the 21 century.

measured m_τ/(MeV/c^2)	year	Exp. group	data sample	method
$1776.91 \pm 0.12^{+0.10}_{-0.13}$	2014	BESIII [185]	23.26 pb^{-1}	threshold-scan
1776.68±0.12±0.41	2009	BaBar [184]	423 fb^{-1}	pseudo-mass
$1776.81^{+0.25}_{-0.23} \pm 0.15$	2007	KEDR [183]	6.7 pb^{-1}	threshold-scan
1776.61±0.13±0.35	2007	Belle [182]	414 fb^{-1}	pseudo-mass

tained using the method of pseudo-mass, while the other experiments used the method of threshold scan. For the pseudo-mass method, huge amount of data acquired at the B-factories was used [179]. Good statistical accuracy was achieved, but large systematic uncertainties exist, which is mainly due to the absolute calibration of the particle momentum. In the threshold scan method, the value of m_τ was extracted from the dependence of the production cross-section on the beam energy. In the KEDR experiment [180], both the resonant depolarization technique and the Compton backscattering technique [187] were used to determine the beam energy. These techniques greatly reduce the uncertainty of the beam energy.

Although the accuracy of the results of the two methods are comparable, it is obvious that the pseudo-mass method is dominated by systematic errors. Additional data taking will not improve this result. For the threshold scan method, however, there still seems to be room for improvement of both the statistical and systematic errors. Therefore, the BESIII collaboration adopted the threshold scan method to measure m_τ. In this approach it is of utmost importance to determine precisely the beam energy and the beam energy spread. For this purpose, starting from 2007, a high accuracy BEMS, located at the north crossing point (NCP) of BEPCII, was designed, constructed, and finally commissioned at the end of 2010 [188-192]. Two days were spent to perform a scan of the $\psi(3686)$ resonance. The difference between the PDG value of the mass in 2010 and the measured mass using BEMS is 1 ± 36 keV, which indicates that the relative accuracy of BEMS is at the level of 2×10^{-5} [191].

Prior to conducting the experiment, a study was carried out using MC simulation and sampling to find the scheme that provides the highest precision of m_τ for a specified period of data taking, or equivalently for a given integrated luminosity. The main conclusions of the optimization study can be summarized as follows [193-197]:

1. For N free parameters, N scan points are sufficient;

2. The optimal position can be obtained by a single parameter scan;

3. Luminosity allocation can be determined analytically or by simulation;

4. The uncertainty of m_τ is proportional to the inverse square root of the luminosity.

On the basis of these conclusions, the optimal scan strategy was designed as follows: first, a scan of the J/ψ resonance (scan points 1-7) is performed, followed by a scan in the vicinity of the τ pair threshold (scan points 8-12), with finally a scan of the $\psi(3686)$ resonance (scan points 13-19). A repeated measurement is then made (in τ region, the data are taken only at scan points 9 and 10). The two-round process was designed to understand the stability of the accelerator and of the detector. The key issue was to acquire 100 pb^{-1} of data in the τ region to guarantee an uncertainty of m_τ of less than 0.1 MeV/c^2. The scan plan and the offline results are summarized in Table 4.3.

Based on these preparations, the BESIII collaboration performed the fine τ mass scan experiment from April 14th to May 3rd, 2018. The actual data taking time was around 11.2 days (269 hours). The J/ψ and $\psi(3686)$ resonances were scanned at seven and nine energy points, respectively, and the data were collected at five scan points near the τ pair production threshold with cms energies 3538.9, 3552.8, 3553.9, 3560.3, and 3599.5 MeV. The first τ scan point is below the mass of the τ pair [163], while the other three are above[1)].

Using these data samples, the goal of the fine scan is to obtain the τ lepton mass with high precision, at the level of 0.1 MeV, which includes statistical errors and

Table 4.3. The scan plan and offline results. Superscript "plan" indicates the planned value for the scan; "exp" indicates the measured value of the scan; "online" denotes the value from the online record. $E_{\rm beam}$ and $\mathcal{L}$ are the beam energy and the integrated luminosity. (†: the planned values are listed in the last two columns; ‡: the measured values are slightly different from the expected due to the fluctuation of the accelerator.

energy region	order	$E^{\rm plan}_{\rm beam}$/MeV	$\mathcal{L}^{\rm plan}$/pb^{-1}	$E^{\rm exp}_{\rm beam}$/MeV	$\mathcal{L}^{\rm online}$/pb^{-1}	$E^{\rm plan}_{\rm beam}$/MeV		
						order	J/ψ	$\psi(3686)$
J/ψ	1-7	†	–	‡	32.6	1/13	1544.0	1838.0
τ	8	1771.0	14	1769.74	25.5	2/14	1547.8	1841.9
	9	1776.6	14+25	1776.43	42.6	3/15	1548.2	1842.5
	10	1777.0	14+12	1776.96	27.1	4/16	1548.6	1843.1
	11	1780.4	7	1780.18	8.3	5/17	1549.0	1843.8
	12	1792.0	14	1800.27	28.8	6/18	1549.4	1844.5
$\psi(3686)$	13-19	†	–	‡	67.2	7/19	1552.0	1847.0

1) The original two-round process was designed mainly to understand the stability of accelerator and detector. During the period of m_τ scan, the status of accelerator and detector was fairly good, so two-round process degenerated into no-circle process.

systematical uncertainties. It is an unprecedented accuracy, and as indicated in Ref. [198], this is a challenging task that needs considerable effort, energy, and great patience.

The statistical uncertainty of the m_τ measurement is roughly equal to the systematical errors. Only when a better way is found to reduce the systematical errors, will BESIII collect more data in order to improve further the precision of m_τ.

4.5.2 Some τ-physics topics at BESIII

As mentioned above, τ is the only lepton heavy enough to decay into hadrons. At present, its partial decay width involving hadrons in the final state is about 65%. The hadronic τ decays turn out to be a beautiful laboratory for studying the non-perturbative regime of QCD, and are useful to understand the hadronization of QCD currents, to study the form factors and to extract resonance parameters.

Rare decays of τ leptons are a very promising area because their interaction is suppressed and the sensitivity to new physics might be enhanced. In SM, the suppression of rare τ decays might be due to several reasons: i) Cabbibo suppression: strange hadronic final states are suppressed with respect to non-strange states since the $|V_{us}|$ element of the CKM matrix enters the description of J^{PC} instead of $|V_{ud}|$; ii) phase space suppression: because of the larger masses of Kaon and η mesons in the final state, the phase space should always be suppressed; iii) second class currents: in hadronic τ decays, the first class currents have $J^{PC} = 0^{++}$, 0^{--}, 1^{+-} or 1^{-+}, and are expected to dominate. The second class currents, which have $J^{PC} = 0^{+-}$, 0^{-+}, 1^{++} or 1^{--}, are associated with a matrix element proportional to the mass difference between up and down quarks. They vanish in the limit of perfect isospin symmetry, but are not prohibited in SM, which indicates that the branching fractions of such τ decays are of the order of 10^{-5}.

The τ lepton provides a clean way to search for second class currents via the decay mode $\tau^- \to \pi^-\eta\nu_\tau$. The $\pi^-\eta$ final state must have either $J^{PC} = 0^{+-}$ or $J^{PC} = 1^{--}$, both of which can only be produced via second class currents.

The CLEO collaboration analyzed 3.5 fb^{-1} of data taken at $\sqrt{s} = 10.6$ GeV, and produced the most stringent limit on $\tau^- \to \pi^-\eta\nu_\tau$ decays, $\mathcal{B}(\tau^- \to \pi^-\eta\nu_\tau) < 1.4\times10^{-4}$ at the 95% confidence level [199]. The BaBar collaboration analyzed 470 fb^{-1} of data taken at $\sqrt{s} = 10.6$ GeV, studied the decay $\tau^- \to \pi^-\eta\nu_\tau$, and set the upper limit $\mathcal{B}(\tau^- \to \pi^-\eta\nu_\tau) < 0.99\times10^{-4}$ at the 95% confidence level [200].

The study of the second class currents is both promising and challenging. On the one hand, the energy region of BEPCII is near the τ pair production threshold and the background is relatively simple. On the other hand, since BEPCII luminosity is relatively low, even if the τ data are taken at the maximum cross-section at 4.25 GeV, BESIII would need to run for ten years to achieve the required precision of 10^{-4}.

The decay of the τ lepton into three pseudoscalar particles can provide information about the hadronic form factors, the Wess-Zumino anomaly, and can also be used for studies of CP violation in the leptonic sector. A study of decays into final states containing three Kaons can provide a direct determination of the strange quark mass and the Cabibbo-Kobayashi-Maskawa (CKM) matrix element $|V_{us}|$.

The BaBar collaboration [201] studied the decay mode $\tau^- \to K^-K^+K^-\nu_\tau$ and obtained the branching fraction $\mathcal{B}(\tau^- \to K^-K^+K^-\nu_\tau) = (1.58\pm0.13\pm0.12)\times10^{-5}$ by analyzing 342 fb^{-1} of data at a cms energy near 10.58 GeV using the BaBar detector at the SLAC PEP-II asymmetric-energy e^+e^- storage ring. The Belle collaboration [202] also measured the branching fraction of this channel and obtained $(3.29\pm0.17\pm0.20)\times10^{-5}$, based on a sample of 666 fb^{-1} of data collected with the Belle detector at the KEKB asymmetric-energy e^+e^- collider at 10.58 GeV. The difference between the two measurements is larger than 3 standard deviations.

BESIII could perform this measurement if enough data are collected.

4.5.3 Measurement of the branching fraction of $\psi(3686)\to\tau^+\tau^-$

$\psi(3686)$ provides a unique opportunity to compare the three lepton generations by studying the leptonic decays $\psi(3686) \to e^+e^-$, $\mu^+\mu^-$, and $\tau^+\tau^-$. The sequential lepton hypothesis leads to a relationship between the branching fractions of these decays, $\mathcal{B}_{e^+e^-}$, $\mathcal{B}_{\mu^+\mu^-}$, and $\mathcal{B}_{\tau^+\tau^-}$ given by

$$\frac{\mathcal{B}_{e^+e^-}}{v_e(\frac{3}{2}-\frac{1}{2}v_e^2)} = \frac{\mathcal{B}_{e^+e^-}}{v_\mu(\frac{3}{2}-\frac{1}{2}v_\mu^2)} = \frac{\mathcal{B}_{e^+e^-}}{v_\tau(\frac{3}{2}-\frac{1}{2}v_\tau^2)} \tag{4.19}$$

with $v_l = [1-(4m_l^2/M^2_{\psi(3686)})]^{1/2}$, $l = e,\mu,\tau$. Substituting the masses of the leptons and $\psi(3686)$ yields

$$\mathcal{B}_{e^+e^-} = \mathcal{B}_{\mu^+\mu^-} = \frac{\mathcal{B}_{\tau^+\tau^-}}{0.3885} \equiv \mathcal{B}_{l^+l^-}. \tag{4.20}$$

BES preformed such a study based on 3.96 million $\psi(3686)$ events at $\sqrt{s} = 3686.36$ MeV [182]. With the BESIII data sample, a more detailed study can be expected.

In 2018, BESIII performed a fine $\psi(3686)$ scan at 10 points with 67 pb^{-1} of data. With this large sample, rather than using Eq. (4.19), it is possible to measure each branching fraction separately and to test the relations between them. Furthermore, with a number of scan points, the interference between the continuum and the resonance can be measured directly, as can the phase angle between them. This will be a very technical and interesting work related to the τ lepton.

4.5.4 Mass measurement for some hadrons

The mass of τ lepton can be determined precisely by means of BEMS. However, not all hadron masses can be determined using BEMS. The details of BEMS can be found in Refs. [193, 203]. Generally speaking, the allowed region of beam energies for BEMS should not exceed 2 GeV. On the one hand, with a high purity germanium detector, the upper limit of the Compton backscattered photons is 10 MeV; on the other hand, there are no suitable radiation sources to calibrate the detector for such high energy backscattered photons. Moreover, the detection efficiency of high Compton backscattered photons is relatively low. Hence, it is better to measure the masses of hadrons, such as D_s^*, D_{s0}, D_{s1}, Λ_c, Σ_c, using the invariant mass method, if we have enough data.

4.5.5 Discussion

The measurements involving τ leptons can be divided into three categories: the mass of τ, the life time of τ and the measurements related to the branching fractions of τ decay. Except for the τ mass measurement, BESIII lacks competitive power for the other measurements due to the limitation of data samples.

4.6 Relative phase in vector charmonium decays

For many years, there has been evidence of an unexpected phenomenon in the decay of narrow charmonium resonances. A relative phase of $|\Delta\Phi| = 90°$ between the strong and EM decay amplitudes of J/ψ was observed [204]. In case of $\psi(3686)$, the available evidence is less compelling. However, $\psi(3686)$ scan data have been collected at BESIII and are being analyzed, e.g. $e^+e^- \to \mu^+\mu^-, KK, \eta\pi^+\pi^-$ and baryon pairs. Concerning $\psi(3770)$, the phase difference was measured in a few cases and $\Delta\Phi = -90°$ was established [205, 206].

Taking into account the aforementioned values, this phase difference implies $\Gamma_P = \Gamma_{\rm EM} + \Gamma_{\rm strong}$, where Γ_P is the total width of the vector charmonium P. This relation might suggest an unconventional hypothesis that J/ψ is a combination of two resonances, one decaying only via the EM processes and the other decaying strongly (see [204] and references therein).

Currently available data are barely sufficient to determine the absolute value of $\Delta\Phi$ for J/ψ in a limited number of decay modes. The process $\eta\pi^+\pi^-$ is observed with low statistics in the J/ψ line shape scan with 16 energy points and a total integrated luminosity of about 100 pb^{-1}, where the fit procedure introduces a systematic uncertainty of 11% [204]. With ten times more data, we could obtain a more precise measurement of $\Delta\Phi$. In a few of those cases it might also be possible to determine the sign of the relative phase of EM and strong amplitudes. However, in J/ψ decays into baryon pairs, the "magnetic" and "electronic" amplitudes might have different phases.

An intriguing situation has been found in $J/\psi \to \pi\pi$. Due to the G parity violation, a purely strong amplitude should be suppressed. However, the EM amplitude is not sufficient to explain the partial with of $J/\psi \to \pi\pi$. As a remedy, an amplitude was suggested with two gluons and one virtual photon as an intermediate state [207]. In order to test this hypothesis, it is most interesting to determine the relative phase between the strong and EM decay amplitudes in the $J/\psi \to \pi\pi$ decay. The currently available data at BESIII, however, do not allow such investigations.

In conclusion, much more data are needed to settle the issue of the phase difference between the strong and EM decay amplitudes of vector charmonium states. If the aforementioned double nature of charmonium is confirmed, an important ingredient is missing in the understanding of the Zweig rule (see Ref. [208] and references therein).

4.7 Study of $\phi(2170)$ with the energy scan method

Quarkonia provide a unique platform to study QCD. Substantial progress has been made over the recent years in the investigation of charmonia ($c\bar{c}$) and bottomonia ($b\bar{b}$). A plethora of interesting new hadronic states was found. New types of hadronic matter, such as hybrids, multiquark states, and hadronic molecules with (hidden) charm and bottom quarks are considered in the interpretations [209-211].

The multitude of results from heavier quarkonia leads to the obvious question whether similar states should exists in the strange sector. However, experimental evidence for a rich spectrum of strangeonium ($s\bar{s}$) or new types of hadronic matter with strange quarks is scarce. Figure 4.20 shows the predicted strangeonium states [212] with identified $s\bar{s}$ resonances [24]. Only 10 probable $s\bar{s}$ resonances out of the 22 expected below 2.2 GeV have been established. A candidate for an exotic type of hadronic matter containing strange quarks is $\phi(2170)$. At BESIII, $\phi(2170)$ can be studied as an intermediate state in charmonium decays, exploiting the unique statistics of the J/ψ data set, and by performing a dedicated energy scan around the mass of $\phi(2170)$. Both methods provide unique opportunities in terms of precision and accuracy, which are necessary to understand the nature of $\phi(2170)$.

$\phi(2170)$, previously referred to as $Y(2175)$, has been observed in $e^+e^- \to \phi f_0(980)$ at B factories using the ISR method [213-215], in the charmonium decay $J/\psi \to \eta\phi f_0(980)$ [216, 217], and in $e^+e^- \to \eta\phi f_0(980)$ at cms energies between 3.7 and 4.6 GeV [218]. Theorists explain it as a traditional $3^3S_1 s\bar{s}$ or $2^3D_1 s\bar{s}$ state [219-222], as a $1^{--} s\bar{s}g$ hybrid [223], as a tetraquark state [224-227], as a $\Lambda\bar{\Lambda}(^3S_1)$ bound state [228-230], and as a $\phi K\bar{K}$ resonance state [231, 232]. According to PDG [24], $\phi(2170)$ has been observed in the final states $\phi f_0(980)$, $\phi\eta$, $\phi\pi\pi$, and $K^+K^- f_0(980)$. For the final state $K^{*0}\bar{K}^{*0}$, only an

upper limit has been reported [233]. Hence, the number of experimentally established decay modes of $\phi(2170)$ is limited. In addition, as shown in Fig. 4.21, there is a large scatter of the measured values of the mass and width of $\phi(2170)$. So far, none of the above theory models has been confirmed or ruled out by the experimental results.

Describing $\phi(2170)$ as a $3^3S_1 s\bar{s}$ or $2^3D_1 s\bar{s}$ state favors the decay modes $K^*\bar{K}^*$, $K\bar{K}(1460)+c.c.$, and $\eta h_1(1380)$, while these modes are forbidden for a $1^{--} s\bar{s}g$ state. Instead, $K\bar{K}_1(1400)+c.c.$ and $K\bar{K}_1(1270)+c.c.$ are favored for the $1^{--} s\bar{s}g$ state [212, 219, 223]. However, all four decays produce the same final state: $K\bar{K}\pi\pi$. Originally, $\phi(2170)$ was observed in the $\phi\pi\pi$ final state, an intermediate state of $K\bar{K}\pi\pi$. The fitted $\phi(2170)$ resonance parameters $m=(2079\pm13)$ MeV/c^2 and $\Gamma=(192\pm23)$ MeV in the $\phi\pi\pi$ mode are slightly lower than $m=(2163\pm32)$ MeV/c^2 and $\Gamma=(125\pm40)$ MeV in the $\phi f_0(980)$ mode [215], which is consistent with the available measurements in the $\phi f_0(980)$ mode (see Fig. 4.21). A PWA analysis of $e^+e^-\to K\bar{K}\pi\pi$ by BESIII would be useful to distinguish between $s\bar{s}$ and $s\bar{s}g$, and to understand the results obtained from the $\phi\pi\pi$ and $\phi f_0(980)$ modes.

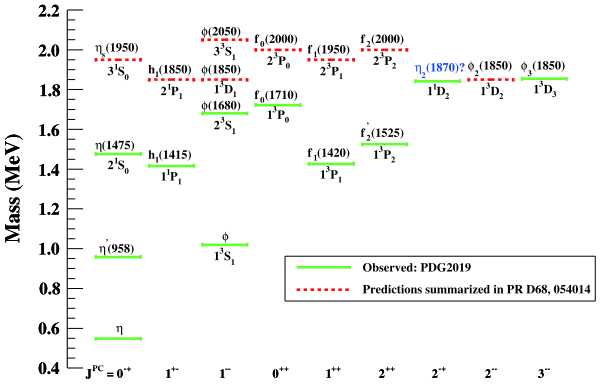

Fig. 4.20. (color online) The strangeonium spectroscopy. The red dotted line corresponds to predicted strangeonium states summarized in Ref. [212], and the green line corresponds to observed $s\bar{s}$ resonances taken from PDG [24].

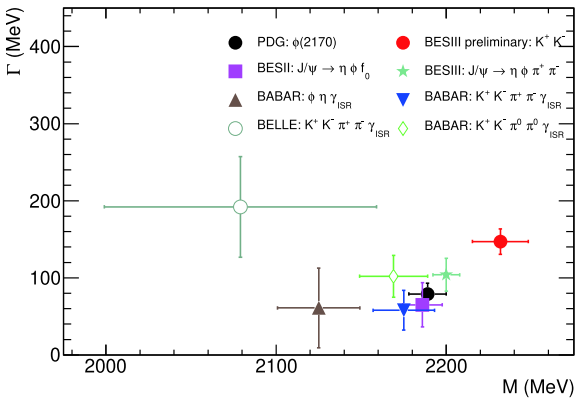

Fig. 4.21. (color online) Mass and width of $\phi(2170)$.

The $e^+e^-\to\phi\eta$ and $e^+e^-\to\phi\eta'$ processes are well suited for studying the excited ϕ states, and useful for estimating the mass and width of strange quarkonia due to the OZI rule. The main decay modes in the tetraquark picture [226] are the $\phi\eta$ and $\phi\eta'$ modes. The predicted decay width of the $1^{--} s\bar{s}g$ state to $\phi\eta$ is much larger than of $\phi\eta'$ [223, 234], whereas $\phi\eta$ is forbidden for $2^3D_1 s\bar{s}$ states [219]. However, the uncertainty of the cross-section of $\phi\eta$ around $\sqrt{s}=2.2$ GeV, measured by BaBar, is at the 50% level [235]. A clear signal of $\phi\eta'$ was observed by BaBar [236]. A precise measurement of $\phi\eta$ and $\phi\eta'$ modes at BESIII would be useful to distinguish between the tetraquark, hybrid and 2^3D_1 pictures of $\phi(2170)$. Besides $\phi(2170)$, there is another possible structure of $\phi f_0(980)$ and $K^+K^-f_0(980)$ around 2.4 GeV [213-217]. BaBar determined its mass and width as (2.37 ± 0.07) GeV/c^2 and (77 ± 65) MeV, while Ref. [237] reported (2436 ± 34) MeV/c^2 and (99 ± 105) MeV, respectively, with a statistical significance smaller than 3σ. A QCD sum rule also predicts two $J^{PC}=1^{--}$ resonances (2.34 ± 0.17) GeV and (2.41 ± 0.25) GeV, both around 2.4 GeV [238]. In the ϕK^+K^- mode, two broad structures were observed at 2.3 GeV and 2.7 GeV, albeit in a different $m(K^+K^-)$ range [213, 214]. A scan in 40 MeV steps in the range [2.35, 2.83] GeV, with an integrated luminosity of 20 pb^{-1} at each energy point, is called for to search for (possible) new resonances.

Last but not least, Refs. [220, 239] predict a broad resonance with a mass around 1.9 GeV, regarded as the $1D$ state of the ϕ family. A new scan between 1.8 and 2.0 GeV is needed to search for $1^3D_1 s\bar{s}$ (shown in Fig. 4.20), and to investigate the threshold production of nucleon pairs and a structure around 1.9 GeV, shown in Ref. [240]. The scan should be performed in 10 MeV steps between 1.8 and 2.0 GeV, with an integrated luminosity of 4 pb^{-1} at each energy point.

Based on the collected data for R values in the energy range between 2.0 and 3.08 GeV, we already studied the final states K^+K^- [241], ϕK^+K^- [242], and $K^+K^-\pi^0\pi^0$ [243], and the investigation of further possible decay modes is ongoing. However, more data at additional energy points are needed, which are listed in Table 4.4.

4.8 Prospects

The different physics aspects addressed in this chapter cannot be studied with a single data set. While studies based on ISR or two-photon collisions require large data samples, taken at masses well above the actual mass range of interest, precise studies of line shapes or threshold effects are best performed with several smaller data sets in an energy scan.

The existing ISR studies were mostly performed with 2.9 fb^{-1} taken at the $\psi(3770)$ peak. The results are already

Table 4.4. Proposed data for τ-QCD study.

energy	physics highlight	current data	expected final data	time/d
1.8-2.0 GeV	R, nucleon, resonances	N/A	96 pb^{-1} at 23 points	66
around 2.2324 GeV	$\Lambda\bar{\Lambda}$ threshold	one point	40 pb^{-1} at 4 points	17
2.35-2.83 GeV	R & resonances	few points	260 pb^{-1} at 13 points	60
2.5 GeV	hyperon	1 pb^{-1} data	100 pb^{-1}	26
J/ψ scan	phase	100 pb^{-1} data	1000 pb^{-1}	150

competitive with previous measurements of hadronic cross-sections. However, one of the key issues, the hadronic contributions to a_μ, is still open. The published BESIII result for the dominant $\pi^+\pi^-$ contribution is currently dominated by systematics, where the largest contributions stem from the uncertainties of the luminosity determination and the theoretical uncertainty of the radiator function. An alternative approach to the normalization of the cross-section can reduce the systematic uncertainty. Using the ratio with respect to the muon cross-section, cancels the two uncertainties mentioned above. However, due to an insufficient muon yield in the current data set, the statistical uncertainty becomes dominant. Based on the published results, it is estimated that an additional data set of 20 fb^{-1} taken at the $\psi(3770)$ peak, and the data set proposed in Chapter 3 for XYZ physics, will allow to collect sufficient statistics to perform the normalization of the hadronic cross-sections with respect to the muon yield. The systematic uncertainty of the pion form factor measurement could be reduced to $O(0.5\%)$, making the BESIII result not only comparable, but competitive with KLOE, BaBar and the announced CMD-3 measurements, as well as with the potential future analyses by Belle II.

At the same time, this data can be used to study TFFs in two-photon collisions. While π^0, η, η', as well as pion pairs, can be studied satisfactorily with a single-tag measurement using the existing data, the statistics is rather low for higher mass resonances or for a double-tagged measurement of the lightest pseudoscalar mesons. However, the latter two are of special interest for understanding the hadronic light-by-light contribution to a_μ at the level of the new direct measurements at FNAL and J-PARC. An additional data set of 20 fb^{-1} at $\sqrt{s}$ = 3.773 GeV would be most beneficial for the TFF measurements by BESIII for two reasons. On the one hand, it would increase the statistics for large invariant masses of the hadronic systems produced. On the other hand, it would allow to perform a first measurement of the doubly-virtual TFF in the energy region which is most relevant for a_μ calculations, with sufficient statistical precision to test the hadronic models and provide valuable input to the new, data-driven theory approaches to $a_\mu^{\rm hLBL}$.

The scan measurements performed by BESIII have allowed to determine baryon EM FFs at the respective thresholds and revealed puzzling features. In order to shed more light on these aspects, further detailed studies with enhanced data sets around the nucleon threshold at cms energies between $\sqrt{s} = (1.8, 2.0)$ GeV, the $\Lambda\bar{\Lambda}$ threshold at 2.2 GeV, and the $\Lambda_c\bar{\Lambda}_c$ threshold at 4.58 GeV, are necessary.

So far, the emphasis has been on the investigation of EM FFs of nucleons and the Λ hyperon. An additional integrated luminosity of 100 pb^{-1} at $\approx$ 2.5 GeV would allow not only precision studies of Λ but also of Σ^0 with a 6% statistical uncertainty, and of $\Sigma^\pm$ with a 4% statistical uncertainty, including the measurement of their effective form factors, their $|G_{\rm E}/G_{\rm M}|$ ratios, and the phase angle between $G_{\rm E}$ and $G_{\rm M}$ for Λ and Σ^+ hyperons.

A high-statistics data set at 2.2 GeV would also be beneficial for improving the understanding of the $\Lambda\bar{\Lambda}$ threshold, and for the studies of $\phi(2170)$. It would allow to perform PWAs of the $\phi\pi\pi$ final state. A structure has been observed in the $\phi\pi\pi$ system around 2.4 GeV. The existing data taken by BESIII at this energy suffer from small statistics. In order to shed light on the nature of this structure, it would be necessary to collect more data, with 20 pb^{-1} for each energy point around 2.4 GeV for a 8% uncertainty.

Table 4.4 summarizes the proposed data for the studies presented in this chapter.

References

1 D. M. Asner *et al*., Int. J. Mod. Phys. A, **24**: S1 (2009)

2 J. B. Guimarães da Costa *et al*. (CEPC Study Group), arXiv:1811.10545 [hep-ex]

3 A. Abada *et al*. (FCC Collaboration), Eur. Phys. J. ST, **228**: 261 (2019)

4 F. Jegerlehner, Springer Tracts Mod. Phys., **274**: 1 (2017)

5 A. Keshavarzi, D. Nomura and T. Teubner, Phys. Rev. D, **97**: 114025 (2018)

6 G. W. Bennet *et al.* (Muon (g-2) Collaboration), Phys. Rev. D 73, 072003 (2006)

7 M. Davier, A. Hoecker, B. Malaescu *et al*., Eur. Phys. J. C, **77**: 827 (2017)

8 B. L. Roberts, Chin. Phys. C, **34**: 741 (2010)
9 J. Grange *et al.*, arXiv:1501.06858
10 Tsutomu Mibe, Chin. Phys. C, **34**: 745 (2010)
11 D. W. Hertzog *et al.*, arXiv:0705.4617
12 J. Prades, E. de Rafael, and A. Vainshtein, Adv. Ser. Direct. High Energy Phys, **20**: 303 (2009)
13 G. Colangelo, M. Hoferichter, M. Procura *et al.*, JHEP, **1409**: 091 (2014)
14 G. Colangelo, M. Hoferichter, B. Kubis *et al.*, Phys. Lett. B, **738**: 6 (2014)
15 G. Colangelo, M. Hoferichter, M. Procura *et al.*, JHEP, **1509**: 074 (2015)
16 G. Colangelo, M. Hoferichter, M. Procura *et al.*, JHEP, **1704**: 161 (2017)
17 G. Colangelo, M. Hoferichter, M. Procura *et al.*, Phys. Rev. Lett., **118**: 232001 (2017)
18 V. Pauk and M. Vanderhaeghen, Phys. Rev. D, **90**: 113012 (2014)
19 V. Pauk and M. Vanderhaeghen, arXiv:1403.7503
20 A. Nyffeler, Phys. Rev. D, **94**: 053006 (2016)
21 T. Blum, A. Denig, I. Logashenko *et al.*, arXiv:1311.2198
22 G. Colangelo, M. Hoferichter, and P. Stoffer, JHEP, **1902**: 6 (2019)
23 Second Plenary Workshop of the *g*-2 Theory Initiative, https://wwwth.kph.uni-mainz.de/g-2/
24 M. Tanabashi *et al.* (Particle Data Group), Phys. Rev. D, **98**: 030001 (2018)
25 S. Binner, J. H. Kühn, and K. Melnikov, Phys. Lett. B, **459**: 279 (1999)
26 M. Benayoun, S. I. Eidelman, V. N. Ivanchenko *et al.*, Mod. Phys. Lett. A, **14**: 2605 (1999)
27 V. P. Druzhinin, S. I. Eidelman, S. I. Serednyakov *et al.*, Rev. Mod. Phys., **83**: 1545 (2011)
28 G. Rodrigo *et al.*, Eur. Phys. J. C, **24**: 71 (2002)
29 H. Czyż, J. H. Kühn, and A. Wapienik, Phys. Rev. D, **77**: 114005 (2008)
30 H. Czyż and J. H. Kühn, Phys. Rev. D, **80**: 034035 (2009)
31 M. Ablikim *et al.* (BESIII Collaboration), Phys. Lett. B, **753**: 629 (2016)
32 A. Hoecker, P. Speckmayer, J. Stelzer *et al.*, PoS A CAT,040 (2007), arXiv:physics/0703039
33 F. Campanario, H. Czyż, J. Gluza *et al.*, JHEP, **1402**: 114 (2014)
34 F. Ambrosino *et al.* (KLOE Collaboration), Phys. Lett. B, **670**: 285 (2009)
35 F. Ambrosino *et al.* (KLOE collaboration), Phys. Lett. B, **700**: 102 (2011)
36 F. Ambrosino *et al.* (KLOE collaboration), Phys. Lett. B, **720**: 336 (2013)
37 B. Aubert *et al.* (BaBar collaboration), Phys. Rev. Lett., **103**: 231801 (2009)
38 M. Ablikim *et al.* (BESIII Collaboration), Phys. Lett. B, **761**: 98 (2016)
39 M. Ablikim *et al.* (BESIII Collaboration), Phys. Lett. B, **774**: 252 (2017)
40 R. R. Akhmetshin *et al.* (CMD-2 Collaboration), Phys. Lett. B, **476**: 33 (2000)
41 M. N. Achasov, K. I. Beloborodov, A. V. Berdyugin *et al.*, Phys. Rev. D, **68**: 052006 (2003)
42 B. Aubert *et al.* (BaBar collaboration), Phys. Rev. D, **70**: 072004 (2004)
43 A. Antonelli *et al.* (DM2 collaboration), Z. Phys. C, **56**: 15 (1992)
44 R. R. Akhmetshin *et al.* (CMD-2 Collaboration), Phys. Lett. B, **466**: 392 (1999)
45 M. N. Achasov *et al.* (SND Collaboration), BUDKER-INP-2001-34
46 J. P. Lees *et al.* (BaBar Collaboration), Phys. Rev. D, **96**: 092009 (2017)
47 J. Z. Bai *et al.* (BES Collaboration), Phys. Rev. Lett., **84**: 594 (2000)
48 J. Z. Bai *et al.* (BES Collaboration), Phys. Rev. Lett., **88**: 101802 (2004)
49 M. Ablikim *et al.* (BES Collaboration), Phys. Lett. B, **641**: 145 (2006)
50 M. Ablikim *et al.* (BES Collaboration), Phys. Lett. B, **660**: 315 (2008)
51 M. Ablikim *et al.* (BES Collaboration), Phys. Lett. B, **677**: 239 (2009)
52 V. V. Anashin *et al.* (KEDR Collaboration), Phys. Lett. B, **753**: 533 (2016)
53 V. V. Anashin *et al.* (KEDR Collaboration), Phys. Lett. B, **770**: 174 (2017)
54 V. V. Anashin *et al.* (KEDR Collaboration), Phys. Lett. B, **788**: 42 (2019)
55 B. Andersson and H. M. Hu, arXiv:hep-ph/9910285
56 Ronggang Ping *et al.*, Chin. Phys. C, **40**: 113002 (2016)
57 F. Jegerlehner, Acta Phys. Polon. B, **44**: 2257 (2013)
58 B. Aubert *et al.* (BaBar Collaboration), Phys. Rev. D, **74**: 012002 (2006)
59 J. P. Lees *et al.* (BaBar Collaboration), Phys. Rev. D, **98**: 112002 (2018)
60 T. Feldmann, P. Kroll, and B. Stech, Phys. Rev. D, **58**: 114006 (1998)
61 T. Feldmann, Int. J. Mod. Phys. A, **15**: 159 (2000)
62 J. F. Donoghue, B. R. Holstein, and Y. C. R. Lin, Phys. Rev. Lett., **55**: 2766 (1985)
63 H. Leutwyler, Nucl. Phys. Proc. Suppl., **64**: 223 (1998)
64 R. Kaiser and H. Leutwyler, Eur. Phys. J. C, **17**: 623 (2000)
65 H. J. Behrend *et al.* (CELLO Collaboration), Z. Phys. C, **49**: 401 (1991)
66 J. Gronberg *et al.* (CLEO Collaboration), Phys. Rev. D, **57**: 33 (1998)
67 B. Aubert *et al.* (BaBar Collaboration), Phys. Rev. D, **80**: 052002 (2009)
68 S. Uehara *et al.* (Belle Collaboration), Phys. Rev. D, **86**: 092007 (2012)
69 M. Hoferichter, B. L. Hoid, B. Kubis *et al.*, Phys. Rev. Lett., **121**: 112002 (2018)
70 M. Hoferichter, B. L. Hoid, B. Kubis *et al.*, JHEP, **1810**: 141 (2018)
71 A. Gérardin, H. B. Meyer, and A. Nyffeler, Phys. Rev. D, **100**: 034520 (2019)
72 I. Danilkin, C. F. Redmer, and M. Vanderhaeghen, Prog. Part. Nucl. Phys., **107**: 20 (2019)

73 H. Czyz and P. Kisza, Comput. Phys. Commun., **234**: 245 (2019)
74 M. Hoferichter and P. Stoffer, JHEP, **1907**: 073 (2019)
75 I. Danilkin, O. Deineka, and M. Vanderhaeghen, arXiv:1909.04158 [hep-ph]
76 M. Masuda *et al.*. (Belle Collaboration), Phys. Rev. D, **93**: 032003 (2016)
77 N. Isgur, Proceedings of NSTAR 2000, JLAB-THY-00-20 (2000)
78 J. Ashman *et al*., Phys. Lett. B, **206**: 206 (1988)
79 C. A. Aidala *et al*., Rev. Mod. Phys., **85**: 655 (2013)
80 G. A. Miller, Phys. Rev. Lett., **99**: 112001 (2007)
81 S. Weinberg, Nucl. Phys. B, **363**: 3 (1991)
82 R. Machleidt and D. R. Entem, Phys. Rep., **503**: 1 (2011)
83 K. G. Wilson, Phys. Rev. D, **10**: 2445 (1974)
84 T. Skyrme, Proc. Roy. Soc. Lond. A, **260**: 237 (1961)
85 G. S. Adkins, C. R. Nappi, and E. Witten, Nucl. Phys. B, **228**: 552 (1982)
86 V. Punjabi, C. F. Perdrisat, and M. K. Jones, Eur. Phys. J. A, **51**: 79 (2015)
87 C. Granados, S. Leupold, and E. Perotti, Eur. Phys. J. A, **53**: 17 (2017)
88 M. A. Belushkin *et al*., Phys. Rev. C, **75**: 035202 (2007)
89 E. C. Titschmarsh, The Theory of Functions, Oxford University Press (1939)
90 A. D. Sakharov, Sov. Phys. Usp, **34**: 375 (1991)
91 A. Sommerfeld, Ann. Phys., **403**: 257 (1931)
92 G. Fäldt, Eur. Phys. J. A, **52**: 141 (2016)
93 G. Fäldt and A. Kupsc, Phys. Lett. B, **772**: 16 (2017)
94 G. I. Gakh and E. Tomasi-Gustafsson, Nucl. Phys. A, **761**: 120 (2005)
95 E. Tomasi-Gustafsson *et al*., Phys. Lett. B, **659**: 197 (2008)
96 A. I. Akhiezer and M. P. Rekalo, Sov. Phys. Dokl., **13**: 572 (1968)
97 A. Akhiezer, and M. P. Rekalo, Sov. J. Part. Nucl., **4**: 277 (1974)
98 A. J. R. Puckett *et al*., Phys. Rev. C, **85**: 045203 (2012)
99 M. Rosenbluth, Phys. Rev., **79**: 615 (1950)
100 P. A. M. Guichon and M. Vanderhaeghen, Phys. Rev. Lett., **91**: 142303 (2003)
101 P. G. Blunden, W. Melnitchouk, and J. A. Tjon, Phys. Rev. Lett., **91**: 142304 (2003)
102 S. Pacetti, R. Baldini Ferroli, and E. Tomasi-Gustafsson, Phys. Rept. 550, 1 (2015), and references therein
103 J. P. Lees *et al*. (BaBar Collaboration), Phys. Rev. D, **87**: 092005 (2007)
104 G. Bardin *et al*. (PS170 Collaboration), Nucl. Phys. B, **411**: 3 (1994)
105 M. Ablikim *et al*. (BESIII Collaboration), Phys. Rev. D, **91**: 112004 (2015)
106 M. Ablikim *et al*. (BESIII Collaboration), Phys. Rev. D, **99**: 092002 (2019)
107 R. R. Akhmetshin *et al*. (CMD-2 Collaboration), Phys. Lett. B, **759**: 634 (2016)
108 M. Ablikim *et al*. (BES Collaboration), Phys. Lett. B, **630**: 14 (2005)
109 A. Antonelli *et al*. (FENICE Collaboration), Nucl. Phys. B, **517**: 3 (1998)
110 T. A. Armstrong *et al*. (E760 Collaboration), Phys. Rev. Lett., **70**: 1212 (1993)
111 M. Ambrogiani *et al*. (E835 Collaboration), Phys. Rev. D, **60**: 032002 (1999)
112 M. Andreotti *et al*. (E835 Collaboration), Phys. Lett. B, **559**: 20 (2003)
113 D. Bisello *et al*. (DM2 Collaboration), Nucl. Phys. B, **224**: 379 (1983)
114 D. Bisello *et al*. (DM2 Collaboration), Z. Phys. C, **48**: 23 (1990)
115 A. Bianconi and E. Tomasi-Gustafsson, Phys. Rev. Lett., **114**: 232301 (2015)
116 J. Haidenbauer *et al*., Nucl. Phys. A, **929**: 102 (2014)
117 J. R. Green *et al*., Phys. Rev. D, **90**: 074507 (2014)
118 B. Jäger *et al*., PoS LATTICE, **2013**: 272 (2014)
119 R. Bijker and F. Iachello, Phys. Rev. C, **69**: 068201 (2004)
120 T. Melde *et al*., Phys. Rev. D, **76**: 074020 (2007)
121 S. J. Brodsky and G. R. Farrar, Phy. Rev. D, **11**: 1309 (1975)
122 M. N. Achasov *et al*., Phy. Rev. D, **90**: 112007 (2014)
123 J. R. Ellis and M. Karliner, New J. Phys., **4**: 18 (2002)
124 M. Karliner and S. Nussinov, Phys. Lett. B, **538**: 321-326 (2002)
125 D. Bisello *et al*. (DM2 Collaboration), Z. Phys. C, **48**: 23 (1990)
126 B. Aubert *et al*. (BaBar Collaboration), Phys. Rev. D, **76**: 092006 (2007)
127 M. Ablikim *et al*. (BESIII Collaboration), Phys. Rev. D, **97**: 032013 (2018)
128 S. Dobbs *et al*., Phys. Lett. B, **739**, 90 (2014); ibid. Phys. Rev. D, **96**, 092004 (2017)
129 M. Anselmino *et al*., Rev. Mod. Phys., **65**: 1199 (1993)
130 R. Jaffe and F. Wilczek, Phys. Rev. Lett., **91**: 232003 (2003)
131 M. Ablikim *et al*. (BESIII Collaboration), Phys. Rev. Lett., **123**: 122003 (2019)
132 J. Haidenbauer and U.-G. Meißner, Phys. Lett. B, **761**: 456 (2016)
133 G. Pakhlova *et al*. (Belle Collaboration), Phys. Rev. Lett., **101**: 172001 (2008)
134 M. Ablikim *et al*. (BESIII Collaboration), Phys. Rev. Lett., **120**: 132001 (2018)
135 R. R. Akhmetshin *et al*. (CMD-3 Collaboration), Phys. Lett. B, **794**: 64-68 (2019)
136 V. F. Dmitriev, A. I. Milstein, and S. G. Salnikov, Phys. Rev. D, **93**: 034033 (2016)
137 A. I. Milstein and S. G. Salnikov, Nucl. Phys. A, **966**: 54 (2017)
138 A. I. Milstein and S. G. Salnikov, Nucl. Phys. A, **977**: 60 (2018)
139 L.-Y. Dai *et al*., Phys. Rev. D, **96**: 116001 (2017)
140 O. D. Dalkarov, P. A. Khakhulin, and A. Yu. Voronin, Nucl. Phys. A, **833**: 104 (2010)
141 B. El-Bennich *et al*., Phys. Rev. C, **79**: 054001 (2009)
142 J. Haidenbauer *et al*., Phys. Lett. B, **643**: 29 (2006)
143 R. Baldini *et al*., Eur. Phys. J. A, **39**: 315 (2009)
144 R. Baldini *et al*., Eur. Phys. J. A, **48**: 33 (2012)
145 M. Anselmino *et al.*, Rev. Mod. Phys., **65:** 1199 (1993), and references therein
146 S. Pacetti, talk presented at the Int. Workshop on Baryon Production in BESIII, Hefei, China, 2019
147 M. Ablikim *et al*. (BESIII Collaboration), Phys. Rev. Lett., **124**: 042001 (2020)

148 S. Albino, Rev. Mod. Phys., **82**: 2489 (2010)
149 M. Radici, Nuovo Cim. C, **035**: 69 (2012)
150 F. Arleo, Eur. Phys. J. C, **61**: 603 (2009)
151 D. De Florian, R. Sassot, and M. Stratmann, Phys. Rev. D, 75, 114010 (2007); D 76 074033 (2007)
152 M. Hirai, S. Kumano, T. H. Nagai *et al.*, Phys. Rev. D, **75**: 094009 (2007)
153 S. Albino, B. A. Kniehl, and G. Kramer, Nucl. Phys. B, **803**: 42 (2008)
154 E. Leader *et al.*, talk presented at 20th International Symposium on Spin Physics (SPIN2012) JINR, Dubna, Russia, 2012
155 E. Leader *et al.*, Phys. Rev. D, **91**: 054017 (2015); Phys. Rev. D, **84**: 014002 (2011)
156 Jozef Dudek *et al.*, Eur. Phys. J. A, **48**: 187 (2012)
157 A. Accardi *et al.*, Eur. Phys. J., **62**: 218 (2016)
158 Isabella Garzia and Francesca Giordano, Eur. Phys. J. A, **52**: 152 (2016)
159 J. C. Collins, Nucl. Phys. B, **396**: 161 (1993)
160 P. Sun and F. Yuan, Phys. Rev. D, **88**: 034016 (2013)
161 M. Ablikim *et al.* (BESIII Collaboration), Phys. Rev. Lett., **116**: 042001 (2016)
162 M. L. Perl *et al.*, Phys. Rev. Lett., **35**: 1489 (1975)
163 J. Beringer *et al.* (Particle Data Group), Phys. Rev. D, **86**: 010001 (2012)
164 W.J. Marciano and A. Sirlin, Phys. Rev. Lett., **61**: 1815 (1988)
165 R. Barate *et al.*, Eur. Phys. J. C, **2**: 395 (1998)
166 Y. Koide, Phys. Rev. D, **28**: 252 (1983)
167 M. L. Perl *et al.*, Phys. Lett. B, **70**: 487 (1977)
168 R. Brandelik *et al.* (DASP Collaboration), Phys. Lett. B, **73**: 109 (1978)
169 W. Bartel *et al.*, Phys. Lett. B, **77**: 331 (1978)
170 W. Bacino *et al.*, Phys. Rev. Lett., **41**: 13 (1978)
171 C. A. BLOCKER *et al.*, Phys. Lett. B, **109**: 119 (1978)
172 H. Albrecht *et al.* (ARGUS Collaboration), Phys. Lett. B, **292**: 221 (1992)
173 J. Z. Bai *et al.* (BES Collaboration), Phys. Rev. Lett., **69**: 3021 (1992)
174 J. Z. Bai *et al.* (BES Collaboration), Phys. Rev. D, **53**: 20 (1996)
175 J. Z. Bai *et al.* (BES Collaboration), HEP&NP, **16**: 343 (1992)
176 R. Balest *et al.* (CLEO Collaboration), Phys. Rev. D, **47**: 3671 (1993)
177 A. Anastassov *et al.* (CLEO Collaboration), Phys. Rev. D, **55**, 2559 (1997); Erratum: [Phys. Rev. D, **58**, 119904 (1998)]
178 G. Abbiendi *et al.* (OPAL Collaboration), Phys. Lett. B, **492**: 23 (2000)
179 K. Belous *et al.* (Belle Collaboration), Phys. Rev. Lett., **99**: 011801 (2007)
180 V. V. Anashin *et al.* (KEDR Collaboration), J. Exp. The. Phys. Lett., **85**: 347 (2007)
181 B. Aubert *et al.* (BaBar Collaboration), Phys. Rev. D, **80**: 092005 (2009)
182 M. Ablikim *et al.* (BESIII Collaboration), Phys. Rev. D, **90**: 012001 (2014)
183 D. E. Groom *et al.* (Particle Data Group), Eur. Phys. J. C, **1**: 15 (2000)
184 K. A. Olive *et al.* (Particle Data Group), Chin. Phys. C, **38**: 090001 (2014)
185 R. M. Barnett *et al.* (Particle Data Group), Phys. Rev. D, **54**: 1 (1996)
186 L. Montanet *et al.* (Particle Data Group), Phys. Rev. D, **50**: 1173 (1994)
187 A. Bogomyagkov *et al.*, the 9th European Particle Accelerator Conference (EPAC 2004), Lucerne, Switzerland, 2004
188 Xiao-Hu Mo *et al.*, Chin. Phys. C, **32**: 995 (2008)
189 M. N. Achasov *et al.*, Nucl. Phys. B (Proc. Suppl.), **189**: 366 (2009)
190 X. H. Mo, E.V. Abakumova, M.N. Achasov *et al.*, Chin. Phys. C, **34**: 912 (2010)
191 E.V. Abakumova *et al.*, Sect. A, **659**: 21 (2011)
192 J. Y. Zhang *et al.*, Nucl. Phys. B (Proc. Suppl.), **225**: 309 (2012)
193 X. H. Mo, Int. J. Mod. Phys. A, **30**: 1550149 (2015)
194 Y. K. Wang, X. H. Mo, C. Z. Yuan *et al.*, Sect. A, **583**: 479 (2007)
195 Y. K. Wang, J. Y. Zhang, X. H. Mo *et al.*, Chin. Phys. C, **33**: 501 (2009)
196 B. Q. Wang, X. H. Mo, and C. Z. Yuan, Int. J. Mod. Phys. A, **27**: 1250150 (2012)
197 B. Q. Wang and X. H. Mo, Chin. Phys. C, **37**: 026202 (2013)
198 X. H. Mo, Mod. Phys. Lett. A, **31**: 1650196 (2016)
199 J. Bartelt *et al.* (CLEO Collaboration), Phys. Rev. Lett., **76**: 4119 (1996)
200 P. del Amo Sanchez *et al.* (BaBar Collaboration), Phys. Rev. D, **83**: 032002 (2011)
201 B. Aubert *et al.* (BaBar Collaboration), Phys. Rev. Lett., **100**: 011801 (2008)
202 M. J. Lee *et al.* (Belle Collaboration), Phys. Rev. D, **81**: 113007 (2010)
203 J. Y. Zhang *et al.*, Chin. Phys. C, **40**: 076001 (2016)
204 M. Ablikim *et al.* (BESIII Collaboration), Phys. Lett. B, **791**: 375 (2019)
205 K. K. Seth, S. Dobbs, A. Tomaradze *et al.*, Phys. Lett. B, **730**: 332 (2014)
206 K. K. Seth, S. Dobbs, Z. Metreveli *et al.*, Phys. Rev. Lett., **110**: 022002 (2013)
207 R. B. Ferroli, A. Mangoni, and S. Pacetti, Phys. Rev. C, **98**: 045210 (2018)
208 K. Zhu, X. H. Mo, and C. Z. Yuan, Int. J. Mod. Phys. A, **30**: 1550148 (2015)
209 Shi-Lin Zhu, Int. J. of Mod. Phys. E, **17**, 283 (2008), and references therein
210 Hua-Xing Chen *et al.*, Phys. Rept, **639**: 1 (2016), and references therein
211 Stephen Lars Olsen *et al.*, Rev. Mod. Phys, **90**: 015003 (2018), and references therein
212 T. Barnes *et al.*, Phys. Rev. D, **68**: 054014 (2003)
213 J. P. Lees *et al.* (BaBar Collaboration), Phys. Rev. D, **86**: 012008 (2012)
214 B. Aubert *et al.* (BaBar Collaboration), Phys. Rev. D, **76**: 012008 (2007)
215 C. P. Shen *et al.* (Belle Collaboration), Phys. Rev. D, **80**: 031101(R) (2009)
216 M. Ablikim *et al.* (BES Collaboration), Phys. Rev. Lett., **100**: 012003 (2008)
217 M. Ablikim *et al.* (BESIII Collaboration), Phys. Rev. D, **95**:

052017 (2015)
218 M. Ablikim *et al*. (BESIII Collaboration), Phys. Rev. D, **99**: 012014 (2019)
219 G. J. Ding and M. L. Yan, Phys. Lett. B, **657**: 49 (2007)
220 X. Wang *et al*., Phys. Rev. D, **85**: 074024 (2012)
221 S. S. Afonin and I. V. Pusenkov, Phys. Rev. D, **90**: 094020 (2014)
222 Cheng-Qun Pang, Phys. Rev. D, **99**: 074015 (2019)
223 G. J. Ding and M. L. Yan, Phys. Lett. B, **650**: 390 (2007)
224 Z. G. Wang, Nucl. Phys. A, **791**: 106 (2007)
225 H. X. Chen *et al*., Phys. Rev. D, **78**: 034012 (2008)
226 N. V. Drenska, R. Faccini, and A. D. Polosa, Phys. Lett. B, **669**: 160 (2008)
227 Hong-Wei Ke and Xue-Qian Li, Phys. Rev. D, **99**: 036014 (2019)
228 L. Zhao *et al*., Phys. Rev. D, **87**: 054034 (2013)
229 C. Deng *et al*., Phys. Rev. D, **88**: 074007 (2013)
230 Yubing Dong *et al*., Phys. Rev. D, **96**: 074027 (2017)
231 A. Martinez Torres *et al*., Phys. Rev. D, **78**: 074031 (2008)
232 S. Gomez-Avila, M. Napsuciale, and E. Oset, Phys. Rev. D, **79**: 034018 (2009)
233 M. Ablikim *et al*. (BES Collaboration), Phys. Lett. B, **685**: 27 (2010)
234 Philip R. Page *et al*., Phys. Rev. D, **59**: 034016 (1999)
235 B. Aubert *et al*. (BaBar Collaboration), Phys. Rev. D, **77**: 092002 (2007)
236 B. Aubert *et al*. (BaBar Collaboration), Phys. Rev. D, **76**: 092005 (2007)
237 C. P. Shen and C. Z. Yuan, Chin. Phys. C, **34**: 1045 (2010)
238 H. X. Chen *et al*., Phys. Rev. D, **98**: 014011 (2018)
239 M. Piotrowska *et al*., Phys. Rev. D, **96**: 054033 (2017)
240 Peter Lichard, Phys. Rev. D, **98**: 113011 (2018)
241 M. Ablikim *et al*., (BESIII Collaboration), Phys. Rev. D, **99**: 032001 (2019)
242 M. Ablikim *et al*., (BESIII Collaboration), Phys. Rev. D, **100**: 032009 (2019)
243 M. Ablikim *et al*., (BESIII Collaboration), Phys. Rev. Lett., **124**: 112001 (2020)

Chapter 5

Charm Physics

5.1 Introduction

The ground states of charmed hadrons, *e.g.* $D^{0(+)}$, D_s^+, and Λ_c^+, can only decay weakly and so precision studies of these charm decays provide important constraints on the weak interaction [1]. Furthermore, as the strong force is always involved in the decays of charmed hadrons and the formation of the final-state hadrons, precise measurements of the decay properties allow tests of non-perturbative quantum chromodynamics (QCD) calculations. The decay rates of the ground states of charmed hadrons are dominated by the weak decay of the charm quark. For comparison, the lifetimes of the charmed hadrons are shown in Fig. 5.1(a); it is surprising that their individual lifetimes differ by up to a factor of 10. As shown in Fig. 5.1(b), the ratio of $\tau(D^+)/\tau(D^0) = 2.54 \pm 0.01$ is very different from that of the corresponding lifetimes in the beauty sector, $\tau(B^+)/\tau(B^0) = 1.076 \pm 0.004$. From these observations one can infer that deviations of the lifetime ratios from unity decrease with increasing heavy-flavor quark mass m_Q. Heavy flavor decays thus constitute an intriguing laboratory for the study QCD. According to the data, the non-perturbative effects in the decays of charmed hadrons are much more important than those in the beauty sector. Comprehensive studies of the decays of charmed mesons and baryons will play an essential role in advancing our understanding of the strong interaction. In particular, the understanding of the different decay mechanisms, such as weak-annihilation, W-exchange and final-state scattering, is essential for developing a complete theory of charmed hadron decays. Therefore, the data from the BESIII experiment will have a leading role in understanding non-perturbative QCD.

BEPCII/BESIII produces charmed hadrons near their mass threshold, which allows exclusive reconstruction of their decay products with well-determined kinematics. Up to now, BESIII has collected data corresponding to the integrated luminosities of 2.9 fb^{-1}, 0.5 fb^{-1}, 3.2 fb^{-1}, and 0.6 fb^{-1} at $\sqrt{s}$ =3.773, 4.009, 4.178, and 4.600 GeV, respectively, as well as data at $\sqrt{s}$ = 4.23, 4.26, and 4.36 GeV. Based on these data sets, many world-leading results have been published. These include the first measurements of the absolute branching fraction (BF) of the Λ_c^+ baryon to hadronic and semi-leptonic (SL) final states, which is an important milestone in the investigation of the charmed baryon sector; the most accurate measurements of the Cabibbo-Kobayashi-Maskawa (CKM) matrix elements $|V_{cs}|$ and $|V_{cd}|$, which is an essential input for tests of the CKM matrix unitarity; and the most precise measurements of the decay constants in leptonic decays as well as the form factors in SL decays, which are crucial for calibrating LQCD for heavy quark studies. Also, it is important to test lepton-flavor universality (LFU) by using the leptonic and SL charmed hadron decays.

However, improved knowledge of the charmed hadron decays is required to match the significantly improved LQCD calculations, and to better understand the strong-force dynamics in the charm region. In addition, more precise measurements of the strong-phase difference between the D^0 and $\bar{D}^0$ decays to final states, which are used to measure the γ angle (also known as ϕ_3) of the

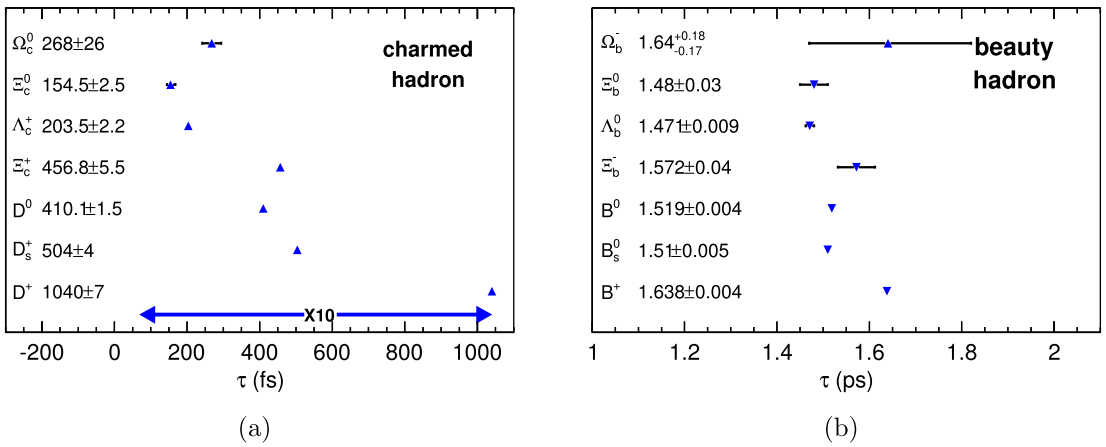

Fig. 5.1. (a) (color online) Comparison of the lifetimes of charmed hadrons [2]. For the lifetimes of Ω_c^0, Ξ_c^0 and Ξ_c^+, we take the recent measurement from LHCb [3]. (b) Comparison of the lifetimes of beauty hadrons. In the left figure, "10×" means that the lifetimes differ by about one order of magnitude.

CKM unitary triangle in $B^+ \to DK^+$ decays, are necessary (D denotes either D^0 or $\bar{D}^0$). Such improved measurements will prevent the γ measurements at LHCb and Belle II from being systematically limited due to uncertainties of the neutral D strong-phase.

This section describes the future pursuit of this rich charm program. Specifically, we focus our discussion on the most important measurements that can be made with the proposed future data taking: $D^{0(+)}$, D_s^+, and Λ_c^+ samples accumulated at $\sqrt{s}$ = 3.773, 4.178, and 4.64 GeV with respective integrated luminosities of 20 fb^{-1}, 6 fb^{-1} and 5 fb^{-1}. Furthermore, it will be interesting to study for the first time the baryons Λ_c and Σ_c at the threshold and at higher cms energies, for example, $e^+e^- \to \Lambda_c^+\bar{\Sigma}_c^-$ and $\Lambda_c^+\bar{\Sigma}_c\pi$. We also discuss the possible energy upgrade of BEPCII to 5 GeV, so that the thresholds would open for baryon pair production $e^+e^- \to \Sigma_c\bar{\Sigma}_c$ and $\Xi_c\bar{\Xi}_c$.

5.2 $D^{0(+)}$ and D_s^+ physics

5.2.1 Leptonic decays

In the Standard Model (SM), the partial widths of the leptonic decays $D_{(s)}^+ \to \ell^+\nu_\ell$ can be written as

$$\Gamma(D_{(s)}^+ \to \ell^+\nu_\ell) = \frac{G_F^2 f_{D_{(s)}^+}^2}{8\pi} |V_{cd(s)}|^2 m_\ell^2 m_{D_{(s)}^+} \left(1 - \frac{m_\ell^2}{m_{D_{(s)}^+}^2}\right)^2, \tag{5.1}$$

where G_F is the Fermi coupling constant, $f_{D_{(s)}^+}$ is the $D_{(s)}^+$ decay constant, $|V_{cd(s)}|$ is the CKM matrix element [2], and m_ℓ [$m_{D_{(s)}^+}$] is the lepton [$D_{(s)}^+$ meson] mass. Using the lifetimes and the measured BFs of these decays, one can determine the product $f_{D_{(s)}^+}|V_{cd(s)}|$. By taking as input $f_{D_{(s)}^+}$ as calculated in LQCD, the value of $|V_{cd(s)}|$ can then be obtained. Alternatively, $|V_{cd(s)}|$ can be taken from the global fits of the other CKM matrix elements, and $f_{D_{(s)}^+}$ can be determined instead.

With the data sets at hand, BESIII has reported the improved measurements of BFs of $D^+ \to \mu^+\nu_\mu$, $D^+ \to \tau^+\nu_\tau$, and $D_s^+ \to \mu^+\nu_\mu$, as well as of $f_{D_{(s)}^+}$ and $|V_{cs(d)}|$ [4-6]. The achieved precision is summarized in Table 5.1. Experimental studies of $D_s^+ \to \tau^+\nu_\tau$ with $\tau^+ \to \pi^+\nu_\tau$, $\tau^+ \to e^+\nu_\tau\nu_e$, $\tau^+ \to \mu^+\nu_\tau\nu_\mu$, and $\tau^+ \to \rho^+\nu_\tau$ are still ongoing. Based on existing measurements at CLEO-c [7-9], BaBar [10], and Belle [11], the expected signal yield of $D_s^+ \to \tau^+\nu_\tau$ will be larger than of $D_s^+ \to \mu^+\nu_\mu$, but will have more background and significant systematic uncer-

Table 5.1. Expected precision of measurements of $D_{(s)}^+ \to \ell^+\nu_\ell$ at BESIII and Belle II. For BESIII, some systematic uncertainties, which are statistically limited by the control samples, are expected to be improved. The total systematic uncertainty is assumed to be comparable to the corresponding statistical uncertainty. For $D^+ \to \tau^+\nu_\tau$, only $\tau^+ \to \pi\nu$ is used currently. However, more τ^+ decay channels could be used. For $D_s^+ \to \tau^+\nu_\tau$, the expectation is based on $\tau^+ \to \pi\nu$, $e\nu\nu$, $\mu\nu\nu$, and $\rho\nu$. Considering that the LQCD uncertainty of f_{D^+} has been reduced from 1.9% to 0.2%, $|V_{cd}|$ measured at BESIII has been re-calculated, and is marked with*. Preliminary results are marked with†. For Belle II, we assume that the systematic uncertainties can be reduced by a factor of 2 compared to the Belle results, and the systematic uncertainty for $D^+ \to \mu^+\nu_\mu$ is the same as for $D_s^+ \to \mu^+\nu_\mu$.

	BESIII	BESIII	Belle	Belle II
Luminosity	2.9 fb^{-1} at 3.773 GeV	20 fb^{-1} at 3.773 GeV	1 ab^{-1} at $\Upsilon(nS)$	50 ab^{-1} at $\Upsilon(nS)$
$\mathcal{B}(D^+ \to \mu^+\nu_\mu)$	$5.1\%_{\rm stat.}1.6\%_{\rm syst.}$[4]	$1.9\%_{\rm stat.}1.3\%_{\rm syst.}$	–	$3.0\%_{\rm stat.}1.8\%_{\rm syst.}$[54]
f_{D^+}(MeV)	$2.6\%_{\rm stat.}0.9\%_{\rm syst.}$[4]	$1.0\%_{\rm stat.}0.8\%_{\rm syst.}$	–	–
$\lvert V_{cd}\rvert$	$2.6\%_{\rm stat.}1.0\%^*_{\rm syst.}$[4]	$1.0\%_{\rm stat.}0.8\%^*_{\rm syst.}$	–	–
$\mathcal{B}(D^+ \to \tau^+\nu_\tau)$	$20\%_{\rm stat.}13\%_{\rm syst.}$ [5]	$8\%_{\rm stat.}5\%_{\rm syst.}$	–	–
$\frac{\mathcal{B}(D^+\to\tau^+\nu_\tau)}{\mathcal{B}(D^+\to\mu^+\nu_\mu)}$	$20\%_{\rm stat.}13\%_{\rm syst.}$ [5]	$8\%_{\rm stat.}5\%_{\rm syst.}$	–	–
Luminosity	3.2 fb^{-1} at 4.178 GeV	6 fb^{-1} at 4.178 GeV	1 ab^{-1} at $\Upsilon(nS)$	50 ab^{-1} at $\Upsilon(nS)$
$\mathcal{B}(D_s^+ \to \mu^+\nu_\mu)$	$2.8\%_{\rm stat.}2.7\%_{\rm syst.}$[6]	$2.1\%_{\rm stat.}2.2\%_{\rm syst.}$	$5.3\%_{\rm stat.}3.8\%_{\rm syst.}$	$0.8\%_{\rm stat.}1.8\%_{\rm syst.}$
$f_{D_s^+}$(MeV)	$1.5\%_{\rm stat.}1.6\%_{\rm syst.}$[6]	$1.0\%_{\rm stat.}1.2\%_{\rm syst.}$	–	–
$\lvert V_{cs}\rvert$	$1.5\%_{\rm stat.}1.6\%_{\rm syst.}$[6]	$1.0\%_{\rm stat.}1.2\%_{\rm syst.}$	–	–
$f_{D_s^+}/f_{D^+}$	$3.0\%_{\rm stat.}1.5\%_{\rm syst.}$[6]	$1.4\%_{\rm stat.}1.4\%_{\rm syst.}$	–	–
$\mathcal{B}(D_s^+ \to \tau^+\nu_\tau)$	$2.2\%_{\rm stat.}2.6\%^\dagger_{\rm syst.}$	$1.6\%_{\rm stat.}2.4\%_{\rm syst.}$	$3.7\%_{\rm stat.}5.4\%_{\rm syst.}$	$0.6\%_{\rm stat.}2.7\%_{\rm syst.}$
$f_{D_s^+}$(MeV)	$1.1\%_{\rm stat.}1.5\%^\dagger_{\rm syst.}$	$0.9\%_{\rm stat.}1.4\%_{\rm syst.}$		
$\lvert V_{cs}\rvert$	$1.1\%_{\rm stat.}1.5\%^\dagger_{\rm syst.}$	$0.9\%_{\rm stat.}1.4\%_{\rm syst.}$	–	–
$f_{D_s^+}^{\mu\&\tau}$(MeV)	$0.9\%_{\rm stat.}1.0\%^\dagger_{\rm syst.}$	$0.6\%_{\rm stat.}0.9\%_{\rm syst.}$	$1.6\%_{\rm stat.}2.0\%_{\rm syst.}$	$0.3\%_{\rm stat.}1.0\%_{\rm syst.}$
$\lvert V_{cs}^{\mu\&\tau}\rvert$	$0.9\%_{\rm stat.}1.0\%^\dagger_{\rm syst.}$	$0.6\%_{\rm stat.}0.9\%_{\rm syst.}$	–	–
$\frac{\mathcal{B}(D_s^+\to\tau^+\nu_\tau)}{\mathcal{B}(D_s^+\to\mu^+\nu_\mu)}$	$3.6\%_{\rm stat.}3.0\%^\dagger_{\rm syst.}$	$2.6\%_{\rm stat.}2.8\%_{\rm syst.}$	$6.4\%_{\rm stat.}5.2\%_{\rm syst.}$	$0.9\%_{\rm stat.}3.2\%_{\rm syst.}$

tainties. After weighing the measurements performed with different τ^+ decays, the sensitivity of the result for $D_s^+ \to \tau^+\nu_\tau$ will be comparable to $D_s^+ \to \mu^+\nu_\mu$. Thus, the measurement precision with $D_s^+ \to \tau^+\nu_\tau$ can be estimated, as summarized in Table 5.1.

There are four reasons why improved measurements of $D_{(s)}^+ \to \ell^+\nu_\ell$ with 20 fb^{-1} of data at 3.773 GeV and 6 fb^{-1} of data at 4.178 GeV are desirable.

1. *Constraints to the LQCD calculations*

Figure 5.2 shows a comparison of $f_{D_{(s)}^+}$ measurements by various experiments and the values obtained in LQCD.

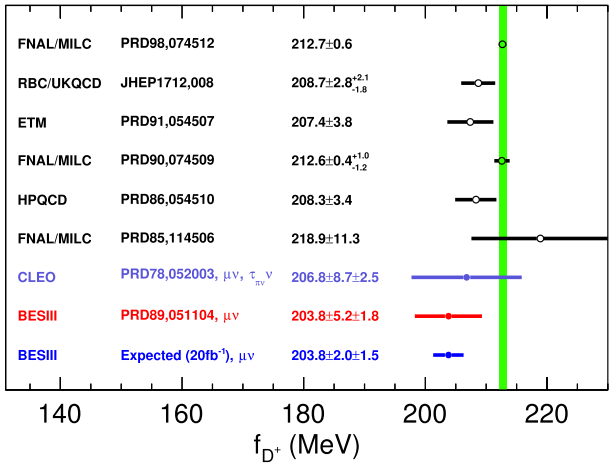

(a)

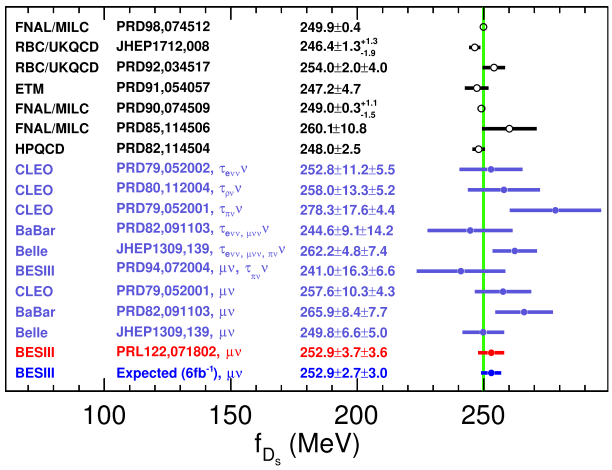

(b)

Fig. 5.2. (color online) Expected precision of the measurements of: (a) f_{D^+}, using $D^+ \to \mu^+\nu_\mu$ with 20 fb^{-1} of data at 3.773 GeV; and (b) $f_{D_s^+}$, using $D_s^+ \to \mu^+\nu_\mu$ with 6 fb^{-1} of data at 4.178 GeV. The green bands show the LQCD uncertainties [12]. The circles and dots with error bars are the LQCD calculations and the experimental measurements, respectively. The value marked in red denotes the best measurement, and the values marked in light blue denote the expected precision.

Focusing on f_{D^+}, it may be seen that BESIII provided the currently most precise individual measurement, which has a statistical uncertainty of around 2.5%. In contrast to the LQCD uncertainty of 0.2%, there is much more room for improvement in the experiment. With 20 fb^{-1} of data at 3.773 GeV, the relative statistical uncertainty on f_{D^+} can be reduced to approximately 1%, which is still larger than the current systematic uncertainty.

2. *Determination of* $|V_{cs(d)}|$

Alternatively, the LQCD calculations of $f_{D_{(s)}^+}$ may be taken as input, and the leptonic BF measurements used to confront weak physics. In SM, quark-flavor mixing is described by the unitary 3×3 CKM matrix

$$V_{\rm CKM} = \begin{pmatrix} V_{ud} & V_{us} & V_{ub} \\ V_{cd} & V_{cs} & V_{cb} \\ V_{td} & V_{ts} & V_{tb} \end{pmatrix}. \tag{5.2}$$

Any deviation from unitarity would indicate new physics beyond SM. Improving the accuracy with which CKM matrix elements are determined is one of the principal goals in flavor physics, as it will test the unitarity of the CKM matrix with higher accuracy.

In the past decade, much progress has been made in LQCD calculations of $f_{D_{(s)}^+}$. The uncertainties of $f_{D_{(s)}^+}$ calculated in LQCD have been reduced from (1-2)% to the 0.2% level [12, 13], thus providing precise information to measure $|V_{cs}|$ and $|V_{cd}|$. Comparison of the measured $|V_{cs(d)}|$ with different methods and experiments is shown in Fig. 5.3. In the figure, the BESIII result for $|V_{cd}|$ has been recalculated with the latest LQCD calculation of $f_{D^+} = 212.7 \pm 0.6$ MeV [12]. Currently, the average is dominated by the BESIII measurements of $D_{(s)}^+ \to \ell^+\nu_\ell$ decays, which have an uncertainty of 2.5% (1.5%) for $|V_{cd(s)}|$. The statistical uncertainty of $|V_{cd}|$ is dominant, whereas the statistical and systematic uncertainties of $|V_{cs}|$ are comparable.

The recalculated value of $|V_{cd}|$ is consistent with the value of $|V_{cd}| = 0.22522 \pm 0.00061$, obtained from the global fit of the other CKM matrix element measurements that assumes unitarity in SM, within 1.7σ. With 20 fb^{-1} of data at 3.773 GeV and 6 fb^{-1} of data at 4.178 GeV, the relative precision of the measurements of $|V_{cs}|$ and $|V_{cd}|$ with leptonic decays will both reach 1.0%.

3. *Tests of lepton flavor universality*

In recent years, hints of LFU violation have emerged in some SL B-meson decays [14-23]. In Ref. [24], it is argued that LFU violation may occur in $c \to s$ transitions due to an amplitude that includes a charged Higgs boson, that arises in a two-Higgs-doublet model, interfering with the SM amplitude involving a $W^\pm$ boson. Therefore, it is important to test LFU with $D_{(s)}^+ \to \ell^+\nu_\ell$ decays.

In SM, the ratio of the partial widths of $D_{(s)}^+ \to \tau^+\nu_\tau$ and $D_{(s)}^+ \to \mu^+\nu_\mu$ is predicted as

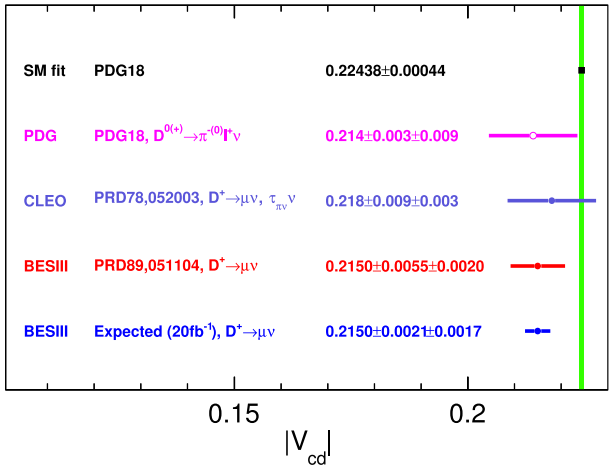

(a)

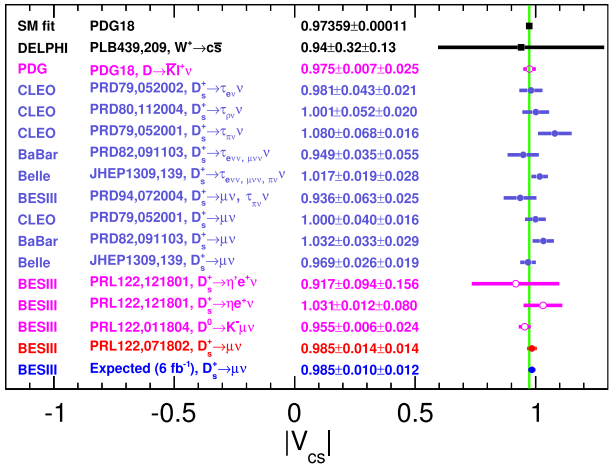

(b)

Fig. 5.3. (color online) Expected precision of the measurements of: (a) $|V_{cd}|$, using $D^+ \to \mu^+\nu_\mu$ with 20 fb^{-1} of data at 3.773 GeV; and (b) $|V_{cs}|$, using $D_s^+ \to \mu^+\nu_\mu$ with 6 fb^{-1} of data at 4.178 GeV. The green bands show the uncertainties of the average values from the global fit in SM [2]. The circles, dots and rectangles with error bars are the values based on SL D decays, leptonic D decays and other methods, respectively. The value marked in red denotes the best measurement, and the values marked in light blue denote the expected precision.

$$R_{D^+_{(s)}} = \frac{\Gamma(D^+_{(s)} \to \tau^+\nu_\tau)}{\Gamma(D^+_{(s)} \to \mu^+\nu_\mu)} = \frac{m^2_{\tau^+}\left(1-\frac{m^2_{\tau^+}}{m^2_{D^+_{(s)}}}\right)^2}{m^2_{\mu^+}\left(1-\frac{m^2_{\mu^+}}{m^2_{D^+_{(s)}}}\right)^2}.$$

With the world average values of the masses of leptons and $D^+_{(s)}$ [2], one obtains $R_{D^+} = 2.67$ and $R_{D_s^+} = 9.74$ with negligible uncertainties. The measurements of $R_{D^+_{(s)}}$ reported by BESIII are $3.21 \pm 0.64 \pm 0.43$ (9.98 ± 0.52), which agree with the SM predictions. However, as previously noted, these measurements are statistically limited. With 20 fb^{-1} of data at 3.773 GeV, the precision of R_{D^+} will be statistically limited to about 8%. With 6 fb^{-1} of data at 4.178 GeV, the precision of $R_{D_s^+}$ will be systematically limited to about 3%.

4. *Comparison with other experiments*

The leptonic decays reconstructed at BESIII and CLEO-c come from data sets accumulated just above the open-charm threshold, where $D^0\bar{D}^0$ or D^+D^- mesons are produced as pairs. BFs can be determined by considering the yields of the single-tagged and double-tagged events. With this method, the background level and systematic uncertainties are lower than in measurements at B factories.

Currently, the best measurements of $D^+ \to \ell^+\nu_\ell$ are from BESIII. So far, no studies of $D^+ \to \ell^+\nu_\ell$ have been reported by BaBar, Belle, and LHCb, which may be due to the higher level of background that these experiments encounter. BESIII is expected to provide unique data in the next decade to improve the knowledge of f_{D^+}, $|V_{cd}|$, and test LFU in $D^+ \to \ell^+\nu_\ell$ decays.

BaBar [10] and Belle [11] have reported measurement of $D_s^+ \to \ell^+\nu_\ell$ using $e^+e^- \to c\bar{c} \to DKXD_s^{*-}$ with $D_s^{*-} \to D_s^-\gamma$, performed with about 0.5 and 1.0 ab^{-1} of data taken around $\Upsilon(4S)$, respectively. The statistical and systematic uncertainties of the measurements of $f_{D_s^+}$ and $|V_{cs}|$ at Belle are 1.6% and 2.5%, respectively. The dominant systematic uncertainties are from normalization, tag bias, particle identification, fit model and D_s^+ background. With 50 ab^{-1} of data at Belle II, the statistical uncertainties of these measurements are expected to be reduced to 0.25%. However, it will be extremely challenging to reduce the systematic uncertainties to match this level. Hence, it is expected that the measurement of $D_s^+ \to \ell^+\nu_\ell$ performed at BESIII with 6 fb^{-1} of data at 4.178 GeV will have a very significant weight in a future world average.

BESIII measurements of purely leptonic D_s^+ decays will be limited to a large degree by systematic uncertainties. This motivates the exploration of taking data at $\sqrt{s} =$ 4.009 GeV, where the $D_s^+D_s^-$ production is only possible. Such a data set will have a considerably reduced background with the double-tag method, thus improving the systematic uncertainties of the measurements. The drawback is the reduction of the cross-section by a factor of three with respect to the operation at 4.178 GeV. Therefore, a data set of 20 fb^{-1} would be required to match the statistical precision of 6 fb^{-1} of data at 4.178 GeV for all measurements of D_s^+ decay. Such a large set corresponds to many years of data taking and as such cannot be considered as the highest priority among the various charm physics data sets requested.

5.2.2 Semi-leptonic decays

In SM, the weak and strong effects in SL $D^{0(+)}$ de-

cays can be well separated [25]. Among them, the simplest case is $D^{0(+)} \to \bar{K}(\pi)\ell^+\nu_\ell$, for which the differential decay rate can be simply written as

$$\frac{\mathrm{d}\Gamma}{\mathrm{d}q^2} = \frac{G_F^2}{24\pi^3}|V_{cs(d)}|^2 p_{K(\pi)}^3 |f_+^{K(\pi)}(q^2)|^2, \tag{5.3}$$

where G_F is the Fermi coupling constant, and $p_{K(\pi)}$ is the kaon (pion) momentum in the D rest frame, $f_+^{K(\pi)}(q^2)$ is the form factor of the hadronic weak current depending on the square of the transferred four-momentum $q = p_D - p_{K(\pi)}$. From the analyses of the dynamics of these decays, one can obtain the product $f_+^{K(\pi)}(0)|V_{cs(d)}|$. By taking $f_+^{K(\pi)}(0)$ calculated in LQCD, or $|V_{cd(s)}|$ from a global fit assuming unitarity in SM, the value of either $|V_{cd(s)}|$ or $f_+^{K(\pi)}(0)$ can be obtained.

● *Form factors of SL decays*

With the data sets at hand, BESIII has reported improved measurements of the absolute BFs and the form factors of the SL decays $D^{0(+)} \to \bar{K}e^+\nu_e$, $D^{0(+)} \to \pi e^+\nu_e$ [26, 27], $D^0 \to K^-\mu^+\nu_\mu$ [28], $D^+ \to \eta e^+\nu_e$ [29], $D^+ \to \bar{K}^{*0}e^+\nu_e$ [30], $D^{0(+)} \to \rho^{-(0)}e^+\nu_e$ [31], $D^+ \to \omega e^+\nu_e$ [32], $D_s^+ \to K^{(*)0}e^+\nu_e$ [33] and $D_s^+ \to \eta^{(\prime)}e^+\nu_e$ [34]. Figure 5.4 shows the form factors $f_+^K(0)$ and $f_+^\pi(0)$ measured by various experiments and calculated in LQCD. The BESIII measurement of $f_+^K(0)$ is dominated by systematic uncertainties, whereas other measurements are dominated by statistical uncertainties. The measurements of the form factors of $D^0 \to K^{*-}e^+\nu_e$, $D^+ \to \eta\mu^+\nu_\mu$, $D_s^+ \to \phi e^+\nu_e$, $D_s^+ \to f_0(980)e^+\nu_e$ and $D_s^+ \to \eta\mu^+\nu_\mu$ are still ongoing, but all will be statistically limited with the current data sets.

Measurements of SL $D^{0(+)}$ decays that contain a scalar or axial-vector meson in the final state, *e.g.* $D^{0(+)} \to \bar{K}_1(1270)e^+\nu_e$ [35] and $D^{0(+)} \to a_0(980)e^+\nu_e$ [36], have been reported by CLEO-c and BESIII. However, these decay samples are about 100 events, which is insufficient to determine the form-factors.

With 20 fb^{-1} of data at 3.773 GeV, all form-factor measurements which are currently statistically limited will be improved by a factor of up to 2.6. We also have an opportunity to determine for the first time the form factors of $D^0 \to K_1^-(1270)e^+\nu_e$, $D^+ \to \bar{K}_1^0(1270)e^+\nu_e$, $D^+ \to \eta' e^+\nu_e$, $D^0 \to a_0^-(980)e^+\nu_e$, and $D^+ \to a_0^0(980)e^+\nu_e$. In addition, studies of the semi-muonic decays $D^{0(+)} \to \bar{K}\mu^+\nu_\mu$ and $D^{0(+)} \to \pi\mu^+\nu_\mu$ will further improve the knowledge of $f_+^K(0)$ and $f_+^\pi(0)$.

With 3.2 fb^{-1} of data at 4.178 GeV, the expected yield for each of the Cabibbo-favored (CF) SL D_s^+ decays is about 1000, while for each of the singly Cabibbo-suppressed (SCS) SL D_s^+ decays it is not more than 200. In this case, all studies of the dynamics of SL D_s^+ decays are restricted by the limited data sets. The measurements of the form factors in these decays will be improved by a factor of up to 1.4 with 6 fb^{-1} of data at 4.178 GeV.

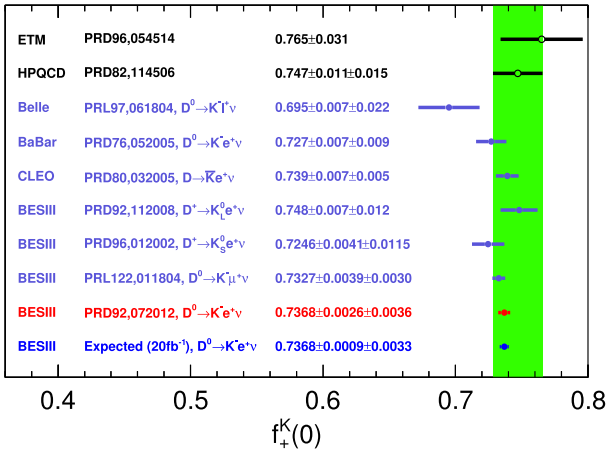

(a)

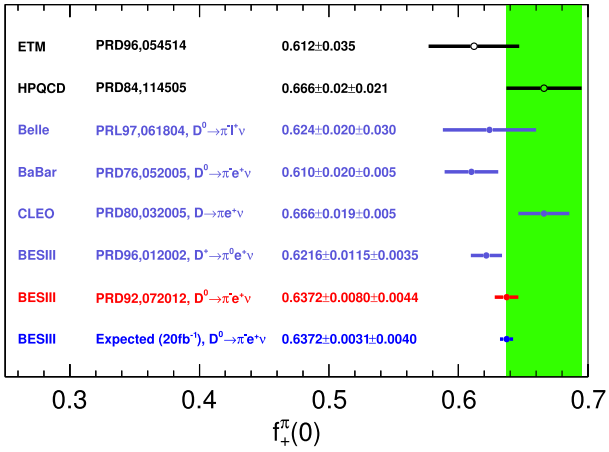

(b)

Fig. 5.4. (color online) Expected precision of the measurements of (a) $f_+^K(0)$ and (b) $f_+^\pi(0)$ with 20 fb^{-1} of data at 3.773 GeV. The green bands show the LQCD uncertainties [37, 38]. The PDG value is combined from the results of Belle, CLEO, BaBar and BESIII. The circles and dots with error bars are the LQCD calculations and experimental measurements, respectively. The value marked in red denotes the best measurement, and the values marked in light blue denote the expected precision.

● *Determination of* $|V_{cs(d)}|$

The CKM elements $|V_{cs}|$ and $|V_{cd}|$ can also be determined from the analyses of SL decays $D^{0(+)} \to \bar{K}\ell^+\nu_\ell$ and $D^{0(+)} \to \pi\ell^+\nu_\ell$ where the values of the form factors are taken from LQCD. The results using this approach are included in Fig. 5.3. At present, the LQCD uncertainties are 2.4% for $f_+^K(0)$ [37] and 4.4% for $f_+^\pi(0)$ [38], which is significantly larger than the associated experimental uncertainties, and therefore limit the determination of $|V_{cs}|$ and $|V_{cd}|$ with this method.

In the coming decade, however, the uncertainties of $f_+^K(0)$ and $f_+^\pi(0)$ calculated in LQCD are expected to be

reduced to the level of 1.0% and 0.5% [39], respectively. Therefore, improved measurements of $f_+^K(0)$ and $f_+^\pi(0)$ will play a key role in the determination of $|V_{cs}|$ and $|V_{cd}|$. With 20 fb^{-1} of $\psi(3770)$ data, the experimental uncertainties of the measurements of $|V_{cs}|$ and $|V_{cd}|$ with the SL $D^{0(+)}$ decays in electron channels are expected to reach the 0.5% level. Studies of $D^{0(+)} \to \bar{K}\mu^+\nu_\mu$ and $D^{0(+)} \to \pi\mu^+\nu_\mu$ will provide additional sensitivity.

In SL D_s^+ decays, the analyses of the dynamics of $D_s^+ \to \eta^{(\prime)}e^+\nu_e$ decays with 6 fb^{-1} of data at 4.178 GeV, where $\eta-\eta'$ mixing is involved, will provide complementary measurements of $|V_{cs}|$. The statistical uncertainty is expected to reach the 2.0% level, which will further improve the measurement precision of $|V_{cs}|$ at BESIII.

● *Tests of lepton flavor universality*

Previous measurements of BFs of $D^0 \to \pi^-\mu^+\nu_\mu$ and $D^0 \to \pi^-e^+\nu_e$ [2] resulted in the ratio of BFs $\mathcal{B}(D^0 \to \pi^-\mu^+\nu_\mu)/\mathcal{B}(D^0 \to \pi^-e^+\nu_e) = 0.82 \pm 0.08$, which deviates from the SM prediction of 0.985 ± 0.002 [40] by 2.1σ. This hint of LFU violation has motivated BESIII to report more precise BF measurements and to obtain the ratios $\mathcal{B}(D^0 \to \pi^-\mu^+\nu_\mu)/\mathcal{B}(D^0 \to \pi^-e^+\nu_e) = 0.922 \pm 0.030 \pm 0.022$ and $\mathcal{B}(D^+ \to \pi^0\mu^+\nu_\mu)/\mathcal{B}(D^+ \to \pi^0e^+\nu_e) = 0.964 \pm 0.037 \pm 0.026$ [41]. These results are consistent with the SM predictions within 1.7σ and 0.5σ, respectively. Considerably more accurate studies will be possible with 20 fb^{-1} of data at 3.773 GeV, besides optimizations of the systematic uncertainties.

As pointed out in Ref. [24], due to the mediation of charged Higgs bosons in the two-Higgs-doublet model, LFU in $c \to s$ transitions may be violated. In charm decays, the semi-tauonic decays involving a kaon in the final state are kinematically forbidden. Measurements of the ratio of the partial widths of $D^{0(+)} \to \bar{K}\mu^+\nu_\mu$ and of $D^{0(+)} \to \bar{K}e^+\nu_e$ in different q^2 intervals constitute a complementary test of LFU to that using semi-tauonic decays. These measurements are currently statistically limited [28, 41], and will be significantly improved with 20 fb^{-1} of data at 3.773 GeV.

● *Studies of meson spectroscopy*

Studies of intermediate resonances in hadronic final states in SL decays provide a clean environment to explore meson spectroscopy as there is no interference from the other particles. This corresponds to a much simpler treatment than similar studies of $D_{(s)}^{0(+)}$ hadronic decays or charmonium decays. For instance, in $D^0 \to K_1^-(1270)e^+\nu_e$ and $D^+ \to \bar{K}_1^0(1270)e^+\nu_e$, the single hadronic current allows to factor out the production of the axial-meson, which provides unique information about the structure of the lightest strange axial-vector mesons. At present, the world average values of the mass, 1272 ± 7 MeV, and width, 90 ± 20 MeV, of $\bar{K}_1(1270)$ have large uncertainties [2]. Furthermore, different analysis channels produce conflicting resonance parameters. Based on the future BESIII data set, the precision of these parameters is expected to be improved by a factor of two to three. Also, we will have an opportunity to study the properties of other particles, *e.g.* $a_0^-(980)$ and $a_0^0(980)$ in SL decays. In addition, it is possible to search for various SL $D_{(s)}^{0(+)}$ transitions to other scalar or axial-vector mesons, as shown in Ref. [42].

● *Comparison with other experiments*

BaBar studied the SL decays $D^0 \to K^-e^+\nu_e$ [43] and $D^0 \to \pi^-e^+\nu_e$ [44] using the decay $D^0 \to K^-\pi^+$ to normalize the measurements. However, BF of $D^0 \to K^-\pi^+$ has an uncertainty of 1% that is larger than the systematic uncertainty of the measurements of $D^0 \to K^-e^+\nu_e$ and $D^0 \to \pi^-e^+\nu_e$ at BESIII. Belle made absolute measurements of $D^0 \to K^-\ell^+\nu_\ell$ and $D^0 \to \pi^-\ell^+\nu_\ell$ using the decay chain $D_{\rm tag}^{(*)}D_{\rm sig}^{*-}X$ with 282 fb^{-1} of data taken around $\Upsilon(4S)$ [45] with the precision summarized in Table 5.2. So far, no other SL measurements have been reported by Belle.

BESIII has the advantage of low background and small systematic uncertainty (<1%) for measurements of semi-electronic $D^{0(+)}$ decays, and with 20 fb^{-1} of data at 3.773 GeV will be competitive with Belle II. On the other hand, the momenta of most muons in semi-muonic $D^{0(+)}$ decays produced at threshold are lower than 0.5 GeV/c, which is outside the detection capability of the muon counter, and hence makes the study of semi-muonic $D^{0(+)}$ decays challenging at BESIII. However, improved and comprehensive measurements of the dynamics of many semi-muonic $D^{0(+)}$ decays into a pseudescalar meson are feasible, as shown in Refs. [28, 41], but will be challenging for the semi-muonic $D^{0(+)}$ transitions into vector, scalar or axial-vector mesons.

SL decays can also be studied at LHCb and its upgrades, particularly in the muon channels. However, studies of the SL $D_{(s)}^{0(+)}$ decays involving electron and photon(s) in the final states are more difficult in the environment of a hadron collider due to larger backgrounds.

5.2.3 Quantum-correlated measurements of D^0 hadronic decays

The quantum correlation of the $D^0\bar{D}^0$ meson pair produced at $\psi(3770)$ provides a unique way to probe the amplitudes of D decays, $D^0\bar{D}^0$ mixing parameters and potential CP violation in D^0 decays [46]. Furthermore, the determination of the strong-phase difference between CF and doubly Cabibbo-suppressed (DCS) amplitudes in the decay of quantum-correlated $D^0\bar{D}^0$ meson pairs has several motivations: understanding the non-perturbative QCD effects in the charm sector; serving as the essential input to extract the angle γ of the CKM unitarity triangle (UT); and relating the measured mixing parameters in hadronic decay (x', y') to the mass and width difference

Table 5.2. Measurements of the form factors of SL $D^{0(+)}$ decays. For the decays involving a pseudoscalar or scalar meson, the decay rate is parametrized by the form factor $f_+(0)$. For the decays involving a vector or axial-vector meson, the decay rate is parametrized by three form factors, $V(0)$, $A_1(0)$, and $A_2(0)$, with the relations $r_V = V(0)/A_1(0)$ and $r_A = A_2(0)/A_1(0)$. $A_1(0)$ for the $D^+ \to \bar{K}^{*0}e^+\nu_e$ decay is reported due to low background and sufficient signal at BESIII. For Belle II, we assume that the systematic uncertainties can be reduced by a factor of 2 compared to the Belle results. The results marked in * for Belle II are based on both the semi-electronic and semi-muonic decays.

	BESIII	BESIII	Belle	Belle II
Luminosity	2.9 fb^{-1}@3.773 GeV	20 fb^{-1}@3.773 GeV	0.28 ab^{-1}	50 ab^{-1}
$D^0 \to K^-e^+\nu_e$	$0.4\%_{\rm stat.}0.5\%_{\rm syst.}$	$0.2\%_{\rm stat.}0.4\%_{\rm syst.}$	$1.0\%_{\rm stat.}3.2\%^*_{\rm syst.}$	$0.1\%_{\rm stat.}1.6\%^*_{\rm syst.}$
$D^0 \to K^-\mu^+\nu_\mu$	$0.5\%_{\rm stat.}0.4\%_{\rm syst.}$	$0.2\%_{\rm stat.}0.4\%_{\rm syst.}$		
$D^0 \to \pi^-e^+\nu_e$	$1.3\%_{\rm stat.}0.7\%_{\rm syst.}$	$0.5\%_{\rm stat.}0.4\%_{\rm stat.}$	$3.2\%_{\rm stat.}4.8\%^*_{\rm syst.}$	$0.2\%_{\rm stat.}2.4\%^*_{\rm syst.}$
$D^0 \to \pi^-\mu^+\nu_\mu$	NA	$0.8\%_{\rm stat.}0.8\%_{\rm syst.}$		
$D^0 \to K^{*-}e^+\nu_e$				
r_V	$5.0\%_{\rm stat.}2.0\%_{\rm syst.}$	$2.0\%_{\rm stat.}2.0\%_{\rm syst.}$	–	–
r_A	$10.\%_{\rm stat.}2.0\%_{\rm syst.}$	$4.0\%_{\rm stat.}2.0\%_{\rm syst.}$	–	–
$D^0 \to a_0^-(980)e^+\nu_e$	NA	$10.\%_{\rm stat.}5.0\%_{\rm syst.}$	–	–
$D^0 \to K_1^-(1270)e^+\nu_e$	NA	$10.\%_{\rm stat.}5.0\%_{\rm syst.}$	–	–
$D^+ \to \bar{K}^0e^+\nu_e$	$0.6\%_{\rm stat.}1.7\%_{\rm syst.}$	$0.2\%_{\rm stat.}1.0\%_{\rm syst.}$	–	–
$D^+ \to K_{\rm L}^0e^+\nu_e$	$0.9\%_{\rm stat.}1.6\%_{\rm syst.}$	$0.4\%_{\rm stat.}1.0\%_{\rm syst.}$	–	–
$D^+ \to \bar{K}^0\mu^+\nu_\mu$	NA	$0.3\%_{\rm stat.}1.0\%_{\rm syst.}$	–	–
$D^+ \to \bar{K}^{*0}e^+\nu_e$				
$A_1(0)$	$1.7\%_{\rm stat.}2.0\%_{\rm syst.}$	$0.7\%_{\rm stat.}1.0\%_{\rm syst.}$	–	–
r_V	$4.0\%_{\rm stat.}0.5\%_{\rm syst.}$	$1.6\%_{\rm stat.}0.5\%_{\rm syst.}$	–	–
r_A	$5.0\%_{\rm stat.}1.0\%_{\rm syst.}$	$2.0\%_{\rm stat.}1.0\%_{\rm syst.}$	–	–
$D^+ \to \pi^0e^+\nu_e$	$1.9\%_{\rm stat.}0.5\%_{\rm syst.}$	$0.7\%_{\rm stat.}0.5\%_{\rm syst.}$	–	–
$D^+ \to \pi^0\mu^+\nu_\mu$	NA	$1.0\%_{\rm stat.}1.0\%_{\rm syst.}$	–	–
$D^+ \to \eta e^+\nu_e$	$4.5\%_{\rm stat.}2.0\%_{\rm syst.}$	$2.0\%_{\rm stat.}2.0\%_{\rm syst.}$	–	–
$D^+ \to \eta' e^+\nu_e$	NA	$10.\%_{\rm stat.}5.0\%_{\rm syst.}$	–	–
$D^+ \to \omega e^+\nu_e$				
r_V	$7.2\%_{\rm stat.}4.8\%_{\rm syst.}$	$3.0\%_{\rm stat.}2.0\%_{\rm syst.}$	–	–
r_A	$14\%_{\rm stat.}5.0\%_{\rm syst.}$	$3.0\%_{\rm stat.}2.0\%_{\rm syst.}$	–	–
$D^+ \to a_0^0(980)e^+\nu_e$	NA	$10.\%_{\rm stat.}5.0\%_{\rm syst.}$	–	–
$D^+ \to \bar{K}_1^0(1270)e^+\nu_e$	NA	$10.\%_{\rm stat.}5.0\%_{\rm syst.}$	–	–
$D^{0(+)} \to \rho^{-(0)}e^+\nu_e$				
r_V	$5.0\%_{\rm stat.}4.0\%_{\rm syst.}$	$2.0\%_{\rm stat.}2.0\%_{\rm syst.}$	–	–
r_A	$8.0\%_{\rm stat.}4.0\%_{\rm syst.}$	$3.0\%_{\rm stat.}2.0\%_{\rm syst.}$	–	–

parameters (x, y) [47].

The measurements of the CKM UT angles α, β, and γ in B decays are important for testing the CKM unitarity and searching for CP violation beyond SM. Any discrepancy in the measurements of the unitarity triangle involving tree and loop dominated processes would indicate high-mass new physics within the loops. Among the three CKM angles, the measurement of γ, where the current world-best measurement from LHCb is $(74.0^{+5.0}_{-5.8})^\circ$ [48], has particular importance as it is the only CP-violating observable that can be determined using tree-level decays. Degree-level precision of γ will allow a rigorous comparison of the loop and tree-level determinations of UT. The independence from loop diagrams means that the measurement of γ has negligible theoretical uncertainty [49]. The precision measurement of γ is one of the top priorities for the LHCb upgrade(s) and Belle II experiments.

The most precise method to measure γ is based on the interference between $B^+ \to \bar{D}^0K^+$ and $B^+ \to D^0K^+$ decays

[50-52]. In the future, the statistical uncertainties of these measurements will be greatly reduced by using the large B meson samples recorded by LHCb and Belle II, and by extending these measurements to other similar B modes such as $B^0 \to DK^{*0}$, where D implies either D^0 or $\bar{D}^0$, $B^+ \to D^*K^+$, $B^+ \to DK\pi\pi$, and $B^+ \to DK^{*+}$ [53, 54]. However, with increased statistical precision, limited knowledge of the strong phases of the D decays will systematically restrict the overall sensitivity. Consequently, improved knowledge of the strong-phase related parameters in D decays is essential to make measurements of γ to the degree-level precision. Strong-phase information in the following D decay modes has been obtained from the CLEO-c experiment and has been used in the most recent γ measurements:

- measurement of the amplitude weighed average cosine and sine of the strong-phase difference, c_i and s_i, where the index i refers to the phase-space region of the self-conjugate multi-body decays, such as $D \to K^0_S\pi^+\pi^-$ and $D \to K^0_S K^+K^-$ [55];
- measurement of the coherence factor and the average strong-phase difference in $D \to K^\pm\pi^\mp\pi^+\pi^-$ and $D \to K^\pm\pi^\mp\pi^0$ [56];
- measurement of the coherence factor and the average strong-phase difference in $D \to K^0_S K^\pm\pi^\mp$ [57];
- measurement of the CP-even content of $D \to \pi^+\pi^-\pi^+\pi^-$, $D \to \pi^+\pi^-\pi^0$, and $D \to K^+K^-\pi^0$ [58];
- measurement of the strong-phase difference in $D \to K^\pm\pi^\mp$ [59];
- measurement of the CP-even content and the strong-phase difference c_i and s_i in $D \to K_S\pi^+\pi^-\pi^0$ [60] .

Complementary constraints on the strong phase in $D \to K^\pm\pi^\mp\pi^+\pi^-$ decays have been obtained from the charm-mixing measurements at LHCb [61]. It should be noted that the precision of the $D \to K^\pm\pi^\mp$ phase is dominated by the combination of charm-mixing measurements at the LHCb and CDF experiments, and the B factories [30], so that the role of threshold data is less important. Recently, BESIII reported the strong-phase measurement of $D \to K^\pm\pi^\mp$ decays [62], and the preliminary results of the strong-phase measurements of $D \to K^0_S\pi^+\pi^-$ decays [63] from the current $\psi(3770)$ data with an integrated luminosity of 2.93 fb^{-1}. The precision of these measurements demonstrated the powerful capabilities of BESIII to determine strong-phase parameters accurately. However, all the current strong-phase measurements are still limited by the size of the $\psi(3770)$ data sets. Therefore, one of the most important goals of the BESIII charm physics program is to improve the strong-phase measurements with a larger $\psi(3770)$ data set.

For the existing determination of γ that is made by combining the CP-violation sensitive observables from different D modes in $B \to D^{(*)}K^{(*)}$ decays, the uncertainty arising from the CLEO-c input has been found to be about 2° for LHCb. The current BESIII $\psi(3770)$ data set is approximately four times larger than of CLEO-c. The full analysis based on this data gave a factor of 2.5(1.9) more precise results for $c_i(s_i)$, which reduces its contribution to the uncertainty of γ to at most 0.7° [63]. As evident from Table 5.3, this precision should be adequate for the LHCb Run-2 measurement, but will not be sufficient for the future LHCb upgrade and Belle II era, in particular because the strong-phase uncertainties will be largely correlated between the two experiments for each mode. To minimize the impact of the strong-phase measurement uncertainties on the next generation experiments, a much larger $\psi(3770)$ data set at BESIII is essential, ideally corresponding to an integrated luminosity of 20 fb^{-1}, as BEPCII is the only machine working at the charm-threshold energy. Furthermore, determining these parameters with radiative return events to $\psi(3770)$ at Belle II will not be achievable with suitable precision even with a data set of 50 ab^{-1}. A 20 fb^{-1} sample of $\psi(3770)$ data would lead to an uncertainty of approximately 0.4° for the γ measurement, which will be necessary for the goals of the LHCb upgrade I and Belle II. Moreover, the improved precision will be essential to allow even larger data of LHCb upgrade II [64] to be fully exploited for further improving the knowledge of γ, and allowing a detailed comparison of the results obtained with different decay modes. A reasonable time frame for taking the $\psi(3770)$ data set with 20 fb^{-1} would be 2025, by when Belle II will complete accumulation of 50 ab^{-1} of data, and the LHCb upgrade I will be mid-way through its period of operation.

The synergy between the BESIII, LHCb, and Belle II experiments is the best way to accurately determine γ in such a manner that the uncertainty of γ is statistically

Table 5.3. Expected γ/ϕ_3 precision of the LHCb [53] and Belle II [54] experiments and their timescales.

Runs	Collected / Expected integrated luminosity	Year attained	γ/ϕ_3 sensitivity
LHCb Run-1 [7, 8 TeV]	3 fb^{-1}	2012	8°
LHCb Run-2 [13 TeV]	6 fb^{-1}	2018	4°
Belle II Run	50 ab^{-1}	2025	1.5°
LHCb upgrade I [14 TeV]	50 fb^{-1}	2030	< 1°
LHCb upgrade II [14 TeV]	300 fb^{-1}	(>)2035	< 0.4°

rather than systematically limited. Table 5.4 lists the decay modes of interest that can be measured at BESIII. Furthermore, for the multi-body D final states, the phase-space binning schemes that could be employed are mentioned. Increasing the number of bins improves the statistical sensitivity of the measurements as the amount of information loss relative to an unbinned method is reduced. The modes are listed in their approximate order of importance for the LHCb measurements. For the Belle II experiment, modes with neutrals are more important due to the larger neutral reconstruction efficiency compared to LHCb. However, LHCb will have an advantage since the two- and four-body D decays contain only prompt charged pions and kaons in the final state.

In addition, it is worth noting the ability of BESIII to efficiently reconstruct D modes containing a K^0_L meson in the final state, and to determine the relevant strong-phases. These K^0_L modes provide additional tags (for example Ref. [66]) that increase the precision of other strong-phase parameter measurements at $\psi(3770)$. Furthermore, it may be possible to use the K^0_L modes at Belle II to reconstruct $B^+ \to DK^+$ given the anticipated improvements in K^0_L reconstruction. This is demonstarted by the fact that the determination of the UT angle β at the B factories benefited from included $B^0 \to J/\psi K^0_L$ decays in the measurement.

The measurements of strong phases using quantum-coherent analyses [69] at BESIII provide important input for the LHCb and Belle II experiments for measurement of the $D^0\bar{D}^0$ mixing parameters and indirect CP violation in charm mixing. All measurement methods, as described in Refs. [70-72], use the charm strong-phase parameters. For example, using the c_i and s_i results as input for time-dependent measurements of $D^0 \to K_S\pi^+\pi^-$, the charm mixing parameters x and y can be determined in a model-independent way [73]. The precise strong-phase measurements listed in Table 5.4, performed with the current and future $\psi(3770)$ data at BESIII, will prevent these studies from being limited by the uncertainties related to the strong-phase. Furthermore, the strong-phase measurements have recently been used in time-dependent CP-violation measurements of the $B^0 \to D^{(*)0}\pi^0$ decays by Belle [74] to make measurements of β/ϕ_1 that are free of uncertainties related to the penguin processes. Such measurements are very attractive at Belle II, and they can be compared to the "golden modes" $B^0 \to J/\psi K^0$ for empirically determining the pollution from the penguin diagrams in β/ϕ_1.

5.2.4 Impact on CKM measurements

In SM, quark-flavor mixing is described by the 3×3 CKM matrix $V_{\rm CKM}$, as shown in Eq. (2) in Sec. 5.2.1. Unitarity is the only, albeit powerful, constraint on $V_{\rm CKM}$. Without loss of generality, $V_{\rm CKM}$ can be parametrized in terms of three mixing angles and one phase [75]

$$V_{\rm CKM} = \begin{pmatrix} c_{12}c_{13} & s_{12}c_{13} & s_{13}e^{-i\delta} \\ -s_{12}c_{23} - c_{12}s_{23}s_{13}e^{i\delta} & c_{12}c_{23} - s_{12}s_{23}s_{13}e^{i\delta} & s_{23}c_{13} \\ s_{12}s_{23} - c_{12}c_{23}s_{13}e^{i\delta} & -c_{12}s_{23} - s_{12}c_{23}s_{13}e^{i\delta} & c_{23}c_{13} \end{pmatrix}, \tag{5.4}$$

Table 5.4. A priority-ordered list of strong-phase related measurements that are important for precision measurements of γ and indirect CP violation in charm mixing [53]. For the states that are not self-conjugate, the coherence factor R, and the average strong-phase difference δ, can be measured [65]. For self-conjugate states, there are two choices: either a measurement of the CP-even fraction F_+ [66], or a measurement of the amplitude weighed average cosine and sine of the strong-phase difference, c_i and s_i, where the index i refers to the phase-space region of the given multi-body decay [67].

Decay mode	Quantity of interest	Comments
$D \to K^0_S\pi^+\pi^-$	c_i and s_i	Binning schemes as used in the CLEO-c analysis. With 20 fb^{-1} of data at 3.773 GeV, it might be worthwhile to explore alternative binning.
$D \to K^0_S K^+K^-$	c_i and s_i	Binning schemes as used in the CLEO-c analysis. With 20 fb^{-1} of data at 3.773 GeV, it might be worthwhile to explore alternative binning.
$D \to K^\pm\pi^\mp\pi^+\pi^-$	R,δ	In bins guided by amplitude models, currently under development by LHCb.
$D \to K^+K^-\pi^+\pi^-$	c_i and s_i	Binning scheme guided by the CLEO-c model [68] or potentially an improved model in the future.
$D \to \pi^+\pi^-\pi^+\pi^-$	F_+ or c_i and s_i	Unbinned measurement of F_+. Measurements of F_+ in bins or c_i and s_i in bins could be explored.
$D \to K^\pm\pi^\mp\pi^0$	R,δ	Simple 2-3 bin scheme could be considered.
$D \to K^0_S K^\pm\pi^\mp$	R,δ	Simple 2 bin scheme where one bin encloses the K^* resonance.
$D \to \pi^+\pi^-\pi^0$	F_+	No binning required as $F_+ \sim 1$.
$D \to K^0_S\pi^+\pi^-\pi^0$	F_+ or c_i and s_i	Unbinned measurement of F_+ required. Additional measurements of F_+ or c_i and s_i in bins could be explored.
$D \to K^+K^-\pi^0$	F_+	Unbinned measurement required. Extensions to binned measurements of either F_+ or c_i and s_i.
$D \to K^\pm\pi^\mp$	δ	Of low priority due to good precision available through charm-mixing analyses.

where $c_{ij} \equiv \cos\theta_{ij}$ and $s_{ij} \equiv \sin\theta_{ij}$ (for $ij = 12$, 23 and 13). The irremovable phase δ is the unique source of CP-violation in quark flavor changing processes in SM. Following the observation of a hierarchy between the different matrix elements, Wolfenstein [76] proposed an expansion of the CKM matrix in terms of four parameters λ, A, ρ, and η, which is widely used in contemporary literature, and which is the parametrization employed in CKMfitter [77].

The allowed region in the ρ and η space can be elegantly displayed by means of UT, described by the rescaled unitarity relation between the first and the third column of the CKM matrix (*i.e.* corresponding to the b-meson system). UT can be described in the complex $(\bar{\rho},\bar{\eta})$ plane, where the apex is given by the following definition, independent of the phase convention [78]

$$\bar{\rho}+i\bar{\eta} \equiv -\frac{V_{ud}V_{ub}^*}{V_{cd}V_{cb}^*}. \tag{5.5}$$

We also propose to represent the combination of CKM constraints in the plane that is relevant for D meson UT. In analogy with the exact and rephasing invariant expression for $(\bar{\rho},\bar{\eta})$, we define the coordinates of the apex of D meson UT [1]

$$\bar{\rho}_{cu}+i\bar{\eta}_{cu} \equiv -\frac{V_{ud}V_{cd}^*}{V_{us}V_{cs}^*}, \tag{5.6}$$

where $\bar{\rho}_{cu} = 1+O(\lambda^4)$ and $\bar{\eta}_{cu} = O(\lambda^4)$. One can see that this triangle has two sides with length very close to 1, and a small side of the order $O(\lambda^4)$, with angles $\alpha_{cu} = -\gamma$, $\beta_{cu} = \gamma+\pi+O(\lambda^4)$ and $\gamma_{cu} = O(\lambda^4)$.

To constrain these parameters, we consider a prospective exercise at the time when BESIII completes taking 20 fb^{-1} of data accumulated at the $D\bar{D}$ threshold [1], and 6 fb^{-1} data at 4.178 GeV, i.e. around 2025 (Phase I). By that time, LHCb will have collected 23 fb^{-1} [79], and CMS/ATLAS 300 fb^{-1} of data, that is after Run 3 of the LHC and prior to the start of HL-LHC. We also take into account the prospective accuracy of Belle II at 50 ab^{-1} at Phase I [54]. The individual constraints as well as the combination of the usual observables that will be available in 2025 are shown in the $(\bar{\rho}_{cu},\bar{\eta}_{cu})$ plane in Fig. 5.5. One can also transfer the constraints to the $(|V_{cs}|,|V_{cd}|)$ plane, as shown in Fig. 5.6, which clearly shows the direct contribution of the BESIII measurements of $|V_{cs}|$ and $|V_{cd}|$, and allows precise tests of the consistency of CKM determination from different quark sectors.

In Phase II, beyond 2035, we assume larger data sets, 300 fb^{-1} for LHCb and 3000 fb^{-1} for CMS/ATLAS. The corresponding perspectives for the individual constraints and the global CKM fit in the $(\bar{\rho},\bar{\eta})$ plane are shown in Fig. 5.7, which involve both the LHC and Belle II measurements related to B and B_s mesons. We use the available sources for the uncertainties [54, 79] assuming that all measurements agree perfectly well with SM. As mentioned in Sec. 5.2.3, thanks to the critical input for charm

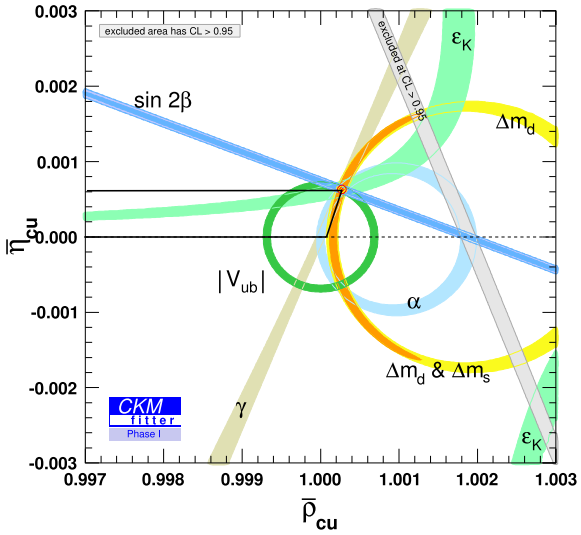

Fig. 5.5. (color online) Individual constraints and the global CKM fit in the $(\bar{\rho}_{cu},\bar{\eta}_{cu})$ plane according to our projection of the experimental status in 2025 (Phase I). The shaded areas have 95% CL. Only a part of D meson UT is visible (black solid lines). The two apices associated with large angles are shown, whereas the missing corner is situated at the origin, on the far left.

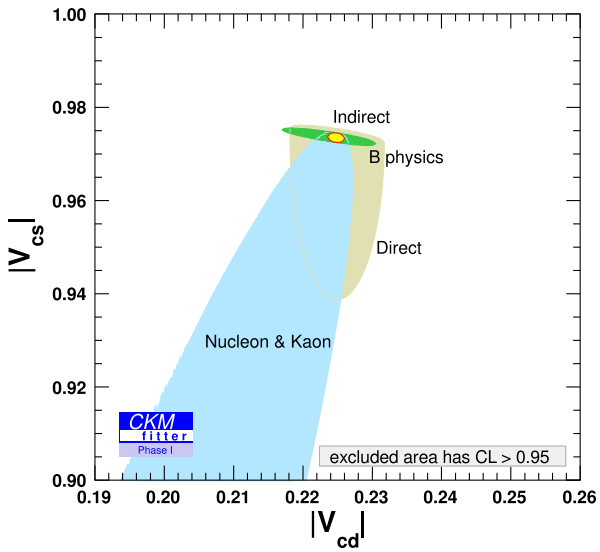

Fig. 5.6. (color online) Constraints in the $(|V_{cd}|,|V_{cs}|)$ plane for the Phase I data. The indirect constraints (from b transitions) are related to $|V_{cd}|$ and $|V_{cs}|$ by unitarity. The direct constraints combine leptonic and SL D and D_s decays from the BESIII experiment. The red hashed region of the global combination corresponds to 68% CL.

strong phases from BESIII with 20 fb^{-1} of data accumulated at the $D\bar{D}$ threshold [1], the knowledge of the angle γ will be improved to 0.4° or better, allowing for extremely precise tests of the CKM paradigm, and providing a sensitive probe for possible new physics contributions.

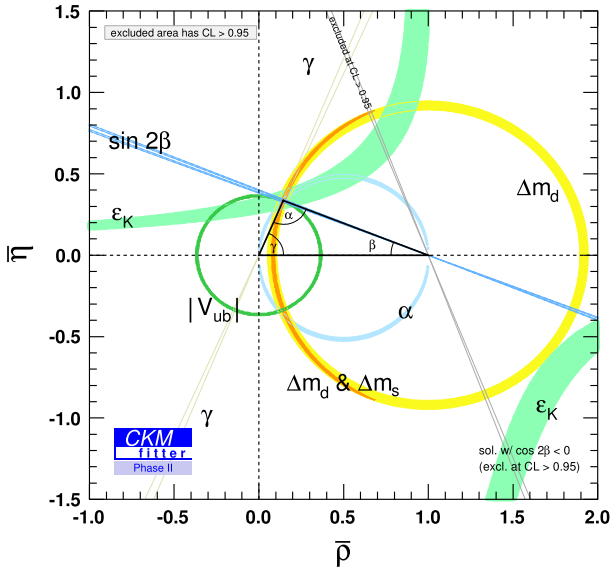

Fig. 5.7. (color online) Evolving constraints and the global fit in the $(\bar{\rho},\bar{\eta})$ plane with the anticipated improvements for the Phase II data (300 fb^{-1} from LHCb [79], 3000 fb^{-1} from CMS/ATLAS, and 50 ab^{-1} from Belle II [54]). γ is expected to have an accuracy around 0.4 degrees (shown in Table 5.3), thanks to the BESIII charm input with 20 fb^{-1} of data accumulated at the $D\bar{D}$ threshold [1]. The shaded areas have 95% CL.

5.2.5 CP violation and D mixing

It is not competitive to search for CP violation and charm mixing parameters at BESIII, since the achievable D^0 and $\bar{D}^0$ samples are smaller by more than 2-4 orders of magnitude than those at LHCb and Belle II. However, BESIII can uniquely explore the quantum coherence of the initial $D^0\bar{D}^0$ state produced at $\psi(3770)$ to provide constraints [80] on the mixing and CP-violating parameters [81, 82] that have completely different systematic uncertainties than those at LHCb or Belle II. For example, decays of each D in the $D^0\bar{D}^0$ state into final states of the same CP would immediately indicate CP-violation in charm, as the D-states produced at $\psi(3770)$ have opposite CP,

$$\Gamma^{++}_{D^0\bar{D}^0} = \left[\left(x^2+y^2\right)\left(\cosh^2 a_m - \cos^2\phi\right)\right]\Gamma^2(D\to f_+),$$

where we employ two CP = + states f, such as $f=\pi^+\pi^-$. Also, $\phi = \arg(p/q)$, $R_m = |p/q|$, and $a_m = \log R_m$ [81]. In addition, superb kinematical constraints might make BESIII competitive in studies of CP-asymmetries in some multi-body D decays [83].

5.2.6 CPT violation in charm mixing

CPT is conserved in all local Lorentz-invariant theories, including SM and all its commonly-discussed extensions. Yet, CPT violation might arise in string theory or some extra-dimensional models with Lorentz-symmetry violations in four dimensions. Time evolution studies of CP-correlated $D^0\bar{D}^0$ states are complementary to CPT-violation studies at B-factories and the LHC. While studies of these models are not particularly well motivated at the charm threshold, CPT-violating effects can still be probed with the quantum-correlated $D^0\bar{D}^0$ states at $\psi(3770)$ [84].

5.2.7 Absolute measurement of hadronic decays

The hadronic decay of charmed hadrons provides important information not only about the charmed hadron itself, but also about the light daughters of the hadron. Therefore, studying the charm multi-body hadronic decays is a powerful tool for light hadron spectroscopy. Analogously, studying the high-statistics hadronic decays of charmed baryon Λ_c^+ with a data set of 5 fb^{-1} produced at 4.64 GeV, as discussed in Sec. 5.3.1, is useful for an improved understanding of the light meson and baryon spectroscopy.

Experimental studies of two-body hadronic decays of D^0, D^+, and D_s^+ mesons are very important for calibrating theoretical models. There are different final-state possibilities, namely PP, VP, VV, SP, AP, and TP, where P, V, S, A, and T represent pseudoscalar, vector, scalar, axial vector, and tensor mesons, respectively. The simplest cases of the PP decays of D^0, D^+, and D_s^+ have been experimentally well investigated in recent years. However, some of these measurements, particularly of the DCS decays, are still statistically limited. Studies of non-PP final states require sophisticated amplitude analyses of multi-body decays of charmed mesons that are not well developed because of either the limited statistics or the high background level. Larger $D^{0(+)}$ and D_s data samples are necessary to guarantee clean signal samples with sufficient yields to perform reliable amplitude analyses, so that all types of two-body process can be well understood.

At present, the sums of BFs for the known exclusive decays of D^0, D^+, and D_s^+ are all more than 80% [2]. However, there is still significant room for exploring many unknown hadronic decays. A 20 fb^{-1} sample of data at $\psi(3770)$ will allow the determination of many BFs of missing decays to $K\pi\pi\pi$, $KK\pi\pi$, and $KK\pi\pi\pi$, as well as further exploration of the sub-structures in these decays. Some of them, for example $D^0\to K^-\pi^+\pi^0\pi^0$ and $D^+\to \bar{K}^0\pi^+\pi^0\pi^0$, are expected to have a BF in the range of 5%-10% [85], which can be significantly improved with the precise detection of π^0 and photons at BESIII.

LHCb has the ability to measure a large number of relative BFs of charm and beauty hadrons, on account of the high yields resulting from large cross-sections for heavy-flavor production in the forward region. Converting from the BF ratio to the absolute BF incurs an additional uncertainty in BF of the reference mode, such as $D^0\to K^-\pi^+$, $D^0\to K^-\pi^+\pi^+\pi^-$, $D^+\to K^-\pi^+\pi^+$, $D_s^+\to K^-K^+\pi^+$, and $\Lambda_c^+\to pK^-\pi^+$. Absolute BF measurements of other charmed baryons, Ξ_c^0 and Ξ_c^+, are also strongly desired.

Although it is acknowledged that these modes are very hard to measure with the current energy of the collisions at BESIII, the importance of these measurements is stressed here in case future developments could make them possible. Relevant discussion of the prospects for measurements of charmed baryons is given in Sec. 5.3.1.

With 20 fb^{-1} of data at 3.773 GeV and 6 fb^{-1} around 4.178 GeV at BESIII, many $D_{(s)}$ decays are expected to be measured with an uncertainty of about 1%, which will then be limited by the systematic uncertainties related to particle reconstruction in different final states. Improved measurements of the absolute BFs at BESIII will be highly beneficial for some key measurements at LHCb, since it is expected that the uncertainty of the reference mode will become the dominant uncertainty of several measurements. One prime example is the LHCb measurement of $B \to D^*\tau^+\nu_\tau$, which is used to test lepton universality [53]. BESIII can make precise measurements of BFs of the D^0, D_s^+, and D^+ inclusive decays to three charged pions and to neutral particles, and exclusive decays to final states with neutral kaons and pions (*e.g.* $D_s^+ \to \eta'\pi^+\pi^0$, $D^+ \to \bar{K}^0\pi^+\pi^+\pi^-\pi^0$, and $D^{0(+)} \to \eta X$, X denotes any possible particle combinations), which will have a significant impact on optimizing the background models. Another example is the determination of the CKM matrix elements $|V_{c(u)b}|$ via inclusive or exclusive SL B decays, such as $B \to D^*\ell^-\nu_\ell$ or $\Lambda_b^0 \to \Lambda_c^+\bar{\ell}^-\nu_\ell$. Precise measurements of absolute BFs of the $D_{(s)}^{0(+)}$ and Λ_c^+ decays (Sec. 5.3.1) are crucial for improvement of the $|V_{c(u)b}|$ measurements.

Due to the interference effects between the CF and DCS contributions, BFs of $D_{(s)} \to K_S^0X$ and $D_{(s)} \to K_L^0X$ are not expected to be equal. The recoil-mass method, or that developed in Ref. [86], allows an efficient reconstruction of $D_{(s)} \to K_L^0X$ decays at BESIII. A difference of about 10% was observed in $D^0 \to K_{S,L}^0\pi^0$ decays at CLEO-c [86], and was confirmed at BESIII [87]. The two-body decays $D^0 \to K_{S,L}^0X$ ($X = \pi^0, \eta, \eta', \omega, \phi$) are expected to have an asymmetry under the same mechanism [88], which can be tested with the current $\psi(3770)$ data, but the uncertainties will be dominated by the statistical uncertainties. Furthermore, measurements of these modes are of interest for understanding the width difference in the neutral D system [89]. With 20 fb^{-1} and 6 fb^{-1} of data taken at $\sqrt{s}$ = 3.773 and 4.178 GeV, these measurements will be performed with a much better precision.

5.3 Charmed baryons

5.3.1 Λ_c^+ physics

Studies of charm baryons have been ongoing since 1975 [90], and all ground states of singly charmed baryons, as well as some excited states, have been observed. The constituents of the lightest charmed baryon (Λ_c^+) are one diquark (ud) and one heavy charm quark (c), where, relative to the heavy quark, the light diquark is in a net quantum state of spin zero and isospin zero. In a naive spectator model, the Λ_c^+ decays dominate via the weak amplitudes $c \to W^+s$ and $c \to W^+d$ at the leading order, which leads to a simpler theoretical description in non-perturbative models than in the case of charmed mesons. Hence, studying the Λ_c^+ decays allows a deeper understanding of the strong and weak interactions in the charm sector, which is complementary to that provided by charmed mesons. In addition, Λ_c^+ is the cornerstone of the charmed baryon spectra. Improved knowledge of the Λ_c^+ decays is essential for the studies of the whole charmed baryon family. Furthermore, this knowledge will provide important information for the studies of beauty baryons that decay into final states involving Λ_c^+.

Compared to the significant progress in the studies of charmed mesons (D^0, D^+, and D_s^+) in both theory and experiment, the advancement of our understanding of charmed baryons has been relatively slow during the past 40 years. Until 2014, no absolute measurements of the decay rates of Λ_c^+ had been performed, with almost all rates measured relative to the normalization mode $\Lambda_c^+ \to pK^-\pi^+$, whose BF suffered from a large uncertainty of 25%. The overall situation changed since 2014, when BESIII collected a data set for e^+e^- annihilation at $\sqrt{s}$ = 4.6 GeV with an integrated luminosity of 567 pb^{-1}. At this energy, the $\Lambda_c^+\bar{\Lambda}_c^-$ pairs are produced in pairs with no accompanying hadrons. The total number of $\Lambda_c^+\bar{\Lambda}_c^-$ pairs produced was approximately 100,000. This threshold data set provided a clean environment to systematically investigate the production and decay of Λ_c^+. Precise BF measurements of $\Lambda_c^+ \to pK^-\pi^+$ were reported by Belle [91] and BESIII [92]. The combined precision of the $\Lambda_c^+ \to pK^-\pi^+$ BF is 5.2%, a five-fold reduction with respect to the previous result. In addition, more analyses were made at BESIII, Belle, and LHCb. At BESIII, a series of BF measurements have been reported, including:

- absolute BF measurement of $\Lambda_c^+ \to \Lambda\ell^+\nu_\ell$ [93, 94], which motivated the first LQCD calculation of this channel [95];
- absolute BF measurements of 12 Cabibbo-favored (CF) decays of Λ_c^+ [92], including $\Lambda_c^+ \to pK_S^0$, $pK^-\pi^+$, $pK_S^0\pi^0$, $pK_S^0\pi^+\pi^-$, $\Lambda\pi^+$, $\Lambda\pi^+\pi^0$, $\Lambda\pi^+\pi^+\pi^-$, $pK^-\pi^+\pi^0$, $\Sigma^0\pi^+$, $\Sigma^+\pi^0$, $\Sigma^+\pi^+\pi^-$, and $\Sigma^+\omega$;
- studies of singly-Cabibbo-suppressed (SCS) decays $\Lambda_c^+ \to p\pi^+\pi^-$, pK^+K^-, $p\eta$, and $p\pi^0$ [96, 97];
- observation of modes with a neutron in the final state, $\Lambda_c^+ \to nK_S^0\pi^+$ [98] and $\Sigma^-\pi^+\pi^+\pi^0$ [99].
- measurements of the absolute BFs of $\Lambda_c^+ \to \Xi^0K^+$, $\Xi^{*0}K^+$ [100], $\Sigma^+\eta$ and $\Sigma^+\eta'$ [101].
- studies of inclusive ΛX decay [102] and inclusive electronic decay [103].

Although much progress has been made since 2014,

the knowledge of Λ_c^+ decays is still very limited in comparison with charmed mesons. Firstly, only a single SL decay mode $\Lambda\ell^+\nu_\ell$ has been observed. Secondly, the DCS modes have not been systematically studied. Thirdly, the known exclusive decays of Λ_c^+ account for only about 60% of the total BF. Many channels are still unobserved. In particular, information about the decays that involve a neutron is minimal, considering that such decays should account for nearly half of the Λ_c^+ decay rate. A thorough investigation of these channels requires a much larger data set taken in the low-multiplicity environment and obtained at the threshold in e^+e^- collisions.

5.3.2 Prospects in Λ_c^+ physics

The approved energy upgrade project of BEPCII will increase the collision energy to 4.9 GeV. Together with the commissioning of the top-up mode, we will be able to take 5 fb^{-1} of data at 4.64 GeV, which corresponds to the energy of the expected peak of the cross-section for $\Lambda_c^+\bar{\Lambda}_c^-$ pairs. This data set will have more than 16 times the statistics of the current BESIII data set at 4.6 GeV, and will allow to improve the precision of Λ_c^+ decay rates to a level comparable to the charmed mesons, as listed in Table 5.5. In addition, it will provide an opportunity to study many unexplored physics observables related to Λ_c^+ decays. In particular, this advance will boost our understanding of the non-perturbative effects in the charmed baryon sector.

A larger data set will guarantee the first absolute measurement of the form factors in the SL decay $\Lambda_c^+ \to \Lambda\ell^+\nu_\ell$, which is crucial for calibrating the various theoretical calculations. Besides $\Lambda_c^+ \to \Lambda\ell^+\nu_\ell$, more SL modes can be identified, as listed in Table 5.6. According to the predicted rates in model calculations, the new CF modes $\Lambda_c^+ \to pK^-e^+\nu_e$ and $\Sigma\pi e^+\nu_e$ will be established for the first time with the double-tag technique. For the SCS mode, studying $\Lambda_c^+ \to ne^+\nu_e$ will be challenging due to the presence of two missing particles in the final state and the dominant $\Lambda_c^+ \to \Lambda e^+\nu_e$ background. However, we still have the opportunity to identify the decay by taking advantage of the well constrained kinematics, the clean reaction environment and the neutron shower information inside the electromagnetic calorimeter. Moreover, another SCS mode $\Lambda_c^+ \to p\pi^-e^+\nu_e$ can be searched for in the enlarged data set.

The hadronic weak decay of a single charmed baryon is expected to violate parity conservation. For instance, the two-body decay $\Lambda_c^+ \to \Lambda\pi^+$ proceeds via a W-interaction, $c \to W^+ + s$, in which parity is not conserved. Λ and π^+ particles are allowed to be in S- or P-wave states. The effects of parity violation are determined from the polarization of the charmed baryons, which is characterized by the angular distribution of Λ in the Λ_c^+ rest frame, and has the form $\frac{\mathrm{d}N}{\mathrm{d}\cos\theta_\Lambda} \propto 1 + \alpha_{\Lambda\pi}\cos\theta_\Lambda$, where $\alpha_{\Lambda\pi}$ is the decay asymmetry parameter [110, 111]. In addition, the decay asymmetry allows discrimination between different theoretical models, as listed in Ref. [111]. Some decay asymmetry parameters, *e.g.* $\alpha_{\Lambda\pi}$ for $\Lambda_c^+ \to \Lambda\pi^+$, $\alpha_{\Sigma^+\pi^0}$ for $\Lambda_c^+ \to \Sigma^+\pi^0$, and $\alpha_{\Xi^-\pi^+}$ for $\Xi_c^0 \to \Xi^-\pi^+$, have been studied previously, but with limited precision [2]. Therefore, improved measurements are desirable, as they will shed light on the decay mechanism and allow searches for CP asymmetries in the charmed baryon sector. In addition,

Table 5.5. Measured or projected precision of charmed hadrons, with the relative precision in parenthesis. For the future Λ_c^+ precision, it is estimated for 5 fb^{-1} of data at $\sqrt{s}$ = 4.64 GeV.

	Leading hadronic decay	Typical two-body decay	Leading SL decay
Λ_c^+	$\mathcal{B}(K^-p\pi^+)$ =	$\mathcal{B}(K_S^0p)$ =	$\mathcal{B}(\Lambda e^+\nu_e)$ =
	2014: (5.0±1.3)% (26%)	2014: (1.2±0.3)% (26%)	2014: (2.1±0.6)% (29%)
	2017(w/ BESIII): (6.35±0.33)% (5.2%)	BESIII: (1.52±0.08)% (5.6%)	BESIII: (3.63±0.43)% (12%)
	5 fb^{-1}: $\frac{\delta\mathcal{B}}{\mathcal{B}}$ <2%	5 fb^{-1}: $\frac{\delta\mathcal{B}}{\mathcal{B}}$ <2%	5 fb^{-1}: $\frac{\delta\mathcal{B}}{\mathcal{B}}$ ~3.3%
D^0	$\mathcal{B}(K^-\pi^+)$ =(3.89±0.04)% (1.0%)	$\mathcal{B}(K_S^0\pi^0)$ =(1.19±0.04)% (3.4%)	$\mathcal{B}(K^-e^+\nu_e)$ =(3.53±0.03)% (0.8%)
D^+	$\mathcal{B}(K^-\pi^+\pi^+)$ =(8.98±0.28)% (3.1%)	$\mathcal{B}(K_S^0\pi^+)$ =(1.47±0.08)% (5.4%)	$\mathcal{B}(K_S^0e^+\nu_e)$ =(4.41±0.07)% (1.5%)
D_s^+	$\mathcal{B}(K^-K^+\pi^+)$ =(5.45±0.17)% (3.8%)	$\mathcal{B}(K_S^0K^+)$ =(1.40±0.05)% (3.6%)	$\mathcal{B}(\phi e^+\nu_e)$ =(2.39±0.23)% (9.6%)

Table 5.6. Expected rates of the SL modes and estimated precision for 5 fb^{-1} of data at $\sqrt{s}$ = 4.64 GeV.

Mode	Expected rate (%)	Relative uncertainty (%)
$\Lambda_c^+ \to \Lambda\ell^+\nu_\ell$	3.6 [95,104]	3.3
$\Lambda_c^+ \to \Lambda^*\ell^+\nu_\ell$	0.7 [105,106]	10
$\Lambda_c^+ \to NKe^+\nu_e$	0.7 [105]	10
$\Lambda_c^+ \to \Sigma\pi\ell^+\nu_\ell$	0.7 [105]	10
$\Lambda_c^+ \to ne^+\nu_e$	0.2 [104,107,108]; 0.4 [109]	17

other decay asymmetry parameters in $\Lambda_c^+ \to \Sigma^0\pi^+$, $p\bar{K}^0$, and $\Xi_c^0 \to \Xi^-\pi^+$ can be accessed. Based on the sensitivity obtained with the current BESIII data set, a 16× larger data set would result in an approximate precision of 4% and 6% for measuring $\alpha_{\Lambda\pi^+}$ and $\alpha_{\Sigma^0\pi^+}$, respectively.

The weak radiative decay $\Lambda_c^+ \to \gamma\Sigma^+$ is predicted to have a BF of 10^{-5} to 10^{-4}. The new data set will push the experimental sensitivity to 10^{-5}, which provides an opportunity to measure this process for the first time. Moreover, the SCS radiative decay $\Lambda_c^+ \to \gamma p$ can be searched for.

We will have better sensitivity to explore the SCS modes, which at present have limited precision or have not been studied before. Meanwhile, more modes with a neutron or Σ^- in the final state can be accessed. This will significantly enhance our knowledge of the less well known decays, and will allow improved studies of $\Lambda_c^+ \to p\pi^0$, and first searches for $n\pi^+$ and nK^+.

Thorough analysis of the involved intermediate states can be carried out in the decays to the multi-body final states. This can be achieved by implementing amplitude analyses of the copious hadronic decays, such as $\Lambda_c^+ \to pK^-\pi^+, pK_S^0\pi^0, pK_S^0\pi^+\pi^-, \Lambda\pi^+\pi^0, \Lambda\pi^+\pi^+\pi^-, pK^-\pi^+\pi^0$, and $\Sigma^+\pi^+\pi^-$. From these analyses, additional two-body decay patterns of $\Lambda_c^+ \to B^{\frac{3}{2}}P$ and $B^{\frac{1}{2}}V$ can be extracted. Here, $B^{\frac{3}{2}}$ and $B^{\frac{1}{2}}$ denote baryon states with isospin $\frac{3}{2}$ and $\frac{1}{2}$, respectively. Also, Λ_c^+ decays act as an isospin filter, and provide a good opportunity to study the light hadron spectroscopy, such as the study of Λ^* and scalar meson states via the weak decays $\Lambda_c^+ \to \Sigma\pi\pi$, $NK\pi$, and $\Lambda\pi^+\eta$ [112-115].

5.3.3 Σ_c and Ξ_c physics

Above 4.88 GeV, the Σ_c baryon can be produced via $e^+e^- \to \Sigma_c\bar{\Lambda}_c^-\pi$. The width of $\Sigma_c^{0(++)}$ has been determined by Belle, while only an upper limit on the width of Σ_c^+ was determined. BESIII will provide an improved width measurement of Σ_c^+ via the dominant decay $\Sigma_c^+ \to \Lambda_c^+\pi^0$, which is useful to test the overall understanding of the decay dynamics. Moreover, BESIII can also search for the decay $\Sigma_c \to \Lambda_c^+\gamma$, which is theoretically expected to occur with a BF of approximately 1%. Above 4.74 GeV, the sum of the Λ_c^+ and Σ_c^+ masses, the isospin-violating EM reaction $e^+e^- \to \Sigma_c^+\bar{\Lambda}_c^-$ occurs. It is interesting to measure its cross-section near the threshold, whose ratio to the cross-section of $e^+e^- \to \Lambda_c^+\bar{\Lambda}_c^-$ will provide insight into the vacuum production of $c\bar{c}$ and $s\bar{s}$ pairs. In addition, it is possible to study the Σ_c baryon pair production at 4.91 GeV via $e^+e^- \to \Sigma_c\bar{\Sigma}_c$. Relative to the production rate of $e^+e^- \to \Lambda_c^+\bar{\Lambda}_c^-$, one can explore the mechanism of generating 'good' spin-0 and 'bad' spin-1 u-d diquarks inside Λ_c and Σ_c, respectively, near the threshold.

For the charmed baryons Ξ_c^0 and Ξ_c^+, the relative uncertainties of the measured BFs are large, and most of the decays have not yet been studied experimentally [2]. Belle performed the first measurements of the absolute BFs of the Ξ_c^0 and Ξ_c^+ decays in $\bar{B}^{-(0)} \to \bar{\Lambda}_c^-\Xi_c^{0(+)}$ [116, 117]. They are given as:

$$\begin{aligned}
&\mathcal{B}(\Xi_c^0 \to \Xi^-\pi^+) = (1.80 \pm 0.50 \pm 0.14)\%,\\
&\mathcal{B}(\Xi_c^0 \to \Lambda K^-\pi^+) = (1.17 \pm 0.37 \pm 0.09)\%,\\
&\mathcal{B}(\Xi_c^0 \to pK^-K^-\pi^+) = (0.58 \pm 0.23 \pm 0.05)\%,\\
&\mathcal{B}(\Xi_c^+ \to \Xi^-\pi^+\pi^+) = (2.86 \pm 1.21 \pm 0.38)\%,\\
&\mathcal{B}(\Xi_c^+ \to pK^-\pi^+) = (0.45 \pm 0.21 \pm 0.07)\%.
\end{aligned}$$

So far, their statistical uncertainties are about 30%~40% and the systematic uncertainties are about 10%. The statistical uncertainties can be suppressed to about 5% at Belle II with a 50 times larger data set by 2025. However, there is less potential for improving further the systematic uncertainties. Hence, the overall uncertainties will be below 10%.

If the cms energy of BEPCII is increased above 4.95 GeV, which is just above the mass of Ξ_c pairs, we will be able to perform absolute BF measurements of Ξ_c decays in the same fashion as is done for Λ_c^+. If we assume that the production cross-sections of $e^+e^- \to \Lambda_c^+\bar{\Lambda}_c^-$ and $\Xi_c\bar{\Xi}_c$ are similar near the mass threshold, the precision at BESIII is expected to be competitive or superior to the Belle II result, depending on the modes. The absolute BF measurements with high precision would be extremely useful as input for studying the b-baryon decays [53]. Furthermore, many of the missing hadronic and SL decays of Ξ_c could be studied for the first time. The data set taken at this energy could also be used to study the triplet states Σ_c^{++}, Σ_c^+, and Σ_c^0.

5.3.4 The EM structure of charmed baryons

As discussed in Chapter 4 of this White Paper, the BESIII experiment is perfectly suited for precision studies of the hyperon structure. The upgrades of BEPCII open new avenues to study single-charm hyperons. In this section, we discuss these possibilities and the prospects of performing tests of CP violation in hyperon decays.

Let us consider a hyperon-antihyperon pair $Y\bar{Y}$, where Y and $\bar{Y}$ have spin 1/2, produced in e^+e^- annihilation. The differential cross-section can be parametrized in terms of the electric and magnetic form factors, $G_E(q^2)$ and $G_M(q^2)$, which are related to the helicity flip and non-flip amplitudes, respectively. They are linear combinations constructed from the Dirac and Fermi unconstrained form factors F_1 and F_2: $G_E = F_1 + F_2$ and $G_E = F_1 + \tau F_2$, where $\tau = \frac{q^2}{4m_Y^2}$, and m_Y is the Y mass. The differential cross-section can be expressed as

$$\frac{\mathrm{d}\sigma}{\mathrm{d}\cos\theta} \propto 1 + \eta\cos^2\theta\,, \tag{5.8}$$

where θ is the polar angle of Λ_c^+ in the e^+e^- center-of-msss system, $-1 \leqslant \eta \leqslant 1$ and is related to the form-factor ratio $R = |G_E/G_M|$ in the following way

$$R = \sqrt{\tau}\sqrt{\frac{1-\eta}{1+\eta}}. \quad (5.9)$$

The form factors are complex in the time-like region, *i.e.* they can be written as $G_M(q^2) = |G_M(q^2)|e^{i\Phi_M}$ and $G_E(q^2) = |G_E(q^2)|e^{i\Phi_E}$, from which the relative phase can be defined as $\Delta\Phi = \Phi_E - \Phi_M$. This non-trivial relative phase has an impact on spin projections and spin correlations of the produced hyperons, and could be detected experimentally via the weak decay of hyperons.

The challenge in the studies of charmed baryons is the lack of prominent decay modes with large BFs. All two-body decay channels have a BF of (1-2)% [2]. Consequently, even a large data set yields only a few hundred reconstructed events per channel. In particular, only the single-tag method can be applied to produce an adequate sample.

The most straightforward mode to study Λ_c^+ polarization is the $\Lambda_c^+ \to K_S^0 p$ channel. The formalism outlined in Ref. [118] can then be used, adapted for single-tag $\Lambda_c^+ \to K_S^0 p$ measurements by integrating over the antiproton angles:

$$\mathcal{W}(\boldsymbol{\xi}) = 4\pi(1 + \eta\cos^2\theta + \alpha_{K_S^0 p}\sqrt{1-\eta^2}\sin(\Delta\Phi) (\sin\theta\cos\theta\sin\theta_1\sin\phi_1)), \quad (5.10)$$

where $\boldsymbol{\xi}$ is a vector of the involved parameters and variables, θ is the polar angle of Λ_c^+ in the e^+e^- center-of-mssss system, θ_1 (ϕ_1) is the solid angle in the Λ_c^+ ($\bar{\Lambda}_c^-$) helicity system, and $\alpha_{K_S^0 p}$ is the decay-asymmetry parameter. The disadvantage is that the decay asymmetry $\alpha_{K_S^0 p}$ is not known, so only the product $\alpha_{K_S^0 p}\sin(\Delta\Phi)$ can be determined. However, if one studies sequential decays, such as $\Lambda_c^+ \to \Lambda\pi^+, \Lambda \to p\pi^-$, by using the formalism outlined in Ref. [119], the asymmetry parameters β and γ are also accessible.

A measurement [120] of $\Delta\Phi$ has been made using a data set collected by the BESIII detector at $\sqrt{s} = 4.6$ GeV (corresponding to $\tau = 1.012$) with an integrated luminosity of $\mathcal{L}_{\rm int} = 0.6\,{\rm fb}^{-1}$. The value reported is $\sin(\Delta\Phi) = -0.28 \pm 0.13 \pm 0.03$. It is expected that the phase initially increases with an increase of $\sqrt{s}$, but the most important improvement should come from larger statistics. Therefore, this motivates a high statistics study of the process $e^+e^- \to \Lambda_c^+\bar{\Lambda}_c^-$ at the energy with the highest yield of Λ_c. In particular, the reaction has a maximum cross-section at about 4.64 GeV, as expected from the Belle data. This energy corresponds to a kinematic factor of $\tau = 1.034$.

Another interesting study of the Λ_c^+ form factor would be with a kinematic factor of approximately $\tau = 1.058$, which is where the BESIII measurement of Λ was made and yielded the result $\Delta\Phi = (37 \pm 12 \pm 7)^\circ$. Such a measurement would enable the first complete extraction of the EM form factor of a charmed hyperon, thus shedding light on the role of strangeness and charm in the hadron structure, and would provide a systematic comparison with the strange partner.

Several three-body decay channels have BFs five to seven times larger than the two-body decays [2]. In Ref. [121], it was found that for an integrated luminosity of 567 pb^{-1}, the number of tagged $\Lambda_c^+ \to pK^-\pi^+$ was around 3000, and similarly for the charge-conjugate $\bar{\Lambda}_c^- \to \bar{p}K^+\pi^-$. It may therefore be a better strategy to construct an angular observable for a three-body decay that is sensitive to the EM phase $\Delta\Phi$ [118, 122, 123]. With the data set proposed, such strategies can be pursued to give complementary measurements of $\Delta\Phi$.

Tests of CP violation can be made for two-body decays of charm hyperons as for strange hyperons. Suitable observables for CP tests have been derived, *e.g.* in Ref. [124]. These asymmetries have in common the asymmetry parameters measured separately for Λ_c^+ and $\bar{\Lambda}_c^-$, which can be done with the proposed large data set above the production threshold.

5.4 Summary

In this chapter, we have presented the physics studies that are possible with data sets corresponding to integrated luminosities of 20 fb^{-1} at $\sqrt{s} = 3.773$ GeV, 6 fb^{-1} at $\sqrt{s} = 4.178$ GeV, and 5 fb^{-1} at $\sqrt{s} = 4.64$ GeV. These cms energies correspond to the optimal values to accumulate samples of $D\bar{D}$, $D_s^{*+}D_s^-$, and $\Lambda_c^+\bar{\Lambda}_c^-$ events at threshold, respectively. Such samples allow a double-tag technique to be employed, as the full event can be reconstructed even if it contains one undetected particle such as a ν or K_L^0 meson. These samples provide a unique environment to measure the absolute BFs of charmed hadrons to leptonic, SL and hadronic final states, with very low levels of background. Such measurements provide rigorous tests of QCD, CKM unitarity and LFU that complement similar studies of beauty hadrons. Furthermore, 20 fb^{-1} of data of coherent $\psi(3770) \to D^0\bar{D}^0$ events allow measurements of the strong-phase difference between D^0 and $\bar{D}^0$ that is an essential input for determining the UT angle γ in a model-independent way from B decays at LHCb and its upgrades, as well as at Belle II. The strong-phase difference can only be determined to the required level of precision using such a data set. In addition, the strong-phase measurement is an important ingredient of the model-independent measurements of $D^0\bar{D}^0$ mixing, and of searches for indirect CP violation in D^0 decay. Finally, additional studies of charmed baryons can be performed related to their electromagnetic form factors. If the BEPCII cms energy is upgraded, studies can also be made of the absolute BFs of Σ_c and Ξ_c. Table 5.7 presents the precision prospects of some key measurements of $D^{0(+)}$, D_s^+, and Λ_c^+ based on the proposed data set, and a comparison with Belle II.

Table 5.7. Prospects of some key measurements at the future BESIII, with a comparison with Belle II. 'NA' means 'not available' and '–' means 'no estimation'.

Observable	Measurement	BESIII	Belle II
$\mathcal{B}(D^+ \to \ell^+\nu)$	$f_{D^+}\lvert V_{cd}\rvert$	1.1%	1.4%
$\mathcal{B}(D_s^+ \to \ell^+\nu)$	$f_{D_s^+}\lvert V_{cs}\rvert$	1.0%	1.0%
$\mathrm{d}\Gamma(D^{0(+)} \to \bar{K}\ell^+\nu)/\mathrm{d}q^2$	$f_+^K(0)\lvert V_{cs}\rvert$	0.5%	0.9%
$\mathrm{d}\Gamma(D^{0(+)} \to \pi\ell^+\nu)/\mathrm{d}q^2$	$f_+^\pi(0)\lvert V_{cd}\rvert$	0.6%	1.0%
$\mathrm{d}\Gamma(D_s^+ \to \eta\ell^+\nu)/\mathrm{d}q^2$	$f_+^\eta(0)\lvert V_{cs}\rvert$	0.8%	–
Strong phases in $D^0\bar{D}^0$	Constraint on γ	$< 0.4^\circ$	N/A
$\Lambda_c^+ \to pK^-\pi^+$	$\mathcal{B}$	2%	3%
$\Lambda_c^+ \to \Lambda\ell^+\nu$	$\mathcal{B}$	3.3%	–

References

1 D. M. Asnesr *et al*., Int. J. Mod. Phys. A, **24**: S1 (2009)
2 M. Tanabashi *et al*. (Particle Data Group), Phys. Rev. D, **98**: 030001 (2018)
3 R. Aaij *et al*. (LHCb Collaboration), Phys. Rev. Lett., **121**: 092003 (2018)
4 M. Ablikim *et al*. (BESIII Collaboration), Phys. Rev. D, **89**: 051104 (2014)
5 M. Ablikim *et al*. (BESIII Collaboration), Phys. Rev. Lett., **123**: 211802 (2019)
6 M. Ablikim *et al*. (BESIII Collaboration), Phys. Rev. Lett., **122**: 071802 (2019)
7 J. P. Alexander *et al*. (CLEO Collaboration), Phys. Rev. D, **79**: 052001 (2009)
8 P. U. E. Onyisi *et al*. (CLEO Collaboration), Phys. Rev. D, **79**: 052002 (2009)
9 P. Naik *et al*. (CLEO Collaboration), Phys. Rev. D, **80**: 112004 (2009)
10 P. del Amo Sanchez *et al*. (BaBar Collaboration), Phys. Rev. D, **82**: 091103 (2010)
11 A. Zupanc *et al*. (Belle Collaboration), JHEP, **1309**: 139 (2013)
12 A. Bazavov *et al*. (Fermilab Lattice and MILC Collaboration), Phys. Rev. D, **98**: 074512 (2018)
13 N. Carrasco *et al*. (ETM Collaboration), Phys. Rev. D, **91**: 054507 (2015)
14 J. P. Lees *et al*. (BaBar Collaboration), Phys. Rev. Lett., **109**: 101802 (2012)
15 J. P. Lees *et al*. (BaBar Collaboration), Phys. Rev. D, **88**: 072012 (2013)
16 A. Matyja *et al*. (Belle Collaboration), Phys. Rev. Lett., **99**: 191807 (2007)
17 I. Adachi *et al*. (Belle Collaboration), arXiv:0910.4301 [hep-ex][hep-ex]
18 A. Bozek *et al*. (Belle Collaboration), Phys. Rev. D, **82**: 072005 (2010)
19 R. Aaij *et al*. (LHCb Collaboration), Phys. Rev. Lett., **115**: 111803 (2015)
20 R. Aaij *et al*. (LHCb Collaboration), JHEP, **1602**: 104 (2016)
21 R. Aaij *et al*. (LHCb Collaboration), JHEP, **1509**: 179 (2015)
22 R. Aaij *et al*. (LHCb Collaboration), Phys. Rev. Lett., **113**: 151601 (2014)
23 S. Wehle *et al*. (Belle Collaboration), Phys. Rev. Lett., **113**: 111801 (2017)
24 S. Fajfer, I. Nisandzic, and U. Rojec, Phys. Rev. D, **91**: 094009 (2015)
25 M. A. Ivanov, J. G. Krner, J. N. Pandya *et al*., Front. Phys. (Beijing), **14**: 64401 (2019)
26 M. Ablikim *et al*. (BESIII Collaboration), Phys. Rev. D, **92**: 072012 (2015)
27 M. Ablikim *et al*. (BESIII Collaboration), Phys. Rev. D, **96**: 012002 (2016)
28 M. Ablikim *et al*. (BESIII Collaboration), Phys. Rev. Lett., **122**: 011804 (2019)
29 M. Ablikim *et al*. (BESIII Collaboration), Phys. Rev. D, **97**: 092009 (2018)
30 M. Ablikim *et al*. (BESIII Collaboration), Phys. Rev. D, **94**: 032001 (2016)
31 M. Ablikim *et al*. (BESIII Collaboration), Phys. Rev. Lett., **122**: 062001 (2019)
32 M. Ablikim *et al*. (BESIII Collaboration), Phys. Rev. D, **92**: 071101 (2015)
33 M. Ablikim *et al*. (BESIII Collaboration), Phys. Rev. Lett., **122**: 061801 (2019)
34 M. Ablikim *et al*. (BESIII Collaboration), Phys. Rev. Lett., **122**: 121801 (2019)
35 M. Artuso *et al*. (Belle Collaboration), Phys. Rev. Lett., **99**: 191801 (2007)
36 M. Ablikim *et al*. (BESIII Collaboration), Phys. Rev. Lett., **121**: 081802 (2018)
37 H. Na *et al*. (HPQCD Collaboration), Phys. Rev. D, **82**: 114506 (2010)
38 H. Na *et al*. (HPQCD Collaboration), Phys. Rev. D, **84**: 114505 (2011)
39 Aida X. EI-Khadra, talk presented at Beauty2014

40 L. Riggio, G. Salerno, and S. Simula, Eur. Phys. J. C, **78**: 501 (2018)
41 M. Ablikim *et al*. (BESIII Collaboration), Phys. Rev. Lett., **121**: 171803 (2018)
42 H. Y. Cheng and X. W. Kang, Eur. Phys. J. C, **77**: 587 (2017) [Erratum: Eur. Phys. J. C 77, 863 (2017)]
43 B. Aubert *et al*. (BaBar Collaboration), Phys. Rev. D, **76**: 052005 (2007)
44 J. P. Lees *et al*. (BaBar Collaboration), Phys. Rev. D, **91**: 052022 (2015)
45 L. Widhalm *et al*. (Belle Collaboration), Phys. Rev. Lett., **97**: 061804 (2006)
46 Z. Z. Xing, Phys. Rev. D, **55**: 196 (1997)
47 Y. Amhis *et al*. (HFLAV Collaboration), Eur. Phys. J. C, **77**: 895 (2017)
48 LHCb Collaboration, Technical Report, LHCb-CONF-2018-002 (2018)
49 J. Brod and J. Zupan, JHEP, **1401**: 051 (2014)
50 M. Gronau and D. London, Phys. Lett. B, **253**: 483 (1991); M. Gronau and D. Wyler, Phys. Lett. B, **265**: 172 (1991)
51 D. Atwood, I. Dunietz, and A. Soni, Phys. Rev. Lett, **78**: 3257 (1997); Phys. Rev. D, **63**: 036005 (2001)
52 A. Giri, Y. Grossman, A. Soffer *et al*., Phys. Rev. D, **68**: (2003)
53 S. S. Malde, Technical Report, LHCb-PUB-2016-025 (2016)
54 E. Kou *et al.* (Belle II Collaboration), PTEP 2019, 123C01 (2019)
55 J. Libby *et al*. (CLEO collaboration), Phys. Rev. D, **82**: 112006 (2010)
56 T. Evans *et al.*, Phys. Lett. B, **757**: 520 (2016); Erratum: [Phys. Lett. B, **765**: 402 (2017)] (2017)]
57 J. Insler *et al*. (CLEO Collaboration), Phys. Rev. D, **85**: 092016 (2012)
58 S. Malde *et al*., Phys. Lett. B, **747**: 9 (2015)
59 D. M. Asner *et al*. (CLEO Collaboration), Phys. Rev. D, **86**: 112001 (2012)
60 P. K. Resmi, J. Libby, S. Malde *et al*., JHEP, **1801**: 082 (2018)
61 R. Aaij *et al*. (LHCb Collaboration), Phys. Rev. Lett., **116**: 241801 (2016)
62 M. Ablikim *et al*. (BESIII Collaboration), Phys. Lett. B, **734**: 227 (2014)
63 M. Ablikim *et al.* (BESIII Collaboration), arXiv:2003.00091 [hep-ex][hep-ex]
64 R. Aaij *et al.* (LHCb Collaboration), Technical Report, CERN-LHCC-2017-003 (2017)17)
65 D. Atwood, I. Dunietz, and A. Soni, Phys. Rev. D, **63**: 036005 (2001)
66 M. Nayak *et al*., Phys. Lett. B, **740**: 1 (2015)
67 A. Giri, Y. Grossman, A. Soffer *et al*., Phys. Rev. D, **68**: 054018 (2003)
68 M. Artuso *et al*. (CLEO Collaboration), Phys. Rev. D, **85**: 122002 (2012)
69 M. Gronau, Y. Grossman, and J. L. Rosner, Phys. Lett. B, **508**: 37 (2001)
70 C. Thomas and G. Wilkinson, JHEP, **1210**: 185 (2012)
71 S. Malde, C. Thomas, and G. Wilkinson, Phys. Rev. D, **91**: 094032 (2015)
72 S. Malde and G. Wilkinson, Phys. Lett. B, **701**: 353 (2011)
73 R. Aaij *et al*. (LHCb Collaboration), JHEP, **1604**: 033 (2016)
74 V. Vorobiev *et al*. (Belle Collaboration), Phys. Rev. D, **94**: 052004 (2016)
75 L. L. Chau and W. Y. Keung, Phys. Rev. Lett., **53**: 1802 (1984)
76 L. Wolfenstein, Phys. Rev. Lett., **51**: 1945 (1983)
77 J. Charles *et al*. (CKMfitter Group), Eur. Phys. J. C, **41**: 1 (2005)
78 A. J. Buras, M. E. Lautenbacher, and G. Ostermaier, Phys. Rev. D, **50**: 3433 (1994)
79 I. Bediaga *et al.* (LHCb Collaboration), arXiv:1808.08865 [hep-ex][hep-ex]
80 M. Ablikim *et al*. (BESIII Collaboration), Phys. Lett. B, **744**: 339 (2015)
81 D. Atwood and A. A. Petrov, Phys. Rev. D, **71**: 054032 (2005)
82 D. M. Asner and W. M. Sun, Phys. Rev. D, **73**: 034024 (2006); [Erratum: Phys. Rev. D, **77**: 019901 (2008)]
83 I. I. Bigi and A. Paul, JHEP, **03**: 021 (2012)
84 V. A. Kostelecky, Phys. Rev. D, **64**: 076001 (2001)
85 S. Barlag *et al*. (ACCMOR Collaboration), Z. Phys. C, **55**: 383 (1992)
86 Q. He *et al*. (CLEO Collaboration), Phys. Rev. Lett., **100**: 091801 (2008)
87 Wenjing Zheng (for the BESIII Collaboration), PoS CHARM2016,075 (2016)
88 Fusheng Yu, presented at 2016 workshop of BESIII Charm Hadron physics, Dec. 27-28, 2016, Beijing, China
89 T. Gershon, J. Libby, and G. Wilkinson, Phys. Lett. B, **750**: 338 (2015)
90 E. G. Cazzoli *et al*., Phys. Rev. Lett., **34**: 1125 (1975)
91 A. Zupanc *et al*. (Belle Collaboration), Phys. Rev. Lett., **113**: 042002 (2014)
92 M. Ablikm *et al*. (BESIII Collaboration), Phys. Rev. Lett., **116**: 052001 (2016)
93 M. Ablikm *et al*. (BESIII Collaboration), Phys. Rev. Lett., **115**: 221805 (2015)
94 M. Ablikim *et al*. (BESIII Collaboration), Phys. Lett. B, **767**: 42 (2017)
95 S. Meinel, Phys. Rev. Lett., **118**: 082001 (2017)
96 M. Ablikm *et al*. (BESIII Collaboration), Phys. Rev. Lett., **117**: 232002 (2016)
97 M. Ablikim *et al*. (BESIII Collaboration), Phys. Rev. D, **95**: 111102 (2017)
98 M. Ablikim *et al*. (BESIII Collaboration), Phys. Rev. Lett., **118**: 112001 (2017)
99 M. Ablikim *et al*. (BESIII Collaboration), Phys. Lett. B, **772**: 388 (2017)
100 M. Ablikim *et al*. (BESIII Collaboration), Phys. Lett. B, **783**:

200 (2018)
101 M. Ablikim *et al*. (BESIII Collaboration), Chin. Phys. C, **43**: 083002 (2019)
102 M. Ablikim *et al*. (BESIII Collaboration), Phys. Rev. Lett., **121**: 062003 (2018)
103 M. Ablikim *et al*. (BESIII Collaboration), Phys. Rev. Lett., **121**: 251801 (2018)
104 R. N. Faustov and V. O. Galkina, Eur. Phys. J. C, **76**: 628 (2016)
105 M. Pervin *et al*., Phys. Rev. C, **72**: 035201 (2005)
106 N. Ikeno and E. Oset, Phys. Rev. D, **93**: 014021 (2016)
107 T. Gutsche *et al*., Phys. Rev. D, **90**: 114033 (2014)
108 Cai-Dian Lü, Wei Wang, and Fu-Sheng Yu, Phys. Rev. D, **93**: 056008 (2016)
109 S. Meinel, Phys. Rev. D, **97**: 034511 (2018)
110 D. Wang, R. G. Ping, L. Li *et al*., Chin. Phys. C, **41**: 023106 (2017)
111 H. Y. Cheng, Front. Phys. (Beijing), **10**: 101406 (2015)
112 T. Hyodo and M. Oka, Phys. Rev. C, **84**: 035201 (2011)
113 K. Miyahara, T. Hyodo, and E. Oset, Phys. Rev. C, **92**: 055204 (2015)
114 J. J. Xie and L. S. Geng, Eur. Phys. J. C, **76**: 496 (2016)
115 M. Ablikim *et al*. (BESIII Collaboration), Phys. Rev. D, **99**: 032010 (2019)
116 Y. B. Li *et al*. (Belle Collaboration), Phys. Rev. Lett., **122**: 082001 (2019)
117 Y. B. Li *et al*. (Belle Collaboration), Phys. Rev. D, **100**: 031101 (2019)
118 G. Fäldt and A. Kupsc, Phys. Lett. B, **772**: 16 (2017)
119 G. Fäldt, Phys. Rev. D, **97**: 053002 (2018)
120 M. Ablikim *et al*. (BESIII Collaboration), Phys. Rev. D, **100**: 072004 (2019), arXiv:1905.04707
121 M. Ablikim *et al*. (BESIII Collaboration), Phys. Rev. Lett., **120**: 132001 (2018)
122 S. Leupold, private communication (2017)
123 S. Bianco *et al*., Nuovo Cim., **26N7**: 1 (2003)
124 N. Hamann *et al*., Technical Report, CERN-SPSLC-92-19 (1992)p;(1992)

Chapter 6

Exotic Decays and New Physics

6.1 Introduction

With the discovery of the Higgs boson in 2012, the Standard Model (SM) has been firmly established. However, there are many compelling reasons to believe that SM is not the ultimate theory, and the search for physics beyond SM is well motivated.

There is strong synergy between direct and indirect searches for New Physics (NP). To identify possible NP paradigms, results from both low energy electron-positron colliders and high energy hadron colliders are needed [1]. Studies performed at electron-positron collider experiments such as BESIII may indicate hints of NP that could be directly probed at an energy frontier experiment, or even make some discoveries directly.

With high luminosity, clean collision environment, and excellent detector performance, the BESIII experiment has a great potential to perform searches for NP. BESIII has already published some NP search results based on the existing data sets. There are still some unique opportunities worth exploring. In general, NP searches at BESIII could be classified into three broad categories, which are discussed in this chapter:

1. Processes that are *allowed* in SM.

NP searches of this type include testing the relations among SM-allowed processes that are known to hold only in SM, but not necessarily in models beyond SM. Some examples have been discussed in depth in previous chapters, such as testing the CKM triangle relations, precision measurement of $D_q \to \ell\bar{\nu}$ ($q = d, s$; $\ell = e, \mu, \tau$), precision QCD tests, etc. We focus on some additional topics, such as weak decays of charmonium states in Sec. 6.2.1, and rare radiative and rare leptonic decays of D mesons in Sec. 6.2.2.

2. Processes that are *forbidden* in SM *at tree level*.

Processes that involve flavor-changing neutral current (FCNC) interactions, which change charm quantum number by one or two units, do not occur in SM at tree level. However, these transitions can happen in SM at loop levels, which makes them rare. Such processes can receive NP contributions from the tree-level interactions mediated by new interactions and from the loop corrections with NP particles. Inclusive and exclusive transitions mediated by $c \to u\gamma$ or $c \to u\ell\bar{\ell}$ are discussed in Sec. 6.2.2. Searches for violation of CP and other symmetries in baryon decays and in $D^0\bar{D}^0$ mixing are discussed in Sec. 6.3. Charged lepton flavor violation decays are discussed in Sec. 6.4.

3. Processes that are *forbidden* in SM.

Some processes, while allowed by space-time symmetries, are forbidden in SM. Even if allowed by NP, searching for these signatures requires high statistics. Their observation, however, would constitute a high-impact discovery, as it would unambiguously point towards physics beyond SM. Examples include searches for the baryon number-violating transitions, discussed in Sec. 6.3.2 and Sec. 6.3.3, and the lepton number violating decays, covered in Sec. 6.4.4. Many well-motivated NP models predict the existence of light, weakly-interacting particles. Since such light particles are not part of the SM particle spectrum, the corresponding processes do not occur in SM. Such processes, which involve invisible signatures, are discused in Sec. 6.5. Some further searches at the off-resonance energies, where the electron and positron are not tuned to the s-channel resonance production of charmonium states, are discussed in Sec. 6.6.

With the accumulation of large data sets and possible increase of luminosity and cms energy, as well as an ever-improving understanding of the detector performance, BESIII will have a great potential for NP searches in the coming years.

6.2 Rare decays of charmonia and charmed hadrons

Experiments at the energy frontier may be able to probe NP via direct production of new particles. The new degrees of freedom could affect low energy observables. Experiments at the intensity frontier can probe the new virtual contributions via decays of charmonia and charmed hadrons, making them complementary to direct searches at the energy frontier.

6.2.1 Weak decays of charmonia states

The decays of $\psi(nS)$ (n=1, 2) below the open-charm threshold are dominated by the strong or electromagnetic interactions where the intermediate gluons or virtual photons are produced by $c\bar{c}$ annihilation. However, flavor-changing weak decays of these states via virtual W bosons are also possible in the SM framework. For instance, the branching fractions of J/ψ inclusive weak decays are estimated to be of the order of 10^{-10} [2]. As mentioned in Refs. [3-6], the branching fractions of $J/\psi \to D(\bar{D})X$ (with X denoting any hadron) can be enhanced by new interactions. Several NP models, such as the top-color model, the minimal supersymmetric standard model (MSSM) with R-parity violation and the general two-Higgs doublet model (2HDM), allow $\psi(nS)$ flavor-changing processes to occur with branching fractions

around 10^{-6} [3,4]. The observation of an anomalous production rate of $\psi(n\mathrm{S})$ weak decays would be a strong hint of NP.

With the newly accumulated 10^{10} J/ψ events, we expect to improve the branching fraction measurements of $\psi(nS)$ weak decays, including the hadronic and semi-leptonic weak decays, by almost one order of magnitude. These measurements will provide a more stringent experimental test of SM than previous searches, and hence further constrain the parameter space of NP models. These weak decays can also be searched for in the expected 3×10^9 $\psi(3686)$ events.

$\psi(nS)\to D_{(s)}P/D_{(s)}V/D^*_{(s)}V$

Several theoretical calculations of the branching fractions of two-body hadronic weak decays $J/\psi\to D_{(s)}P/D_{(s)}V/D^*_{(s)}V$, where D represents a charmed meson, and P and V are pseudoscalar and vector mesons, are summarized in the last column of Table 6.1. The charge conjugate states are implicitly included.

The BESII experiment searched for the hadronic decays $J/\psi\to D_s^-\pi^+$, $J/\psi\to D^-\pi^+$, and $J/\psi\to D^0K^0$ and set upper limits of the order of $10^{-4}\sim10^{-5}$ using a sample of 5.8×10^7 J/ψ events [11]. BESIII searched for the rare decays $J/\psi\to D_s^-\rho^+$ and $J/\psi\to D^0K^{*0}$ with a sample of 2.25×10^8 J/ψ events [12]. No signal was observed, and upper limits at the 90% C.L. were set on the branching fractions, $\mathcal{B}(J/\psi\to D_s^-\rho^+)<1.3\times10^{-5}$ and $\mathcal{B}(J/\psi\to D^0K^{*0})<2.5\times10^{-6}$. These results are several orders of magnitude above the SM predictions and can be improved with larger data sets. The expected sensitivity with a sample of 10^{10} J/ψ events are estimated in the third column of Table 6.1.

$\psi(nS)\to D_{(s)}l^+\nu/D^*_{(s)}l^+\nu$

Semi-leptonic decays of $\psi(nS)$ mesons are induced by weak transitions $c\to s$ or $c\to d$ via a virtual intermediate W boson. Theoretical calculations predict the branching fractions of $J/\psi\to D_s^{(*)}l^+\nu$ and $J/\psi\to D^{(*)}l^+\nu$ to be at the level of 10^{-9} and 10^{-10}, respectively, by using QCD sum rules [8], the covariant light-front quark model [9], and the covariant constituent quark model [13]. It is therefore interesting to search for semi-leptonic weak decays of $\psi(nS)$ states in high intensity and low background experiments.

The BESII experiment searched for several semi-leptonic weak decays of J/ψ. Using 5.8×10^7 J/ψ decay events, the upper limits at the 90% C.L. for $\mathcal{B}(J/\psi\to D_s^-e^+\nu)$ and $\mathcal{B}(J/\psi\to D^-e^+\nu)$ were found to be 3.6×10^{-5} and 1.2×10^{-5}, respectively [14]. BESIII has searched for the decay $J/\psi\to D_s^-e^+\nu/D_s^{*-}e^+\nu$ with a much higher sensitivity than previous analyses, based on a sample of 2.25×10^8 J/ψ events [15]. At the 90% C.L., the upper limits were determined to be $\mathcal{B}(J/\psi\to$

Table 6.1. Predicted branching fractions and expected sensitivities with a sample of 10^{10} J/ψ events of two-body hadronic weak decays $J/\psi\to D_{(s)}P, D_{(s)}V$ and $D^*_{(s)}V$.

	Decay type	Example	exp. sensitivity($\times10^{-6}$)	predicted $\mathcal{B}$ [7-10]($\times10^{-10}$)
$c\to s$	$D_{(s)}P$	$J/\psi\to D_s^-\pi^+$	9.9	2.00~8.74
		$J/\psi\to D^0K^0$	13.0	0.36~2.80
	$D_{(s)}V$	$J/\psi\to D_s^-\rho^+$	2.0	12.60~50.50
		$J/\psi\to D^0K^{*0}$	0.38	1.54~10.27
	$D^*_{(s)}V$	$J/\psi\to D_s^{*-}\rho^+$	1.7	52.60
$c\to d$	$D_{(s)}P$	$J/\psi\to D_s^-K^+$	9.8	0.16~0.55
		$J/\psi\to D^-\pi^+$	0.21	0.08~0.55
		$J/\psi\to D^0\eta$	0.72	0.016~0.070
		$J/\psi\to D^0\eta'$	0.25	0.003~0.004
		$J/\psi\to D^0\pi^0$	0.48	0.024~0.055
	$D_{(s)}V$	$J/\psi\to D_s^-K^{*+}$	5.4	0.82~2.79
		$J/\psi\to D^-\rho^+$	0.35	0.42~2.20
		$J/\psi\to D^0\rho^0$	0.77	0.18~0.22
		$J/\psi\to D^0\omega$	0.35	0.160.18
		$J/\psi\to D^0\phi$	0.22	0.41~0.65
	$D^*_{(s)}V$	$J/\psi\to D_s^{*-}K^{*+}$	4.5	2.6
		$J/\psi\to D^{*-}\rho^+$	0.083	2.8
		$J/\psi\to D^{*-}K^{*+}$	0.027	9.6

$D_s^- e^+\nu) < 1.3\times10^{-6}$ and $\mathcal{B}(J/\psi \to D_s^{*-} e^+\nu) < 1.8\times10^{-6}$. Both are consistent with the SM predictions, but can be improved with more data.

$\psi(nS) \to D^{(*)0} l^+ l^- / D^{(*)0}\gamma$

The rates of $c \to u$ transitions of $\psi(nS)$ are predicted to be tiny in SM [3,16]. However, some NP scenarios allow larger FCNC transition rates. For example, Ref. [3] argues that the branching fraction of $J/\psi \to DX_u$ (where X_u denotes mesons containing the u quark), which is mediated by the $c \to u$ quark transition, could be enhanced and to be of the order of $10^{-6} - 10^{-5}$. Thus, an observation of FCNC in the low-lying charmonium decays would indicate NP.

In practice, it is difficult to isolate pure $c \to u$ mediated transitions from $c \to s$ and $c \to d$ in hadronic weak decays of the type $\psi(nS) \to D^{(*)}X_u$. Instead, theoretically (relatively) clean semi-leptonic or radiative rare decays $\psi(nS) \to D^{(*)0} l^+ l^-$ and $\psi(nS) \to D^{(*)0}\gamma$ should be employed. The energy distributions of the final state photons or lepton pairs could be used as kinematic constraints to identify these decays.

6.2.2 Rare radiative and rare leptonic $D_{(s)}$ decays

The decays of D mesons that are mediated by quark-level FCNC transitions $c \to u\gamma$ (rare radiative) and $c \to u\ell\ell$ (rare leptonic and semi-leptonic) only proceed at the one loop level in SM. The absence of a super-heavy down-type quark in SM implies that Glashow-Iliopoulos-Maiani cancellation mechanism is very effective, making the charm sector of special interest for probing NP. The predicted short-distance (SD) contributions in SM of FCNC in the charm sector are well beyond the sensitivity of current experiments. Yet, theoretical estimates suggest that the rates of FCNC processes could be enhanced by long-distance (LD) effects by several orders of magnitude.

There are a number of interesting FCNC processes in the charm sector. Such examples include $D \to h(h')\ell\ell'$ and $D \to h\nu\bar{\nu}$, where h represents light hadron states and ℓ is a charged lepton. Such decays could be interesting probes of NP, especially in light of the renewed interest in lepton flavor universality (LFU) studies in B decays. While the SM interactions in general respect LFU, recent experimental observations (see, *e.g.*, [17]) show hints of LFU violation in rare semi-leptonic decays of B mesons. Theoretically, such violation could come from new lepton-flavor non-universal interactions [18], which might also be detectable in D-decays [19]. Such interactions might also induce lepton-flavor violating effects [20] (see section 6.4), although this depends on a particular model of NP.

Even though the charm production rate in e^+e^- collisions near the charm threshold is lower than at hadron colliders and B-factories, BESIII has the benefit of lower multiplicity and the ability to impose powerful kinematic constraints, which can deliver high purity final states with invisible energy or photons.

Rare radiative decays (such as $D \to \rho\gamma$) are most likely dominated by the LD SM contributions, which are quite difficult to compute [21-23]. Yet, there are opportunities to study NP effects in rare radiative transitions. These include a possibility that NP dominates the SM signal at least in portions of the available phase space [24], using particular combinations of radiative transitions [25], including CP-violating asymmetries [26,27], or by studying photon polarization patterns [28] that could be more sensitive to NP contributions.

Two-body rare decays with charged leptons

The simplest rare leptonic decays, such as $D^0 \to \ell^+\ell^-$, have a very small SM contribution (both SD and LD), and they are potentially very clean probes of NP amplitudes. In this section we concentrate on the lepton-flavor conserving decays.

Experimentally, there exist at present only upper limits on the $D^0 \to \ell^+\ell^-$ decays [29]. Theoretically, all possible NP contributions to $c \to u\ell^+\ell^-$ can be summarized in the effective Hamiltonian,

$$\mathcal{H}_{\rm NP}^{\rm rare} = \sum_{i=1}^{10} \tilde{C}_i(\mu)\tilde{Q}_i, \tag{6.1}$$

where $\tilde{C}_i$ are Wilson coefficients, and $\tilde{Q}_i$ are the effective operators. In this case, there are ten of them,

$$\begin{aligned}
&\tilde{Q}_1 = (\bar{\ell}_L\gamma_\mu\ell_L)\,(\bar{u}_L\gamma^\mu c_L)\,, \quad \tilde{Q}_4 = (\bar{\ell}_R\ell_L)\,(\bar{u}_R c_L),\\
&\tilde{Q}_2 = (\bar{\ell}_L\gamma_\mu\ell_L)\,(\bar{u}_R\gamma^\mu c_R)\,, \quad \tilde{Q}_5 = (\bar{\ell}_R\sigma_{\mu\nu}\ell_L)\,(\bar{u}_R\sigma^{\mu\nu} c_L)\,,\\
&\tilde{Q}_3 = (\bar{\ell}_L\ell_R)\,(\bar{u}_R c_L)\,,
\end{aligned} \tag{6.2}$$

and five other operators $\tilde{Q}_6, \cdots, \tilde{Q}_{10}$ that can be obtained from the operators in Eq. (6.2) by the substitutions $L \to R$ and $R \to L$. It is worth noting that only eight operators contribute to $D^0 \to \ell^+\ell^-$, as $\langle\ell^+\ell^-|\tilde{Q}_5|D^0\rangle = \langle\ell^+\ell^-|\tilde{Q}_{10}|D^0\rangle = 0$. The most general $D^0 \to \ell^+\ell^-$ decay amplitude can be written as

$$\mathcal{M} = \bar{u}(\boldsymbol{p}_-, s_-)\,[A + B\gamma_5]\,v(\boldsymbol{p}_+, s_+), \tag{6.3}$$

which results in the branching fractions

$$\mathcal{B}_{D^0\to\ell^+\ell^-} = \frac{M_D}{8\pi\Gamma_{\rm D}}\sqrt{1-\frac{4m_\ell^2}{M_D^2}}\left[\left(1-\frac{4m_\ell^2}{M_D^2}\right)|A|^2 + |B|^2\right]\,. \tag{6.4}$$

Any NP contribution described by the operators of Eq. (6.2), gives the amplitudes A and B,

$$\begin{aligned}
|A| &= G\frac{f_D M_D^2}{4m_c}\left[\tilde{C}_{3-8} + \tilde{C}_{4-9}\right]\,,\\
|B| &= G\frac{f_D}{4}\left[2m_\ell\left(\tilde{C}_{1-2} + \tilde{C}_{6-7}\right) + \frac{M_D^2}{m_c}\left(\tilde{C}_{4-3} + \tilde{C}_{9-8}\right)\right]\,,
\end{aligned} \tag{6.5}$$

with $\tilde{C}_{i-k} \equiv \tilde{C}_i - \tilde{C}_k$. Any NP model that contributes to $D^0 \to \ell^+\ell^-$ can be constrained using the constraints on the

Wilson coefficients in Eq. (6.5). It will be advantageous to study the *correlations* of various processes to isolate and constrain the NP contributions [30,31]. Such correlations exist, for instance, in $D^0\bar{D}^0$ mixing and rare decays [30]. In general, the rare decay rate can not be predicted just on the basis of the mixing rate, even if both x_D and $\mathcal{B}_{D^0\to\ell^+\ell^-}$ are dominated by a given NP contribution. However, this is possible for a restricted subset of NP models [30]. Predictions of the $D^0\to\mu^+\mu^-$ branching fraction for $x_D$of about 1% can be found in Ref. [30] together with the definitions of NP model parameters.

Three-body rare decays with charged leptons

Theoretical predictions of the decay rates of di-lepton modes such as $D\to h(h')e^+e^-$ are complicated due to the LD contributions. The rates with a lepton-pair mass in the non-resonant regions could provide access to NP [31-34], at least for some particular BSM models. Table 6.2 gives some interesting $D\to h(h')e^+e^-$ modes that can be studied at the BESIII experiment. The corresponding experimental upper limits on the branching fractions are also summarized. In a recent BESIII paper [35], some of the limits have been improved by several orders of magnitude. With more data in the future, we expect to improve these limits. Some new modes could also be probed, depending on the background of a given mode. The expected BESIII sensitivities with the expected final charm data set listed in Sec. 7 are also shown in the last column of Table 6.2.

Three-body rare decays with neutrinos

Neutral modes, such as $D^0\to\pi^0\nu\bar{\nu}$, have never been studied at the charm threshold before. It is possible that the LD SM effects are under better theoretical control in such transitions [23]. Belle reported a similar search for the rare decays $B\to h^{(*)}\nu\bar{\nu}$ [38], and BaBar searched for $B^0\to\gamma\nu\bar{\nu}$ [39]. With the 20 fb^{-1} data sample at $\sqrt{s}$ = 3.773 GeV, the sensitivity of the $\mathcal{B}(D^0\to\pi^0\nu\bar{\nu})$ measurement at BESIII could reach 10^{-4} or better.

Radiative decay modes $D^0\to\gamma\nu\bar{\nu}$ serve as physics background to searches for light Dark Matter (DM), as described in Sec. 6.5.1. This transition has an extremely small branching fraction of $\mathcal{B}(D^0\to\gamma\nu\bar{\nu}) = 3.96\times10^{-14}$ in SM [40], making the final state of a photon with missing energy a suitable topology for searches for light DM at BESIII.

6.3 Symmetry test in hyperon decays

The Sakharov conditions for baryogengesis underline the role of *CP* violation as one of the central pieces of the matter-antimatter asymmetry puzzle [41]. However, the CKM mechanism for *CP* violation in SM fails to fully explain the puzzle of the matter-antimatter asymmetry by more than 10 orders of magnitude [42]. This suggests that

Table 6.2. The latest experimental upper limits on the branching fractions (in units of 10^{-6}) of the rare D and D_s decays into $h(h')e^+e^-$. The expected BESIII sensitivities with the expected final charm data set listed in Sec. 7 are also shown in the last column.

Decay	Upper limit	Experiment	Year	Ref.	BESIII Expected
$D^0\to\pi^0e^+e^-$	0.4	BESIII	2018	[35]	0.1
$D^0\to\eta e^+e^-$	0.3	BESIII	2018	[35]	0.1
$D^0\to\omega e^+e^-$	0.6	BESIII	2018	[35]	0.2
$D^0\to K^0_Se^+e^-$	1.2	BESIII	2018	[35]	0.5
$D^0\to\rho e^+e^-$	124.0	E791	2001	[36]	0.5
$D^0\to\phi e^+e^-$	59.0	E791	2001	[36]	0.5
$D^0\to\bar{K}^{*0}e^+e^-$	47.0	E791	2001	[36]	0.5
$D^0\to\pi^+\pi^-e^+e^-$	0.7	BESIII	2018	[35]	0.3
$D^0\to K^+K^-e^+e^-$	1.1	BESIII	2018	[35]	0.4
$D^0\to K^-\pi^+e^+e^-$	4.1	BESIII	2018	[35]	1.6
$D^+\to\pi^+e^+e^-$	1.1	BaBar	2011	[37]	0.12
$D^+\to K^+e^+e^-$	1.0	BaBar	2011	[37]	0.46
$D^+\to\pi^+\pi^0e^+e^-$	1.4	BESIII	2018	[35]	0.5
$D^+\to\pi^+K^0_Se^+e^-$	2.6	BESIII	2018	[35]	1.0
$D^+\to K^0_SK^+e^+e^-$	1.1	BESIII	2018	[35]	0.4
$D^+\to K^+\pi^0e^+e^-$	1.5	BESIII	2018	[35]	0.6
$D^+_s\to\pi^+e^+e^-$	13.0	BaBar	2011	[37]	70.0
$D^+_s\to K^+e^+e^-$	3.7	BaBar	2011	[37]	1.7

additional, as yet undiscovered, *CP* violating processes exist, which has motivated aggressive searches for new sources of *CP* violation in *b*-quark decays and neutrino oscillations [43]. *CP* violation in charm decay is very small and had not yet been found until the discovery in 2019 at LHCb. LHCb finds a non-zero *CP* violation in $D^0 \to \pi^+\pi^-$ and $D^0 \to K^+K^-$ decays with a significance of 5.3σ. The time-integrated *CP* asymmetry is given as

$$\begin{aligned}\Delta a_{\rm CP} =& \frac{\Gamma(D\to K^+K^-)-\Gamma(\bar{D}\to K^+K^-)}{\Gamma(D\to K^+K^-)+\Gamma(\bar{D}\to K^+K^-)}\\ &-\frac{\Gamma(D\to \pi^+\pi^-)-\Gamma(\bar{D}\to \pi^+\pi^-)}{\Gamma(D\to \pi^+\pi^-)+\Gamma(\bar{D}\to \pi^+\pi^-)}\\ =&(-0.154\pm 0.029)\%, \end{aligned} \tag{6.6}$$

where $D(\bar{D})$ is a $D^0(\bar{D}^0)$ at time $t=0$ [44]. This result is at the high end of the SM theoretical estimates which range from 10^{-4} to 10^{-3}. The LHCb result is intriguing, because it may be a sign of the long-sought non-SM mechanism of *CP* violation. However, uncertainties in the SM theoretical calculations of $\Delta a_{\rm CP}$ make it impossible to rule out this possibility. The current BESIII level of sensitivity of $10^{-3} \sim 10^{-2}$ for charm meson *CP* violation is still more than one order of magnitude above the highest conceivable SM effects. In addition to charmed mesons, BESIII has accumulated huge data samples of strange and charmed baryons, thus providing a unique opportunity to examine the strong dynamics of strange/charm decays, which is another route to probe the phenomenon of *CP* violation. In this section we briefly discuss strange/charmed baryon decays and outline various paths to the observation of *CP* violation and baryon number violation (BNV).

6.3.1 Probing *CP* asymmetry in hyperon decays

BESIII has the capability of testing *CP* symmetry in hyperon decays, produced via $J/\psi \to B\bar{B}$, with $B\bar{B}$ denoting polarized, quantum-entangled hyperon pairs, which adds an exciting new dimension to the study of *CP* violations.

A weak two-body decay of a spin one-half baryon under charge and parity transformations is illustrated in Fig. 6.1 for the most prominent decay mode $\Lambda \to p\pi^-$. The picture is in the Λ rest frame and the spin polarization vector $\boldsymbol{P}_\Lambda$ is pointing upwards. The daughter proton emitted at angles θ_d and ϕ_d with respect to the polarization vector $\boldsymbol{P}_\Lambda$ is transformed under *CP* into an antiproton emitted at angles $\pi-\theta_d$ and $-\phi_d$ with respect to the polarization vector of the parent $\bar{\Lambda}$. In addition, in the weak decay the polarization of the final proton could have a transverse component (along the $\boldsymbol{p}_p \times \boldsymbol{p}_\Lambda$ vector). For the antiproton, this component has an opposite direction.

Direct *CP* asymmetry

The most straightforward *CP*-odd observable is the difference between the partial decay rate for the decay and the *CP*-transformed process:

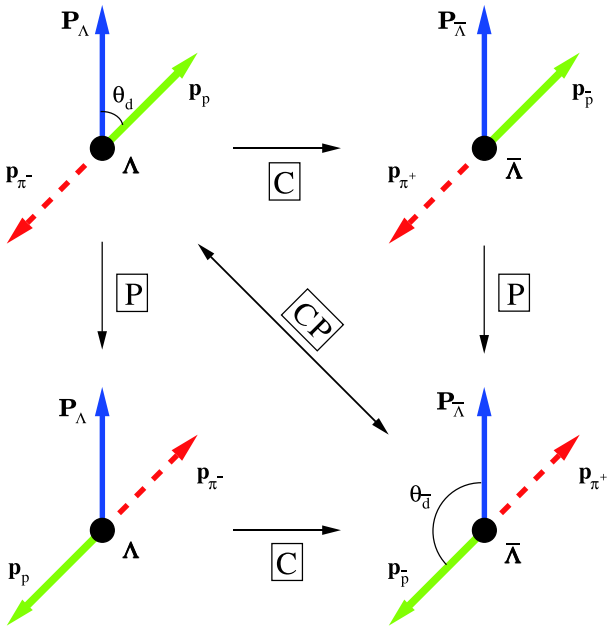

Fig. 6.1. (color online) Illustration of the charge (C), parity (P) and *CP* transformations in the $\Lambda \to p\pi^-$ decay.

$$\Delta = \frac{\Gamma-\overline{\Gamma}}{\Gamma+\overline{\Gamma}}\,. \tag{6.7}$$

Furthermore, the parity violation in the hyperon decays allows much more sensitive tests to be constructed. The two-body nonleptonic weak decay $1/2 \to 1/2+0$ can be described by the partial width Γ and decay parameters α, β, γ:

$$\begin{aligned}&\alpha = \frac{2{\rm Re}(S^*P)}{|S|^2+|P|^2}, \quad \beta = \frac{2{\rm Im}(S^*P)}{|S|^2+|P|^2} = \sqrt{1-\alpha^2}\sin\phi,\\ &\gamma = \sqrt{1-\alpha^2}\cos\phi. \end{aligned} \tag{6.8}$$

Only two parameters are independent, and it is convenient to use α and ϕ. The parameter α has a simple interpretation due to the asymmetry of the angular distribution of the daughter proton, given by

$$\frac{{\rm d}\Gamma}{{\rm d}\Omega_d} \propto \frac{1}{4\pi}(1+\alpha P_\Lambda \cos\theta_d)\,. \tag{6.9}$$

A comparison of the decay parameters of the hyperon and antihyperon leads to sensitive tests of *CP* symmetry. The *CP*-odd observables are

$$A = \frac{\alpha+\overline{\alpha}}{\alpha-\overline{\alpha}}\,, \quad B = \frac{\beta+\overline{\beta}}{\beta-\overline{\beta}}\,. \tag{6.10}$$

Here, α corresponds to α_- in the $\Lambda \to p\pi^-$ decay, while $\overline{\alpha}$ corresponds to α_+ in the $\bar{\Lambda} \to \bar{p}\pi^+$ decay. The quantity β can not be measured in the joint $J/\psi \to \Lambda\bar{\Lambda} \to p\pi^-\bar{p}\pi^+$ decay. In general, the sensitivity of these asymmetries to *CP* violation scales as $\Delta : A : B \sim 1 : 10 : 100$. The asymmetry A has been studied in $\bar{p}p$ experiments and at e^+e^- colliders [45-48]. The present world average is $A = 0.006 \pm 0.021$, while the CKM mechanism predicts a

value of $A \sim 10^{-5} - 10^{-4}$ [49-51]. Predictions in scenarios beyond SM are given in Refs. [52-54]. There also exist dynamical calculations, shown in Refs. [55,56]. Experimental prospects of *CP*-symmetry tests for the charmed baryon by determination of α are discussed in Ref. [57].

At BESIII, J/ψ mesons are produced in the annihilation of unpolarized electron-positron beams, and therefore the spin-density matrix of J/ψ depends only on the scattering angle θ_Λ between the electron beam direction and the Λ momentum in the reaction cms system. The helicity frames for the subsequent decay chains are shown in Fig. 6.2.

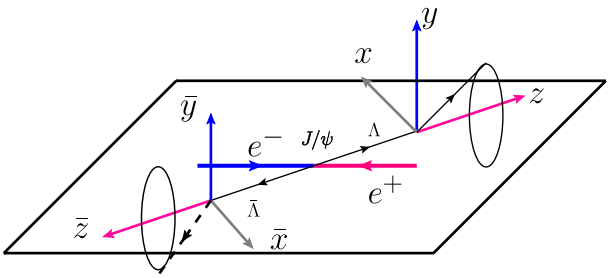

Fig. 6.2. (color online) Definition of the helicity frames for $J/\psi \to \Lambda\bar{\Lambda} \to p\pi^-\bar{p}\pi^+$.

The coherent production of $\Lambda/\bar{\Lambda}$ pairs from the decay $J/\psi \to \Lambda\bar{\Lambda}$ with subsequent weak decays of Λ and $\bar{\Lambda}$ is a very simple spin-entangled quantum system where the final state is specified by four real parameters summarized in Table 6.3.

A recent BESIII study with 1.3×10^9 J/ψ events observed a transverse spin polarization of $\Lambda/\bar{\Lambda}$, and the phase between the hadronic form factors was determined [58]. The polarization effect is illustrated by dividing the data sample into 50 $\cos\theta_\Lambda$ bins and plotting the $\cos\theta_\Lambda$ dependence of the moment $\mu(\cos\theta_\Lambda) = 1/N\sum_i^{N(\theta_\Lambda)}(\sin\theta_1^i\sin\phi_1^i - \sin\theta_2^i\sin\phi_2^i)$, where N is the total number of events in the data sample and $N(\theta_\Lambda)$ is the number of events in the $\cos\theta_\Lambda$ bin. This dependence enables to extract simultaneously $\alpha_- = 0.750\pm0.009\pm0.004$ and $\alpha_+ = -0.758\pm0.010\pm0.007$, and to calculate the most precise value of A as $-0.006\pm0.012\pm0.007$, where a large value of the correlation coefficient $\rho(\alpha_+,\alpha_-) = 0.82$ is included in the propagation of the statistical uncertainty.

New BESIII data with 10^{10} J/ψ events will enable an improved measurement of the parameter A. In the future measurements, the systematic uncertainty will be significantly improved since this simple system permits several internal consistency checks. In the general case of two spin one-half particles, we have 16 polarization and spin correlation distributions to fully describe using only four global parameters. In addition, the use of other monitoring and calibration channels allows to determine independent corrections for any bias. Also, if a similar polarization is observed for other hyperons, then similar studies will be possible, *e.g.* for the Ξ hyperon with its cascade decays, B asymmetry tests would be possible.

The triple-product asymmetry

Apart from the above mentioned direct measurement, we can also exploit the triple-product asymmetry as a *CP*-violating observable. Studies of *CP* violation in the Λ and other hyperon decays using this approach were proposed in Ref. [59]. The direct *CP*-violating asymmetry $\mathcal{A}_{\rm dir}$ and the triple-product asymmetry $\mathcal{A}_T$ depend on the weak phase ϕ and the strong-phase δ as:

$$A_{\rm dir} \propto \sin\phi\sin\delta, \quad A_T \propto \sin\phi\cos\delta. \tag{6.11}$$

The direct asymmetry only survives if there is a non-zero strong phase, whereas the triple-product asymmetry with the strong phase vanishes. Therefore the two methods are complementary, particularly if the strong phase is unknown.

The triple product is defined as $\vec{v}_1\cdot(\vec{v}_2\times\vec{v}_3)$, where $\vec{v}$ can be a three-momentum or a spin vector. Under time reversal the triple product changes sign, and thus it is a *T*-violating signal. However, final-state interactions (FSI) can give a false *CP*-violation signal. As a result, a channel must be compared to its conjugate. For an illustration of this point, we refer to Refs. [60,61]. Such considerations have led to the corresponding proposal for BESIII [62,63], as well as in beauty decays [64-68], and in the search for NP effects [69,70].

We illustrate the method with the process $e^+e^- \to J/\psi \to \Lambda\bar{\Lambda} \to [p\pi^-][\bar{p}\pi^+]$. This process is transformed to itself under charge conjugation. Since the polarization of the proton and antiproton is not measured, we have four independent vectors to construct triple products. Two of them are $\boldsymbol{k}$ and $\boldsymbol{p}_\Lambda$ – the three-momenta of incoming electron and outgoing Λ in the reaction cms frame. The remaining ones are $\boldsymbol{q}_1$ and $\boldsymbol{q}_2$ – the momenta of the proton and antiproton in the Λ and $\bar{\Lambda}$ rest frames. For example, defining $C_T = (\boldsymbol{p}_\Lambda\times\boldsymbol{q}_1)\cdot\boldsymbol{p}_\Lambda$, and $\bar{C}_T = -(\boldsymbol{p}_\Lambda\times\boldsymbol{q}_2)\cdot\boldsymbol{p}_\Lambda$, we can define the following triple-product asymmetries

Table 6.3. List of kinematic variables (helicity angles) and parameters used in the analysis of the decay chain.

Decay	Coordinate system	Helicity angles	Parameters
$J/\psi \to \Lambda\bar{\Lambda}$	cms	$(\theta_\Lambda,\phi_\Lambda)$	α_ψ, $\Delta\Phi$
$\Lambda \to p\pi^-$	(x, y, z)	(θ_1,ϕ_1)	α_-
$\bar{\Lambda} \to \bar{p}\pi^+$	$(\bar{x}, \bar{y}, \bar{z})$	(θ_2,ϕ_2)	α_+

$$\langle A_T\rangle = \frac{N(C_T>0)-N(C_T<0)}{N(C_T>0)+N(C_T<0)}, \tag{6.12}$$

$$\langle \bar{A}_T\rangle = \frac{N(-\bar{C}_T>0)-N(-\bar{C}_T<0)}{N(-\bar{C}_T>0)+N(-\bar{C}_T<0)}. \tag{6.13}$$

Therefore, CPT invariance implies that

$$\mathcal{A}_T = \langle A_T\rangle - \langle \bar{A}_T\rangle \neq 0 \tag{6.14}$$

is a *CP*-odd observable, which can be measured simply by event counting. Another triple product is $(\boldsymbol{q}_1\times\boldsymbol{q}_2)\cdot\boldsymbol{p}_\Lambda$, related to the $C_{x\bar{z}}-C_{z\bar{x}}$ spin correlation term. This last triple product allows to improve the limits on the Λ electric-dipole moment d_Λ, as discussed in Refs. [71,72].

The *CP* asymmetries can also be studied locally as a function of the kinematic variable $\cos\theta_\Lambda$, limiting the range of the triple-product values:

$$\mathcal{A}_T(d) = \frac{N(C_T>|d|)-N(C_T<-|d|)}{N(C_T>|d|)+N(C_T<-|d|)}. \tag{6.15}$$

By considering the efficiency of the BESIII detector, the number of observed events and the corresponding statistical errors for various channels were estimated. The expected sensitivity with 10^{10} J/ψ events is shown in Table 6.4.

A wide range of *CP* tests in the hyperon sector can also be performed in a single measurement of the spin entangled Ξ-$\bar{\Xi}$ system [73]. From the joint distributions for $e^+e^-\to\Xi\bar{\Xi}$, it can be shown that the role of the transverse polarization is fully replaced by the diagonal spin correlations between the cascades. All decay parameters can be determined simultaneously, and the statistical uncertainties do not depend on the transverse polarization in the production process. The sensitivities at BESIII are given in Table 6.5 , including the correlations between parameters. Practically, the results do not change between the two extreme cases: $\Delta\Phi=0$ and $\pi/2$. The results for the decays $\psi(3686)\to\Xi^-\bar{\Xi}^+$ and $J/\psi,\psi(3686)\to\Xi^0\bar{\Xi}^0$ are similar. The results are also shown for the asymptotic case $e^+e^-\to\Xi^-\bar{\Xi}^+$ with $\alpha_\psi=0$, and for the scalar charmonium decay to $\Xi\bar{\Xi}$. Contrary to $e^+e^-\to\Lambda\bar{\Lambda}$, the polarization in the production process plays practically no role. The weak decay phases ϕ_Ξ and $\phi_{\bar{\Xi}}$ are not correlated with each other or with any other parameter.

6.3.2 Constraint on BNV from $\Lambda-\bar{\Lambda}$ oscillations

The stability of ordinary matter implies baryon number (B) conservation. However, the observed baryon asymmetry in the Universe shows that the baryon number should be broken. There are many theoretical models in which B is not exactly conserved, with B and lepton number (L) violated simultaneously while conserving $B-L$.

It was pointed out long ago [74] that the crucial test of baryon number violation are the neutron-antineutron (n-$\bar{n}$) oscillations, and many corresponding experiments have been conducted [43]. If n-$\bar{n}$ oscillations exist, Λ-$\bar{\Lambda}$ oscillations may also take place [75]. There is a proposal to search for Λ-$\bar{\Lambda}$ oscillations in the decay $J/\psi\to\Lambda\bar{\Lambda}$ [76]. Until recently, however, there have not been any direct experimental searches for this process.

At BESIII, the decay $J/\psi\to pK^-\bar{\Lambda}$ has a very simple final state and is almost background free, so it is well suited for searching for $\Lambda-\bar{\Lambda}$ oscillations. Initially, J/ψ decays into the $pK^-\bar{\Lambda}$ final state (defined as a right-sign event, as $\bar{\Lambda}\to\bar{p}\pi^+$ is detected along with pK^-), and then, with some $\bar{\Lambda}$ oscillating into Λ, the final state becomes $pK^-\Lambda$ (defined as a wrong-sign event, as $\Lambda\to p\pi^-$ is detected with pK^-). Hence, the probability of generating a final Λ from an initial $\bar{\Lambda}$ can be determined by the ratio of

Table 6.4. The number of reconstructed events, taking into account the decay branching fractions, tracking and particle identification, with 10^{10} J/ψ events. The sensitivity is estimated without the possible background dilution, which is small at BESIII. Systematic uncertainties are expected to be of the same order as the statistical uncertainties.

Channel	Number of events	Sensitivity on $\mathcal{A}_T$
$J/\psi\to\Lambda\bar{\Lambda}\to[p\pi^-][\bar{p}\pi^+]$	2.6×10^6	0.06%
$J/\psi\to\Sigma^+\bar{\Sigma}^-\to[p\pi^0][\bar{p}\pi^0]$	2.5×10^6	0.06%
$J/\psi\to\Xi^0\bar{\Xi}^0\to[\Lambda\pi^-][\bar{\Lambda}\pi^+]$	1.1×10^6	0.1%
$J/\psi\to\Xi^-\bar{\Xi}^+\to[\Lambda\pi^0][\bar{\Lambda}\pi^0]$	1.6×10^6	0.08%

Table 6.5. The sensitivities at BESIII of the extracted parameters in the spin entangled Ξ-$\bar{\Xi}$ system, given as the estimated uncertainty multiplied by the square root of the observed signal yield. The errors for the parameters of the charge conjugated decay modes are identical. The input values of the Ξ parameters have only a minor effect on the sensitivities.

	α_Ξ	α_Λ	ϕ_Ξ	α_ψ	$\Delta\Phi$	$\langle\alpha_\Xi\rangle$	A_Ξ	$\langle\alpha_\Lambda\rangle$	A_Λ	$\langle\alpha_\Xi\alpha_\Lambda\rangle$	$A_{\Xi\Lambda}$	$\langle\phi_\Xi\rangle$	B_Ξ
$J/\psi\to\Xi^-\bar{\Xi}^+$ ($\Delta\Phi=0$)	2.0	3.1	5.8	3.5	6.0	1.4	3.7	1.7	3.5	0.78	4.0	4.1	110
$J/\psi\to\Xi^-\bar{\Xi}^+$ ($\Delta\Phi=\pi/2$)	1.9	2.8	5.4	3.0	13	1.4	3.5	1.6	3.1	0.76	3.9	3.8	100
$e^+e^-\to\Xi^-\bar{\Xi}^+$ ($\alpha_\psi=1$)	1.9	2.7	5.0	–	–	1.3	3.4	1.4	3.1	0.76	4.0	3.5	96
$\eta_c,\chi_{c0}\to\Xi^-\bar{\Xi}^+$	1.6	2.2	3.7	–	–	1.1	2.9	1.0	2.6	0.72	3.9	2.6	71

wrong sign events to right sign events.

The time evolution of the Λ-$\bar{\Lambda}$ oscillation can be described [73] by the Schroedinger-like equation,

$$i\frac{\partial}{\partial t}\begin{pmatrix}\Lambda(t)\\ \bar{\Lambda}(t)\end{pmatrix}=M\begin{pmatrix}\Lambda(t)\\ \bar{\Lambda}(t)\end{pmatrix},$$

where the matrix M is Hermitian,

$$M=\begin{pmatrix}m_{\Lambda}-\Delta E_{\Lambda} & \delta m_{\Lambda\bar{\Lambda}}\\ \delta m_{\Lambda\bar{\Lambda}} & m_{\bar{\Lambda}}-\Delta E_{\bar{\Lambda}}\end{pmatrix},$$

and $\delta m_{\Lambda\bar{\Lambda}}$ is the $\Delta B=2$ oscillation parameter due to some NP effect, m_{Λ} ($m_{\bar{\Lambda}}$) is the mass of the $\Lambda(\bar{\Lambda})$ baryon, and ΔE is the energy split due to an external magnetic field. For an unbound Λ propagating in vacuum without an external field, both ΔE_{Λ} and $\Delta E_{\bar{\Lambda}}$ are zero.

Starting with a beam of free Λ particles, the probability $P(\bar{\Lambda},t)$ of generating $\bar{\Lambda}$ after time t, is given by

$$P(\bar{\Lambda},t)=\sin^2(\delta m_{\Lambda\bar{\Lambda}}\cdot t).$$

BESIII can measure the time integral of the probability, *i.e.* the oscillation rate,

$$P(\bar{\Lambda})=\frac{\int_0^{T_{\rm max}}\sin^2(\delta m_{\Lambda\bar{\Lambda}}\cdot t)\cdot e^{-t/\tau_{\Lambda}}\cdot {\rm d}t}{\int_0^{\infty}e^{-t/\tau_{\Lambda}}\cdot {\rm d}t},$$

where $P(\bar{\Lambda})$ is the time-integrated probability of $\Lambda\to\bar{\Lambda}$, τ_{Λ} is the lifetime of the Λ baryon, and $T_{\rm max}$ is the maximum flight time. If we assume that $T_{\rm max}$ is large enough in the BESIII tracking system, the oscillation parameter can be deduced as

$$\delta m_{\Lambda\bar{\Lambda}}=\sqrt{\frac{P(\bar{\Lambda})}{2\cdot(\tau_{\Lambda}/\hbar)^2}}.$$

With the accumulated data sample of 10^{10} J/ψ events, the upper limit of the Λ-$\bar{\Lambda}$ oscillation rate will be at the level of 10^{-6} (90% C.L.) based on the analysis of $J/\psi\to pK^-\bar{\Lambda}$ events, and the constraint on $\delta m_{\Lambda\bar{\Lambda}}$ will be reduced to 10^{-16} MeV (90% CL). On the other hand, a time-dependent analysis of Λ-$\bar{\Lambda}$ pairs produced in J/ψ decays can be investigated, taking advantage of their long mean flight distance of 7.6 cm in the detector. Therefore, BESIII could provide a very stringent constraint on NP in this channel.

6.3.3 More symmetry violation in hyperon decays

Since BESIII has a rather large hyperon data set, Λ from hyperons can also be used to study symmetry violations and search for NP, as was recently summarized in the review [77]. We reproduce here the summary table (Table 6.6) showing the lepton or baryon-number violating hyperon decays and their expected sensitivities with future BESIII data sets. More information can be found in the original paper [77].

6.4 Charged Lepton Flavor (Number) Violation decays

Charged Lepton Flavor Violation (CLFV) processes are highly suppressed in SM by the tiny but finite neutrino masses. Their branching fractions are predicted to be negligibly small – and no such processes have been observed. Yet, there are various theoretical models that predict the rates for CLFV transitions to be large enough to be observed experimentally. Examples include the SUSY grand unified theories [78], SUSY with a right-handed neutrino [79], gauge-mediated SUSY breaking [80], SUSY with vector-like leptons [81], SUSY with R-parity violation [82], models with Z' [83], or models with Lorentz non-invariance [84]. While the discovery of neutrino oscillations has confirmed the existence of neutrino masses and LFV in the neutral lepton sector, detection of LFV in the charged lepton sector would provide direct evidence of NP.

Experimentally, searches for CLFV effects have been carried out in a variety of ways, including decays of leptons, pseudoscalar, and vector mesons, as well as in other processes. In the charmonium system, BESII obtained the limit $\mathcal{B}(J/\psi\to e\mu)<1.1\times10^{-6}$ [85] by analyzing a data sample of 58 million J/ψ events. BESIII has so

Table 6.6. Lepton or baryon number violating hyperon decays and expected sensitivities with 10^{10} events at the J/ψ peak, and 3×10^9 events at the $\psi(3686)$ peak. The current J/ψ data are from CLAS, as listed in PDG. "–" indicates "not available", $l=e$ or μ, and $M^{\pm}$ refers to the charged stable mesons ($M^{\pm}=\pi^{\pm}$ or $K^{\pm}$). Each reaction shows evidence of $\Delta L=\pm1$ or/and $\Delta B\neq0$, and conserves the electric charge and the angular momentum [77].

Decay mode	Current data $\mathcal{B}$ ($\times10^{-6}$)	Expected BESIII $\mathcal{B}$ ($\times10^{-6}$)(at the 90% C.L.)	ΔL	ΔB
$\Lambda\to M^+l^-$	$<0.4\sim3.0$	<0.1	+1	−1
$\Lambda\to M^-l^+$	$<0.4\sim3.0$	<0.1	−1	−1
$\Lambda\to K^0_S\nu$	<20	<0.6	+1	−1
$\Sigma^+\to K^0_Sl^+$	–	<0.2	−1	−1
$\Sigma^-\to K^0_Sl^-$	–	<1.0	+1	−1
$\Xi^-\to K^0_Sl^-$	–	<0.2	+1	−1
$\Xi^0\to M^+l^-$	–	<0.1	+1	−1
$\Xi^0\to M^-l^+$	–	<0.1	−1	−1
$\Xi^0\to K^0_S\nu$	–	<2.0	+1	−1

far analyzed 255 million J/ψ decays. Four events have been observed, which is consistent with the background estimate. As a result, BESIII set the upper limit $\mathcal{B}(J/\psi \to e\mu) < 1.6\times10^{-7}$ at the 90% C.L. [86], which is currently the best upper limit on CLFV in charmonium decays. BESII also placed bounds on $\mathcal{B}(J/\psi \to \mu\tau) < 2.\times10^{-6}$ and $\mathcal{B}(J/\psi \to e\tau) < 8.3\times10^{-6}$ [87]. The limits on these decay channels will be updated at BESIII with the data set of 10^{10} J/ψ decays, and an improvement of several orders of magnitude is expected.

CLFV and lepton-number-violating (LNV) processes can also be probed in D meson decays at BESIII. No evidence has been found for D meson decays with either CLFV or LNV. The present experimental bounds on the branching fractions are generally set at the level of 10^{-6} to 10^{-5} (with a notable exception of $D^0 \to \mu e$, where $\mathcal{B}(D^0 \to \mu^\pm e^\mp) < 1.3\times10^{-8}$) [88]. D decays with LNV, such as $D^+ \to l^+l^+X^-$ and $D_s^+ \to l^+l^+X^-$, are also forbidden in the minimal SM, but are possible if massive neutrinos are Majorana particles.

However, for CLFV processes such as $D^0 \to l^+l'^-$ and $D^0 \to l^+l'^-X$, LHCb will dominate the searches even if BESIII increases the available data set of D meson decays by an order of magnitude. On the other hand, BESIII has a potential to search for LNV transitions such as $D^+ \to l^+l^+X^-$ and $D_s^+ \to l^+l^+X^-$, due to the clean environment and low charge confusion rates.

Effective Lagrangian and NP models

NP models probed at BESIII include those predicting lepton-flavor violating interactions. They can be probed in decays to flavor-non-diagonal combination of final state leptons $\ell_i = e,\mu,\tau$. Due to a multitude of NP models contributing to CLFV processes, it is advantageous to introduce an effective Lagrangian that economically encodes all NP models. The details of the models are encoded in the Wilson coefficients, while the quark-lepton dynamical effects are described by a set of CLFV operators.

The effective Lagrangian $\mathcal{L}_{\rm eff}$ that involves CLFV can in general be written as

$$\mathcal{L}_{\rm eff} = \mathcal{L}_{\ell q} + \mathcal{L}_D + \mathcal{L}_G + \cdots, \tag{6.16}$$

where $\mathcal{L}_D$ is the dipole part, $\mathcal{L}_{\ell q}$ is the part that contains four-fermion interactions, and $\mathcal{L}_G$ is the gluonic part [89,90].

The dipole part $\mathcal{L}_D$ has been extremely well constrained by purely leptonic CLFV decays of the type $\ell_1 \to \ell_2\gamma$ [91,92]. It appears that any possible contribution of $\mathcal{L}_D$ to charmed particle decays is four-to-six orders of magnitude smaller than from the other sectors of $\mathcal{L}_{\rm eff}$, and it is neglected in the following discussion [89].

The four-fermion dimension-six lepton-quark part of the effective Lagrangian, Eq. (6.16) is [91]

$$\begin{aligned}\mathcal{L}_{\ell q} = -\frac{1}{\Lambda^2}\sum_{q=u,c}\Big[&\left(C_{VR}^{qc\ell_1\ell_2}\,\bar{\ell}_1\gamma^\mu P_R\ell_2 + C_{VL}^{qc\ell_1\ell_2}\,\bar{\ell}_1\gamma^\mu P_L\ell_2\right)\bar{q}\gamma_\mu c\\ &+\left(C_{AR}^{qc\ell_1\ell_2}\,\bar{\ell}_1\gamma^\mu P_R\ell_2 + C_{AL}^{qc\ell_1\ell_2}\,\bar{\ell}_1\gamma^\mu P_L\ell_2\right)\bar{q}\gamma_\mu\gamma_5 c\\ &+ m_2m_cG_F\left(C_{SR}^{qc\ell_1\ell_2}\,\bar{\ell}_1P_L\ell_2 + C_{SL}^{qc\ell_1\ell_2}\,\bar{\ell}_1P_R\ell_2\right)\bar{q}c\\ &+ m_2m_cG_F\left(C_{PR}^{qc\ell_1\ell_2}\,\bar{\ell}_1P_L\ell_2 + C_{PL}^{qc\ell_1\ell_2}\,\bar{\ell}_1P_R\ell_2\right)\bar{q}\gamma_5 c\\ &+ m_2m_cG_F\left(C_{TR}^{qc\ell_1\ell_2}\,\bar{\ell}_1\sigma^{\mu\nu}P_L\ell_2 + C_{TL}^{qc\ell_1\ell_2}\,\bar{\ell}_1\sigma^{\mu\nu}P_R\ell_2\right)\\ &\times\bar{q}\sigma_{\mu\nu}c + h.c.\Big].\end{aligned} \tag{6.17}$$

Here, $P_{R,L} = (1\pm\gamma_5)/2$ is the right (left) chiral projection operator. In general, the Wilson coefficients are different for the lepton flavors ℓ_i and quark flavors $q = u,c$. This implies that decays of charmonium states and D mesons probe different terms (and different models of NP) in the effective CLFV Lagrangian.

The dimension seven gluonic operators in $\mathcal{L}_G$ appear for flavor-diagonal quark transitions, *i.e.* for $q = c$ [90,93],

$$\begin{aligned}\mathcal{L}_G = -\frac{m_2G_F}{\Lambda^2}\frac{\beta_L}{4\alpha_s}\Big[&\left(C_{GR}^{\ell_1\ell_2}\,\bar{\ell}_1P_L\ell_2 + C_{GL}^{\ell_1\ell_2}\,\bar{\ell}_1P_R\ell_2\right)G^a_{\mu\nu}G^{a\mu\nu}\\ &+\left(C_{\tilde{G}R}^{\ell_1\ell_2}\,\bar{\ell}_1P_L\ell_2 + C_{\tilde{G}L}^{\ell_1\ell_2}\,\bar{\ell}_1P_R\ell_2\right)G^a_{\mu\nu}\tilde{G}^{a\mu\nu} + h.c.\Big].\end{aligned} \tag{6.18}$$

Here, $\beta_L = -9\alpha_s^2/(2\pi)$ is defined for the number of light active flavors L, relevant for the scale of the process, which we take as $\mu \approx 2$ GeV. All Wilson coefficients should also be calculated at the same scale. G_F is the Fermi constant, and $\tilde{G}^{a\mu\nu} = (1/2)\epsilon^{\mu\nu\alpha\beta}G^a_{\alpha\beta}$ is the dual of the gluon field strength tensor.

Each term in Eqs. (6.17)-(6.18) can be separately probed in two-body decays of charmonium states with different J^{PC} and D mesons, as their constrained kinematics only selects operators with particular quantum numbers. As will be shown below, $J/\psi \to \bar{\ell}_1\ell_2$ decays select vector and tensor operators, while $\chi_c \to \bar{\ell}_1\ell_2$ and $\eta_c \to \bar{\ell}_1\ell_2$ only select scalar and pseudoscalar/axial operators in Eq. (6.17).

6.4.1 Decays $J/\psi, \psi(3686) \to l_1l_2, l_1l_2\gamma$

Experimental constraints on the $J/\psi \to \ell_1\ell_2$ branching fractions can be effectively converted to bounds on the Wilson coefficients of vector and tensor operators in Eq. (6.17). The Wilson coefficients can then be related to the model parameters of explicit realizations of possible UV completions of the effective Lagrangian in Eq. (6.16). Examples of particular new physics models include the Z' scenarios [94], R-parity violating supersymmetric models [95-97], and other approaches [98,99].

The most general expression for the J/ψ (or any $\psi(nS)$) $\to \ell_1\bar{\ell}_2$ decay amplitude can be written as

$$\begin{aligned}\mathcal{A}(V \to \ell_1\bar{\ell}_2) = &\bar{u}(p_1,s_1)\Big[A_V^{\ell_1\ell_2}\gamma_\mu + B_V^{\ell_1\ell_2}\gamma_\mu\gamma_5\\ &+\frac{C_V^{\ell_1\ell_2}}{m_V}(p_2-p_1)_\mu + \frac{iD_V^{\ell_1\ell_2}}{m_V}(p_2-p_1)_\mu\gamma_5\Big]\\ &\times v(p_2,s_2)\,\epsilon^\mu(p),\end{aligned} \tag{6.19}$$

where $V = J/\psi$ or $\psi(3686)$, and $A_V^{\ell_1\ell_2}$, $B_V^{\ell_1\ell_2}$, $C_V^{\ell_1\ell_2}$, and $D_V^{\ell_1\ell_2}$

are dimensionless constants which depend on the underlying Wilson coefficients of the effective Lagrangian in Eq. (6.17), as well as on the hadronic effects associated with the meson-to-vacuum matrix elements or decay constants. We shall neglect the dipole and tensor operator contributions, which implies that $C_V^{\ell_1\ell_2} = D_V^{\ell_1\ell_2} = 0$ [89]. The branching fractions of the vector ψ states are calculated from Eq. (6.19), and yield the ratio

$$\frac{\mathcal{B}(\psi \to \ell_1\bar{\ell}_2)}{\mathcal{B}(\psi \to e^+e^-)} = \left(\frac{m_V\left(1-y^2\right)}{4\pi\alpha f_\psi Q_q}\right)^2 \left[\left|A_V^{\ell_1\ell_2}\right|^2 + \left|B_V^{\ell_1\ell_2}\right|^2\right]. \quad (6.20)$$

Here, α is the fine structure constant, $Q_c = 2/3$ is the charge of the c quark, the mass of the lighter of the two leptons has been neglected, and $y = m_2/m_V$. The coefficients $A_V^{\ell_1\ell_2}$ and $B_V^{\ell_1\ell_2}$ depend on the initial state meson,

$$A_V^{\ell_1\ell_2} = \frac{f_V m_V}{2\Lambda^2}\left(C_{VL}^{cc\ell_1\ell_2} + C_{VR}^{cc\ell_1\ell_2}\right),$$
$$B_V^{\ell_1\ell_2} = -\frac{f_V m_V}{2\Lambda^2}\left(C_{VL}^{cc\ell_1\ell_2} - C_{VR}^{cc\ell_1\ell_2}\right). \quad (6.21)$$

The constraints on the Wilson coefficients also depend on the meson decay constants,

$$\langle 0|\bar{q}\gamma^\mu q|V(p)\rangle = f_V m_V \epsilon^\mu(p), \quad (6.22)$$

where $\epsilon^\mu(p)$ is the V meson polarization vector, and p is its momentum [100]. The decay constants are $f_{J/\psi} = 418\pm 9$ MeV and $f_{\psi(3686)} = 294 \pm 5$ MeV. They are both known experimentally from the leptonic decays, and theoretically from the lattice or QCD sum rule calculations.

There is an ongoing analysis based on the existing data set of 1.3×10^9 J/ψ decays. In this study the selection efficiencies for both $J/\psi \to \mu\tau$ and $J/\psi \to e\tau$ are around 14%. Based on the same Cut and Count (CC) analysis technique, with the assumption of similar efficiencies, we can make a projection of the future BESIII sensitivity in this channel. By constructing cocktail samples from the 1.3×10^9 data set, and then performing toy MC (pseudo-experiment) studies, the sensitivity with 10^{10} J/ψ events is evaluated. The 90% C.L. upper limit on the number of signal events is estimated according to the recoil τ mass distribution. With 10^{10} J/ψ decays, the projected sensitivities of the two channels are estimated to be at the 10^{-8} level. Such results would represent an improvement of almost two orders of magnitude compared to BESII. The systematic uncertainties have also been estimated, and are expected to be sub-dominant even for this very large sample. With more advanced analysis techniques, such as multivariate analyses (MVA), the efficiencies could be increased due to reduced background levels, which would result in even better sensitivities. The current and future BESIII constraints on $\mathcal{B}(J/\psi \to \ell_1\ell_2)$ are summarized in Table 6.7. Based on these projections, the current and projected constraints on the combination of Wilson coefficients and NP scale Λ are given in Table 6.8.

A promising approach for increasing the sensitivity of J/ψ decays to CLFV operators is to consider radiative charged lepton-flavor violating (RCLFV) transitions. The addition of a photon to the final state certainly reduces the number of events available for studies of CLFV decays. However, theJ/ψ data set accumulated by BESIII is large, which makes it possible to detect the contribution of other operators in $\mathcal{L}_{\rm eff}$. Since the final state kinematics is less constrained than in two-body decays, the constraints on the Wilson coefficients of the effective Lagrangian depend on a set of $V \to \gamma$ form factors that are not very well known [89]. To place meaningful constraints on the Wilson coefficients from non-resonance J/ψ RCLFV decays, it is necessary to employ the single-operator dominance hypothesis, *i.e.* to assume that only one operator contributes at a time. For the axial, scalar, and pseudoscalar operators, one has [89]

$$\Gamma_A(J/\psi \to \gamma\ell_1\bar{\ell}_2) = \frac{1}{18}\frac{\alpha Q_q^2}{(4\pi)^2}\frac{f_V^2 m_V^3}{\Lambda^4} \times\left[\left(C_{AL}^{cc\ell_1\ell_2}\right)^2 + \left(C_{AR}^{cc\ell_1\ell_2}\right)^2\right],$$
$$\Gamma_S(J/\psi \to \gamma\ell_1\bar{\ell}_2) = \frac{1}{144}\frac{\alpha Q_q^2}{(4\pi)^2}\frac{f_V^2 G_F^2 m_V^7}{\Lambda^4} \times\left[\left(C_{SL}^{cc\ell_1\ell_2}\right)^2 + \left(C_{SR}^{cc\ell_1\ell_2}\right)^2\right]y^2,$$
$$\Gamma_P(J/\psi \to \gamma\ell_1\bar{\ell}_2) = \frac{1}{144}\frac{\alpha Q_q^2}{(4\pi)^2}\frac{f_V^2 G_F^2 m_V^7}{\Lambda^4} \times\left[\left(C_{PL}^{cc\ell_1\ell_2}\right)^2 + \left(C_{PR}^{cc\ell_1\ell_2}\right)^2\right]y^2. \quad (6.23)$$

The $J/\psi \to \gamma e\mu$ channel is experimentally challenging at BESIII, so we focus on $J/\psi \to \gamma\mu\tau$ and $J/\psi \to \gamma e\tau$, for which the analysis with the current data set is ongoing. If MVA were to be used, the efficiency would be about 35% for both channels. There is no detailed projection yet, but the sensitivity to branching fractions could then reach $(1-3)\times10^{-8}$.

Table 6.7. Current [89] and future BESIII constraints on $\mathcal{B}(J/\psi \to \ell_1\ell_2)$. The projections with CC and MVA methods provide conservative and aggressive estimates.

$\ell_1\ell_2$	$\mu\tau$	$e\tau$	$e\mu$
Current upper limit	2.0×10^{-6}	8.3×10^{-6}	1.6×10^{-7}
BESIII projected (CC)	3.0×10^{-8}	4.5×10^{-8}	1.0×10^{-8}
BESIII projected (MVA)	1.5×10^{-8}	2.5×10^{-8}	6.0×10^{-9}

Table 6.8. Constraints on the Wilson coefficients of four-fermion operators. Note that the constraints on the right-handed couplings ($L \to R$) are the same. "−" means that no constraint is currently available, "FPS" means that the decay is forbidden by the phase space, and "N/A" means that the BESIII sensitivity studies are yet to be performed. Current constraints are from [89].

Wilson coeff (GeV^{-2})	Leptons	Constraints	
	$\ell_1\ell_2$	Current	Projected
$\left\|C_{VL}^{cc\ell_1\ell_2}/\Lambda^2\right\|$	$\mu\tau$	5.5×10^{-5}	$[5.0, 7.1]\times10^{-6}$
	$e\tau$	1.1×10^{-4}	$[6.5, 8.7]\times10^{-6}$
	$e\mu$	1.0×10^{-5}	$[2.8, 3.7]\times10^{-6}$
$\left\|C_{AL}^{cc\ell_1\ell_2}/\Lambda^2\right\|$	$\mu\tau$	–	7.4×10^{-4}
	$e\tau$	–	7.4×10^{-4}
	$e\mu$	–	N/A
$\left\|C_{SL}^{cc\ell_1\ell_2}/\Lambda^2\right\|$	$\mu\tau$	–	2.0
	$e\tau$	–	2.0
	$e\mu$	–	N/A
$\left\|C_{AL}^{uc\ell_1\ell_2}/\Lambda^2\right\|$	$\mu\tau$	FPS	FPS
	$e\tau$	–	N/A
	$e\mu$	1.3×10^{-8}	2.2×10^{-8}

6.4.2 $\chi_c(\eta_c) \to l_1 l_2$ via photon tagging in $\psi(3686) \to \gamma\chi_c(\eta_c)$

Similarly to probing operators with vector quantum numbers described in Sec. 6.4.1, the scalar and pseudoscalar operators in Eq. (6.17) can be probed in decays of scalar and pseudoscalar charmonia. Although these states are not produced directly in e^+e^- collisions, they can be studied in the radiative decays of vector charmonia [89]. Since at resonance

$$\mathcal{B}(V \to \gamma\ell_1\bar{\ell}_2) = \mathcal{B}(V \to \gamma M)\mathcal{B}(M \to \ell_1\bar{\ell}_2), \tag{6.24}$$

states with large $\mathcal{B}(V \to \gamma M)$ can be used to probe $\mathcal{B}(M \to \ell_1\bar{\ell}_2)$ [89]. An example includes

$$\mathcal{B}(\psi(3686) \to \gamma\chi_{c0}) = (9.99 \pm 0.27)\%\,,$$
$$\mathcal{B}(\psi(3770) \to \gamma\chi_{c0}) = (0.73 \pm 0.09)\%\,,$$

for probing the scalar operators in decays of the scalar states $M = \chi_c$. BESIII will have the highest sensitivity for the decay channels $\psi(3686) \to \gamma\chi_{c0}$, and $\chi_{c0} \to \mu\tau$ and $\chi_{c0} \to e\tau$. It is estimated that the efficiency for $\mathcal{B}(\psi(3686) \to \gamma\chi_{c0})$ could be about 10%.

If BESIII could collect a data set with about 3×10^9 $\psi(3686)$ events, the sensitivity for $\chi_{c0} \to \mu\tau$ and $\chi_{c0} \to e\tau$ could reach $(1-3)\times10^{-7}$. Similarly,

$$\mathcal{B}(J/\psi \to \gamma\eta_c) = (1.7 \pm 0.4)\%\,,$$
$$\mathcal{B}(\psi(3686) \to \gamma\eta_c) = (0.34 \pm 0.05)\%\,,$$

for the pseudoscalar state $M = \eta_c$. BESIII will be sensitive to the decay channels $J/\psi \to \gamma\eta_c$, $\eta_c \to \mu\tau$ and $\eta_c \to e\tau$. With 10^{10} J/ψ events and a detection efficiency of 10%, the sensitivity for $\eta_c \to \mu\tau$ and $\eta_c \to e\tau$ could reach $(2-5)\times10^{-7}$.

It must be pointed out that in the cases of χ_{c0} and η_c, the decay to $e\mu$ is more challenging, as the level and complexity of the background is expected to be higher. It is nevertheless still possible to probe these decay channels with the final BESIII data set, although a separate dedicated analysis is needed. It is expected that in these cases as well, BESIII will be able to probe the decay branching fractions at the level of 10^{-7} .

The most general expression for scalar and pseudoscalar decays $M \to \ell_1\bar{\ell}_2$ is

$$\mathcal{A}(M \to \ell_1\bar{\ell}_2) = \bar{u}(p_1, s_1)\left[E_M^{\ell_1\ell_2} + iF_M^{\ell_1\ell_2}\gamma_5\right]v(p_2, s_2), \tag{6.25}$$

where $E_M^{\ell_1\ell_2}$ and $F_M^{\ell_1\ell_2}$ are dimensionless constants for the scalar $M = \chi_c$ and pseudoscalar $M = \eta_c$ decay amplitudes, which depend on the Wilson coefficients of the operators in Eq. (6.17), and on the decay constants. The corresponding branching fraction is

$$\mathcal{B}(M \to \ell_1\bar{\ell}_2) = \frac{m_M}{8\pi\Gamma_M}\left(1-y^2\right)^2\left[\left|E_M^{\ell_1\ell_2}\right|^2 + \left|F_M^{\ell_1\ell_2}\right|^2\right]. \tag{6.26}$$

Here, Γ_M is the total decay width and $y = m_2/m_M$. The generic expressions for the coefficients $E_M^{\ell_1\ell_2}$ and $F_M^{\ell_1\ell_2}$ for the pseudoscalar $M = P$ and scalar $M = S$ states are given in [89]. We can simplify them by neglecting the contribution of the gluonic operators of Eq. (6.18), as η_c and χ_c are not expected to contain large gluonic components in their wave functions. The Wilson coefficients of the gluonic operators are better probed in CLFV tau decays, where the low energy theorems [93], or experimental data [90], constrain the gluonic matrix elements in a model-independent manner.

Hence, $P=\eta_c$ CLFV decays are mainly sensitive to the axial operator contributions in $\mathcal{L}_{\ell q}$ of Eq. (6.17) [89],

$$\begin{aligned} E_P^{\ell_1\ell_2} =& y\frac{m_P}{4\Lambda^2}\Big[-if_P\Big[2\left(C_{AL}^{cc\ell_1\ell_2}+C_{AR}^{cc\ell_1\ell_2}\right)\\ &-m_P^2G_F\left(C_{PL}^{cc\ell_1\ell_2}+C_{PR}^{cc\ell_1\ell_2}\right)\Big]\Big],\\ F_P^{\ell_1\ell_2} =& -y\frac{m_P}{4\Lambda^2}\Big[f_P\Big[2\left(C_{AL}^{cc\ell_1\ell_2}-C_{AR}^{cc\ell_1\ell_2}\right)\\ &-m_P^2G_F\left(C_{PL}^{cc\ell_1\ell_2}-C_{PR}^{cc\ell_1\ell_2}\right)\Big]\Big], \end{aligned} \tag{6.27}$$

while scalar $S=\chi_c$ CLFV decays uniquely probe the scalar CLFV operators of Eq. (6.17),

$$\begin{aligned} E_S^{\ell_1\ell_2} =& iyf_S m_c\frac{m_S^2G_F}{2\Lambda^2}\left(C_{SL}^{ccl_1l_2}+C_{SR}^{ccl_1l_2}\right),\\ F_S^{\ell_1\ell_2} =& yf_S m_c\frac{m_S^2G_F}{2\Lambda^2}\left(C_{SL}^{ccl_1l_2}-C_{SR}^{ccl_1l_2}\right), \end{aligned} \tag{6.28}$$

where the decay constants are $f_{\eta_c}=(387\pm7)$ MeV [100], and $f_{\chi_c}\approx 887$ MeV [101], for the pseudoscalar and scalar states, respectively. The current and projected constraints on the combination of Wilson coefficients and NP scale Λ are given in Table 6.8.

6.4.3 (Radiative) Leptonic decays $D^0\to l_1l_2,\gamma l_1l_2$

Studies of lepton flavor violation can also be performed with D^0 decays into $\ell_1\ell_2$ and $\gamma\ell_1\ell_2$ final states. These decays involve FCNC transitions in the quark and lepton currents, and the set of effective operators tested is given in Eq. (6.17) for $q=u$. It should be emphasized that they are different from the operators discussed in Sects. 6.4.1 and 6.4.2, although particular NP models could give contributions to both sets of operators, in which case the Wilson coefficients of Eq. (6.17) for $q=c$ and $q=u$ would depend on parameters of the same NP model.

As D mesons are pseudoscalar states, the branching fraction of the flavor off-diagonal leptonic decays of D mesons is given by Eq. (6.26) with $M\to D$, where Γ_D is the total width of D^0. Calculating the form factors $E_D^{uc\ell_1\ell_2}$ and $F_D^{uc\ell_1\ell_2}$ for the $\bar{D}^0$ ($q_1q_2=cu$) states yields [91]

$$\begin{aligned} E_D^{q_1q_2\ell_1\ell_2} =& \frac{m_Df_Dy}{2\Lambda^2}\Big[\left(C_{AL}^{uc\ell_1\ell_2}+C_{AR}^{uc\ell_1\ell_2}\right)\\ &+m_D^2G_F\left(C_{PL}^{q_1q_2\ell_1\ell_2}+C_{PR}^{q_1q_2\ell_1\ell_2}\right)\Big],\\ F_D^{q_1q_2\ell_1\ell_2} =& i\frac{m_Df_Dy}{2\Lambda^2}\Big[\left(C_{AL}^{uc\ell_1\ell_2}-C_{AR}^{q_1q_2\ell_1\ell_2}\right)\\ &+m_D^2G_F\left(C_{PL}^{uc\ell_1\ell_2}-C_{PR}^{uc\ell_1\ell_2}\right)\Big], \end{aligned} \tag{6.29}$$

where $f_D=207.4\pm3.8$ MeV is the D meson decay constant.

The current and projected constraints on the combination of Wilson coefficients and NP scale Λ are given in Table 6.8. It should be noted that other operators can also be probed in D decays. To access them, one can consider three-body decays of a D meson into $\gamma\ell_1\ell_2$ [91], or semileptonic CLFV decays. While increasing the reach of the experiment, these decays complicate the theoretical interpretation of the bounds, forcing the introduction of additional hypotheses, such as the single-operator dominance, as well as model dependence. Using the results of Ref. [91], a set of constraints on CLFV operators can be obtained. If BESIII could take about 20 fb^{-1} data at $\psi(3770)$, the sensitivity for $D^0\to\gamma e\mu$ could reach $(5-10)\times10^{-7}$.

6.4.4 CLFV and LNV $D_{(s)}$ decays with light mesons

CLFV searches can include decays with light mesons in the final states, such as $D\to\pi\ell_1\ell_2$ or $D_s\to K\ell_1\ell_2$. A clear advantage in using these transitions is that both charged and neutral D mesons can be used for analyses. Just as in $D\to\gamma\ell_1\ell_2$, the disadvantages are the difficulties with the theoretical interpretation of the experimental bounds (unless directly projected onto particular NP models), and increased model dependence of the bounds, as long-distance contributions become increasingly more pronounced.

Finally, lepton-number violating processes such as $D_{(s)}^+\to\pi^-(K^-)\ell^+\ell^+$ can also be probed at BESIII. In particular, with 20 fb^{-1} of $\psi(3770)$ data, BESIII could improve the best upper limit to 4.6×10^{-7} and 2.3×10^{-7} for $D^+\to\pi^-e^+e^+$ and $D^+\to K^-e^+e^+$, respectively, extrapolated from the current analysis.

6.5 Searches for light (invisible) NP particles

Several well-motivated proposals of BSM physics include new degrees of freedom (DOF) that do not interact with the SM particles directly. Such DOFs constitute the so-called "Dark Sector". Particles that populate the Dark Sector could form a part or whole of the DM in our Universe. There are only a few interactions allowed by SM symmetries that provide a portal from the SM sector into the Dark Sector [102,103]. Depending on the masses, such DM and portal DOFs could be probed at the low-energy high-intensity frontier experiments, such as BESIII.

6.5.1 Physics of the Dark Sector

The presence of cold DM in our Universe provides the most natural explanation of several observational puzzles. If DM has a particle origin, it should be eventually detected in particle physics experiments. In particular, if DM particles are light, with masses in the keV-MeV range, as suggested by our understanding of small-scale gravitational clustering in numerical simulations, it should be possible to detect them in the decays of heavy meson states at BESIII. These DM particles could be fermions, scalars, or even vector bosons. In many models they are produced in pairs, as such models feature the Z_2 symmetry requirements for Lagrangians with such particles.

In other models light new particles can be produced not only in pairs, but also individually, in which case they could serve the role of mediators (portals) between the Dark Sector and SM. A particular motivation for such scenarios comes from the observations of anomalous fluxes of cosmic-ray positrons. In 2008, the PAMELA collaboration reported an excess of positrons above 10 GeV [104], which has now been confirmed by many other experiments, such as ATIC [105], Fermi-LAT [106] and AMS02 [107]. In a class of models, DM particles with masses of O(TeV) annihilate into a pair of light bosons with masses of O(GeV), which subsequently decay into charged leptons [108,109]. An exchange of light bosons would increase the DM annihilation cross-section, which would allow to explain the observations of anomalous cosmic-ray positrons. Moreover, if the mediator is light enough, no extra antiproton will be produced due to the kinematics. This feature is consistent with the PAMELA antiproton data. The light boson may be a massive dark photon in the models with an extra $U(1)$ gauge symmetry.

The dark photon field V_μ couples to the SM photon A_μ via kinetic mixing [110],

$$\mathcal{L}_k = -\frac{\kappa}{2} V_{\mu\nu} F^{\mu\nu}, \tag{6.30}$$

where $V_{\mu\nu}$ is the dark photon's field tensor $V_{\mu\nu} = \partial_\mu V_\nu - \partial_\nu V_\mu$. Note that this construction is gauge invariant. The dark photon can acquire a mass via the spontaneous symmetry breaking mechanism. Some models predict that the mass of the dark photon is at the scale ranging from O(MeV) to O(GeV) [110,111]. The kinetic mixing coupling κ is assumed to to be very small. Similarly to the case of neutral meson mixing, the introduction of the term mixing A_μ and V_μ implies that neither of the fields is a mass eigenstate. Diagonalizing the Lagrangian [110,112] introduces a small coupling g between the new, weakly-interacting vector field V'_μ, $g \approx \kappa e$, where e is the electric charge. Thus, dark photons can be searched for in the decays of charmed particles [112] and/or charmonia.

The structure of the Dark Sector can be complicated, possibly with a class of light particles including scalars, pseudo-scalars, gauge bosons and fermions at the GeV scale. Since the interaction between the Dark Sector and the SM sector is very weak, the constraints on the mixing parameter and dark photon mass mainly come from the intensity frontier, such as the measurements of the electron and muon anomalous magnetic moments, low-energy electron-positron colliders, beam-dump experiments and fixed-target experiments [102,103].

Light Dark Matter (LDM) with Z_2 symmetry

Let us consider, as an example, the generic case of a complex neutral scalar field χ_0 describing LDM. The discussion of other spin assignments of LDM and their effects in charm decays can be found in [40]. The generic effective Hamiltonian of lowest dimension describing $c \to u\chi_0^*\chi_0$ interactions is

$$\mathcal{H}_{\rm eff}^{(s)} = 2\sum_i \frac{C_i^{(s)}}{\Lambda^2} O_i, \tag{6.31}$$

where Λ is the scale associated with the particle (s) mediating interactions between the SM and LDM fields, and $C_i^{(s)}$ are the relevant Wilson coefficients of the operators

$$\begin{aligned} O_1 &= m_c(\bar{u}_R c_L)(\chi_0^*\chi_0), \\ O_2 &= m_c(\bar{u}_L c_R)(\chi_0^*\chi_0), \\ O_3 &= (\bar{u}_L\gamma^\mu c_L)(\chi_0^* \overleftrightarrow{\partial}_\mu \chi_0), \\ O_4 &= (\bar{u}_R\gamma^\mu c_R)(\chi_0^* \overleftrightarrow{\partial}_\mu \chi_0), \end{aligned} \tag{6.32}$$

where $\overleftrightarrow{\partial} = (\overrightarrow{\partial} - \overleftarrow{\partial})/2$, and χ_0^* is the conjugated state of χ_0. Operators $O_{3,4}$ disappear for real scalar LDM, in which case $\chi_0^* = \chi_0$. In Eq. (6.32), it is implied that the mediator of interactions between the LDM and SM fields is heavy, $M_\Lambda > m_D$. The discussion can be modified for the case of a light mediator (see [40]).

The simplest decay that is mediated by Eq. (6.32) is the transition $D^0 \to \chi_0\chi_0$, which could contribute to the invisible D decay width,

$$\mathcal{B}(D^0 \to \chi_0\chi_0) = \frac{\left(C_1^{(s)} - C_2^{(s)}\right)^2}{4\pi M_D \Gamma_D}\left(\frac{f_D M_D^2 m_c}{\Lambda^2(m_c+m_u)}\right)^2 \sqrt{1-4x_\chi^2}, \tag{6.33}$$

where $x_\chi = m_\chi/M_D$ is the rescaled LDM mass. Clearly, this rate is not helicity suppressed, so it could be quite a sensitive tool for determining LDM properties at BESIII. Current experimental constraints imply that

$$\frac{\left(C_1^{(s)} - C_2^{(s)}\right)}{\Lambda^2} \leqslant 8\times 10^{-8}, \tag{6.34}$$

for $m_\chi \ll m_D$, which corresponds to probing NP scales above 3.5 TeV. These constraints could be improved with the updated bounds for the $D^0 \to$ invisible decays. The constraints obtained in Eq. (6.34) can be used for constraining the parameters of particular models of light DM [40,113].

Similarly, the decay width of the radiative decay $D^0 \to \chi_0^*\chi_0\gamma$ can be computed as

$$\begin{aligned} \mathcal{B}(D^0 \to \chi_0^*\chi_0\gamma) &= \frac{f_D^2 \alpha C_3^{(s)} C_4^{(s)} M_D^5}{6\Lambda^4\Gamma_D}\left(\frac{F_D}{4\pi}\right)^2 \\ &\times\left(\frac{1}{6}\sqrt{1-4x_\chi^2}(1-16x_\chi^2-12x_\chi^4) - 12x_\chi^4 \log\frac{2x_\chi}{1+\sqrt{1-4x_\chi^2}}\right). \end{aligned} \tag{6.35}$$

We observe that Eq. (6.35) does not depend on $C_{1,2}^{(s)}$. This can be easily seen from the fact that the $D \to \gamma$ form factors of scalar and pseudoscalar currents are zero.

LDM without Z_2 symmetry

If DM particles are very light, in the kev-MeV range, they do not need to obey the Z_2 symmetry, as their decays to pairs of SM states could be either suppressed kinematically or by a small coupling. This implies that DM particles can be emitted and absorbed by SM particles. Due to their extremely small couplings to SM particles, experimental searches for such light states require large samples and the ability to resolve signals with missing energy. BESIII is ideally suited for such searches. For example, such particles could be searched for in leptonic $D/D_s \to \ell\bar{\nu}$ decays, which are helicity suppressed in SM. Additional emission of a dark photon or an axion-like particle (ALP) a could lift the helicity suppression and change the energy spectrum of the lepton [112]. Similarly, flavor-changing transitions of the type $D \to a\pi$, which result in a two-body-like spectrum of pions in $D \to \pi + invisible$, could become possible [114].

Searches for dark photons can be performed in decays of charmonium states. BESIII has the largest J/ψ data sample in the world. Associated production of dark photons with other Dark Sector particles, such as the dark Higgs h', is also possible and has been studied [115,116], provided that $m_{h'}$ is such that the production of this state is not kinematically suppressed.

6.5.2 (radiative) Invisible decays of charmonia

Invisible decays of quarkonium states might provide a window into what may lie beyond SM. In SM, the invisible decays of J/ψ and other charmonium states are given by their decays into neutrino final states,

$$\frac{\Gamma(J/\psi \to \nu\bar{\nu})}{\Gamma(J/\psi \to e^+e^-)} = \frac{9N_\nu G_F^2}{256\pi^2\alpha^2} M_{J/\psi}^4 \left(1 - \frac{8}{3}\sin^2\theta_W\right)^2 \simeq 4.54\times10^{-7}, \tag{6.36}$$

where G_F is the Fermi coupling, θ_W is the weak mixing angle, and $N_\nu = 3$ is the number of light non-sterile neutrinos. It is interesting to note that this result is about three orders of magnitude smaller than the corresponding decay of an Upsilon state [117]. Similarly, the SM branching fraction of radiative decays of J/ψ with missing energy is also very tiny [118]. Thus, we may neglect the neutrino background effects when confronting the theoretical predictions of J/ψ decays into invisible states with the experimental data. This implies that invisible decays of charmonium states provide an important opportunity to search for glimpses of BSM physics. In BSM scenarios, the decay rate might be enhanced either by new heavy particles which modify the interactions of neutrinos with heavy quarks, or by opening new decay channels into light DM states.

It is therefore possible to use invisible decays of charmonium states to set constraints on various models of light DM, provided that DM states couple to charmed quarks [118-121]. Predictions for radiative decays with missing energy in light DM models are given in Ref. [122].

Due to its superb kinematic reconstruction capabilities, BESIII can search for the invisible and radiative invisible decays of J/ψ, and via decay chains $\psi(3686) \to \pi^+\pi^- J/\psi(\to \text{invisible})$ using $\pi^+\pi^-$ as a trigger, similar to the invisible decay search for $\Upsilon(1S)$ at BaBar [123]. With the data set of 3×10^9 $\psi(3686)$ events, the branching fraction of the J/ψ invisible decay could be probed to 3×10^{-5}.

6.5.3 Invisible decays of D mesons

Decays of D mesons into invisible final states can also provide an excellent probe of light Dark Matter models. Similarly to Sect. 6.5.2, the invisible decays of D mesons in SM are constituted by their decays into neutrino final states, which can be computed. A major difference between the heavy quarkonium and D decays into neutrinos includes long-distance effects, which are currently poorly known. However, they are not expected to dominate the short-distance (SD) estimates by many orders of magnitude. The SD contributions to the branching fractions of $D^0 \to \nu\bar{\nu}$ decays can be readily computed. It can be immediately noted that the left-handed structure of the Hamiltonian should result in helicity suppression of these transitions. Assuming that the neutrino masses are $m_\nu \sim \sum_i m_{\nu_i} < 0.62$ eV [124], where m_{ν_i} is the mass of one of the neutrinos,

$$\mathcal{B}(D^0 \to \nu\bar{\nu}) = \frac{G_F^2\alpha^2 f_D^2 m_D^3}{16\pi^3\sin^4\theta_W\Gamma_{D^0}} |V_{bc}V_{ub}^*|^2 X(x_b)^2 x_\nu^2 \simeq 1.1\times10^{-30}. \tag{6.37}$$

Here, $x_\nu = m_\nu/m_D$ and $\Gamma_D = 1/\tau_D$ is the total width of the D^0 meson. Such tiny rates imply that decays of heavy mesons into neutrino-antineutrino final states in SM can be safely neglected as sources of background in the searches for DM in D decays. Such helicity suppression in the final state can be overcome by adding a third particle to the final state, such as a photon. In fact, the SM contribution to the invisible width of the D meson is dominated by D decays into the four-neutrino final state with the branching fraction $\mathcal{B}(D^0 \to 4\nu) = (2.96\pm0.39)\times10^{-27}$ [125]. The resulting branching fractions of $D^0 \to \gamma\nu\bar{\nu}$ are also larger than $D^0 \to \nu\bar{\nu}$ by orders of magnitude [40,126].

The Belle collaboration published a limit on the branching fraction of D decays to invisible final states, setting it at 9.4×10^{-5} at the 90% C.L. [127]. BESIII could improve this limit to the order of $10^{-6} \to 10^{-5}$ with the final charm data set. Many NP models predict much larger branching fractions of D mesons into light DM states than of $D \to \nu\bar{\nu}$. This implies that the measurement of the invisible D width provides a practically SM-background-free search for such states [40]. Searches for D decays into a meson state and missing energy can also probe light DM states [113,128].

6.5.4 Invisible decays of light mesons

Decays of light mesons produced at BESIII can also probe new light particles [129]. In the case of dark photons, the general rule is that if light mesons can decay into regular photons then they can also decay into dark photons [115,130]. Since low-energy electron-positron colliders produce numerous mesons, it is also possible to investigate dark photons in rare decays of mesons. For instance, one can search for a resonance in the processes $\phi \to \eta + V'$ and $\pi/\eta \to \gamma + V' \to \gamma l^+ l^-$.

The invisible decay of η and η' mesons was studied [131] with 2.25×10^8 J/ψ events at BESIII, which improved the previous limits from BESII. Invisible decays of vector states, such as ω or ϕ, were also probed [132]. The sensitivities of these results are dominated by the available statistics. With $10^{10} J/\psi$ events recorded, the statistical uncertainty will be correspondingly reduced. The expected upper limits could then be further improved to 2.8×10^{-5} and 4.5×10^{-5} for the ω and ϕ invisible decays.

6.6 Off-resonance searches

The clean collision environment and excellent detector performance of BESIII offer opportunities for NP searches in kinematic regions where the energies of the electron and positron are not tuned to the s-channel resonance production of $\psi(nS)$ states.

6.6.1 Rare charm production: $e^+e^- \to D^*(2007)$

As mentioned in Sect. 6.2.2, the rate of the simplest FCNC decay $D^0 \to \ell^+\ell^-$ is helicity suppressed. This is demonstrated by the decay amplitude that is proportional to the mass of the final state lepton. This fact makes the observation of the branching fraction of $D^0 \to e^+e^-$ a near-impossible task, and complicates the study of lepton flavor universality in charm transitions.

An interesting alternative to the studies of D decays is to measure the corresponding *production* process $e^+e^- \to D^*$, as shown in Fig. 6.3 [133]. This is possible if BEPCII were to take data at the collision energy corresponding to the mass of D^* meson, $\sqrt{s} \approx 2007$ MeV. The production process, $e^+e^- \to D^{*0}$, which is inverse of the $D^* \to e^+e^-$ decay, is rather rare, as it is driven by FCNC. Yet, the produced D^{*0} resonance, tagged by a single charmed particle in the final state, decays strongly ($D^{*0} \to D^0\pi^0$) or electro-magnetically ($D^{*0} \to D^0\gamma$) with huge branching fractions of $(64.7\pm0.9)\%$ and $(35.3\pm0.9)\%$, respectively. This production mechanism, albeit very rare, has clear advantages for NP studies compared to the $D^0 \to e^+e^-$ decay: helicity suppression is absent, and a richer set of effective operators can be probed. It is also interesting to note that contrary to other rare decays of charmed mesons, long-distance SM contributions are under theoretical control and are of the same order of magnitude as the short-distance contributions [133].

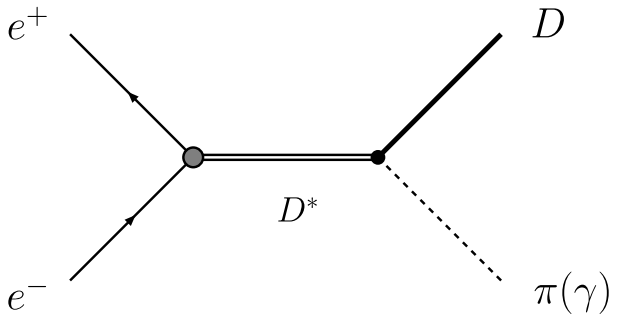

Fig. 6.3. Probing the $c\bar{u} \to e^+e^-$ vertex with $D^*(2007)^0$ resonant production in e^+e^- collisions.

Some preliminary studies of this process were performed by CMD-3 at VEPP-2000 collider in Novosibirsk [134].

It is interesting to estimate the sensitivity of BESIII to detect the process $e^+e^- \to D^* \to D\pi$. It can be shown [133] that crudely,

$$\mathcal{B}_{D^*\to e^+e^-} \geqslant \left(\frac{1}{\epsilon\int L\mathrm{d}t}\right)\times\frac{m_{D^*}^2}{12\pi\,\mathcal{B}_{D^*\to D\pi}}, \tag{6.38}$$

assuming that the beam energy resolution is smaller than the spread of the resonance cross-section. An average luminosity of $L \approx 1.0\times10^{32}\ \mathrm{cm^{-2}s^{-1}}$ with a year ($\sim 10^7$ s) of running at the D^* resonance yields $\int L\mathrm{d}t = 1.0\ \mathrm{fb}^{-1}$. Thus, the single-event sensitivity estimated from Eq. (6.38) implies that

$$\mathcal{B}_{D^*\to e^+e^-} > 4\times10^{-13} \tag{6.39}$$

could be probed in an ideal way. However, the beam energy resolution around $\sqrt{s} = 2$ GeV at BEPCII would in practice be more than several hundred keV, which is at least one order of magnitude wider than the D^* resonance width. Hence, a realistic upper limit for one-year data taking could be a few orders of magnitude worse than the number given in Eq. (6.39).

To estimate the NP scale sensitivity implied by Eq. (6.39), one can assume single operator dominance with the Wilson coefficient C to obtain [133]

$$\Lambda \sim \left(\frac{1}{3\pi}\frac{m_{D^*}^3 f_{D^*}^2}{32\Gamma_0}\frac{C^2}{\mathcal{B}(D^*\to e^+e^-)}\right)^{1/4}. \tag{6.40}$$

With the upper bound of Eq. (6.39), the observation of a single event in a year of running would probe NP scales of the order of $\Lambda \sim 2.7$ TeV, provided that $C \sim 1$. Taking into account the current experimental bound $\mathcal{B}_{D\to e^+e^-} = 7.9\times10^{-8}$, one finds that only the scale $\Lambda \sim 200$ GeV is currently probed by the $D \to e^+e^-$ decay. It is the presence of the lepton mass factor that severely limits the NP scale sensitivity in $D^0 \to e^+e^-$.

It should be noted that single-charm final states required for this analysis can also be produced in non-leptonic weak decays of heavy quarkonium states, such as $J/\psi \to D\pi$, discussed in Sect. 6.2.1, albeit in different kin-

ematic regions. Since the heavy charmonium states lie far away from the energy region required for this analysis, these transitions will not produce any background in $e^+e^- \to D^* \to D\pi$, and can be used to study the experimental systematics associated with such final states (see Sect. 6.2.1).

6.6.2 Dark photon and dark Higgs searches

Electron-positron colliders are suitable for probing dark photons via either the direct production or rare decays of mesons (see Sect. 6.5). Dark photons, directly produced in e^+e^- annihilation, could subsequently decay into charged leptons [116,130,135-137], which could be detected at BESIII. In comparison with the irreducible QED background, dark photon production is highly suppressed. To reduce the background, precise reconstruction of the dark photon mass and high luminosity are important. Such analyses have been performed by the BaBar experiment [130,138,139]. The mixing parameter κ (see Sect. 6.5.1 for definition) is constrained for the dark photon with a mass of about 1 GeV. The limits can be further improved at Belle II [140]. The potential reach of BESIII was discussed in Ref. [115], where 20 fb^{-1} of data collected at $\psi(3770)$ is assumed.

At BESIII, the most promising channel to search for dark photons is via the radiative decay $e^+e^- \to \gamma V'^\star \to \gamma e^+e^-$. The published BESIII result [141], based on 2.9 fb^{-1} of $\psi(3770)$ data, is competitive with the upper limit from BaBar [142], based on nine years of running.

BESIII searches would also be competitive if the dark photon decays invisibly (or is detector stable, *i.e.* it mostly decays outside of the detector volume). An estimate of the possible constraints from the existing data set shows that BESIII could reach or exceed the existing BaBar limit. In the future, the $\psi(3770)$ and XYZ data sets will be increased, so that the exclusion limit will be further reduced by BESIII. However, it will be difficult to reach the relic density limit, since it is 2-4 orders of magnitude lower. Future data sets will provide an opportunity for studying other channels that are feasible for dark photon searches, such as $J/\psi \to e^+e^- + V'$ [135] or $\psi(3686) \to \chi_c + V'$.

Another search strategy is to look for dark photons indirectly. This applies to BSM models with light dark Higgs particles h'. We can search for a dark photon associated with a dark Higgs h' via the Higgs-strahlung $e^+e^- \to V'h'$. Masses of the dark Higgs and dark photon are unknown. The dark Higgs h' decay modes strongly depend on the relation between these two masses.

1. $m_{h'} > 2\times m_{V'}$: $h' \to V'V'$;

2. $m_{V'} < m_{h'} < 2\times m_{V'}$: $h' \to V'V'^*$, where V'^* decays into leptons;

3. $m_{h'} < m_{V'}$: h' decays to lepton pairs or hadrons, or $h' \to$ invisible.

There may also be other light bosons in the dark sector, for instance gauge bosons associated with extra non-Abelian symmetries [143]. The final states of the direct production could contain more lepton pairs. In this case, it is easier to extract the signals from large QED background via the reconstruction of resonances. BESIII published two results from a light Higgs search, exploiting $\psi(3686)$ [144] and J/ψ [145] decays. These results can also be interpreted to constrain the dark photon. They are still limited by statistics, so the sensitivity will be improved with more data.

6.6.3 Axion-like particles

Axion-like particles (ALP), commonly denoted as a, are present in many possible extensions of SM. ALPs arise as Goldstone bosons in theories with additional Peccei-Quinn symmetry (PQ) [146,147], which is a spontaneously broken global symmetry that is anomalous with respect to the SM gauge interactions. a mainly couples to a photon-pair via $\mathcal{L} = \frac{g_{a\gamma\gamma}}{8}\epsilon_{\mu\nu\alpha\beta}F^{\mu\nu}F^{\alpha\beta}a$. The search for an axion-like particle at BESIII can be performed via $D \to K^*a$ [148], ALP-strahlung ($e^+e^- \to \gamma a$) and photon fusion ($e^+e^- \to e^+e^-a$) processes [149]. Searches for axion-like particles have not yet been made at the BESIII experiment, nor at any other e^+e^- collider experiment. Belle II has a planned program of searches for this kind of new particle [150].

At BESIII, ALP can be searched for via radiative decays of quarkonium states, such as $J/\psi \to \gamma a$. The branching fraction of $J/\psi \to \gamma a$ can be computed as $\mathcal{B}(J/\psi \to \gamma a) = \frac{1}{8\pi\alpha}g^2_{a\gamma\gamma}m^2_c\mathcal{B}(J/\psi \to e^+e^-)$ [151]. The large data sets collected by BESIII at J/ψ and $\psi(3686)$ provide a unique opportunity to explore ALPs. One of the possible difficulties could arise from the method of selecting two best photons for $a \to \gamma\gamma$ reconstruction. One of the easiest methods would be to combine all three possible combinations of di-photon invariant mass spectra, and then search for a narrow resonance 'a' signal. Assuming $\mathcal{B}(J/\psi \to \gamma A^0)\times\mathcal{B}(A^0 \to \mu^+\mu^-) = \mathcal{B}(J/\psi \to \gamma a)\times\mathcal{B}(a \to \gamma\gamma)$, the 90% C.L. upper limit on $g_{a\gamma\gamma}$ is expected to be in the range $(8.7-115.9)\times10^{-5}$, with the J/ψ sample of 10^{10} events, in the absence of any significant signal.

6.6.4 Searches for fractionally charged particles

The electric charges of all known elementary particles are either zero, $\pm e$, $\pm\frac{1}{3}e$, or $\pm\frac{2}{3}e$, where e is the electron charge. While it is known that such charge assignments are required for the cancellation of electroweak anomalies [152], we can not explain why this particular pattern of charges was chosen in Nature. Furthermore, quarks always combine into composite particles with charges ne, where $n = 0, \pm1, \pm2...$, so that all observable particles have zero or integer charge in terms of e. This seems quite natural but we do not understand the physical law behind this simplicity.

Some BSM models predict the existence of fraction-

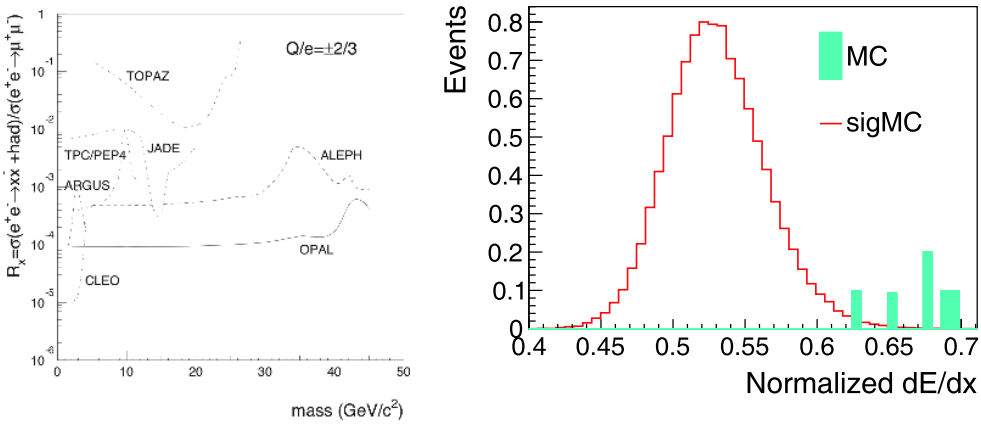

Fig. 6.4. (color online) (Left) Existing limits for fractionally charged particles in the low-mass region. (Right) A typical $\mathrm{d}E/\mathrm{d}x$ distribution of the signal for $m(F) = 1.3$ GeV/c^2 and $Q(F) = \frac{2}{3}e$, where the red histogram shows the signal and the cyan histogram the background estimate.

Table 6.9. Projection of BESIII limit on $\sigma(e^+e^- \to F^{+\frac{2}{3}}F^{-\frac{2}{3}})$ at $\sqrt{s} = 3.773$ GeV (with statistical uncertainties only) at the 90% C.L.

$m(F)/(\mathrm{GeV}/c^2)$	$N_{\rm bkg}$	$N_{\rm obs}$(MC)	ϵ(signal)	σ (fb) for 2.9 fb^{-1}	σ (fb) for 20 fb^{-1}
0.3	0	0	0.73	0.94	0.14
1.3	0.57	0.57	0.76	1.39	0.28
1.7	5.38	5.38	0.77	1.90	0.78

ally charged particles, such as leptoquarks [153], modified QCD [154-156], etc. In the past 80 years, physicists have searched for fractionally charged particles by employing various methods and technologies, such as particle accelerators in fixed target and collider modes, space science, analyses of bulk matter etc., without any confirmed observation [157].

In collider experiments, the ionization energy loss $\mathrm{d}E/\mathrm{d}x$ can be used to search for a fractionally charged particle F with low background. The energy loss scales roughly as $(Q/e)^2$, where Q is the charge of F. Such searches have been performed by experiments at LEP, Tevatron, as well as earlier facilities, with the assumed mass of F larger than 45 GeV/c^2. The existing search results for low-mass fractionally charged particles are shown in Fig. 6.4(a), presented as the ratio of $\sigma(e^+e^- \to F\bar{F} + had)/\sigma(e^+e^- \to \mu^+\mu^-)$. The most sensitive low-mass search was performed by CLEO [158] and OPAL [159]. With significant integrated luminosity in the tau-charm energy region, BESIII can search for fractionally charged particles in the low-mass regime to improve the bounds set by CLEO.

The BESIII drift chamber can measure $\mathrm{d}E/\mathrm{d}x$ precisely, and the process $e^+e^- \to F\bar{F}$ can be searched for by counting the number of events in the corresponding $\mathrm{d}E/\mathrm{d}x$ distribution. Figure 6.4(b) shows a typical $\mathrm{d}E/\mathrm{d}x$ distribution from a simulation with $m(F) = 1.3$ GeV/c^2 and $Q(F) = \frac{2}{3}e$, where only 0.57 background events are expected for 2.9 fb^{-1} $\psi(3770)$ of data. Using the Rolke method [160], the upper limit on $\sigma(e^+e^- \to F^{+2/3}F^{-2/3})$ at the 90% C.L. can be extracted. Table 6.9 shows the expected BESIII sensitivity for the cross-section with several assumptions for the mass. The expected signal and background are from MC simulations, and only the statistical uncertainties are taken into account in the upper limits. It is clear that BESIII can provide improved constraints on the mass of F in the low-mass region.

To facilitate the comparison with existing results, the expected BESIII results can also be presented as the ratio $R_F = \sigma(e^+e^- \to F\bar{F})/\sigma(e^+e^- \to \mu^+\mu^-)$. Using the information given in Table 6.9, the BESIII projection corresponds to $R_F \approx 10^{-7}$. This result would be several orders of magnitude lower than the existing data shown in Fig. 6.4(a). Using all data samples with large integrated luminosity ($\geqslant$500 pb^{-1}) for each collision energy at BESIII, and by varying the charge of F, better constraints on the parameters of fractionally charged particles are expected.

References

1 S.-H. Zhu, arxiv: 1410.2042

2 M. A. Sanchis, Z. Phys. C, **62**: 271 (1994)

3 A. Datta, P. O 'Donnell, S. Pakvasa *et al.*, Phys. Rev. D, **60**: 014011 (1999)

4 X. M. Zhang, High Energy Phys. Nucl. Phys., **25**: 461 (2001)
5 H.-B. Li and S.-H. Zhu, Chin. Phys. C, **36**: 932 (2012)
6 C. Hill, Phys. Lett. B, **345**: 483 (1995)
7 R. Dhir, R.C. Verma, and A. Sharma, Adv. High Energy Phys., **2013**: 706543 (2013)
8 Y.-M. Wang, H. Zhou, Z.-T. Wei *et al*., Eur. Phys. J. C, **55**: 607 (2008)
9 Y.-L. Shen and Y.-M. Wang, Phy. Rev. D, **78**: 074012 (2008)
10 K. K. Sharma and R.C. Verma, Int. J. Mod. Phys. A, **14**: 937 (1999)
11 M. Ablikim *et al*. (BES Collaboration), Phys. Lett. B, **663**: 297 (2008)
12 M. Ablikim *et al*. (BESIII Collaboration), Phys. Rev. D, **89**: 071101 (2014)
13 M. A. Ivanov and C. T. Tran, Phys. Rev. D, **92**: 074030 (2015)
14 M. Ablikim *et al*. (BES Collaboration), Phys. Lett. B, **639**: 418 (2006)
15 M. Ablikim *et al*. (BESIII Collaboration), Phys. Rev. D, **90**: 112014 (2014)
16 Y.-M. Wang *et al*., J. Phys. G, **36**: 105002 (2009)
17 R. Aaij *et al*. (LHCb Collaboration), JHEP, **08**: 055 (2017)
18 W. Altmannshofer, P. Stangl, and D. M. Straub, Phys. Rev. D, **96**: 055008 (2017)
19 I. Dorsner, S. Fajfer, D. A. Faroughy *et al*., JHEP, **10**: 188 (2017)
20 S. L. Glashow, D. Guadagnoli, and K. Lane, Phys. Rev. Lett., **114**: 091801 (2015)
21 G. Burdman, E. Golowich, J. L. Hewett *et al*., Phys. Rev. D, **52**: 6383 (1995)
22 C. Greub, T. Hurth, M. Misiak *et al*., Phys. Lett. B, **382**: 415 (1996)
23 G. Burdman, E. Golowich, J. L. Hewett *et al*., Phys. Rev. D, **66**: 014009 (2002)
24 S. de Boer and G. Hiller, Phys. Rev. D, **98**: 035041 (2018)
25 S. Fajfer, S. Prelovsek, P. Singer *et al*., Phys. Lett. B, **487**: 81 (2000)
26 G. Isidori and J. F. Kamenik, Phys. Rev. Lett., **109**: 171801 (2012)
27 S. de Boer and G. Hiller, JHEP, **08**: 091 (2017)
28 S. de Boer and G. Hiller, Eur. Phys. J. C, **78**: 188 (2018)
29 Y. Amhis *et al*. (Heavy Flavor Averaging Group), Eur. Phys. J. C, **77**: 895 (2017)
30 E. Golowich, J. Hewett, S. Pakvasa *et al*., Phys. Rev. D, **79**: 114030 (2009)
31 A. Paul, A.De La Puente, and I. I. Bigi, Phys. Rev. D, **90**: 014035 (2014)
32 S. Fajfer, Sasa Prelovsek, and P. Singer, Phys. Rev. D, **64**: 114009 (2001)
33 S. Fajfer and N. Kosnik, Phys. Rev. D, **87**: 054026 (2013)
34 S. de Boer and G. Hiller, Phys. Rev. D, **93**: 074001 (2016)
35 M. Ablikim *et al*. (BESIII Collaboration), Phys. Rev. D, **97**: 072015 (2018)
36 E. M. Aitala *et al*. (E791 Collaboration), Phys. Rev. Lett., **86**: 3969 (2001)
37 J. P. Lees *et al*. (BaBar Collaboration), Phys. Rev. D, **84**: 072006 (2011)
38 K. F. Chen *et al*. (Belle Collaboration), Phys. Rev. Lett., **99**: 221802 (2007)
39 J. P. Lees *et al*. (BaBar Collaboration), Phys. Rev. Lett., **93**: 091802 (2004)
40 A. Badin and A. A. Petrov, Phys. Rev. D, **82**: 034005 (2010)
41 A. D. Sakharov, Pisma Zh. Eksp. Teor. Fiz., **5**: 32 (1967); Usp. Fiz. Nauk, **161**: 61 (1991)
42 D. E. Morrissey and M. J. Ramsey-Musolf, New J. Phys., **14**: 125003 (2012)
43 M. Tanabashi *et al*. (Particle Data Group), Phys. Rev. D, **98**: 030001 (2018)
44 R. Aaij *et al*. (LHCb Collaboration), Phys. Rev. Lett., **122**: 211803 (2019)
45 P. Chauvat *et al*. (R608 Collaboration), Phys. Lett. B, **163**: 273 (1985)
46 P. D. Barnes *et al*., Phys. Rev. C, **54**: 1877 (1996)
47 M. H. Tixier *et al*. (DM2 Collaboration), Phys. Lett. B, **212**: 523 (1988)
48 M. Ablikim *et al*. (BESIII Collaboration), Phys. Rev. D, **81**: 012003 (2010)
49 J. F. Donoghue and S. Pakvasa, Phys. Rev. Lett., **55**: 162 (1985)
50 J. F. Donoghue, X.-G. He, and S. Pakvasa, Phys. Rev. D, **34**: 833 (1986)
51 J. Tandean and G. Valencia, Phys. Rev. D, **67**: 056001 (2003)
52 X.-G. He and G. Valencia, Phys. Rev. D, **52**: 5257 (1995)
53 K. B. Luk, arXiv: hep-ex/9803002
54 J. Tandean, Phys. Rev. D, **69**: 076008 (2004)
55 H.-Y. Cheng and B. Tseng, Phys. Rev. D, **46**: 1042 (1992); [Erratum: Phys. Rev. D, **55**: 1697 (1997)]
56 H.-Y. Cheng, X.-W. Kang, and F. Xu, Phys. Rev. D, **97**: 074028 (2018)
57 J. Liu, R.-G. Ping, and H.-B. Li, J. Phys. G, **42**: 095002 (2015)
58 M. Ablikim *et al.* (BESIII Collaboration), Nature Phys., **15**: 631 (2019)1 (2019)
59 I. I. Bigi, X.-W. Kang, and H.-B. Li, Chin. Phys. C, **42**: 013101 (2018)
60 G. Valencia, Phys. Rev. D, **39**: 3339 (1989)
61 I. I. Bigi and A. I. Sanda, Part. Phys. Nucl. Phys. Cosmol., **9**: 1 (2009)
62 X.-W. Kang and H.-B. Li, Phys. Lett. B, **684**: 137 (2010)
63 X.-W. Kang, H.-B. Li, G.-R. Lu *et al*., Int. J. Mod. Phys. A, **26**: 2523 (2011)
64 M. Duraisamy and A. Datta, JHEP, **09**: 005 (2013)
65 W. Bensalem, A. Datta, and D. London, Phys. Lett. B, **538**: 309 (2002)
66 A. Datta and D. London, Int. J. Mod. Phys. A, **19**: 2505 (2004)
67 M. Gronau and J. L. Rosner, Phys. Rev. D, **84**: 096013 (2011)
68 M. Gronau and J. L. Rosner, Phys. Lett. B, **749**: 104 (2015)
69 E. Di Salvo and Z. J. Ajaltouni, Mod. Phys. Lett. A, **28**: 135004 (2013)
70 Z. J. Ajaltouni and E. Di Salvo, Int. J. Mod. Phys. A, **27**: 1250086 (2012)
71 X. G. He, J. P. Ma, and B. McKellar, Phys. Rev. D, **47**: R1744 (1993)
72 X. G. He, J. P. Ma, and B. McKellar, Phys. Rev. D, **49**: 4548 (1994)
73 P. Adlarson and A. Kupsc, arXiv: 1908.03102[hep-ph]
74 R. N. Mohapatra and R. E. Marshak, Phys. Rev. Lett., **44**: 1316

(1980)
75 K.-B. Luk, in *International Workshop on the Search for Baryon and Lepton Number Violations*, LBNL, 2007
76 X. W. Kang, H. B. Li, and G. R. Lu, Phys. Rev. D, **81**: 051901(R) (2010)
77 H.-B. Li, Frontiers of Physics, **12**: 121301 (2017)
78 S. Dimopoulos and H. Georgi, Nucl. Phys. B, **193**, 150 (1981); N. Sakai, Z. Phys. C, **11**, 153 (1981)
79 F. Borzumati and A. Masiero, Phys. Rev. Lett., **57**: 961 (1986)
80 M. Dine, Y. Nir, and Y. Shirman, Phys. Rev. D, **55**: 1501 (1997); S. L. Dubovsky and D. S. Gorbunov, Phys. Lett. B, **419**: 223 (1998)
81 R. Kitano and K. Yamamoto, Phys. Rev. D, **62**: 073007 (2000)
82 J. E. Kim and D. G. Lee, Phys. Rev. D, **56**: 100 (1997); K. Huitu *et al.*, Phys. Lett. B, **430**: 355 (1998); A. Faessler *et al.*, Nucl. Phys. B, **587**: 25 (2000); M. Chaichian and K. Huitu, Phys. Lett. B, **384**: 157 (1996)old>: 157 (1996)
83 J. Bernabeu, E. Nardi, and D. Tommasini, Nucl. Phys. B, **409**: 69 (1993)
84 S. Coleman and S. L. Glashow, Phys. Rev. D, **59**: 116008 (1999)
85 J. Z. Bai *et al.* (BES Collaboration), Phys. Lett. B, **561**: 49 (2003)
86 M. Ablikim *et al.* (BESIII Collaboration), Phys. Rev. D, **87**: 112007 (2013)
87 M. Ablikim *et al.* (BESIII Collaboration), Phys. Lett. B, **598**: 172 (2004)
88 R. Aaij *et al.* (LHCb Collaboration), Phys. Lett. B, **754**: 167 (2016)
89 D. E. Hazard and A. A. Petrov, Phys. Rev. D, **94**: 074023 (2016)
90 A. Celis, V. Cirigliano, and E. Passemar, Phys. Rev. D, **89**: 095014 (2014)
91 D. E. Hazard and A. A. Petrov, Phys.Rev. D, **98**: 015027 (2018)
92 M. Raidal *et al.*, Eur. Phys. J. C, **57**: 13 (2008)
93 A. A. Petrov and D. V. Zhuridov, Phys. Rev. D, **89**: 033005 (2014)
94 S. Nussinov, R. D. Peccei, and X. M. Zhang, Phys. Rev. D, **63**: 016003 (2001)
95 H. K. Dreiner, G. Polesello, and M. Thormeier, Phys. Rev. D, **65**: 115006 (2002)
96 H. K. Dreiner, M. Kramer, and B. O'Leary, Phys. Rev. D, **75**: 114016 (2007)
97 K.-S. Sun, T.-F. Feng, T.-J. Gao *et al.*, Nucl. Phys. B, **865**: 486 (2012)
98 A. Abada, D. Becirevic, M. Lucente *et al.*, Phys. Rev. D, **91**: 113013 (2015)
99 D. Black, T. Han, H.-J. He *et al.*, Phys. Rev. D, **66**: 053002 (2002)
100 D. Becirevic, G. Duplancic, B. Klajn *et al.*, Nucl. Phys. B, **883**: 306 (2014)
101 S. Godfrey and H. E. Logan, Phys. Rev. D, **93**: 055014 (2016)
102 R. Essig *et al.*, arXiv: 1311.0029
103 J. Alexander *et al.*, arXiv: 1608.08632
104 O. Adriani *et al.* (PAMELA Collaboration), Nature, **458**: 607 (2009)
105 J. Chang *et al.*, Nature, **456**: 362 (2008)
106 A. A. Abdo *et al.* (Fermi-LAT Collaboration), Phys. Rev. Lett., **102**: 181101 (2009)
107 M. Aguilar *et al.* (AMS Collaboration), Phys. Rev. Lett., **110**: 141102 (2013)
108 N. Arkani-Hamed, D. Finkbeiner, T. Slatyer *et al.*, Phys. Rev. D, **79**: 015014 (2009)
109 M. Pospelov and A. Ritz, Phys. Lett. B, **671**: 391 (2009)
110 N. Arkani-Hamed and N. Weiner, JHEP, **0812**: 104 (2008)
111 C. Cheung, J. T. Ruderman, L.-T. Wang *et al.*, Phys. Rev. D, **80**: 035008 (2009)
112 Y. G. Aditya, K. J. Healey, and A. A. Petrov, Phys. Lett. B, **710**: 118 (2012)
113 C. Bird, R. V. Kowalewski, and M. Pospelov, Mod. Phys. Lett. A, **21**: 457 (2006)
114 L. Calibbi, F. Goertz, D. Redigolo *et al.*, Phys. Rev. D, **95**: 095009 (2017)
115 H.-B. Li and T. Luo, Phys. Lett. B, **686**: 249 (2010)
116 P.-F. Yin, J. Liu, and S.-H. Zhu, Phys. Lett. B, **679**: 362 (2009)
117 L. N. Chang, O. Lebedev, and J. N. Ng, Phys. Lett. B, **441**: 419 (1998)
118 G. K. Yeghiyan, Phys. Rev. D, **80**: 115019 (2009)
119 B. McElrath, Phys. Rev. D, **72**: 103508 (2005)
120 P. Fayet, Phys. Rev. D, **81**: 054025 (2010)
121 N. Fernandez, J. Kumar, I. Seong *et al.*, Phys. Rev. D, **90**: 015029 (2014)
122 N. Fernandez, I. Seong, and P. Stengel, Phys. Rev. D, **93**: 054023 (2016)
123 B. Aubert *et al.*, Phys. Rev. Lett., **103**: 251801 (2009)
124 A. Goobar, S. Hannestad, E. Mortsell *et al.*, JCAP, **0606**: 019 (2006)
125 B. Bhattacharya, C. Grant, and A. Petrov, arXiv: 1809.04606
126 T. M. Aliev, A. Ozpineci, and M. Savci, Phys. Lett. B, **393**: 143 (1997)
127 Y. T. Lai *et al.*, Phys. Rev. D, **95**: 011102 (2017)
128 D. McKeen, Phys. Rev. D, **79**: 114001 (2009)
129 H. K. Dreiner, S. Grab, D. Koschade *et al.*, Phys. Rev. D, **80**: 035018 (2009)
130 M. Reece and L.-T. Wang, JHEP, **07**: 051 (2009)
131 M. Ablikim *et al.* (BESIII Collaboration), Phys. Rev. D, **87**: 012009 (2013)
132 M. Ablikim *et al.* (BESIII Collaboration), Phys. Rev. D, **98**: 2001 (2018)
133 A. Khodjamirian, T. Mannel, and A. A. Petrov, JHEP, **1511**: 142 (2015)
134 E. P. Solodov *et al.*, PoS, EPS-HEP2017: 407, 2017
135 S.-H. Zhu, Phys. Rev. D, **75**: 1 (2007)
136 P. Fayet, Phys. Rev. D, **75**: 115017 (2007)
137 R. Essig, P. Schuster, and N. Toro, Phys. Rev. D, **80**: 42 (2009)
138 J. Bjorken, R. Essig, P. Schuster *et al.*, Phys. Rev. D, **80**: 1 (2009)
139 B. Aubert *et al.* (BaBar Collaboration), Phys. Rev. Lett., **103**: 081803 (2009)
140 B. O'Leary *et al.* (SuperB Collaboration), arXiv: 1008.1541
141 M. Ablikim *et al.* (BESIII Collaboration), Phys. Lett. B, **774**: 252 (2017)
142 J. P. Lees *et al.* (BaBar Collaboration), Phys. Rev. Lett., **113**: 201801 (2014)
143 M. Baumgart, C. Cheung, J. T. Ruderman *et al.*, JHEP, **04**: 014

(2009)
144 M. Ablikim *et al*. (BESIII Collaboration), Phys. Rev. D, **85**: 092012 (2012)
145 M. Ablikim *et al*. (BESIII Collaboration), Phys. Rev. D, **93**: 052005 (2016)
146 R. D. Peccei and H. Quinn, Phys. Rev. Lett., **38**: 1440 (1977); Phys. Rev. D, **16**: 1791 (1977)
147 S. Weinberg, Phys. Rev. Lett., **40**: 223 (1978); F. Wilczek, Phys. Rev. Lett., **40**: 279 (1978)
148 E. Izaguirre, T. Lin, and B. Shuve, Phys. Rev. Lett., **118**: 111802 (2017)
149 M. J. Dolan, T. Ferber, C. Hearty *et al*., JHEP, **12**: 92 (2017)
150 G. D. Pietro, arXiv: 1808: 00776
151 E. Masso and R. Toldra, Phys. Rev. D, **52**: 1755 (1995)
152 E. Golowich and P. B. Pal, Phys. Rev. D, **41**: 3537 (1990)
153 J. L. Hewett and T. G. Rizzo, Phys. Rev. D, **56**: 5709 (1997)
154 A. De Rujula, R. C. Giles, and R. L. Jaffe, Phys. Rev. D, **17**: 285 (1978)
155 R. Slansky, J. T. Goldman, and G. L. Shaw, Phys. Rev. Lett., **47**: 887 (1981)
156 D. G. Caldi and S. Nussinov, Phys. Rev. D, **28**: 3138 (1983)
157 M. L. Perl, E. R. Lee, and D. Loomba, Ann. Rev. Nucl. Part. Sci., **59**: 47 (2009)
158 T. J. V. Bowcock *et al*., Phys. Rev. D, **40**: 263 (1989)
159 R. Akers *et al*., Z. Phys. C, **67**: 203 (1995)
160 W. A. Rolke, A. M. Lópezand J. Conrad, Nucl. Instrum. Methods Phys. Res., Sect. A, **551**: 493 (2005)

Chapter 7

Summary

The BESIII experiment has been running very successfully since 2009, and has now collected around 30 fb^{-1} of integrated luminosity at a variety of critical energy points. The physics output to date comprises more than 270 papers in highly-ranked peer-reviewed journals, including one publication with more than 500 citations [1], and three others with more than 250 citations [2-4]. BESIII is now recognized as one of the leading experiments in hadronic physics in the world, and has made many significant measurements that are important entries in the Review of Particle Physics [5].

Noteworthy areas of study have included the spectroscopy of hadronic states containing the charm quark, the spectroscopy of light-hadron states produced in the decay of charmonia, and open-charm physics. Other significant results have been achieved in the precision tests of SM, checks of various predictions of QCD, and probes for new physics beyond SM.

The outstanding physics output has been enabled through the interplay between the well-running accelerator and the superb capabilities of the BESIII detector, which have allowed for new programs of operation and studies never previously attempted, for example high precision energy scans. Open questions have been answered, but new ones have arisen, which require higher precision measurements and even larger data sets. This requirement, therefore, provides compelling motivation for an extended running program, accompanied by upgrades to both the machine and the detector to deliver optimal performance.

BESIII has a crucial and unique role to play in the world-wide effort to explore and characterize the behavior of QCD in the non-perturbative regime, which is one of the least understood areas of SM. BESIII is the only hadron-physics experiment in the world that exploits electron-positron annihilation in the τ-charm energy region.

Globally, new experiments are starting to run or are planned. Belle II in Japan runs at a higher energy; the JLab experiments GlueX and CLAS12 in the USA use photon and electron beams, respectively; LHCb at CERN studies proton-proton collisions, and PANDA in Germany will be a fixed-target experiment with antiproton beams. Given the complexity of the underlying physics, all these complementary approaches are necessary to tackle the unsolved problems in our understanding of the strong interaction. The active and planed experiments highlight the importance of the physics that BESIII studies and excels at.

With more data BESIII can address many critical questions regarding charm physics. The study of leptonic and semileptonic charmed-hadron decays can greatly improve our knowledge of the decay constants, CKM matrix elements, form factors, and lepton flavor universality. LQCD, which plays a central role in these analyses, can be validated through stringent tests. Quantum-correlated

Table 7.1. List of data samples collected by BESIII/BEPCII up to 2019, and the proposed samples for the remainder of the physics program. The rightmost column shows the number of required data taking days with the current (T_C) and upgraded (T_U) machine. The machine upgrades include top-up implementation and beam current increase.

Energy	Physics motivations	Current data	Expected final data	T_C / T_U
1.8 - 2.0 GeV	R values Nucleon cross-sections	N/A	0.1 fb^{-1} (fine scan)	60/50 days
2.0 - 3.1 GeV	R values Cross-sections	Fine scan (20 energy points)	Complete scan (additional points)	250/180 days
J/ψ peak	Light hadron & Glueball J/ψ decays	3.2 fb^{-1} (10 billion)	3.2 fb^{-1} (10 billion)	N/A
$\psi(3686)$ peak	Light hadron & Glueball Charmonium decays	0.67 fb^{-1} (0.45 billion)	4.5 fb^{-1} (3.0 billion)	150/90 days
$\psi(3770)$ peak	$D^0/D^{\pm}$ decays	2.9 fb^{-1}	20.0 fb^{-1}	610/360 days
3.8 - 4.6 GeV	R values XYZ/Open charm	Fine scan (105 energy points)	No requirement	N/A
4.180 GeV	D_s decay XYZ/Open charm	3.2 fb^{-1}	6 fb^{-1}	140/50 days
4.0 - 4.6 GeV	XYZ/Open charm Higher charmonia cross-sections	16.0 fb^{-1} at different $\sqrt{s}$	30 fb^{-1} at different $\sqrt{s}$	770/310 days
4.6 - 4.9 GeV	Charmed baryon/XYZ cross-sections	0.56 fb^{-1} at 4.6 GeV	15 fb^{-1} at different $\sqrt{s}$	1490/600 days
4.74 GeV	$\Sigma_c^+\bar{\Lambda}_c^-$ cross-section	N/A	1.0 fb^{-1}	100/40 days
4.91 GeV	$\Sigma_c\bar{\Sigma}_c$ cross-section	N/A	1.0 fb^{-1}	120/50 days
4.95 GeV	Ξ_c decays	N/A	1.0 fb^{-1}	130/50 days

$D^0\bar{D}^0$ production, accessible only at BESIII, permits strong-phase measurements which are a necessary and invaluable input to CP-violation studies at other facilities. Recent BESIII progress in mapping out the decay modes of Λ_c will be expanded to include the currently missing channels, and new data involving e^+e^- production of charmed baryon pairs will provide information about the form factors in the time-like domain.

In Table 7.1, we present the current data samples available at BESIII and the samples needed to execute the physics program presented in this White Paper. To meet all requirements would mean another 12 years of operation assuming current BEPCII luminosity performance, and the collection by BESIII of another 56 fb^{-1} of integrated luminosity.

The BESIII physics goals laid out herein will benefit greatly from the improved BEPCII e^+e^- collision luminosity. The accelerator group is strongly encouraged to implement top-up injection and to operate BEPCII close to the peak instantaneous luminosity in order to achieve overall integrated luminosity improvement, and develop an effective upgrade plan to further enhance the luminosity performance and energy range. With these efforts, BESIII can achieve its science goals in less than 12 years, as estimated in this White Paper. It would be reasonable to conclude that BESIII can continue for 10 more years with a high quality physics program. It is important that the collaboration allocates resources to evaluate the status of the detector system, develop upgrade plans, optimize the data taking strategy and maximize the physics output of the experiment.

The authors thank the international review committee: Alexander E. Bondar (Chair), Cesare Bini, Kuang-Ta Chao, Shaomin Chen, Marco Gersabeck, Marek Karliner, Giovanni Passaleva and Yoshihide Sakai, for their great effort in reviewing the program and providing valuable comments and suggestions to improve this White Paper. The BESIII collaboration thanks the staff of BEPCII and the IHEP computing center for their strong support.

References

1 M. Ablikim *et al*. (BESIII Collaboration), Phys. Rev. Lett., **110**: 252001 (2013)
2 M. Ablikim *et al*. (BESIII Collaboration), Phys. Rev. Lett., **111**: 242001 (2013)
3 M. Ablikim *et al*. (BESIII Collaboration), Phys. Rev. Lett., **112**: 132001 (2014)
4 M. Ablikim *et al*. (BESIII Collaboration), Phys. Rev. Lett., **112**: 022001 (2014)
5 M. Tanabashi *et al*. (Particle Data Group), Phys. Rev. D, **98**: 030001 (2018)